THESIS

Contribution to engineering of WDM Nx160 Gbit/s optical transmission systems. Analysis of optical signal degradation induced by propagation impairments.

to obtain the

DOCTORATE DEGREE

in

THE LOUIS PASTEUR UNIVERSITY OF STRASBOURG

Speciality: Physics - Photonics

by

BENJAMIN CUENOT

Host laboratory: France Telecom R&D Division – Metropolitan and Core Network Lannion (22300, France)
University laboratory: Laboratoire des Systèmes Photoniques – Illkirch (67400, France)

The 29th of September 2004 before the doctoral committee:

FONTAINE Joël	Professor – ENSPS, INSA, Strasbourg, France
GALLION Philippe	Professor – ENST, Paris, France
GOSSELIN Stéphane	Engineer – FT R&D Division, Lannion, France
LIEBER Winfried	Prof. Dr.-Ing. – FachHochschule Offenburg, Germany
LACH Eugen	Doctor – Alcatel SEL, Stuttgart, Germany
RICHTER Andre	Doctor – VPI Systems, Berlin, Germany
MEYRUEIS Patrick	Professor – ENSPS, Strasbourg, France

Table of contents

General introduction

1 General definitions in optical communications

The aim of this chapter will be to get acquainted with some technical words and definitions used in optical telecommunications in order to understand clearly this document. To achieve this goal, we present different definitions within their context and briefly describe the objective of this study.

At first, we describe an optical line in a generic way. An optical transmission is composed of the following elements:

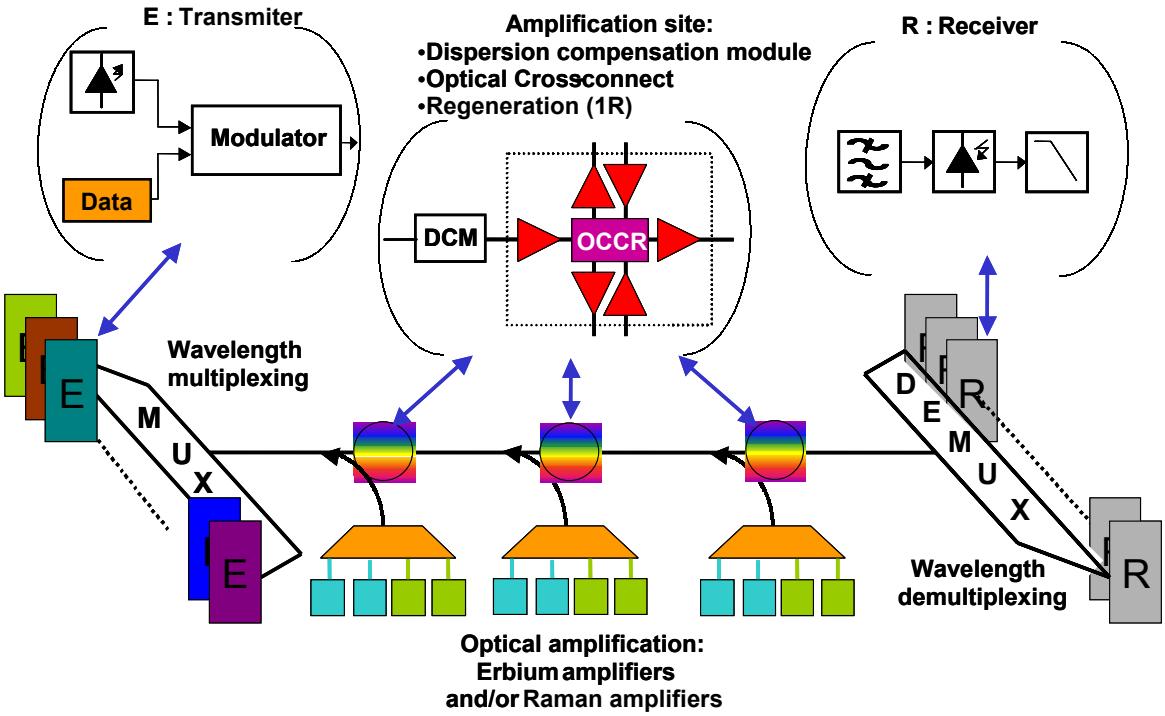

Figure 1. 1: scheme of an optical line.

As we can see on the previous figure, the emission part can be generally represented by 3 blocks: the data block generates data that will be transmitted in the line but it's generally electric and need to be converted into optical data. The optical coding of these data can be realized in various ways. Most usual ways of encoding are known as NRZ and RZ. An optoelectronic modulator is the key component for the emission of these optical data: this device modulates the input optical signal by the magnitude of its data input as shown in Figure 1. 2.

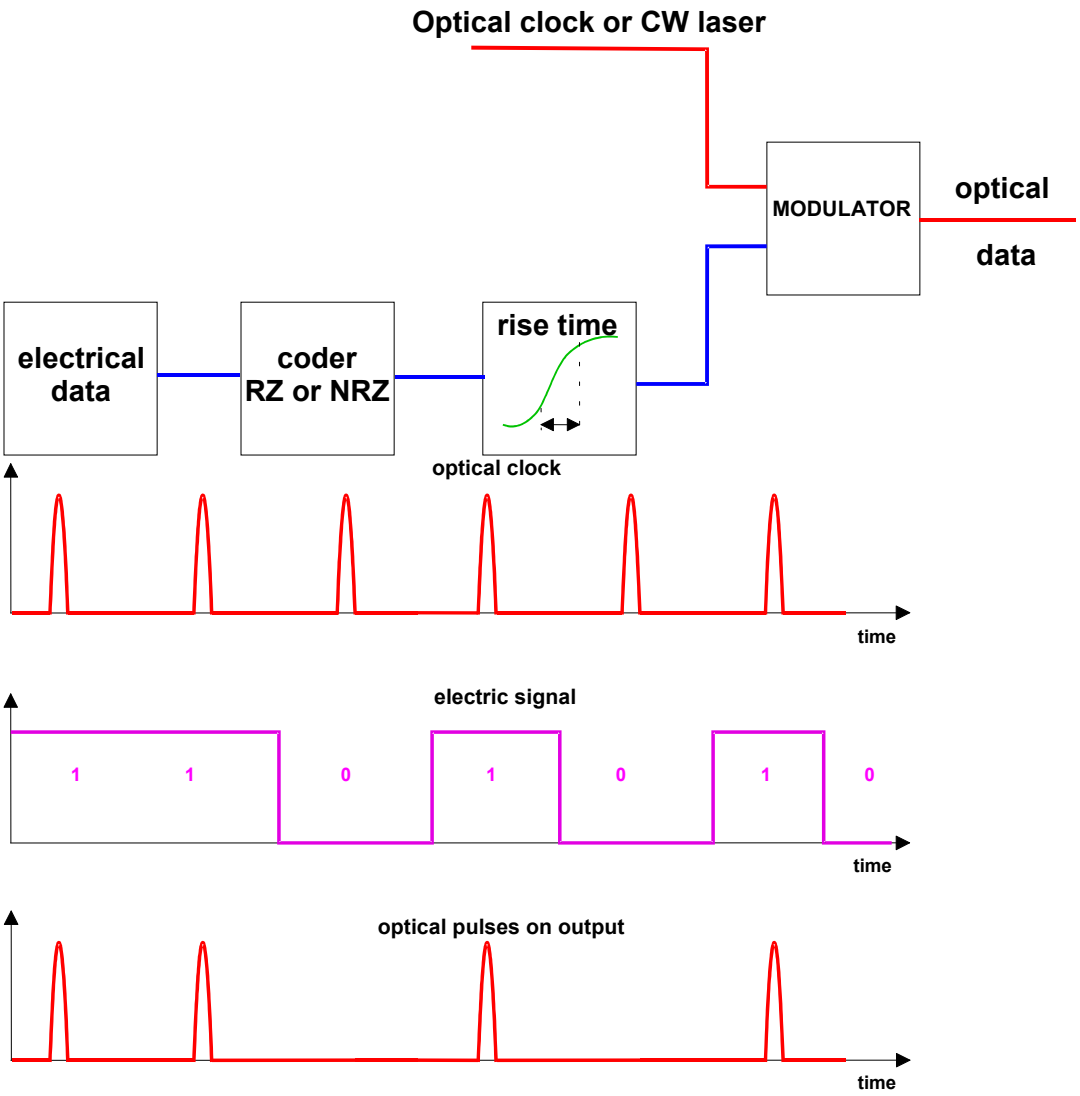

Figure 1. 2: representation and behavior of a data modulator.

Use of wavelength multiplexing enables higher capacity transmission. Several channels can be multiplexed in an optical fibre. All channels are equally spaced in the spectral domain by a parameter called the channel spacing and the efficiency of the multiplexing can be defined by the ratio:

$$\text{Spectral efficiency} = \frac{Channel\_bit\_rate}{Channel\_Spacing}$$

The line is composed of several spans, which are separated one from another by amplification sites. In a terrestrial transmission configuration, a span length is typically between 80 and 100 km.

The amplification site has two main functions. It is responsible for the amplification of the signal to compensate for the loss of inline fibre and dispersion compensating fibre. This amplification can be either lumped or distributed. Lumped amplification is implemented with erbium doped fibre amplifiers. Distributed amplification is obtained by using Raman effect in fibre.

The amplification site is also responsible for dispersion compensation as the chromatic dispersion of inline fibre broadens the pulse, and its width after transmission is not the same as at the emission. Dispersion compensating module is used in order for the pulse to recover its original width.

If noise is ignored, non-linear effects and polarisation effects in the fibre, we obtain the same optical pulses at the reception as at the emission when dispersion is fully compensated.

An optical add-drop site is used to extract some of the data in the entire amount of data transmitted by the optical signal or to insert some data to it. To drop data from an optical signal, the optical signal must be demultiplexed with an appropriate optical filter and converted in an electronic signal. In order to add some data, similar operations must be done in reverse order: electronic data is converted into optical data and multiplexed with other optical signals.

At the reception, the optical signal is first demultiplexed to separate different channels. It is then converted into an electric signal using a photodiode. An electric filter is used to reshape the electric signal.

In order to measure the quality of transmission, we define the bit error rate as the ratio of errored bits to the total number of bits. A good transmission quality is obtained if the bit error rate (BER) is lower than 10^{-9}. When using simulations, it is not possible to reach so low values of the as we generally work with a data sequence length lower than 1024 bits. As a consequence, it is obvious we have to estimate this quality of transmission. Thus, we can define the transmission quality factor depending the opening of the eye on an eye diagram. A bit error rate of 10^{-9} corresponds to a quality factor of 6.

The purpose of this study is to determine the maximum reach of a WDM system when increasing the bitrate to 160 Gbit/s per channel. Indeed, there are three main categories of effects that degrade the signal during the propagation in optical fibre. Firstly, the accumulation of noise due to amplification is limiting the quality of the transmission. Secondly, non-linear effects, which are due to the intensity dependence of the refraction index, degrade the quality of the optical signal. At last, statistical effects due to polarisation mode dispersion also affects the signal.

2 Brief review of optical telecommunications

In this chapter, I will give a brief summary of the history of optical telecommunications and see how it has become unavoidable nowadays. The aim is to answer this question: what were the developments of optical telecommunications up to now?

2.1 Historical background

Fibre optics telecommunication systems are nowadays the major component of terrestrial and submarine long distance networks. This is the result of intensive research and the situation is still in progress currently.

In years 1970 to 1980, communication networks were based on two key medias: the coaxial cable and radio systems (using electromagnetic wave). This double choice was motivated by the possibility of mutual help between cable and radio which are linked to different risks: for cable, an accidental breaking of the cable requires an intervention whereas an outage linked to the wave propagation for radio systems is intrinsically repaired automatically.

The apparition of the first optical transmission systems is the result of many years of research in order to achieve good quality of fibres (presenting attenuation compatible with the needs of a telecommunication network) and also high-performance components or devices (in particular laser sources) which must be reliable.

These important evolutions had a great impact in the first years of optical communications:

- The use of monomode fibre instead of multimode fibre. Monomode fibre is leading to more difficult problems in terms of connector industry but it offers a much bigger potential capacity and reach.
- The change of telecommunication window from 800 nm wavelength to 1300 nm wavelength and to 1550 nm, which presents a minimal attenuation.

First optical systems are installed during years of the 80s with a bitrate of a few Mbit/s to 560 Mbit/s. The capacity of these systems is comparable to capacity of coaxial cable systems but they present a key advantage, which is the distance between regenerators (typically around 70 km for terrestrial transmissions). The consequence is the diminution of the number of optical repeaters, which is a major issue for submarine transmission. The first transatlantic cable, TAT 8, is installed in 1988 and operates at 1300 nm wavelength. Its reach is 6740 km and its capacity is 280 Mbit/s per fibre. In 1991, TAT 9 is installed and operates at 1550 nm wavelength allowing transmission of 560 Mbit/s per fibre.

The introduction of the SONET standard (Synchronous Optical NETworks) is a decisive factor for the development of optical communication. It will lead to the introduction, outside the United States, of the SDH standard (Synchronous Digital Hierarchy).

In the beginning of 90s, first high capacity optical systems were born. They are characterised by a bitrate of 2,5 Gbit/s at 1550 nm with a repeater spacing of 90 km (either amplifier or OEO regenerator). From this period, optical systems present more capacity and much higher quality than radio systems. Between 1992 and 1996, optical transport networks will be built using standard fibre G.652 in France. Each fibre is equipped with a transmission system delivering 2,5 Gbit/s with a typical repeater spacing of 90 km. In 1993, the accumulate length of optical fibre in the communication network is around 170000 km in France.

The rapid expansion of worldwide networks is due to the development of the Web and of its online applications. This results in a need for increasing capacity in order to ensure data transmission. The technical context, essentially based on optical technologies, is full of hopes for this development as a major breakthrough occurs with the apparition of WDM transmission and new optical amplifiers.

2.2 Optical amplification: a technological breakthrough

Apparition and industrial development of optical amplifiers is responsible for the evolution of optical transmission systems at the end of the 1980s. Basically, these components use a power transfer mechanism from an optical power to the signal in an erbium-doped fibre. Their conception is relatively simple and they show good performances in terms of noise. They were first used to increase the transmission length of mono-channel systems by replacing electronics regenerators. In a second time, the idea was to associate this technology to wavelength division multiplexing (WDM) techniques. This way, the transmission media is used to propagate several channels and its cost becomes lower. Using WDM transmission, a unique optical amplifier will replace N regenerators in each site of the transmission line and enable a reduction of the cost proportional to the transmission length and to the number of channels. This was the beginning for the development of long reach optical WDM transmission systems (typically between 150 and 600 km). As any type of amplification, Raman and EDFA amplifications are producing noise, which degrades the quality of the optical signal.

2.3 Parameters of WDM systems

Systems are mainly characterised by three parameters. The first one is the transmission length, which influences the number of regeneration sites. As a matter of fact, the transmission length is generally limited by the amount of noise in reception and thus by the optical signal to noise

ratio (OSNR). Another limitation comes from the accumulation of propagation impairments such as non-linearities or dispersion due to polarization… Second parameter is the spacing between amplifiers, characterized by its length in km and its attenuation in dB. Reducing this spacing allows to increase the OSNR and finally the transmission length. For terrestrial systems, this spacing is typically between 80 and 120 km (with optical losses between 20 and 30 dB). For submarine transmissions, it can be reduced to 40 km (approximately 10 dB attenuation). The last one is the capacity of the system, which results from the choice of two parameters: the number of channels and the capacity of each of them. These key parameters are summarized in Figure 1. 3.

The driving force behind the innovation and the evolution of WDM systems is the reduction of the cost of the bit per second transmitted per km. The research for this aim is considering two directions. Firstly, the number of channels may be increased but the frequency window of optical amplifiers and/or non-linear impairments and filtering issues limit this goal. Secondly, the bitrate of each channel can be increased in order to reduce, for a given total bitrate, the number of channels and the cost for non-shared equipment (regenerators for example).

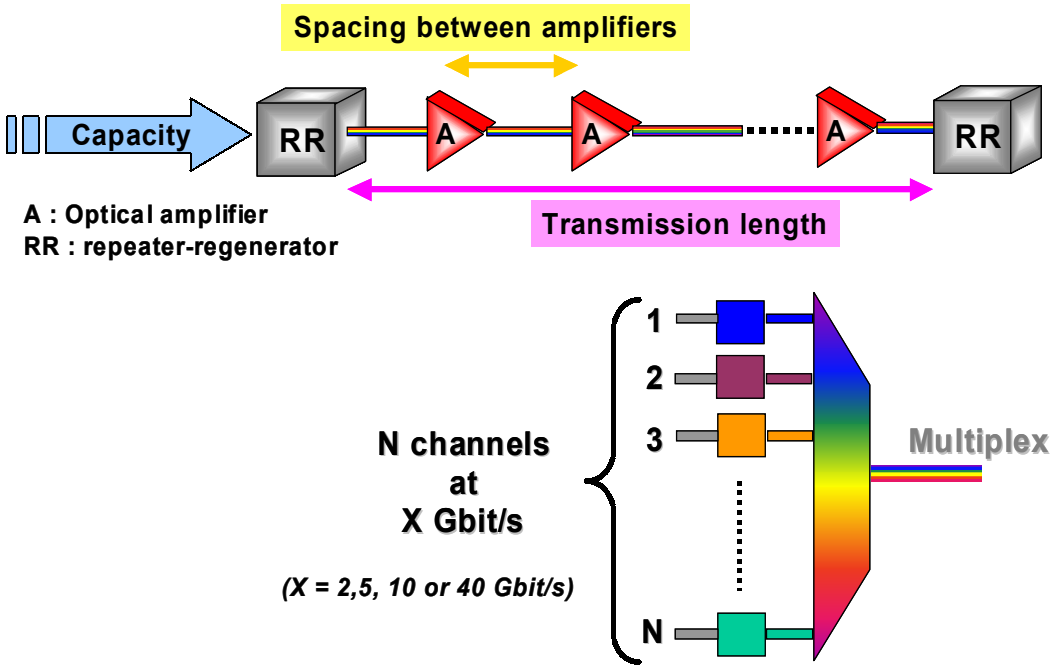

Figure 1. 3: parameters of a transmission link.

2.4 Why increasing the channel bitrate in WDM systems is unavoidable?

Strong restrictions are imposed to optical fibre infrastructure by WDM systems at 10 Gbit/s per channel and especially at 40 Gbit/s per channel when we achieve the same spectral efficiency than at 2,5 Gbit/s per channel. Last developments announce 40 Gbit/s systems with spectral efficiency of 0.4 bit/s/Hz with a channel spacing of 100 GHz. Thus, WDM systems can transmit the same total capacity of 1,6 Tbit/s with 40 channels at 40 Gbit/s or with 160 channels at 10 Gbit/s or with 640 channels at 2,5 Gbit/s. The diminution of channel spacing results in higher degradation due to cross non-linear effects, which is either caused by four wave mixing and crossed phase modulation.

On one hand, the technical viability of optical communication systems is based on improved multiplexing/demultiplexing techniques and also on improved laser sources, which results in a higher cost per channel. On the other hand, for a given spectral efficiency, crossed effects between channels are all the more important since the channel bitrate is low. The degradation is consequently higher at 2.5 Gbit/s than at 40 Gbit/s. The chromatic dispersion of the fibre is a key factor in the understanding of these effects as it influences the relative phase conditions between channels.

Increasing the channel bitrate is necessary for economic reasons. This is why currently, 10 Gbit/s systems are replacing 2,5 Gbit/s systems. Since the beginning of WDM systems, the evolution of spectral efficiency has been increasing linearly with a ratio of 60 % per year as can be seen on Figure 1. 4.

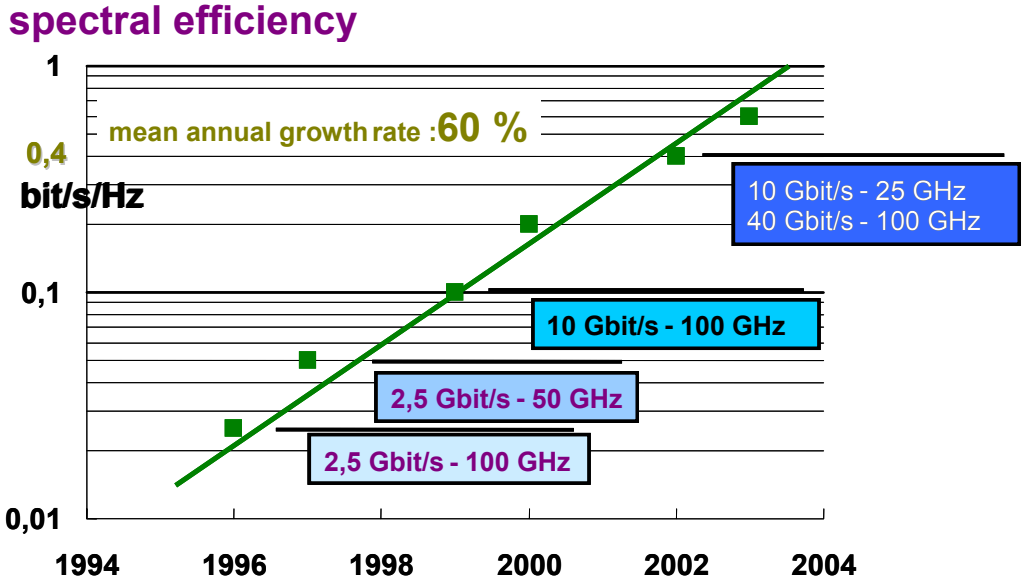

Figure 1. 4: increase of the spectral efficiciency.

In order to ensure the increase of channel bitrate, it is necessary to have all the basic electronic and opto-electronic components. This way, modulations and demodulations of optical waves can be realised. These devices were available in the early 90s at 2,5 Gbit/s bitrate but only in 1998 at 10 Gbit/s. At 40 Gbit/s, the first modules appeared in 2001.

Furthermore, transmitting with a higher capacity requires, for the same performance, a higher optical signal to noise ratio (6 dB higher for 4 times the bitrate). It is possible to obtain such a gain either by increasing the signal power (if non-linear impairments are kept under control) or by using binary error corrector codes.

At last, the sensibility to propagation defaults is increasing with the channel bitrate. This is the case for both the linear effects due to chromatic dispersion or polarisation dispersion of the fibre and non-linear effects essentially due to Kerr effect (refraction index of the fibre depending the optical intensity that propagates in the fibre).

The stake of the evolution is to choose the best engineering scenarios. The implementation and exploitation of these solutions should present as low complexity as possible.

The frequency band, which characterises erbium doped fibre amplifiers, is now extended to 40 nm (5 THz or 50 channels at 40 Gbit/s with a spectral efficiency of 0,4 bit/s/Hz). The main technological advances linked to equipments (except amplifiers) concern the selectivity of optical demultiplexing devices. The various techniques (thin films, diffractive grating, arrayed wave guide grating…) confirm the innovation in this field. We must also note the progress that has been done concerning the source performance in terms of stability.

Another way to raise the number of channels is to widen amplification band to others bands than traditional C band (1535-1560 nm) such as L band (1560-1610 nm) or S band (1500-1530 nm). The problem is then to amplify these channels or to compensate the accumulated dispersion in each site of the line: a demultiplexing is then necessary and adds additional losses as shown in Figure 1. 5.

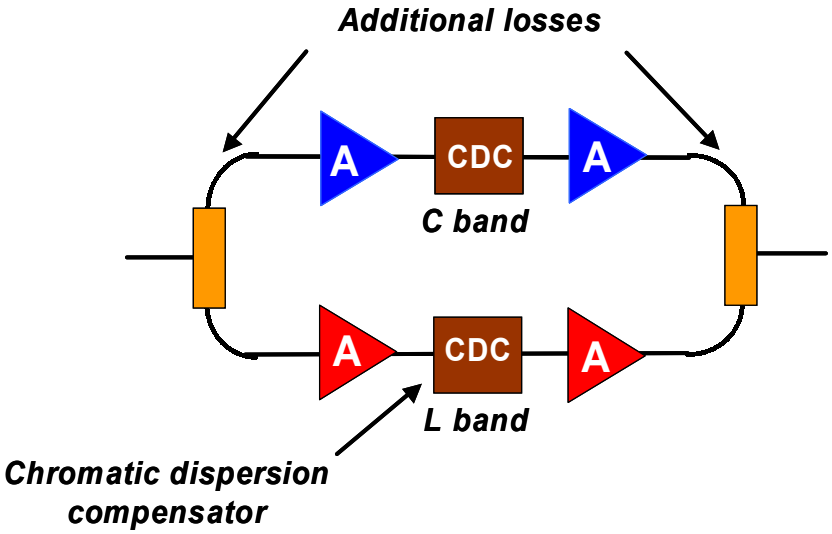

Figure 1. 5: demultiplexing and amplifying a multi-band WDM multiplex.

Final interest depends on the context of the need for such a capacity increase. Figure 1. 6 shows that, without requiring technological breakthrough, a maximal capacity of 5 Tbit/s can be achieved.

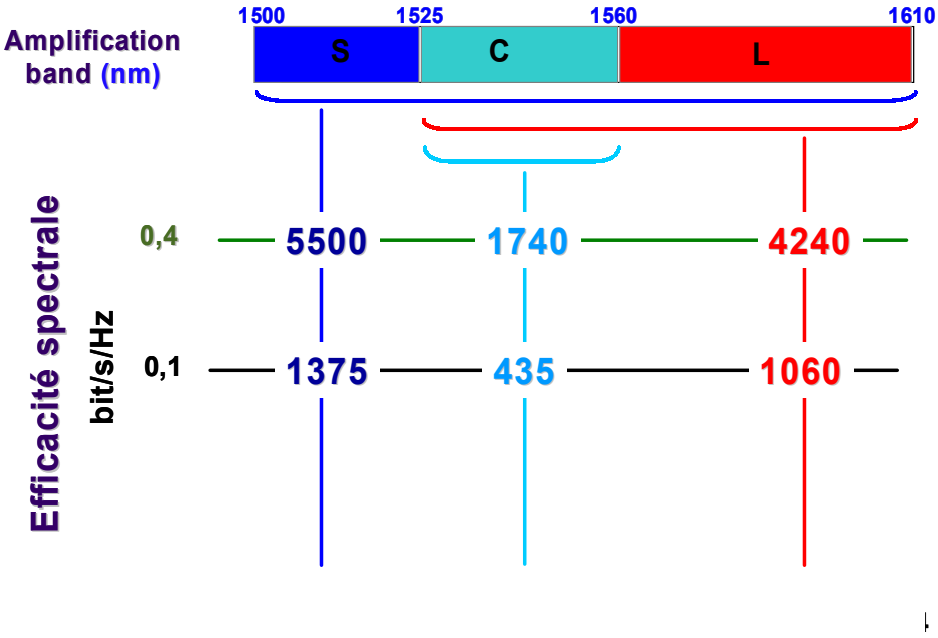

Figure 1. 6: capacity transmitted in telecommunication window.

The offer of equipment in WDM transmission is schemed in Figure 1. 7 where we distinguish commercially available systems, the systems announced with preliminary characteristics and also the R&D experimentations that are the base of a system development.

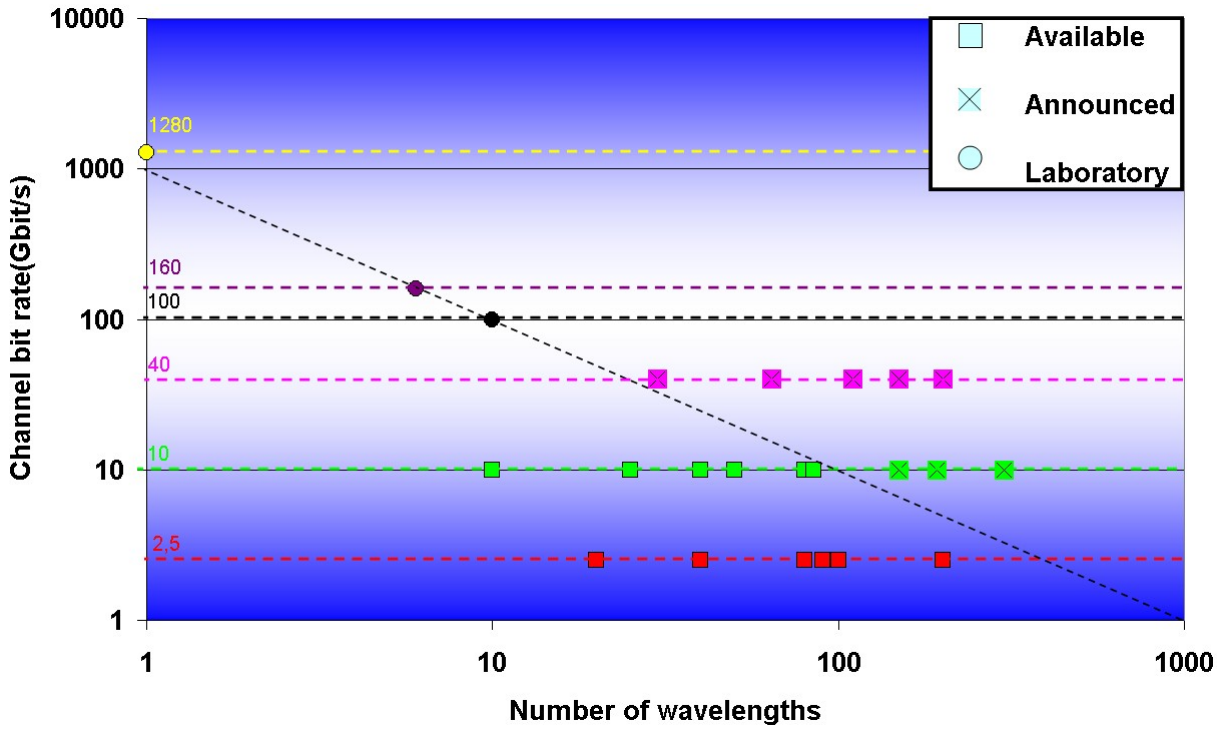

Figure 1. 7: offer of equipments in WDM transmission.

2.5 WDM system engineering

First generations of WDM systems based on 2,5 Gbit/s were typically propagating on 5 spans, each of them attenuating from 25 to 30 dB, and the total transmission length was around 500 km. Since, technological evolutions have enabled transmissions at 40 Gbit/s per channel on more than 1000 km. We will note two major progresses in this evolution: firstly, the error corrector coding techniques are powerful algorithm techniques encoded in the binary data that allow the detection and correction of errors. The gain [1] of a typical error correcting scheme is around 6 dB. Secondly, the Raman amplification consists in injecting an optical wave acting as a pump in the fibre. This optical wave is shifted by 110 nm from the optical signal. A power transfer occurs in the fibre due to Raman scattering but the conversion ratio is lower than in erbium-doped fibre and requires high power pumps. Raman amplification is used alone or in complement with erbium amplification. This type of amplification called distributed amplification is very interesting because it is characterised by a lower noise factor than erbium amplifiers. Another advantage of Raman amplification is that it enables the amplification of several channels in an entire band or in several bands.

Depending on their reach, systems are classified in 3 categories as shown in Table 1. 1:

System class	Long Haul (LH)	Very Long Haul (VLH)	Ultra Long Haul (ULH)
Reach (in km)	150 - 700	700 – 1500	1500 – 3000

Table 1. 1: Different classes of WDM systems.

A high constraint is due to the location of the amplification sites. As a matter of fact, it is not possible to reduce the distance between these amplification sites because it is not realistic to insert an amplification scheme between two locations. Otherwise, it would have been possible to increase the bit rate only by decreasing the span length.

3 Context of the bit rate increase with the help of wavelength multiplexing and channel bit rate increase up to 40 Gbit/s

As explained in the previous chapter, there were many progresses in electronics, opto-electronics, and fibre technologies. Recently, some experiments in laboratory have been possible thanks to these technologies. In this chapter, we briefly detail some of the evolutions that enable the realization of WDM systems at 40 Gbit/s.

A key factor for increasing the bitrate is compatibility with optical fibres. The constraints are stronger in terms of polarisation dispersion due to PMD (polarization mode dispersion). The most common fibre is referenced as G652 and named SSMF (for standard single mode fibre). It is characterised by a high chromatic dispersion of 17 ps/nm/km at 1550 nm. The following table summarizes the main fibres used in optical telecommunications and their physical characteristics.

Fibre type	Dispersion in ps/nm/km	Dispersion slope in ps/nm²/km	Effective area in µm²
SMF	17	0,08	80
DCF	-90	-0,45	20
LEAF	4,2	0,085	72
Truewave	4,5	0,045	50
Teralight	8	0,057	65

Table 1. 2: characteristics of main telecommunication fibres.

All the propagation problems occurring for WDM systems at 10 Gbit/s per channel will be reinforced at 40 Gbit/s and exacerbated at 160 Gbit/s. Tolerance for cumulated dispersion is around 1000 ps/nm at 10 Gbit/s (which is the equivalent of 60 km of G652 fibre) but it is only 60 ps/nm at 40 Gbit/s (only 4 km of G652 fibre). Inline fibre dispersion is generally compensated by dispersion compensation fibre (DCF). Several sorts of DCF exist in order to match the slope of the different inline fibres. The attenuation of these dispersion compensation fibres is higher than the one of inline fibre. At 1550 nm, the signal attenuation is typically 0,6 dB/km for DCF and 0,2 dB/km for whatever inline fibre type. We note the recent development of higher order mode (HOM) modules with lower losses. These devices currently compensate for all the second and third order chromatic dispersion of any fibre.

This requirement for higher precision concerning chromatic dispersion is also the reason of the introduction of automatic dispersion compensation devices. The realization of a chromatic dispersion compensator with the possibility to adjust the dispersion slope for C and L band (from 1525 to 1610 nn) has been achieved in 2002. Teraxion has also designed some components using Bragg gratings in fiber and achieving adjustable dispersion compensation on several channels from -300 to -2700 ps/nm.

Another aspect of the deformations induced by fibre is statistic and concerns the polarisation mode dispersion. Generally, a limit of 15% of the time bit is required for polarisation mode dispersion effect. For example, if the bit rate is set to 10 Gbit/s and the fibre PMD value is 0,1, the maximum transmission distance is:

$$L = \left(\frac{T_b \times 15\%}{PMD_{fibre}} \right)^2 = \left(\frac{100.0{,}15}{0{,}1} \right)^2 = 22500\,\text{km}$$

Table 1. 3 gives the limitations of typical transmission reach as a function of mean PMD value of inline fibre and for different bitrates.

	G652A (ITU recommandation)	G652D (ITU recommandation)	Good fibre in laboratory	Fibre in field
PMD(in $ps/\sqrt{km}$)	0,5	0,2	0,04	0,08
10 Gbit/s	900 km	5625 km	140000 km	35000 km
40 Gbit/s	56 km	350 km	8800 km	2200 km
160 Gbit/s	3 km	22 km	550 km	140 km

Table 1. 3: theoretical limitations to polarisation mode dispersion for different bitrates and fibres

Indeed, the tolerance to PMD is one of the critical points for the deployment of 40 Gbit/s WDM systems. Polarisation mode dispersion effect introduces a propagation delay between the two principal axes of polarisation. This PMD can reach 2 ps/$\sqrt{km}$ for some critical sections of deployed fibre. It means that propagation in 25 km of such a fibre is responsible for a mean differential group delay of 10 ps, which is nearly the half of the bit duration at 40 Gbit/s.

At last, spectral width associated to high bitrate optical signals (such as 40 Gbit/s and 160 Gbit/s) is high and increases the impact of intrachannel non-linear effects. In order to lower the degradations of these effects, the signal power should be reduced but it is not easy since a gain of 6 dB is necessary to ensure the same level of optical signal to noise ratio when increasing the bitrate by 4.

Beyond 40 Gbit/s per channel, WDM systems are a real challenge. First experimentations in laboratory at 160 Gbit/s per channel are being developed and even beyond this bitrate (1,28 Tbit/s on one channel propagating on some tens kilometres). The very first difficulties are linked to the generation of an optical pulse sequence. As a matter of fact, electronic circuits are not operating currently at bitrates higher than 40 Gbit/s. Very last developments have enabled the production of high performance electro-absorption modulators and lithium niobate modulators, which have been shown in ECOC 2001 exposition by Corning or JDS Uniphase [2]. The lithium niobate technology is not the only one at this bitrate: in february 2002, Oki announced the development of electro-absorption modulators based on GaInAsP technology. Compared to lithium niobate, these modulators require a lower control voltage but produce more chirp [3], which is not good for long distance transmission.

Concerning lasers, Mitsubishi has developed a DFB laser in September 2002: it is characterized by a high emission power (60 mW) and a high suppression mode ratio (40 dB).

As a consequence, electric multiplexing is possible at 40 Gbit/s but optical multiplexing is at the moment the only way to achieve a transmitter at 160 Gbit/s. The principle of a transmitter and receiver at 160 Gbit/s is shown on Figure 1. 8.

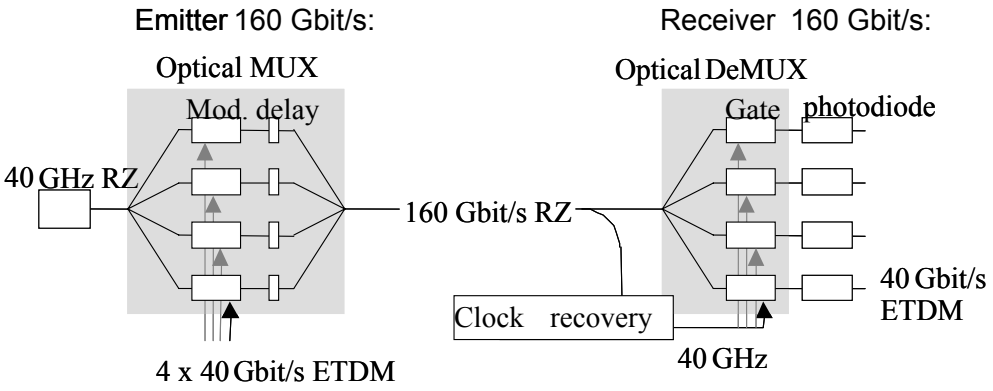

Figure 1. 8: scheme of emitter and receiver based on optical multiplexing.

On the receiver site, it is necessary to use photodiodes operating at 40 Gbit/s. VSK Photonics has developed such components in april 2002 [4]. Most of the detectors are based on photodiodes where photons are absorbed by a semiconductor adapted to the wavelength and give rise to electrical depending on light flood.

In order to increase the capacity transmitted in an optical fibre, the solution used in last decade was to use wavelength division multiplexing. As a consequence, the number of 2.5 Gbit/s channels rised from 4 to 40 and even 80. From there, there was no more spectrum in the conventional C-band of erbium doped fiber amplifiers (1530-1565 nm) and this is why increasing the bitrate became the main driver of WDM developments. This also enabled to increase spectral efficiency and to reduce transmission costs.

The problem is that while increasing the bitrate to 40 Gbit/s and beyond, the tolerance margin is also reduced in terms of polarisation mode dispersion or chromatic dispersion. In order to extend transmission reaches at 40 Gbit/s with the same quality, dynamic functions may be necessary.

These adaptive devices already exist for PMD compensation. Currently, this transformation is operated channel by channel and requires demultiplexing wavelengths, which introduces a greater cost. The aim for the future is to develop functions that are processing the whole WDM multiplex. Lucent [5] has recently shown that PMD compensation for all channels is possible using one of the following schemes:

- Demultiplexing and process similar actions for several channels with an ultra-fast switcher.
- Compensators connected in series with an adjustable delay (DGD).
- Compensators connected in series with a fixed delay.

Dynamic functions also exist in order to flatten the gain at the output of optical amplifiers so that all channels approximately have the same power. Such features are used by Onetta in their optical amplifiers and have been shown in November 2001 within an application for ultra long haul transmission. Lightconnect has also developped in 2002 some components based on MEMS technology in order to achieve dynamic equalization of optical powers. Corning has also developed products since 2000 for dynamic equalization: it uses liquid crystal as “wavelength blockers” enabling the extinction in a range of 20 dB.

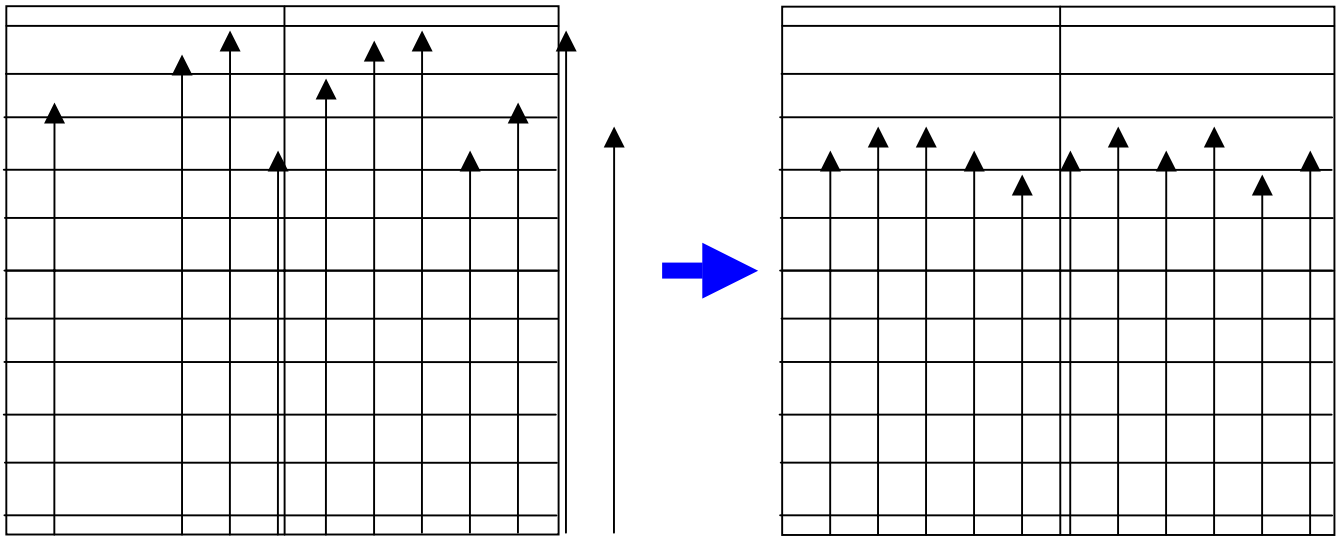

Figure 1. 9: principle of a gain equalizer.

An important function for optical communication is regeneration. Alcatel has demonstrated all optical regeneration based on saturable absorber at 40 Gbit/s in March 2002. Transmission distance could be increased from 1300 km to 7600 km for a unique wavelength and to 2200 km using WDM transmission of 5 channels with 200 GHz channel spacing [6].

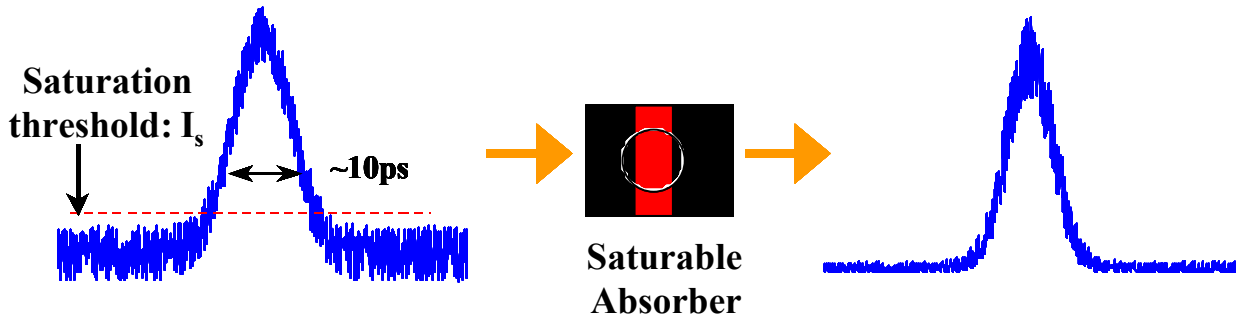

Figure 1. 10: principle of a saturable absorber.

I now report some system demonstrations at 40 Gbit/s in terrestrial configuration on Table 1. 4. These experimentations are remarkable because they use some key technologies (such as multi-level phase-shift keying modulations, Raman amplification, FEC correction, higher-order-mode dispersion compensation…) for capacity increased transmissions that will be useful at 160 Gbit/s per channel.

Ref.	Fibre	Channels number	Spectral efficiency (in bit/s/Hz)	Propagation distance (in km)	Modulation format	Use of Raman amplification	Use of FEC
7	NZDSF	8	1,6	320	CSRZ-DQPSK	No	No
8	NZDSF	1	-	2000	RZ-AMI	Yes	Desirable
9	SLA-IDF	40	0,8	2000	CSRZ	Yes	Yes
10	SMF	4	2	400	RZ-DQPSK	No	Desirable
11	SMF	128	0,8	1280	CSRZ	Yes	Desirable
12	SMF	43	0,4	1600	NRZ	Yes	Desirable
13	SMF	1	-	1980	9 different modulation formats	Yes	depends on the modulation format
14	Teralight	80	0,8	300	PSB	Yes	No
15	Teralight	125	0,64	1200	NRZ	Yes	Desirable
16	Teralight	256	?	100	?	Yes	Yes
17	Truewave	160	0,8	3200	CSRZ-DPSK	Yes	Desirable
18	Truewave Reach	89	0,4	4000	CSRZ-DPSK	Yes	Desirable
19	Truewave-RS	25	0,8	1600	DPSK	Yes	No
20	Truewave-RS	64	transmission of 10 and 40 Gbit/s data	2500	RZ-DPSK	Yes	Desirable

21	Truewave-RS	1	-	1700	RZ	Yes	No
22	Truewave-RS	64	0,4	4000	RZ-DPSK	Yes	Desirable

Table 1. 4: demonstrations of 40 Gbit/s WDM terrestrial transmissions using new technologies.

We remark the use of mainly 3 fibres, which is TrueWave Rs, Teralight and single mode fibre. It is also very interesting to note that nearly almost all of these demonstrations are using hybrid amplification in order to reduce the amount of noise and the impact of non-linear effects. It is also noticeable that the use of a particular modulation format lowers the degradation of the signal. On Figure 1. 11, we represent these experiments indicating the number of channels versus the propagation distance. We also indicate the inline fibre type and some of these key technologies

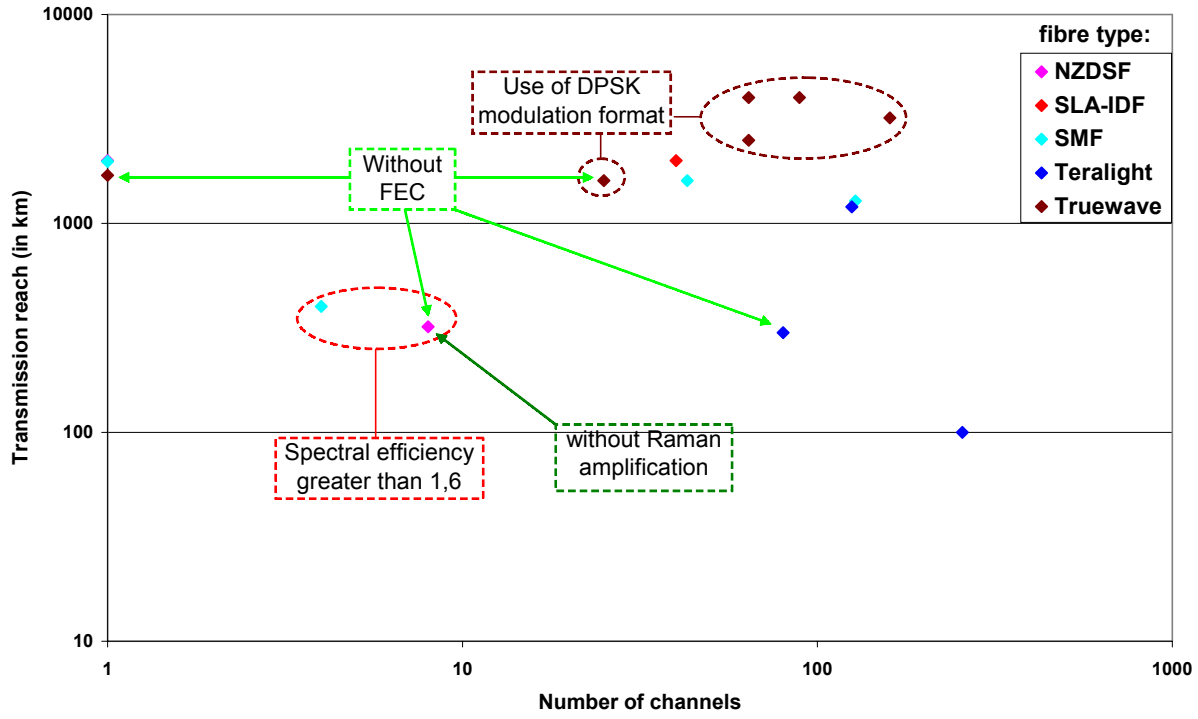

Figure 1. 11: some 40 Gbit/s experiments using key technologies.

I now report a state of the art of system demonstrations [23-46] at 160 bit/s with a terrestrial scenario on Table 1. 5.

Ref.	Number of channels	Fibre type	Dispersion @ data wavelength in ps/nm/km	Modulation format	Spectral efficiency in bit/s/Hz	amplification	Channel power in dBm	Length(in km) and number of spans	FEC
23	1	TW-RS	4,5	RZ		Erbium	10,5	1x120	No
24	1	SMF	16	RZ		Erbium	11,5	1x160	No
25	1	Teralight	8	RZ		Erbium	12,5	2x100	No
26	4	Teralight (and RTL)	8	RZ	0,4	Erbium	7	3x80	No
27	8	Teralight	8	CSRZ	0,53	Erbium	6	1x85	No
28	6	TW	5,9	RZ	0,53	Raman	2,5	4x100	No
29	1	SMF	17	RZ		Erbium	4	6x80	No
30	6	TW-RS	4,5	RZ	0,53	Erbium		1x80	No
31	1	SMF	16	CSRZ		Erbium	9	3x100	No

32	1	SMF	17	CSRZ		Hybrid		12x100	Yes
32	7	SMF	17	CSRZ	0,53	Hybrid		6x100	Yes
33	1	SMF et SLA/IDF	17 et 20/-40	RZ-DPSK		Erbium	10	110;3x80;60	No
34	8	SMF	17	RZ	0,4	Erbium	14	1x140	No
35	1	TW	4,5	CSRZ		Erbium	10	1x40	No
36	1	SMF	17	RZ-CSRZ		Hybrid	1	8x80	No
37	1	SMF	17	RZ		Erbium	3 to 8	3x80	No
37	1	SLA-IDF	20/-40	RZ		Erbium	6 to 12	3x80	No
38	1	DSF	0	RZ		Erbium		1x140	No
39	19	DSF	Slightly positive	RZ	0,33	Erbium	7,5	1x40	No
40	1	SMF	17	RZ		Raman	-4	80-44-50	No
41	1	SMF	17	RZ		Erbium		2x54	No
42	4	NZDSF	4	CSRZ	0,4	Erbium	5	3x75	No
43	1	SMF	17	RZ		Erbium		3x54	No
44	1	SMF	17	RZ		Erbium		4x70	No
45	6	TW-RS	4,5	RZ-DPSK	0,53	Hybrid	3	20x100	Yes
46	1	SMF	17	RZ		Hybrid	5	2x60	No

Table 1. 5: state of the art of 160 Gbit/s WDM terrestrial transmissions

These experimentations are represented on the following figure where we focus on the main characteristics in order to compare them.

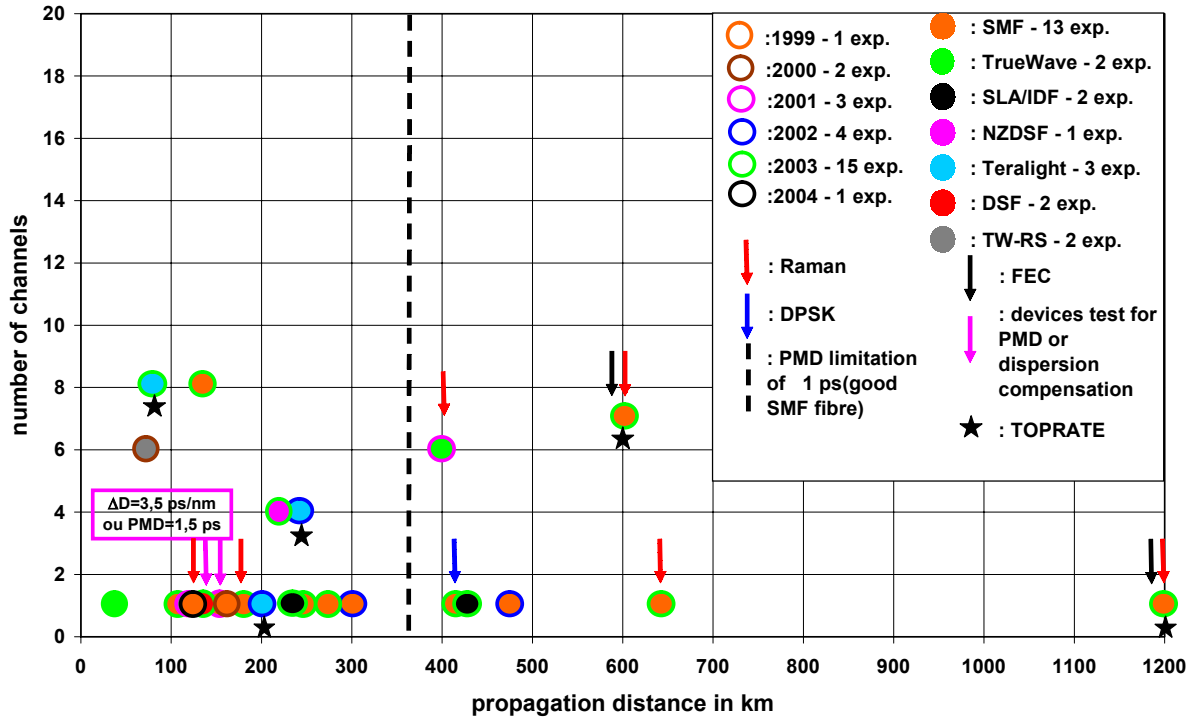

Figure 1. 12: main 160 Gbit/s experiments.

We can first outline that these demonstrations of 160 Gbit/s per channel transmission have covered a wide range of exploration since 1999. As a matter of fact, such high bit rate transmission has

been investigated with almost every fibre type with inline fibre dispersion from 0 to 20 ps/nm and effective areas from 50 to 107 μm². We also remark that different modulation formats have been investigated such as RZ, CSRZ and RZ-DPSK in order to reduce the amount of non-linear effects. Despite this diversity, we remark the preponderance of SMF in the choice for such high bit rate transmissions probably because of its high dispersion and effective area, which reduces non linear effects. We also observe that, in order to obtain a good signal quality, devices for PMD or dispersion compensation and FEC have been used. At last, Raman/hybrid amplification seems unavoidable for transmission reaches greater than 600 km. As a matter of fact, transmission over these distances requires

4 Conclusion

In this chapter, I have summarized the main aspects of the evolution of optical communication since its beginning. We have seen that this evolution has been possible because of progress made in opto-electronic technologies and in particular concerning the performance and reliability of laser sources, the introduction of wavelength division multiplexing and error-correcting code. These developments have enabled the increase of global capacity of the transmission. We have also presented and compared various experiments at 40 Gbit/s and we realize the importance of some transmission parameters such as inline fibre, amplification type, modulation format, dynamic functions...

5 References

1. "Coding gain of basic FEC block-codes in the presence of ASE noise", Faraj P. et al, Transparent Optical Networks, 2003. Proceedings of 2003 5th International Conference on , Volume: 2 , 29 June-3 July 2003, Pages:80 - 83 vol.2
2. "Lithium niobate modulators for 10 Gb/s and beyond", Hallemeier P., Lasers and Electro-Optics Society 1999 12th Annual Meeting. LEOS '99. IEEE , Volume: 2 , 8-11 Nov. 1999, Pages:713 - 714 vol.2
3. Press release: http://www.oki.com/en/press/ov/2002/0202.html#21-1
4. Press release: http://www.vskphotonics.com/about/pr_041602.html
5. "Analysis of multichannel PMD mitigation strategies based on worst channel equalization.", Moller, L.; Sinsky, J.H.;Optical Communication, 2001. ECOC '01. Volume: 2 , 30 Sept.-4 Oct. 2001, Pages:212 - 213 vol.2
6. OFC 2002, PostDeadLine, FD11.
7. "1,6 bit/s/Hz orthogonally polarized CSRZ-DQPSK transmission of 8x40 Gbit/s over 320 km NDSF", Y. Zhu et al, Optical Fiber Communication 2004, Los Angeles, USA, Paper TuF1
8. "40-Gb/s return-to-zero alternate-mark-inversion (RZ-AMI) transmission over 2000 km", Winzer, P.J. et al, Photonics Technology Letters, IEEE , Volume: 15 , Issue: 5 , May 2003, Pages:766 - 768
9. "1,6 Tbit/s (40 x 42,7 Gbit/s) transmission over 2000 km of fiber with 100-km dispersion-managed spans", B. Zhu et al, European conference on optical communication 2001, Amsterdam, Netherlands.
10. "Investigation of 2-b/s/Hz 40-gb/s DWDM transmission over 4/spl times/100 km SMF-28 fiber using RZ-DQPSK and polarization multiplexing", Cho, P.S. et al, Photonics Technology Letters, Volume: 16 , Issue: 2 , Feb. 2004, Pages:656 - 658
11. "Ultra-high-capacity long-haul 40-Gb/s WDM transmission with 0.8-b/s/Hz spectral efficiency by means of strong optical filtering", Agarwal, A. et al, Photonics Technology Letters, IEEE , Volume: 15 , Issue: 3 , March 2003, Pages:470 - 472
12. "43-Gbit/s x 40 ch transmission over 1,600 km of conventional single-mode fiber in NRZ modulation scheme", Nakamura, K., Optical Fiber Communications Conference, 2003. OFC 2003 , 23-28 March 2003, Pages:745 - 746
13. "Comparison of modulation formats for 42.7-gb/s single-channel transmission through 1980 km of SSMF", Gnauck, A.H. et al, Photonics Technology Letters, IEEE ,Volume: 16 , Issue: 3 , March 2004, Pages:909 - 911
14. "3,2 Tbit/s (80 x 40 Gbit/s) C-band transmission over 3 x 100 km with 0,8 bit/s/Hz efficiency", H. Bissessur et al, European conference on Optical communication 2001, Amsterdam, Netherlands
15. "Transmission of 125 WDM channels at 42,7 Gbit/s (5 Tbit/s capacity) over 12x100 km of Teralight Ultra fibre", S. Bigo et al, European conference on optical communication 2001, Amsterdam, Netherlands
16. Press release by Alcatel on 21st March 2001
17. "High spectral density long-haul 40-Gb/s transmission using CSRZ-DPSK format", Zhu, B. et al, Journal of Lightwave Technology, Volume: 22 , Issue: 1 , Jan. 2004, Pages:208 - 214
18. "72-nm continuous single-band transmission of 3,56 Tbit/s (89x42,7 Gbit/s) over 4000 km of NDF fiber", B. Zhu et al, European conference on optical communication 2003, Rimini, Italy, Paper TU462
19. "25 x 40-Gb/s copolarized DPSK transmission over 12 x 100-km NZDF with 50-GHz channel spacing", Gnauck, A.H. et al, Photonics Technology Letters, IEEE , Volume: 15 , Issue: 3 , March 2003, Pages:467 - 469
20. "Ultralong-haul transmission of 40-Gb/s RZ-DPSK in a 10/40 G hybrid system over 2500 km of NZ-DSF", Agarwal, A. et al, Photonics Technology Letters, IEEE , Volume: 15 , Issue: 12 , Dec. 2003, Pages:1779 - 1781

21. "1700 km transmission at 40 Gbit/s with 100 km amplifier spacing enabled by higher-order-mode dispersion compensation", Ramachandran, S. et al, Electronics Letters , Volume: 37 , Issue: 22 , 25 Oct 2001, Pages:1352 - 1354
22. "2,5 Tb/s (64 x 42.7 Gb/s) transmission over 40 x 100 km NZDSF using RZ-DPSK format and all-Raman-amplified spans", Gnauck, A.H. et al, Optical Fiber Communication Conference and Exhibit, 2002. OFC 2002 , 17-22 March 2002, Pages:FC2-1 - FC2-3
23. "160 Gbit/s demultiplexer with clock recovery using SOA-based interferometric switches and its application to 120 km fiber transmission", Yamamoto, T. et al, 27th European Conference on Optical Communication 2001, Volume: 2 , 30 Sept. 2001; Pages: 192 -193 vol.2
24. "Unrepeatered 160 Gbit/s RZ single-channel transmission over 160 km of standard fibre at 1.55 μm with hybrid MZI optical demultiplexer", Ludwig, R. et al, Electronics Letters, Volume: 36 Issue: 16 , 3 Aug. 2000, pages 1405 -1406
25. "Advanced 160 Gbit/s OTDM system based on wavelength transparent 4x40 Gbit/s ETDM transmitters and receivers", E. Lach et al, Optical Fiber Communication Conference and Exhibit 2002, Paper TuA2.
26. "4x160 Gbit/s DWDM / OTDM transmission over 3x80 km TeraLight™-Reverse TeraLight™ fibre", Schuh K. et al, Proceedings European Conference on Optical Communication 2002, Copenhagen, Paper 2.1.2.
27. "8x160 Gbit/s (1.28 Tbit/s) DWDM transmission with 0.53 bit/s/Hz spectral efficiency using single EA-modulator based RZ pulse source and demux", M. Schmidt et al, European Conference on Optical Communication 2003.
28. "High spectral efficiency (0.53 bit/s/Hz) WDM transmission of 160 Gb/s per wavelength over 400 km of fiber", Mikkelsen, B. et al, Optical Fiber Communication Conference and Exhibit 2001, 17-22 March 2001, Pages: ThF2 -T1-3 vol.4
29. "Single channel 160 GB/s OTDM propagation over 480 km of standard fiber using a 40 GHz semiconductor mode-locked laser pulse source"; Augier J.-L. et al, Optical Fiber Communication Conference and Exhibit, 2002, 17-22 March 2002, Pages: 4 –5
30. "160 Gb/s TDM transmission systems", B. Mikkelsen et al, European Conference on Optical Communication 2000, Munich, Sept. 3-7 2000, Paper 6.1.1
31. "Single Channel 160 Gbit/s (40 Gbit/s x 4) 300 km - Transmission Using EA Modulator based - OTDM Module and 40 GHz External - Cavity Mode-locked", LD Murai et al, Electric Industry Co., Ltd., Japan., NEC Corporation, Japan, European Conference on Optical Communication 2002, Paper 2.1.4.
32. "7x170 Gbit/s (160 Gbit/s + FEC overhead) DWDM transmission with 0,53 bit/s/hz spectral efficiency over long haul distance of standard SMF", E. Lach et al, Proc. European Conference on Optical Communication 2003, Rimini, Sept. 22-25, 2003, PD Th 4.3.5.
33. "Comparison of DPSK and OOK modulation format in a 160 Gb/s transmission system", S. Ferber et al, Proc. European Conference on Optical Communication 2003, Rimini, Sept. 22-25, 2003, page(s): 1004-1005.
34. "8x160 Gbit/s(1,28 Tbit/s) DWDM/OTDM unreapeatered transmission over 140 km standard fiber by semiconductor-based devices", A. Suzuki et al., Proc. European Conference on Optical Communication 2003, Rimini, Sept. 22-25 2003, Mo 3.6.1
35. "Generation of 160 Gbit/s Carrier-Suppressed Return-to-Zero Signals", L. Möller et al, Proc. European Conference on Optical Communication 2003, Rimini, Sept. 22-25 2003, Mo 3.6.3
36. "Single Channel 160 Gbit/s Carrier-Suppressed RZ Transmission over 640 km with EA modulator based OTDM module", H. Murai et al, Proc. European Conference on Optical Communication 2003, Rimini, Sept. 22-25 2003, Mo 3.6.4
37. '160 Gbit/s Transmission over dispersion-managed fibre set", J. Berger et al., Proc. European Conference on Optical Communication 2003, Rimini, Sept. 22-25 2003, Mo 3.6.6
38. "160 Gbit/s adaptive dispersion equalizer using a chirp monitor with a balanced dispersion configuration", T. Inui et al, Proc. European Conference on Optical Communication 2003, Rimini, Sept. 22-25 2003, Tu 3.6.3
39. "3 Tbit/s (160 Gbit/s×19 ch) OTDM/WDM transmission experiment", Kawanishi S. et al, Optical Fiber Communication Conference 1999.

40. "Experimental characterization of distributed Raman amplification in a standard single mode fibre based 160 Gbit/s transmission system", Z. Xu et al, Proc. European Conference on Optical Communication 2003, Rimini, Sept. 22-25 2003, Tu 4.7.2.
41. "160 Gbit/s RZ pulse generation based on fiber optical parametric amplification", T. Torounidis et al, Proc. European Conference on Optical Communication 2003, Rimini, Sept. 22-25 2003, We 1.6.3.
42. "160-Gb/s four WDM quasi-linear transmission over 225-km NZ-DSF with 75-km spacing", Daikoku M. et al, Photonics Technology Letters, Volume: 15, Issue: 8 , Aug. 2003, Page(s): 1165 - 1167.
43. "Long-Term 160 Gbit/s-TDM, RZ Transmission with automatic PMD compensation and System monitoring using an optical sampling system", H. Sunnerud et al, Proc. European Conference on Optical Communication 2001, P.D. M.1.9
44. "Siemens Claims 160-Gbit/s Milestone", Light Reading, http://www.lightreading.com/document.asp?doc_id=44067
45. "160-Gb/s OTDM Transmission Using Integrated All-Optical MUX/DEMUX With All-Channel Modulation and Demultiplexing", Ohara, T. et al, Photonics Technology Letters, IEEE , Volume: 16 , Issue: 2 , Feb. 2004.
46. "160 Gbit/s transmission over 116 km field-installed fibre using 160 Gbit/s OTDM and 40 Gbit/s ETDM", Feiste, U. et al, Electronics Letters , Volume: 37 , Issue: 7 , 29 March 2001. Pages:443 – 445.

Problematics

State of the art

As we have seen in the previous chapters, two ways seem possible to increase the capacity of the transmission: it is needed either to increase the number of channels or to extend the bit rate per channel to 160 Gbit/s. The first solution seems the simpler as channel multiplexing is now a mature techonlogy but it also has some drawbacks: for example, the limitation of bandwidth in the optical amplifiers will restrain the total number of channels that it is possible to transmit in a WDM multiplex.

In march 2002, Tyco presented experimental results [47] of submarine transmission on 11000 km (with 256 channels at 10 Gbit/s) or on 6200 km (with 38 channels at 40 Gbit/s). Back to terrestrial transmission, Bell Labs obtained a transmission [48] over 40 spans of 100 km using Raman amplification only. The modulation format was RZ-DPSK (Return-to-zero Differential Phase Shift Keying). The channels were distributed from 1555 to 1607 nm using a channel spacing of 100 GHz. We understand from this result that the choice of modulation format is a key point at high bit rate.

In September 2002, Mintera announced the record transmission [49] of 40 channels at 40 Gbit/s each over 5200 km (with a channel spacing of 100 GHz)) without optical regeneration but using forward error correction. Raman amplifiers have also been used in this transmission and the modulation format was CCS-RZ (Chirped Carrier Suppressed Return-to-zero). Same company announced later that using CSRZ-DPSK (Carrier Suppressed Return-to-zero Differential Phase Shift Keying), the transmission [50] was possible over 10000 km with the same span length. OFS had already presented a transmission of 160 channels at 40 Gbit/s each in march 2002. The transmission was made on 3200 km using Raman amplification with the same modulation format. At last, a capacity record of 10 Tbit/s was obtained by Alcatel with a transmission [51] of 256 channels on 300 km.

The idea of optical time division multiplexing was first introduced by Kensel and Denton [52] in 1967 but it's only twenty years after that the first experimentations were made using this concept: in 1988, Tucker[53] and Lord[54] achieved Gbit/s transmission. More recently, OTDM-based experimental transmissions have been shown over some hundreds kilometres [55, 56, 57, 58].

1 Basics of optical time division multiplexing

The basic principle of optical time division multiplexing is to introduce a delay on 2 or more optical lines so that the combination of these N signals at the bit rate B_o results in one signal at the bit rate $N \times B_o$. The following scheme illustrates this device:

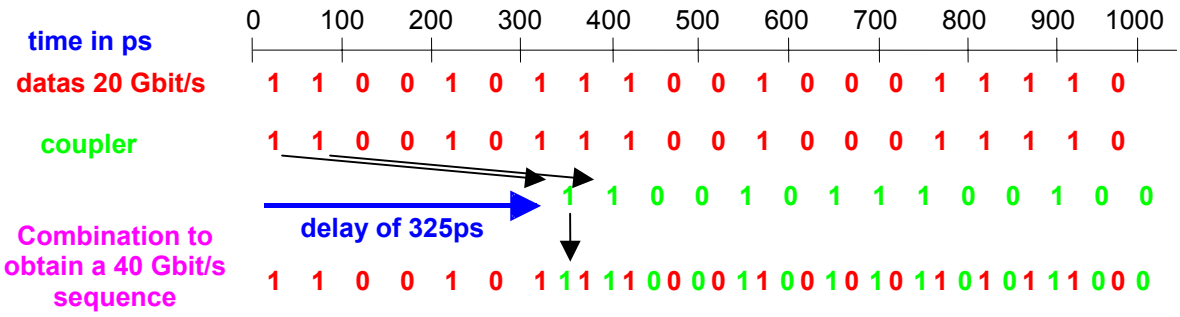

Figure 1. 13: illustration of the OTDM device (40 Gbit/s from 2 sequences at 20 Gbit/s bit rate)

From Figure 1. 13, we understand that a requirement for each pulse on the different optical time division multiplexing lines is to be short enough: in the previous example, even if the bit rate is 20 Gbit/s on each line, the pulse must be shorter than 25 ps which is the time bit at 40 Gbit/s bit rate.

2 Main issues of the study

As we have seen in the introduction, raising the bit rate is a source of constraints for engineering rules. The problem is to know if it is possible to realize optical transmission at 160 Gbit/s and what are the key points to achieve this transmission. I will also see what distance is reachable at this bit rate.

In order to answer to these questions, we will particularly be interested in transmission issues. Therefore, we will not mainly deal with how the OTDM emitter and receiver are built.

In the first part of this study, I will focus on noise impairments and study their influence at 160 Gbit/s bit rate. For this reason, I will first see what is the impact of noise on the quality of a transmission. I will study the relative importance of each noise on the receiver side and also see the importance of accumulated noise in the transmission. I will then be able to measure the impact of filtering and design some engineering rules linking noise and transmission distance.

In a second part, I will concentrate on linear and non-linear propagation effects. As an introduction to this part, I will present some of the methods I have used to simulate the propagation of optical pulses in a fibre. I will then define some immediate rules concerning the design of a transmission at 160 Gbit/s and also present some linked constraints. The study of non-linear effects will aim to identify the impact of each non-linear effect separately in order to measure its importance and to define a solution avoiding this impact. After this, I will be able to summarize the hot keys to present the optimization of linear and non-linear propagation effects.

In a third part, I will see how polarization effects impact the propagation of optical pulses at 160 Gbit/s bit rate. This study will try to define some engineering rules in order to directly measure the consequence of polarization effects in the transmission. I will then present some ideas for compensating these effects and see how they can be applied here.

Following this study of transmission effects, I will validate all these solutions with transmission simulations and see some different cases depending on the transmission distance.

Involvement in European project

The beginning of this study in October 2001 coincides with the beginning of a European project that deals with the same subject. Briefly, the aim of the project is to study and design the conception of OTDM-based emitter and receiver in order to realize a field transmission at 160 Gbit/s bit rate. Inside the project, the work has been separated into several work packages. My work is part of the first work package, which is in charge of the engineering rules for transmission. This collaboration within a European project is a real benefit as it has brought me some different views on the work I did and it has also pointed out some interesting facts for the evolution of the project.

3 References

47. "2.56 Tb/s (256/spl times/10 Gb/s) transmission over 11,000 km using hybrid Raman/EDFAs with 80 nm of continuous bandwidth", Foursa D.G. et al, Optical Fiber Communication Conference and Exhibit 2002, 17-22 March 2002, Pages:FC3-1 - FC3-3
48. "2.5 Tb/s (64/spl times/42.7 Gb/s) transmission over 40/spl times/100 km NZDSF using RZ-DPSK format and all-Raman-amplified spans", Gnauck A.H. et al, Optical Fiber Communication Conference and Exhibit, 2002., 17-22 March 2002, Pages:FC2-1 - FC2-3.
49. Press release: http://www.mintera.com/news/minteraworldrecord.html or Post Deadline paper at ECOC 2002.
50. "DWDM 40G transmission over trans-pacific distance (10 000 km) using CSRZ-DPSK, enhanced FEC, and all-Raman-amplified 100-km UltraWave fiber spans", Rasmussen C. et al, Journal of Lightwave Technology, Vol. 22 , N°1 , January 2004, pages:203 - 207.
51. "Multiplexage en longueur d'onde et en polarisation pour la transmission de données à 10 Tbit/s (256x40 Gbit/s) dur 3x100 km", Frignac Y. et al, Journées nationales de l'optique guidée 2002 (JNOG2002), Dijon.
52. "Multiplexing and demultiplexing techniques for an optical pulse code modulation (PCM) transmission system", Kinsel T. et al; Journal of Quantum Electronics, Vol. 3, N°6, June 1967, pages 251 –252.
53. "Optical time-division multiplexing for very high bit-rate transmission", Tucker R.S. et al, Journal of Lightwave Technology, Vol. 6, N°11 , November 1988, pages 1737 –1749.
54. "Optical multiplexing techniques for future Gbit/s transmission systems", Lord A. et al, Communications, 1988. ICC 88. Digital Technology - Spanning the Universe. Conference Record. IEEE International conference on , 12-15 Jun 1988, Page(s): 21 -25 vol.1.
55. "Single channel 160 GB/s OTDM propagation over 480 km of standard fiber using a 40 GHz semiconductor mode-locked laser pulse source", Auge J.-L. et al, Optical Fiber Communication Conference and Exhibit 2002, 17-22 March 2002, pages: 4 –5.
56. "Enabling transmission at 160 Gbit/s", Ludwig R. et al; Optical Fiber Communication Conference and Exhibit, 2002, 17-22 March 2002, pages: 1 –2.
57. "High spectral efficiency (0.53 bit/s/Hz) WDM transmission of 160 Gbit/s per wavelength over 400 km of fiber", Mikkelsen B. et al, Optical Fiber Communication Conference and Exhibit 2001, pages: ThF2 -T1-3 vol.4.
58. "Dispersion compensation schemes for 160 Gb/s TDM-transmission over SSMF and NZDSF", Konrad B. et al, 27th European Conference on Optical Communication 2001, Vol.2, pages 188 –189

Optical noise and power analysis

In this chapter, we focus our study on noise impairments and energetic considerations. After a brief summary of the scheme used in these studies, we express the different sources of noise and quantify each of them in order to derive some rules concerning transmission reach. Therefore, we introduce a certain number of formulas that have already been proved within certain conditions. Here is a summary of the assumptions that are made.

- **Spectral densities of noise (generally denoted N_B or N_{ASE}) are given per state of polarization.**
- **Optical noise powers and related definitions, for example optical signal to noise ratios, are calculated taking into account the two states of polarization.**
- The photons in the optical line will be governed by a Poisson distribution, whose mean value is <n>, the mean number of photons in a given section of the optical line, and variance is σ^2=<n>.
- The noise figure of an EDFA will be described assuming an input power high enough such that just after the amplifier, the number of photons representing the signal is largely greater than the number of photons produced by spontaneous emission.
- We will consider optical noise as uniformly distributed over a large bandwidth. This bandwidth is assumed to be greater than the optical bandwidth B_O of optical amplifiers so that the resulting noise bandwidth will be B_O.
- This distribution of noise is centered at the frequency ν_S=193.1 THz. We will assume all the photons to have the same energy $h.\nu_S$.
- This noise will also be equally distributed on the two polarizations.
- Some formulas express the average power as a function of other parameters. This average power assumes that "0" and "1" are equiprobable so that the average power is half the mean power for symbols "1".

1 The optical receiver

1.1 Introduction

An optical preamplifier followed by basic photo detection constitutes the receiver I will consider basically. The layout of the receiver is given below:

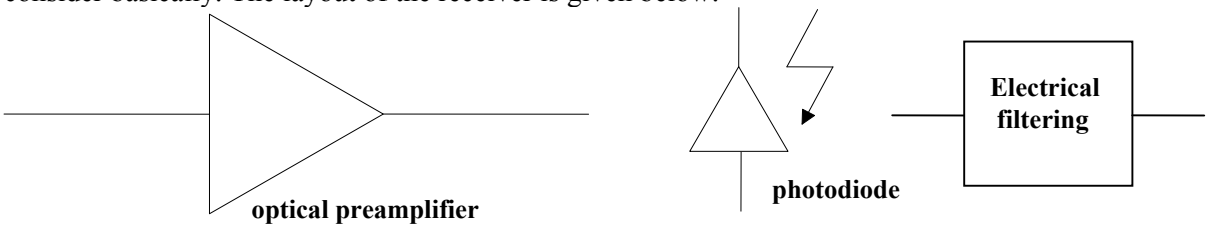

Figure 2. 1: scheme of the optical receiver.

The characteristics of the optical amplifier are the followings:

- The gain G.
- The optical bandwidth Bo.

- The equivalent input noise factor n_{eq} matches the spontaneous emission factor n_{sp} at high gain. In fact, we have the relation:

$$n_{eq} = \frac{n_{sp}(G-1)}{G}$$

so that the optical noise figure is defined by:

$$F_0 = \frac{1+2.n_{sp}(G-1)}{G} = \frac{1}{G} + 2.n_{eq}$$

Using this definition, the total amplified spontaneous emission spectral density per state of polarization is [1]: $N_{ASE} = h\nu.n_{eq}.G$ which is finite. The amplified spontaneous emission power is distributed over M modes where M is the number of ASE modes (M=2 with single-mode EDFAs if no polarizer is used between the EDFA and the detector). Consequently, the total noise power in the optical bandwidth B_0 is [1,2]:

$$P_{ASE} = M.N_{ASE}.B_0 = M.h\nu.G.n_{eq}.B_0$$

For the photodiode, we shall consider the quantum efficiency η. Electrical filtering is characterized by its electrical bandwidth Be.

Typically, the values we will consider for these parameters of the optical amplifier are the following:

- The gain G of the optical preamplifier will vary from 0 to 20 dB.
- The optical and electrical bandwidths will depend on the bit rate.
  For a 10 Gbit/s transmission, we will have:
  Bo = 20 GHz and Be = Bo/2 = 10 GHz

  Indeed, the minimum value for Bo is two times the bit rate whereas it is usual to set Be to 0.7 or 0.8 times the bit rate which is a compromise between signal-ase beat noise and intercrossing between symbols.
- The quantum efficiency η is also set to 1 considering a perfect conversion.

1.2 Definitions and quality factor

The goal of the photo receiver is to sample the signal at the decision time t_D and to make a decision concerning its value, as shown in Figure 2. 2.

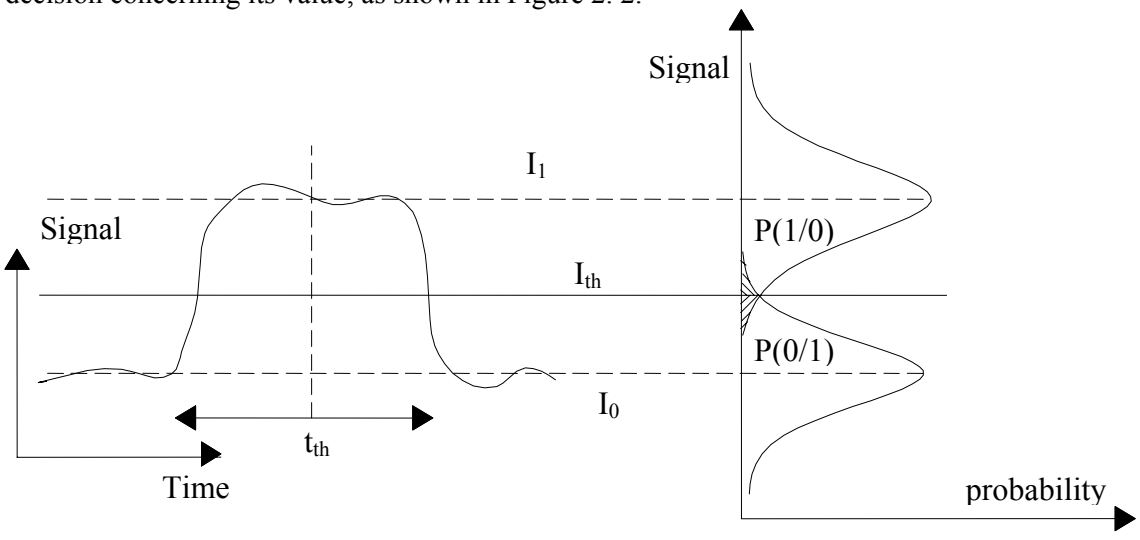

Figure 2. 2: electrical signal after photo detection and conditional gaussian densities of probability.

The decision circuit compares the received sampled value to the threshold value I_{th} and forces the bit value to '1' when $I>I_{th}$ and to '0' when $I<I_{th}$. An error occurs when $I> I_{th}$ whereas the value of the bit symbol is 0 and vice versa. We can define the error probability as:

$$\text{Error probability} = p(1) \times p(0 \mid 1) + p(0) \times p(1 \mid 0)$$

where p(1) and p(0) are the probability to transmit a symbol '1' and '0' respectively. p(0|1) and p(1|0) are the probability of incorrect identification. Assuming the same number of symbols 0 and 1, we have:

$$p(1) = p(0) = \frac{1}{2}$$

$$\text{Error probability} = \frac{1}{2} \times \left[p(0 \mid 1) + p(1 \mid 0) \right]$$

Assuming that the distribution of the different sources of noise is gaussian, we can deduce that the distribution of noise on symbols '1' and '0' is also gaussian and can be defined by their variances σ_1^2 and σ_0^2. It is then possible to define the conditional probabilities p(1|0) and p(0|1) [1]:

$$p(0|1) = \frac{1}{\sigma_1 \sqrt{2\pi}} \int_{-\infty}^{I_{th}} e^{-\frac{(I-I_1)^2}{2\sigma_1^2}} dI = \frac{1}{2} erfc\left(\frac{I_1 - I_{th}}{\sigma_1 \sqrt{2}} \right)$$

$$p(1|0) = \frac{1}{\sigma_0 \sqrt{2\pi}} \int_{I_{th}}^{+\infty} e^{-\frac{(I-I_0)^2}{2\sigma_0^2}} dI = \frac{1}{2} erfc\left(\frac{I_{th} - I_0}{\sigma_0 \sqrt{2}} \right)$$

where erfc is the complementary error function defined by:

$$erfc(x) = \frac{2}{\sqrt{\pi}} \int_{x}^{+\infty} e^{-y^2} dy$$

The bit error ratio can then be expressed as:

$$BER = \frac{1}{4} \times \left[erfc\left(\frac{I_1 - I_{th}}{\sigma_1 \sqrt{2}} \right) + erfc\left(\frac{I_{th} - I_0}{\sigma_0 \sqrt{2}} \right) \right]$$

This rate depends on the decision threshold I_{th}. Generally, the decision threshold is chosen to minimize the bit error rate. A good approximation for I_{th} is:

$$\frac{I_1 - I_{th}}{\sigma_1} = \frac{I_{th} - I_0}{\sigma_0} \text{ leading to } I_{th} = \frac{\sigma_0 \times I_1 + \sigma_1 \times I_0}{\sigma_0 + \sigma_1}$$

We associate the quality factor to the bit error rate through the relationship:

$$BER = \frac{1}{2} erfc\left(\frac{Q}{\sqrt{2}} \right) = \frac{1}{\sqrt{\pi}} \int_{\frac{Q}{\sqrt{2}}}^{+\infty} e^{-y^2} dy \approx \frac{e^{-\frac{Q^2}{2}}}{Q\sqrt{2\pi}}$$

This last approximation is valid for Q>3.

And thus, we have the relation:

$$Q = \frac{I_1 - I_0}{\sigma_1 + \sigma_0}$$

1.3 Description of the different sources of noise in the receiver

1.3.1 Shot Noise

The shot noise is due to the photodiode and is related to quantum characteristics of photocurrent. Its expression is given by [1]:

$$\sigma_{shot}^{\ 2} = 2.\eta.e.B_e.(G.Is + \mathrm{M}.I_N)$$

where M is the number of ASE modes and:

$$\frac{I_S}{e} = \frac{P_S}{h.\nu} \text{ and } \frac{I_N}{e} = \frac{P_{ASE}}{h.\nu} = G.n_{eq}.B_o$$

with P_S the input signal power at the receiver and P_{ASE}, the noise power per state of polarization. Indeed, Is is the photocurrent corresponding to the signal power P_s.

In this relation, $G.I_S$ is the photocurrent due to optical signal and I_N is the ASE noise corresponding to the noise power P_{ASE}. That's why we have a contribution of the signal and of the amplified spontaneous emission to the shot noise.

$$\sigma_{shot-0}^{\ 2} = 2.\eta.e.B_e.\mathrm{M}.P_{ASE}.\frac{e}{h.\nu}$$

$$\sigma_{shot-1}^{\ 2} = 2.\eta.e.B_e.(G.P_S + \mathrm{M}.P_{ASE}).\frac{e}{h.\nu}$$

We note that shot noise variance depends linearly on received optical power.

1.3.2 Thermal Noise

The thermal noise is associated to the electronic circuit of the receiver and defined by [1]:

$$\sigma_{th}^{\ 2} = \frac{4.k_B.T.B_e}{R}$$

where k_B is Boltzmann's constant (k_B=1.38.10^{23} J.K^{-1}), T the absolute temperature and R the load resistor.

1.3.3 Amplified Spontaneous Emission (ASE)

The amplified spontaneous emission noise is generated within the optical amplifiers. This is a wide band noise so it will be considered to have the same spectral density above the whole optical bandwidth Bo of the amplifier. The expression of its power is given by [1,2]:

$$P_{ase} = h.\nu.G.n_{eq}B_o \text{ per state of polarization}$$

At 193.1 THz, the photon energy is h ν_s = 1.279.10^{-19} J.

1.3.4 ASE and ASE-signal beat noise

The expressions of beat noise contributions will not be justified in this study. Their expressions are detailed in the references. These noises are due to interferences between optical fields at photodiode input. The signal-ASE beat noise is due to the beat of the spontaneous emission noise with the signal noise [1,8]:

$$\sigma_{S-ASE}^{\ 2} = 4.\eta^2.G.P_S.P_{ASE}.\frac{B_e}{B_o}.\left(\frac{e}{h.\nu}\right)^2$$

We note that this noise depends linearly on signal power.

The ASE-ASE beat noise is due to the beat of the spontaneous emission noise with itself. Its expression is [1,8]:

$$\sigma_{ASE-ASE}^{\ 2} = M.\eta^2.P_{ASE}^{\ 2}.\frac{B_e}{B_o^{\ 2}}.(2.B_o - B_e).\left(\frac{e}{h\nu}\right)^2$$

We can outline the introduction of the factor M due to the number of ASE modes.

1.3.5 Total receiver noise

Thus, we can express the total electrical noise power in case of a mark or a space:

$$\sigma_1^{\ 2} = \sigma_{shot-1}^{\ 2} + \sigma_{S-ASE}^{\ 2} + \sigma_{ASE-ASE}^{\ 2} + \sigma_{th}^{\ 2}$$

$$\sigma_0^{\ 2} = \sigma_{shot-0}^{\ 2} + \sigma_{ASE-ASE}^{\ 2} + \sigma_{th}^{\ 2}$$

1.4 Simulation of the electrical noise variances as a function of input power, optical preamplifier gain and bit rate

Thanks to figure 1, 2 and 3, we can see which type of noise(s) will be predominant over the others. These simulations have been obtained with the following parameters:

- $\eta = 1$
- $M = 2$
- $R = 500\ \Omega$
- $T = 300$ K
- $n_{eq} = 2$

The input signal power will vary from –40 dBm to –10 dBm. The OSNR is the ratio between signal power and noise power in a reference bandwidth. In order to evaluate the different contributions of noise, it is set to 18 dB at the input of the optical receiver (with a reference bandwidth $B_{ref} = 1.6$ nm). Usually, OSNR values are given in a 0,1 nm bandwidth. In this case, the OSNR value equals 30 dB. For this computation, the optical bandwidth is set to 80 GHz. The electric bandwidth is set to 40 GHz. The different noise powers are evaluated in figure 3 as a function of the mean power in front of the optical receiver and for three different gains of the optical preamplifier.

Therefore, we can see that for low signal powers, the signal-ASE beat noise is predominant but we cannot neglect the other noises whereas when Ps becomes greater than –30 dBm, at least two orders of magnitude separates the signal-ASE beat noise from the others and so, this last one can be considered only. This fact is quite interesting because it will allow us to predict the limit of the transmission factor when Ps grows, as we will see in Chapter I. 4.

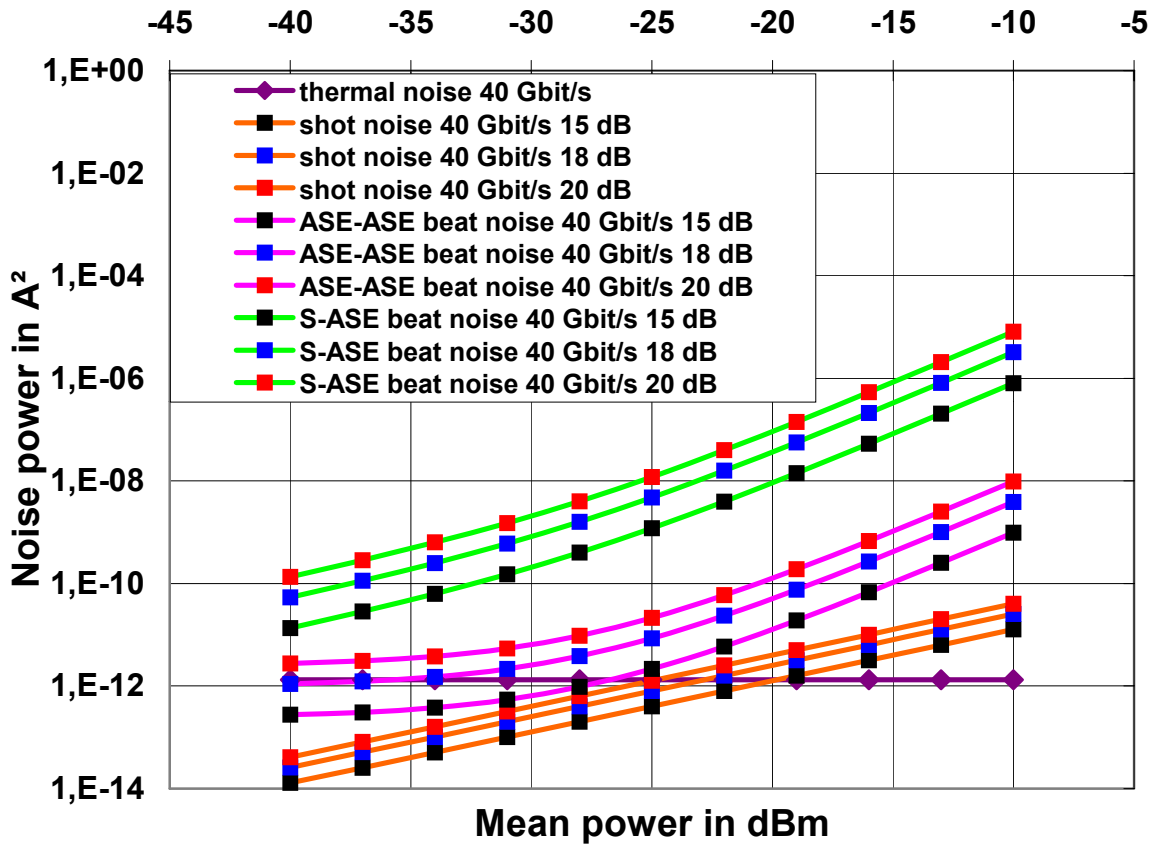

Figure 2. 3: noise variances versus mean power in dBm at 40 Gbit/s for various values of pre-amplifier gain. Bo=80 GHz; Be=40 GHz, OSNR=30 dB in 0,1 nm optical bandwidth.

1.5 The receiver sensitivity

1.5.1 Without ASE noise at the input

The receiver sensitivity is, by definition, the input signal power P for which BER= 10^{-9}. To obtain its expression, we investigate the definition of the transmission quality factor Q assuming Gaussian distribution for the marks and spaces:

$$Q = \frac{< i_1 > - < i_0 >}{\sqrt{\sigma_0^{\,2}} + \sqrt{\sigma_1^{\,2}}}$$

where $<i_1>$ (respectively $<i_0>$) and $\sigma_1^{\,2}$ (respectively $\sigma_0^{\,2}$) are the mean and the variance of photocurrent for symbol 1(respectively 0):

$< i_0 >= \eta.\mathrm{M}.I_N$ is the photocurrent due to noise.

$< i_1 >= \eta.(G.I_S + \mathrm{M}.I_N)$ is the photocurrent due to noise and amplified signal.

$$\sigma_0^{\,2} = \eta.e.2.B_e.\mathrm{M}.I_N + \mathrm{M}.\eta^2.I_N^{\,2}.\frac{2.B_e}{B_o^{\,2}}.(B_o - \frac{B_e}{2}) + \frac{4.k_B.T.B_e}{R}$$

where we recognize $\sigma_0^{\,2} = \sigma_{shot-0}^{\,2} + \sigma_{ASE-ASE}^{\,2} + \sigma_{th}^{\,2}$

$$\sigma_1^{\,2} = \sigma_0^{\,2} + \eta.e.2B_e.G.I_S + 2.\eta^2.G.I_S.I_N.\frac{2.B_e}{B_o}$$

which can also be written $\sigma_1^{\,2} = \sigma_0^{\,2} + \left(\sigma_{shot-1}^{\,2} - \sigma_{shot-0}^{\,2}\right) + \sigma_{S-ASE}^{\,2}$.

Substituting these four equations in the definition of Q, we will obtain a relation between Q, Ps and G [1]:

$$P_S = Q^2.h.\nu_S.B_e.\left[2.F_o + \frac{2}{Q}\sqrt{\mathrm{M}.n_{eq}^{\,2}.\left(2.\frac{B_o}{B_e} - 1\right) + \mathrm{M}.n_{eq}.\frac{2}{\eta.G}.\frac{B_o}{B_e} + \frac{4.k_B.T}{R.e^2.\eta^2.G^2.B_e}}\right]$$

where F_o is the amplifier optical noise figure [1]:

$$F_o = \frac{\frac{1}{\eta} + 2.n_{eq}.G}{G}$$

To express the value as an average power per bit, we will rather look at the mean power P_{mean} which is half the signal power due to the equiprobability of symbols "0" and "1". The expression of the sensitivity is:

$$P_{mean} = 36.h.\nu_S.Be.\left[F_o + \frac{1}{6}\sqrt{\mathrm{M}.n_{eq}^{\,2}.\left(2.\frac{B_o}{B_e} - 1\right) + \mathrm{M}.n_{eq}.\frac{2}{\eta.G}.\frac{B_o}{B_e} + \frac{4.k_B.T}{R.e^2.\eta^2.G^2.B_e}}\right]$$

Three series of computations are shown on figure 4 corresponding to transmissions at three different bit rates (i.e. 2.5, 10 and 40 Gbit/s).

We notice that, when increasing the gain of the optical preamplifier, the sensibility reaches a limit which is proportional to the bit rate as we have a 6 dB difference between the different curves. This is due to the fact that shot noise and thermal noise contributions can then be neglected compared to beat noises. More generally, it means that the noise figure of the optical preamplifier, i.e. the first element in the reception device, determines the minimal optical power. This value of 6 dB is due to the increase of the spectral bandwidth of the signal: from 2,5 to 10 Gbit/s or from 10 to 40 Gbit/s, the electric bandwidth is multiplied by 4. Consequently, the noise terms contributions are greater by 6 dB.

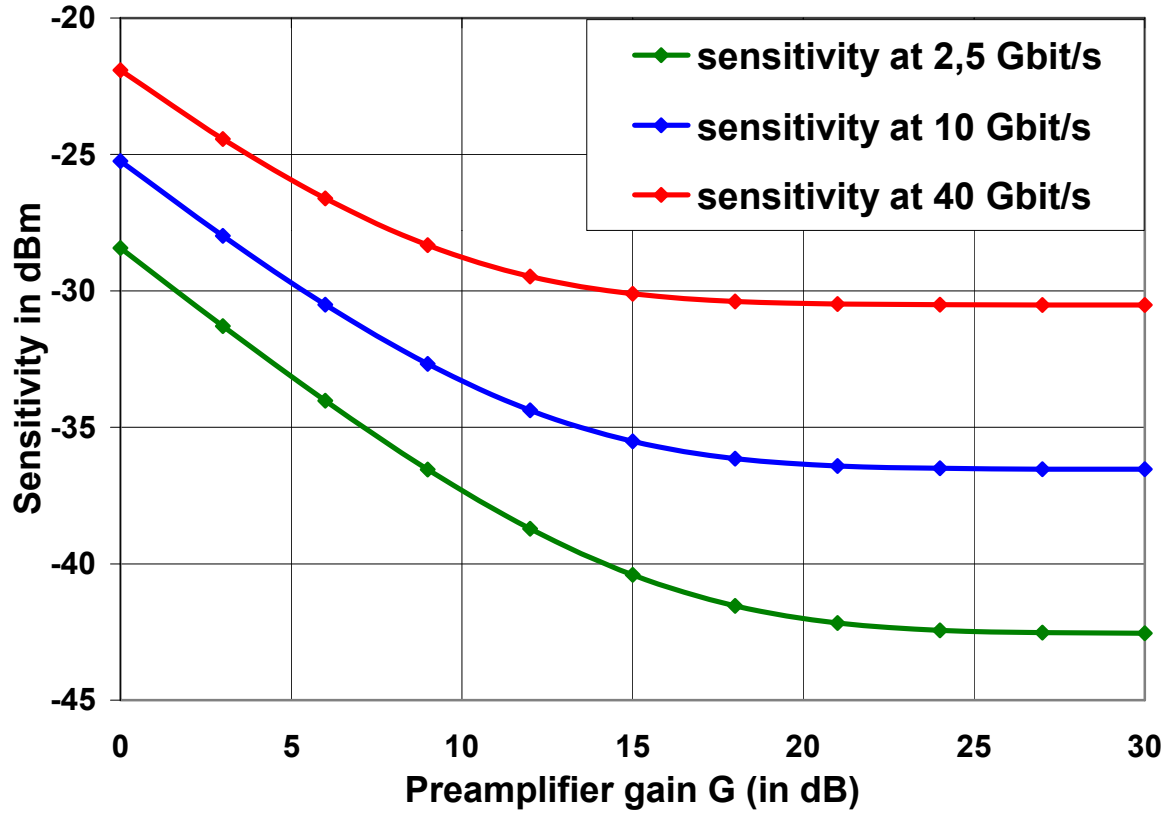

Figure 2. 4: sensitivity of the receiver as a function of the optical preamplifier gain G. Bo=2*Be=5, 20 and 80 GHz for 2.5, 10 and 40 Gbit/s respectively.

1.5.2 Adding ASE noise at the input of the receiver

We now consider that we have noise at the input of the optical amplifier. In chapter 2, we have evaluated the different contributions of noise. In this chapter, we evaluate the quality factor as a function of signal and noise powers. We can consider that this noise has been emitted by spontaneous amplification by inline optical amplifiers. In this case, the noise at the input of the optical preamplifier will be amplified by a gain G. Amplified spontaneous emission noise due to this amplifier remains as described on the following scheme:

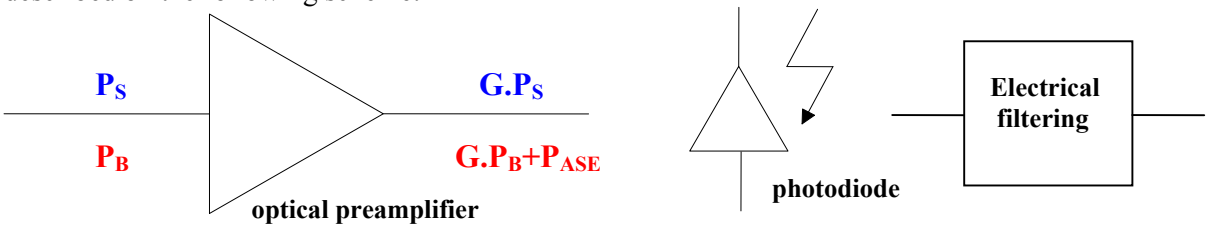

Figure 2. 5: description of the receiver and notations of optical signal (blue) and noise (red) powers.

We should be aware that the noise power P_B is distributed over each of the M ASE modes so that, in the usual case of 2 modes, the total noise power is equal to $2.P_B$.

Assuming the input noise is distributed over a large bandwidth, we will have equivalent terms appearing in the definition of σ_0 and σ_1. Thus, we have the following definitions:

- The thermal noise remains the same: $\sigma_{th}^{\ 2} = \dfrac{4.k_B.T.B_e}{R}$
- The shot noise is now: $\sigma_{shot}^{\ 2} = 2.\eta.e.B_e.[G.P_S + \mathrm{M}.(P_{ASE} + G.P_B)].\left(\dfrac{e}{h.\nu}\right)$
- The signal-ASE beat noise is defined by:

$$\sigma_{S-ASE}^{\ 2} = 2.\eta^2.G.P_S.(P_{ASE} + G.P_B).\frac{2.B_e}{B_o}.\left(\frac{e}{h\nu}\right)^2$$

with the same expression for I_B and I_N as before.

- The beat between noise and itself (called the ASE-ASE beat noise in the previous chapters) can also be deduced:

$$\sigma_{ASE-ASE}^{\ 2} = M.\eta^2.(P_{ASE} + G.P_B)^2 \frac{B_e}{B_o^{\ 2}}.(2.B_o - B_e).\left(\frac{e}{h\nu}\right)^2$$

Therefore, it is possible to obtain a relation between Q, P_S and P_B because we have the relations:

$$Q = \frac{< i_1 > - < i_0 >}{\sqrt{\sigma_0^{\ 2}} + \sqrt{\sigma_1^{\ 2}}}$$

The substitution of these contributions leads to the following relation:

$$Q = \frac{\eta.G.(\frac{e}{h.\nu}).P_S}{\sqrt{\sigma_0^{\,2}}.(1+\sqrt{1+\frac{2.\eta.\frac{e^2}{h.\nu}.G.\left[B_e+\frac{\eta}{h.\nu}.\frac{2.B_e}{B_o}.\left(G.P_B+P_{ASE}\right)\right].P_S}{\sigma_0^{\,2}}})}$$

Adding noise on the input of the receiver, we can define the signal and noise powers P_S and P_B. Considering the equiprobability between marks and spaces, the optical signal to noise ratio (OSNR) in the bandwidth B_{ref} at the input of the receiver is: $OSNR = \frac{P_S}{2.M.P_B}.\frac{B_o}{B_{ref}}$ and the mean power is $P_{mean} = \frac{P_S}{2}$ where P_s is the optical power for symbol 1.

Reciprocally, it is possible to obtain P_S as a function of Q and P_B because we can write:

$$Q = \frac{A.P_S}{(\sigma_0 + \sqrt{\sigma_0^{\,2} + B.P_S})}$$

$$Q = \frac{A.P_S.(\sigma_0 - \sqrt{\sigma_0^{\,2} + B.P_S})}{-B.P_S}$$

We finally obtain:

$$P_S = \frac{Q.\left(2.A.\sigma_0 + B.Q\right)}{A^2}$$

$$P_S = \frac{Q.\left(2.\sigma_0 + 2.e.\left[B_e + \frac{\eta}{h.\nu}.\frac{2.B_e}{B_o}.(G.P_B + P_{ASE})\right].Q\right)}{\eta.G.\left(\frac{e}{h.\nu}\right)}$$

and

$$\sigma_0^{\,2} = M.\eta.e.2.B_e.(G.P_B + P_{ASE}).\frac{e}{h\nu} + M.\eta^2.(G.P_B + P_{ASE})^2.(\frac{e}{h.\nu})^2.\frac{B_e}{B_o^{\,2}}.(2.B_o - B_e) + \frac{4.k_B.T.B_e}{R}$$

Therefore, the transmission quality factor can be estimated when the mean power varies for a given OSNR and for various bitrates and preamplifier gains. Results are shown on Figure 2. 6 for an optical signal to noise ratio of 20 dB in 0,1 nm bandwidth for a bit rate of 2.5, 10 and 40 Gbit/s and for a preamplifier gain of 15, 18 and 20 dB.

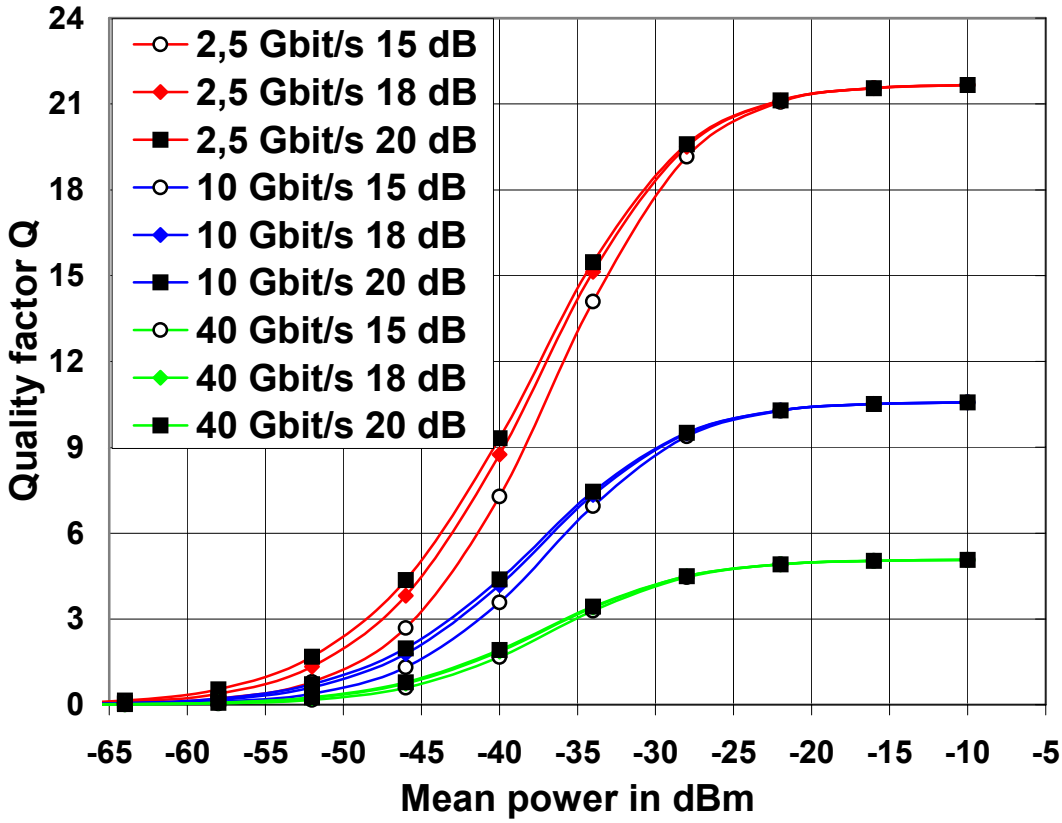

Figure 2. 6: quality factor versus mean power for different preamplifier gains (G = 15, 18 and 20 dB). OSNR=20 dB in B_{ref}=0,1 nm.Bo=2*Be=5, 20 and 80 GHz for 2.5, 10 and 40 Gbit/s respectively.

1.6 Limit of the quality factor

We see that when the input signal power grows, the quality factor reaches a limit. Considering the noise terms can also lead to this conclusion. We have seen in chapter I. 2. that when P_S is high, the signal-ASE beat noise is predominant and so we can write:

$$\sqrt{\sigma_0^{\,2}} + \sqrt{\sigma_1^{\,2}} \approx \sqrt{\sigma_{S-ASE}^{\,2}}$$

and :

$$\sigma_{S-ASE}^{\,2} = 4.\eta^2.G.I_S.(I_N + G.I_B).\frac{B_e}{B_o} = 4.\eta^2.G.P_S.(G.P_B + P_{ASE}).(\frac{e}{h.\nu})^2.\frac{B_e}{B_o}$$

From the definition of Q, we obtain:

$$Q \approx \frac{2.\eta.G.\left(\frac{e}{h.\nu}\right).P_{mean}}{\sqrt{\sigma_{S-ASE}^{\,2}}}$$

where P_{mean} is the average power per bit or the mean power.
Replacing $\sigma_{S\text{-}ASE}^2$ and introducing OSNR, we obtain:

$$Q^2 \approx \frac{OSNR}{\left(1 + \frac{P_{ASE}}{G.P_B}\right).\frac{B_e}{B_{ref}}} \approx \frac{OSNR}{\left(\frac{B_e}{B_{ref}}\right)}$$

Actually, the term $\frac{P_{ASE}}{G.P_B}$ can be neglected compared to 1 because typically, $\frac{P_{ASE}}{G.P_B}$ is less than 0,001 (i.e. -30 dB) when the limit is nearly reached.

This last equation is important because it allows us to see what the limit of Q is when Ps grows. The following values of the asymptotic transmission quality factor are obtained with $Bref = 0{,}1\,\text{nm}$ (corresponding to 12,5 GHz). Up to now, the electrical filter bandwidth was set to one time the bit rate. However, we usually consider a ratio of 0,7 between this figure and the bit rate. For example, at 40 Gbit/s bit rate, the electrical filter bandwidth is Be=28 GHz. The maximum transmission quality factor is evaluated below for different optical signal to noise ratios at 40 Gbit/s.

OSNR (in dB)	15	18	21	24
Limit for Q	3,8	5,3	7,5	10,6

Table 2. 1. Limit for Q factor (in linear scale) as a function of optical signal-to-noise ratio (in dB) for an electric filter bandwidth equal to 28 GHz.

Similar results can be obtained if we assume the receiver to operate at 160 GHz. This time, the electric bandwidth is 112 GHz but the OSNR is still measured in 0,1 nm:

OSNR (in dB)	21	24	27	30
Limit for Q	3,7	5,3	7,5	10,6

Table 2. 2. Limit for Q factor (in linear scale) as a function of optical signal-to-noise ratio (in dB) for an electric filter bandwidth equal to 112 GHz.

This equation also shows that, in order to obtain Q=6 (i.e. BER=10^{-9}), we shall have at least an optical signal to noise ratio of 19 dB at 40 Gbit/s and of 25 dB at 160 Gbit/s bit rate.

We have seen that this maximum quality factor is obtained when the signal power is sufficiently high, i.e. with a high gain of the optical preamplifier. We see that this asymptotic quality factor is reached for a mean power around -15 dBm in front of the photodiode when the receiver does not include any optical preamplifier. In the following figure, the quality factor is estimated as a function of mean power without optical preamplifier and for a ratio of 0,7 between electrical filter bandwidth and the bit rate. The OSNR is set to 20 dB and we consider three different bit rates.

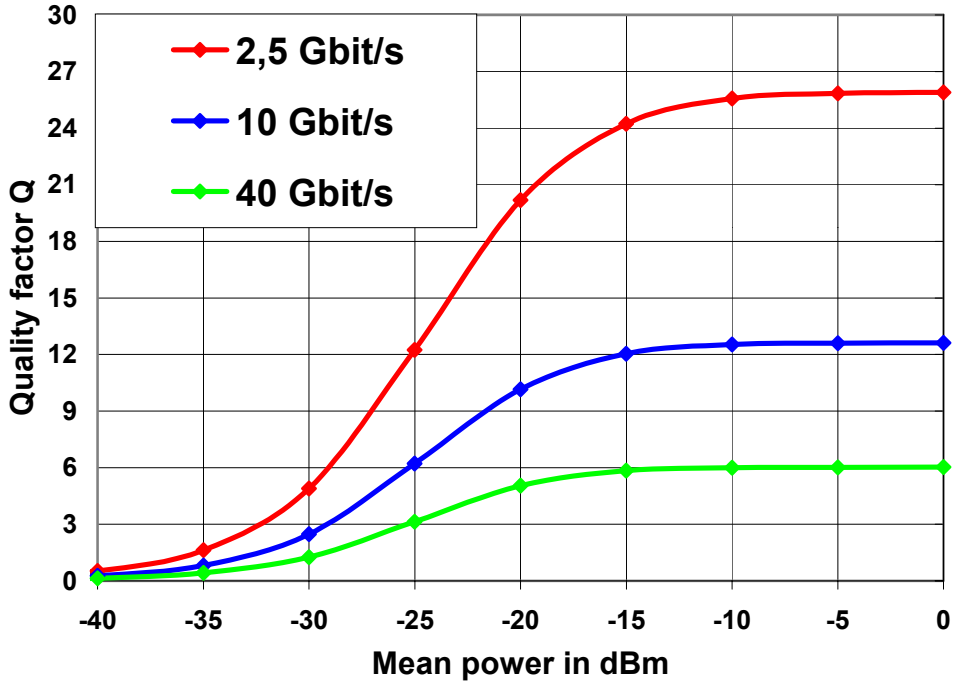

Figure 2. 7: quality factor versus mean power (OSNR = 20 dB in 0,1 nm) without optical preamplifier. Bo = 2 x BitRate and Be = 0,7x BitRate = 1.75, 7 and 28 GHz for 2.5, 10 and 40 Gbit/s respectively.

Conclusion: the receiver

In this first chapter, we have evaluated the different noise contributions at the detection of the signal and we have shown that signal-ASE beat noise is predominant for high signal power (see Figure 2. 3). We have also seen how the quality factor could be expressed as a function of the mean power. This leads directly to the determination of the minimum signal power on the input of the preamplifier in order to obtain a transmission quality factor of 6 (see Figure 2. 4).

At last, we have seen that the introduction of optical noise at the input of the receiver, which leads to the definition of the optical signal to noise ratio, was determining a limit for the quality factor of the transmission (see Figure 2. 6 and Figure 2. 7). For this reason, a minimum of 25 dB is required for the optical signal to noise ratio in order to obtain a quality factor of 6, corresponding to a bit error rate of 10^{-9} which is mostly used in telecommunications.

2 Filtering issues

In the previous chapters, filtering has not been considered since the bandwidth of optical filters was always set to 320 GHz for a 160 Gbit/s signal. In this chapter, we analyze the impact of optical filtering in two cases: first, we consider the case of a native 160 Gbit/s signal with an OSNR of 30 and 40 dB. In a second time, the 160 Gbit/s signal is obtained by optically multiplexing four signals at 40 Gbit/s each. After optical demultiplexing from 160 to 40 Gbit/s, the quality factor is only estimated on one of the OTDM lines. This optical demultiplexing is obtained by a rectangular temporal gating which width is equal to the time bit. Therefore, this non-optimized function does not induce any change on the optical signal-to-noise ratio. We would like to mention that improved switching windows, more adapted to the signal, enable more efficient conversion [3,4]. The optical filter bandwidth is varying from 150 to 500 GHz and the optical pulse width is varying from 1,25 ps (duty cycle=0,2) to 4,5 ps (duty cycle=0,72). This simulation is schemed on the following figure. For these simulations, we do not take into account photo detection noises and we only consider signal-ASE and ASE-ASE beat noises.

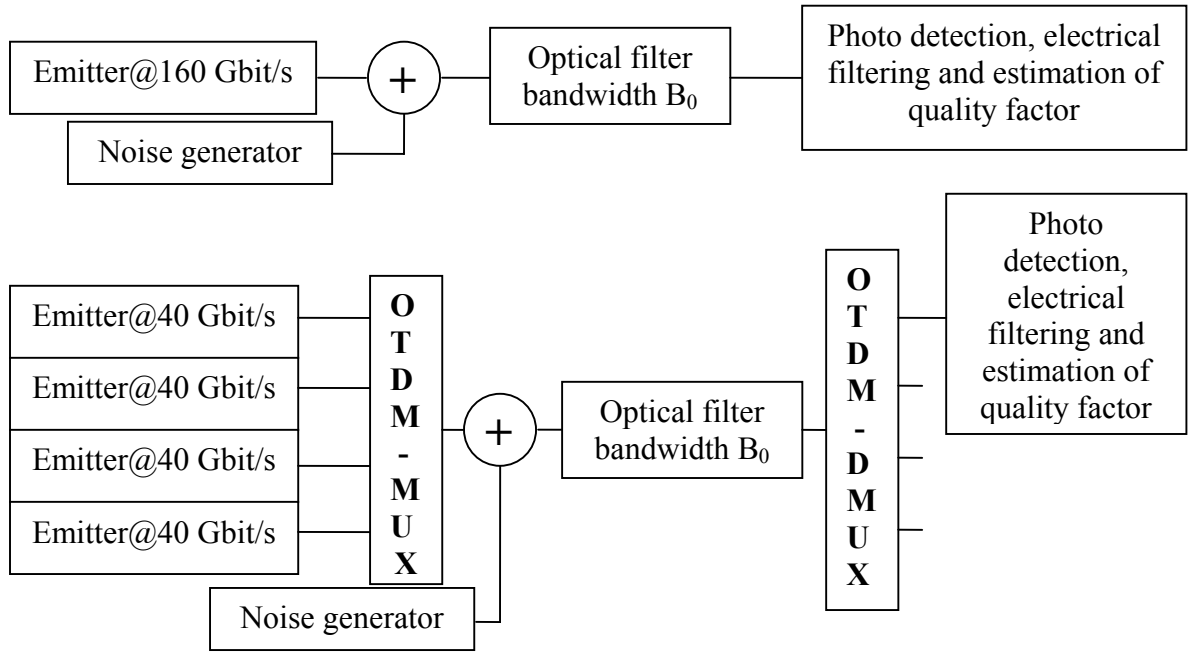

Figure 2. 8: Scheme of the simulation: optimization of optical filtering in cases of native and OTDM signals.

The electric filter bandwidth is set to 0,7 times the bitrate in order to filter noise as much as possible and to avoid inter symbol interference [5]. In the case of a native 160 Gbit/s signal, we can make the following comments:

- We obtain high values for Q^2 factor when the pulse width is lower than 3 ps in the two cases (for OSNR values of 30 and 40 dB) as, when the pulse width is greater than 3 ps, pulses interfere with the neighbouring bits which cause pulse distortion(ISI).
- When the OSNR is 30 dB, we notice that for small pulse width (less than 2 ps), the requirement for filter bandwidth increases from 175 GHz to more than 325 GHz when the pulse width changes from 2,25 ps to 1,25 ps. The reason for it is linked to inter symbol interference: for a small initial pulse width τ_i, the pulse width after optical filtering τ_f is determined by the optical filter as $\tau_f \approx \tau_i + \frac{1}{B_0} \approx \frac{1}{B_0}$ and as a consequence, a large optical bandwidth is required to avoid inter symbol interference. At the opposite, when the initial pulse width is high, we have $\tau_f \approx \tau_i + \frac{1}{B_0} \approx \tau_i$ and the filter bandwidth has a small impact on inter symbol interference.

- We can remark that the optimum value for Q^2 factor is between 20 and 21 dB when the OSNR is 30 dB and between 30 and 31 dB when the OSNR is 40 dB which is coherent: an OSNR difference of 10 dB induces a difference of 10 dB for the quality factor as shown previously. Furthermore, we verify that signal-ASE beat noise is predominant as the difference between OSNR and Q^2 values is between 9 and 10 dB, which is equal to the ratio between the electric bandwidth (112 GHz) and the reference bandwidth (12,5 GHz).

In the case of an OTDM 160 Gbit/s signal, we can make the following comments:

- We do not encounter degradation due to high pulse width as seen for a native 160 Gbit/s signal. This is due to the fact that optical demultiplexing reduces the impact of adjacent bits. As a matter of fact, time gating associated to optical demultiplexing transforms 160 Gbit/s signal into a 40 Gbit/s signal with a duty cycle 4 times lower.
- For optimum filter bandwidth, we obtain better values for the Q^2 factor than in the case of a native signal. This improvement is about 5 to 6 dB when the OSNR is 30 dB. This is due to the fact that the electric filter bandwidth is 28 GHz (0,7 times 40 GHz) in this case whereas it is 112 GHz (0,7x160 GHz) for a native signal. Thus, the electric filter reduces much more the amount of noise in the OTDM case.

This last characteristic is really important because it means that considering noise only, we need the same OSNR when we consider a native 40 Gbit/s signal and an OTDM 4x40 Gbit/s in order to obtain a given quality factor. Furthermore, it is possible to implement the optical demultiplexing function before optical filtering and to use a narrower optical filter and more efficient noise suppression with a bandwidth equal to $B_0/4$ for example [6].

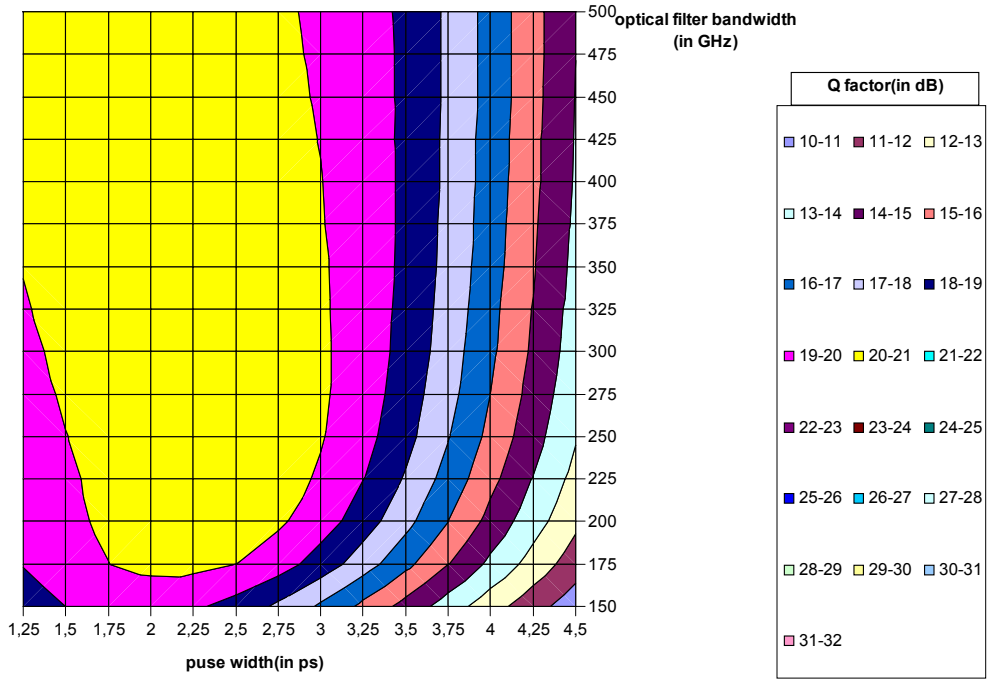

Figure 2. 9: Q factor as a function of pulse width and optical filter bandwidth for a native 160 Gbit/s signal with OSNR=30 dB.

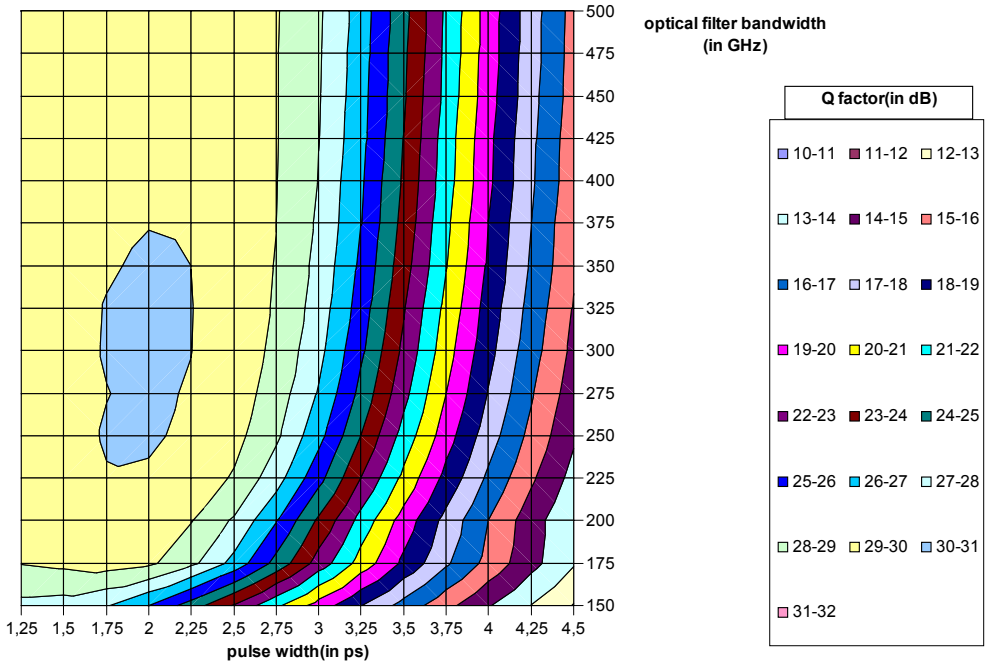

Figure 2. 10: Q factor as a function of pulse width and optical filter bandwidth for a native 160 Gbit/s signal with OSNR=40 dB.

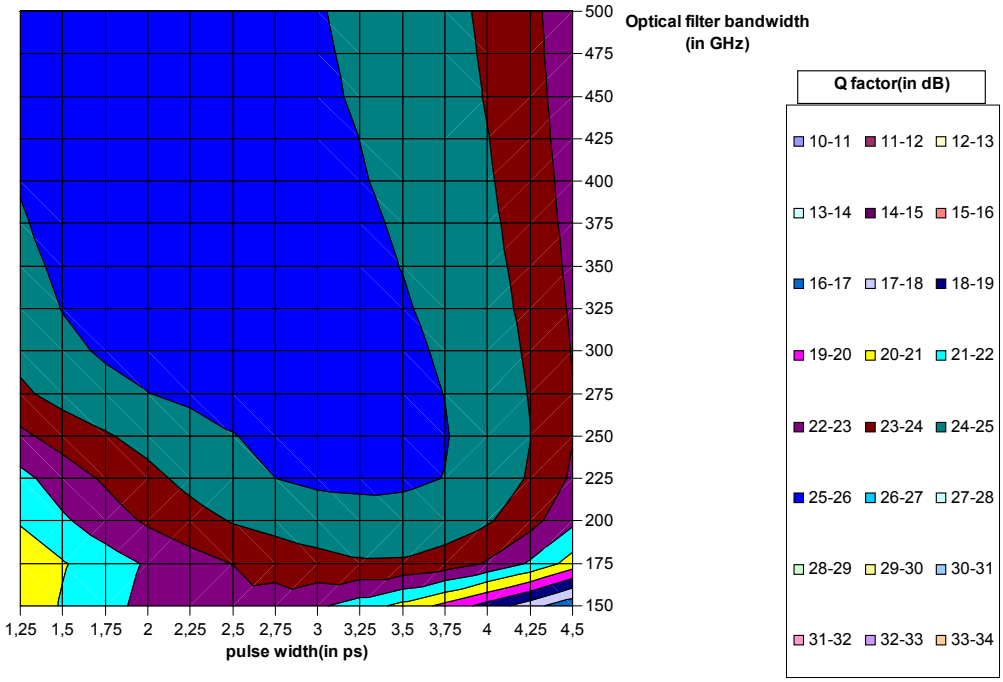

Figure 2. 11: Q factor as a function of pulse width and optical filter bandwidth for an OTDM 160 Gbit/s signal with OSNR=30 dB.

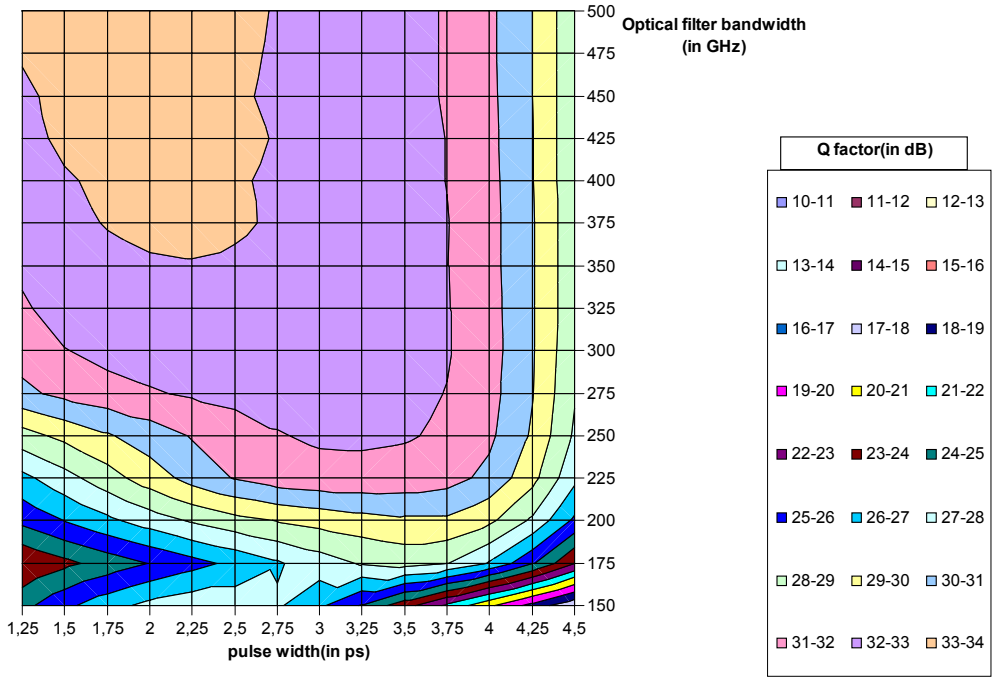

Figure 2. 12: Q factor as a function of pulse width and optical filter bandwidth for an OTDM 160 Gbit/s signal with OSNR=40 dB.

Conclusion: filtering issues

In this chapter, we have investigated the choice of the optical filter bandwidth for 160 Gbit/s bitrate optical communications. We have seen that this choice is not influenced by the nature of the signal (OTDM or native signal) as the optimal filter bandwidth is the same in both cases. However, an improvement of nearly 6 dB is obtained in the case of a four-tributaries-OTDM signal linked to the fact that the electric bandwidth can be divided by four compared to native bit rate signal. For more simplicity, most of the simulations performed during this study are considering native 160 Gbit/s signal. From a noise point of view, it means that when we consider a quality factor of 15,6 dB at the reception, an enhancement of a few dB (up to 6 theoretically) can be obtained by optical time division demultiplexing. However, in these studies, we did not consider the losses due to optical time demultiplexing and the supplementary amplification needed to cover these losses. That's why we will still consider a quality factor of 15,6 dB as a reference.

3 Optical time division multiplexing impact on power penalty

Basically, we can define a return-to-zero pulse sequence at a given bit rate by the following parameters: pulse width, peak level of ones, mean level of zeros as shown in the following figure.

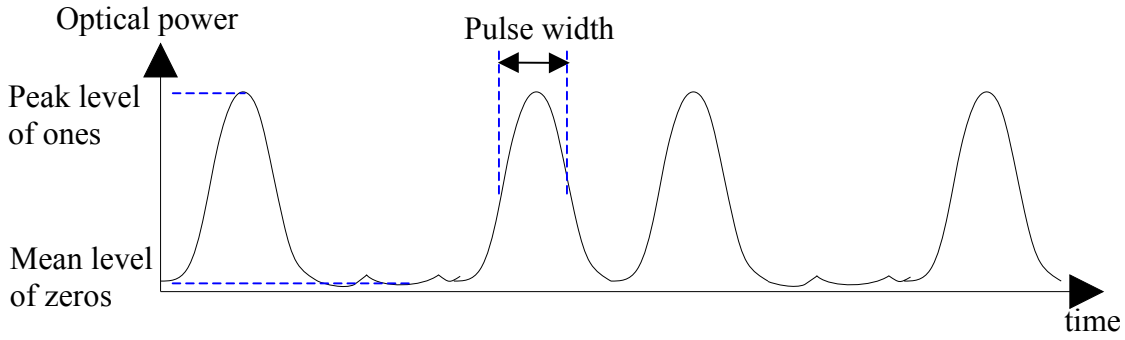

Figure 2. 13. Parameters of a return-to-zero pulse sequence.

The optical multiplexing of N lines at the bit rate Bo produces an optical pulse sequence at the bit rate NxBo. However, an imperative condition needs to be respected concerning the pulse width, which should be smaller than $\frac{1}{N.B_0}$. Furthermore, the addition of optical signals during the multiplexing process impacts the peak level of ones and the mean level of zeros. These two values are modified as shown in the following figure.

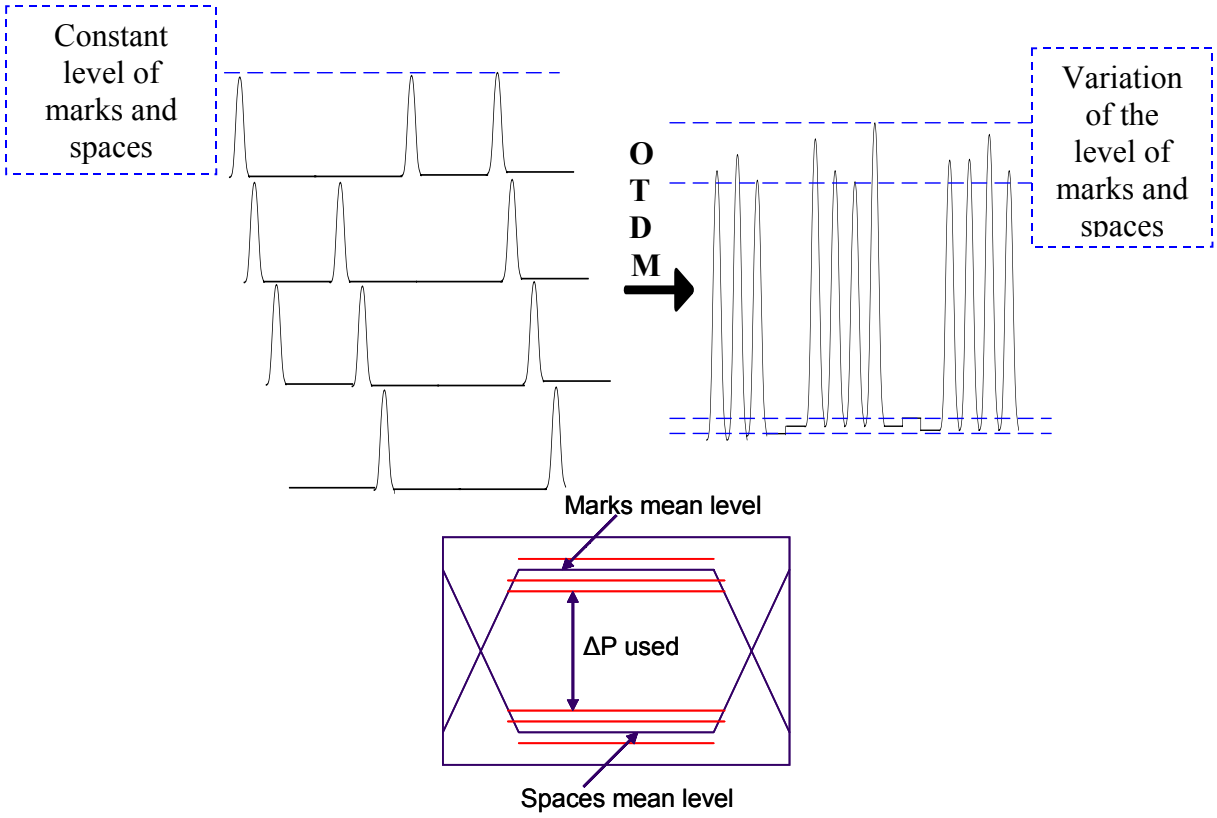

Figure 2. 14. Modification of peak level of ones and mean level of zeros by optical time division multiplexing and resulting eye diagram.

In order to simplify the transformation, we here consider that the pulses have a rectangular shape and that the condition on the width is valid. Before optical multiplexing, the peak level of marks is μ_1 and the level of zeros is μ_0. We can introduce the contrast parameter defined by:

$$contrast = \frac{\mu_1}{\mu_0}$$

After optical multiplexing of N lines, these parameters change and their evolution is described in the following equations where we introduce the phases of the N pulse sequences called Φ_1, Φ_2, Φ_3,… Φ_N:

$$\mu_0 \rightarrow \left\langle \left| \sum_{k=1}^{N} \sqrt{\mu_0}.e^{i.\phi_k} \right|^2 \right\rangle$$

where < > stands for the mean value of coefficients inside.

$$\mu_{1j} \rightarrow \left\langle \left| \sqrt{\mu_1} \times e^{i\phi_j} + \sqrt{\mu_0} \times \sum_{\substack{k=1 \\ k \neq j}}^{N} e^{i.\phi_k} \right|^2 \right\rangle$$

These alterations of the level changes have an impact on the contrast parameter of the optically multiplexed pulse sequence since it is now:

$$contrast = \frac{\left\langle \left| \sqrt{\mu_1} \times e^{i\phi_j} + \sqrt{\mu_0} \times \sum_{\substack{k=1 \\ k \neq j}}^{N} e^{i.\phi_k} \right|^2 \right\rangle_{j=1..N}}{\mu_0 \times \left| \sum_{k=1}^{N} e^{i.\phi_k} \right|^2}$$

In order to have an idea of this change, we consider as an example the case where the phases of the N optical sequences are equal ($\Phi_1=\Phi_2=\ldots=\Phi_N$). The contrast parameter of the optical multiplexed pulse sequence is:

$$contrast = \frac{\mu_1 + (N-1)^2 \times \mu_0 + 2(N-1) \times \sqrt{\mu_1.\mu_0}}{N^2 \times \mu_0}$$

$$contrast = \frac{\mu_1}{N^2 \times \mu_0} + \frac{(N-1)^2}{N^2} + \frac{2.(N-1)}{N^2} \times \sqrt{\frac{\mu_1}{\mu_0}}$$

Values of the contrast parameter depend of the modulator used to convert electrical data into optical data. We here consider the case of an initial contrast of 30 dB. This parameter is then a function of N (the number of multiplexed optical lines) as shown in the following table:

Number N of optical lines	2	4	8	16	32
Output contrast in dB	24,2	18,7	13,7	9,3	3,8

Table 2. 3. Contrast of an optically multiplexed line as a function of the number of optical lines N (the initial contrast of each optical line is set to 30 dB).

Indeed, we can easily understand that this case of equal optical phases corresponds to the worst case in terms of output contrast. This phenomenon can be studied by introducing the following parameter:

$$\frac{\Delta P_{used}}{P_{total}} = \frac{\mu_1 - \mu_0}{\mu_1 + \mu_0} = 1 - \frac{2}{\frac{\mu_1}{\mu_0} + 1} = 1 - \frac{2}{1 + contrast}$$

Using this definition, we can define the power ratio penalty by:

$$Power\_ratio\_Penalty = \frac{\Delta P_{used})_{after}}{\Delta P_{used})_{before}} \times \frac{P_{total})_{before}}{P_{total})_{after}}$$

In case of equal optical phases, the power penalty is a function of the number N of optical lines:

$$Power\_ratio\_Penalty = \frac{\left[1 - \frac{2}{1 + \left(\frac{\mu_1}{N^2 \times \mu_0} + \frac{(N-1)^2}{N^2} + \frac{2.(N-1)}{N^2} \times \sqrt{\frac{\mu_1}{\mu_0}} \right)}\right]}{1 - \frac{2}{1 + \frac{\mu_1}{\mu_0}}}$$

In the case of an initial contrast of 30 dB, the values of this power ratio penalty are given in the following table:

Number N of optical lines	2	4	8	16	32
Power ratio penalty in dB	-0,03	-0,1	-0,362	-1,02	-3,85

Table 2. 4: power-ratio penalty of an optically multiplexed line as a function of the number of optical lines N (the initial contrast of each optical line is set to 30 dB).

4 The optical line

4.1 Erbium amplification

The optical line will be constituted by successive patterns. A pattern is made of a certain length of fiber followed by an optical amplifier. The characteristics taken into account are:

- The fiber length.
- The attenuation of the fiber.
- The gain of the amplifier.
- The optical bandwidth of the amplifier.
- The equivalent input noise factor n_{eq} (which has the same definition than in chapter I.).

The following figure illustrates this design.

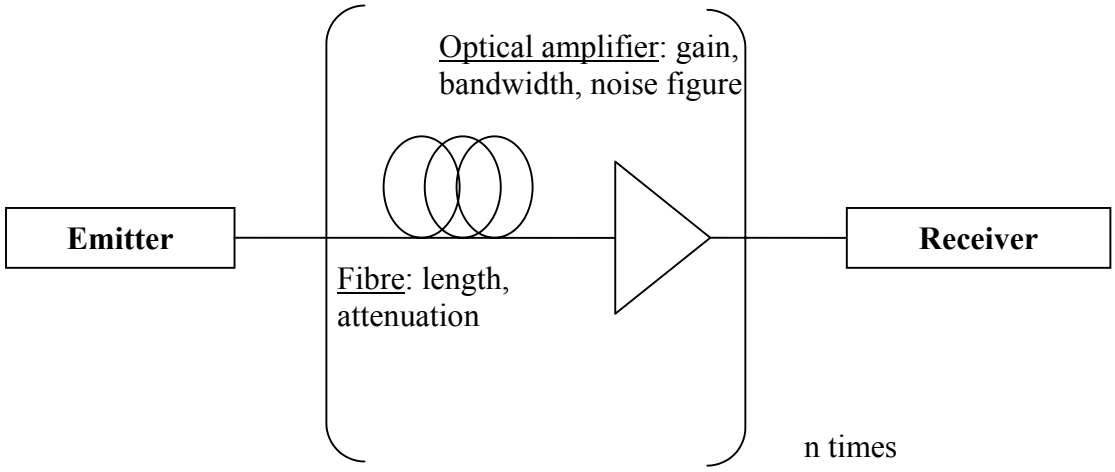

Figure 2. 15: scheme of the optical line for noise consideration.

In this firs example, we will not consider separately the attenuation of inline fibre and dispersion compensating fibre. Additionally, we only investigate the case of a single stage amplifier. As we will see later, double stage amplification will gain some advantage in terms of noise reduction.

Moreover, we consider that signal and noise powers are equally attenuated by the fibre. The gain of the amplifier is also the same when looking at signal or noise.

We first investigate the evolution of noise power with an optical amplifier. Considering the optical amplifier gain G, the spectral density of noise N_{noise} is multiplied by a gain G and added to the spectral density of the spontaneous emission noise of the amplifier:

$$N_{noise} \longrightarrow G.N_{noise} + N_{ASE}$$

We will consider that all the noises have the same bandwidth so that when considering the same optical band Bo, we can write:

$$N_{noise}.B_o \longrightarrow G.N_{noise}.B_o + N_{ASE}.B_o$$

$$P_{noise} \longrightarrow G.P_{noise} + P_{ASE}$$

We shall consider an optical line made of a unique pattern repeated N times, i.e. we have N spans. The first study will consider the number of spans and will aim to see its contribution to the degradation of the $OSNR_{max}$. The parameters of the first simulation are:

- The gain of the amplifier G is set to 20 dB.
- The length of the fiber is 100 km
- The attenuation of the fiber is set to 0.2 dB/km.
- The bandwidth of the optical filter (after the amplifier) is set to 320 GHz because the bit rate which is taken into account is 160 Gbit/s on the line and as the minimum value for Bo is twice the bit rate: $B_0 \geq 320$ GHz.
- The bandwidth of the Optical Spectrum Analyser is 0,1 nm (i.e. 12,5 GHz) for the measure of the OSNR. This value has been set by considering the broadening of the signal spectra.

If T is set to be the total attenuation of the fibre (or the transmission factor) then after transmission over one span, the evolution of signal and noise powers are described by:

$$P_{signal} \longrightarrow G.T.P_{signal}$$

$$P_{noise} \longrightarrow G.T.P_{noise} + P_{ASE}$$

For a transmission over n spans, these formulas naturally become:

$$P_{signal} \longrightarrow (G.T)^n.P_{signal}$$

$$P_{noise} \longrightarrow (G.T)^n.P_{noise} + P_{ASE}.(1 + G.T + G^2.T^2 + ... + G^{n-1}.T^{n-1})$$

This last equation can be written in a simpler way:

$$P_{noise} \longrightarrow (G.T)^n.P_{noise} + P_{ASE}.\frac{1-(G.T)^n}{1-G.T} \text{ if G.T} \neq 1$$

$$P_{noise} \longrightarrow (G.T)^n.P_{noise} + (n-1).P_{ASE} \text{ if G.T} = 1$$

The following figure shows the variation of OSNR on the output of the line with the number of spans and the input signal power Ps whereas the OSNR has been set at 40 dB in 0,1 nm bandwidth on the input. It is obvious that the results are critical if the input signal power is lower than –5 dBm just without considering the number of spans because we have to obtain at least 25 dB on the output of the line.

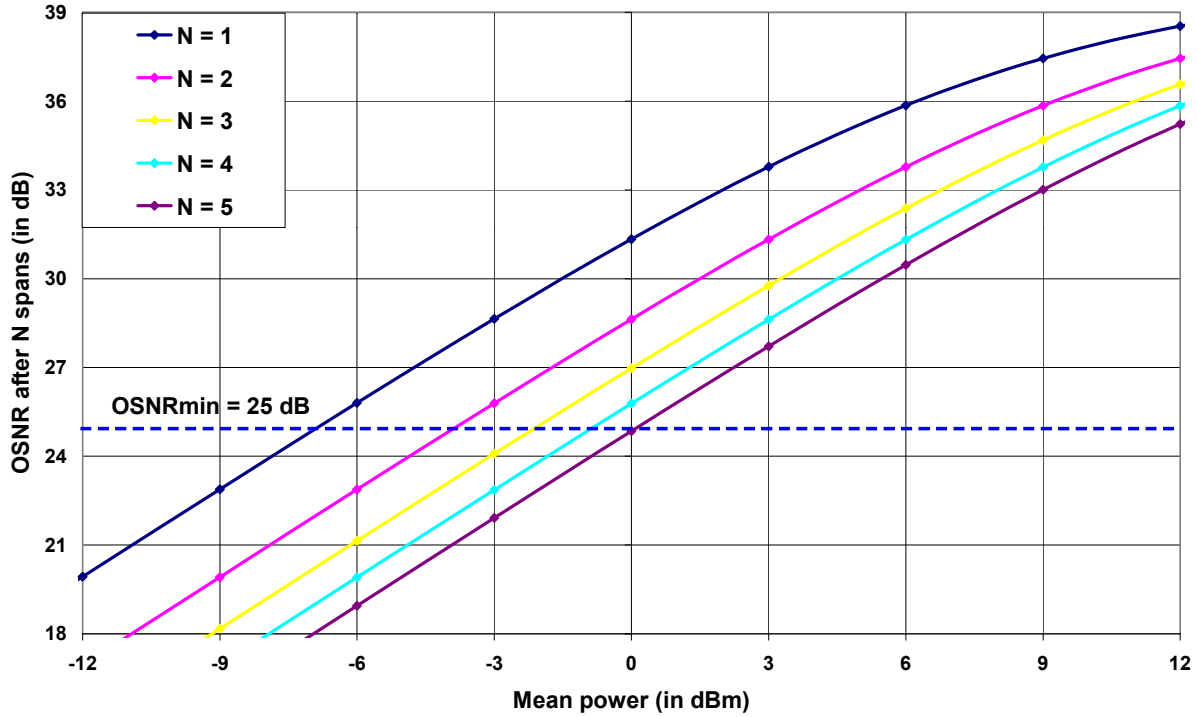

Figure 2. 16: OSNR (in 0,1 nm bandwidth) as a function of mean power and the number of spans (attenuation of 20 dB per span). The input OSNR is 40 dB in 0,1 nm.

We remark from Figure 2. 16 that an increase of the mean power by 3 dB is necessary to maintain the same OSNR when the transmission reach is increased from 1 to 2 spans or from 2 to 4 spans.

Furthermore, it is interesting to see which distance of transmission could be achieved if, due to longer or smaller span lengths, the span attenuation is 15, 20 or 25 dB. We know from chapter I.3. that a condition to obtain a quality factor greater than 6 is that the OSNR is greater than 25 dB. We can see from Figure 2. 17 that there is a considerable difference between these three choices. For example, if Ps is set to 0 dBm, then the maximum transmission distance is about 400 km if the span attenuation is 20 dB and more than 1000 km if G=15 dB whereas it is only 125 km if G=25 dB.

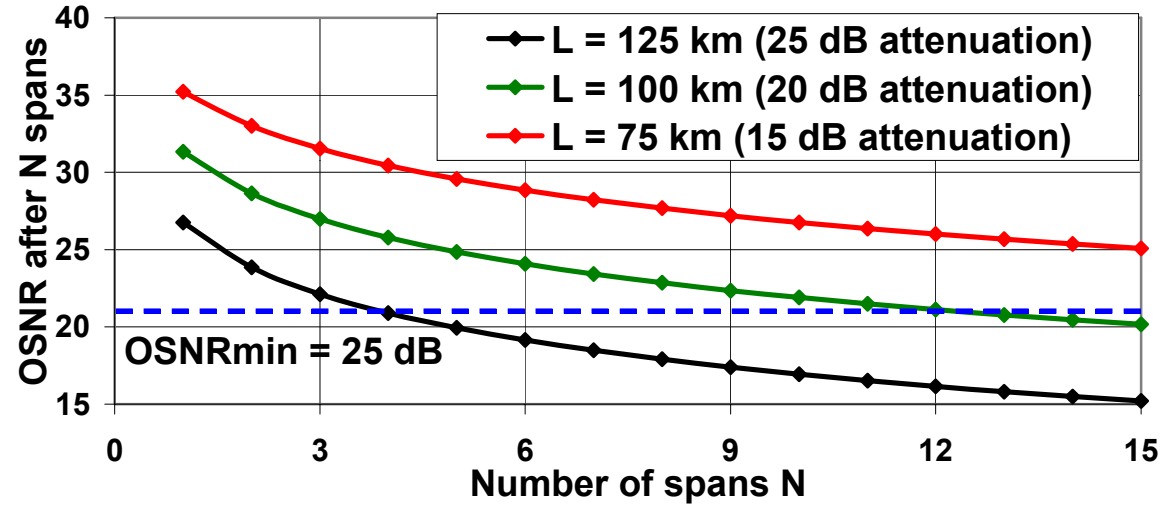

Figure 2. 17: OSNR (in 0,1 nm) as a function of the distance for 3 different span lengths. The input OSNR is 40 dB in 0,1 nm. Required OSNR for a quality factor of 6 is 25 dB.

4.2 Raman amplification

We only consider the case of a unique pump at frequency ν_P. The evolution of signal and pump powers in case of Raman amplification is ruled by the following equations [7]:

$$\frac{dP_p}{dz} = -\frac{\nu_p}{\nu_s} C_r \left(P_s + P_o\right) P_p - \alpha_p P_p$$

$$\frac{dP_S}{dz} = C_r \left(P_s + P_o\right) P_p - \alpha_s P_s$$

where :

- α_S (respectively α_P) is the attenuation coefficient of the signal (respectively of the pump) in the fibre.
- C_r is the Raman gain measured for frequency ν_P and depends on the frequency difference $\nu_P - \nu_S$.
- P_0 is representing spontaneous emission.

If we neglect the pump depletion, the gain provided by Raman amplification is [9]:

$$G(z) = \frac{P_s(z)}{P_s(0)} = \exp\left(\frac{C_r(\lambda)}{\alpha_p} P^+_{pompe} \left(1 - \exp\left(-\alpha_p z\right)\right) - \alpha_s z \right)$$

This expression does not correspond to the on/off gain but to the gain from the fibre input to the fibre output. The amplified spontaneous emission spectral density per state of polarization is given by:

$$N_{ASE} = h\nu_s \int_0^L C_r P^+_{pompe} \exp\left(-\alpha_p z\right) \exp\left(\frac{C_r(\lambda)}{\alpha_p} \left\{ P^+_{pompe} \left(\exp\left(-\alpha_p z\right) - \exp\left(-\alpha_p L\right)\right)\right\} - \alpha_s \left(L - z\right) \right) dz$$

As a matter of fact, the power spectral density of noise N is ruled by the following equation:

$$\frac{dN}{dz} = \left(C_r . P_p - \alpha_S\right) N + C_r . P_p . h . \nu$$

We can understand this last equation as following: the noise power is amplified by the Raman pumps and attenuated due to the fibre attenuation and this appears in the first term. The last term of the equation is due to the Raman spontaneous emission noise which is proportional to the pump power.

With this simple modelling, we can numerically calculate the evolution of pump, signal and noise power using Raman amplification. In the following figures, we compare the evolution of Raman gain and accumulated noise power versus backwards Raman pump power for different fibre types. Plain lines correspond to measures which have been made by E. Pincemin [10] over different fibre types with 100 km length and broken lines are representative of numerical applications.

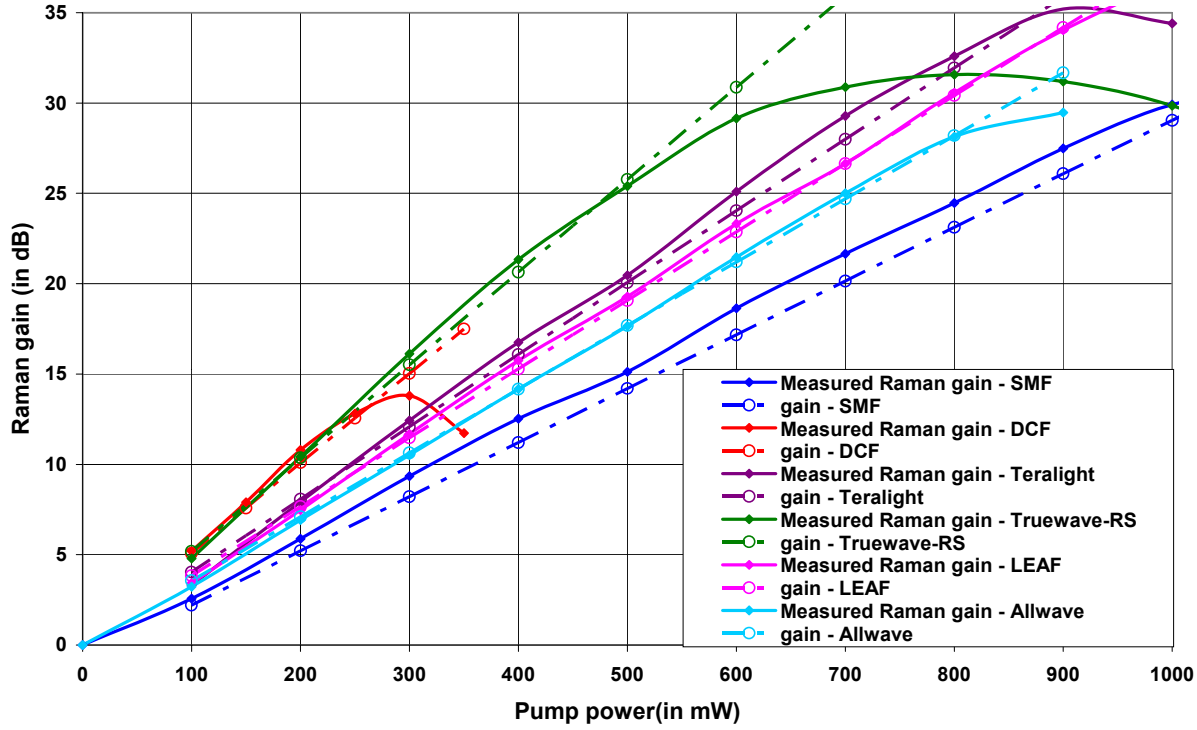

Figure 2. 18: Raman gain as a function of backwards Raman pump power for different fibre types. Comparison between experimental (plain lines) and numerical (broken lines) results.

We obtain a good approximation of Raman gain for all fibre types as the difference between experimental and numerical results is around 1 dB only. This is true only when the Raman pump power is low (for example, less than 300 mW for DCF or 800 mW for Allwave) because a saturation phenomenon [11] appears when the Raman pump power exceeds a threshold. This difference may also be linked to the pump depletion.

Concerning noise power, the matching between simulations and measurements is quite good, as can be seen in Figure 2. 19. We also observe a difference for high Raman pump power. Differences of 7 dB are observed in the case of Truewave-RS when the Raman pump power is greater than 600 mW. These differences between the modelling and the experiment may be due to double-Rayleigh backscattering which occurs for relatively high Raman gain [12,13].

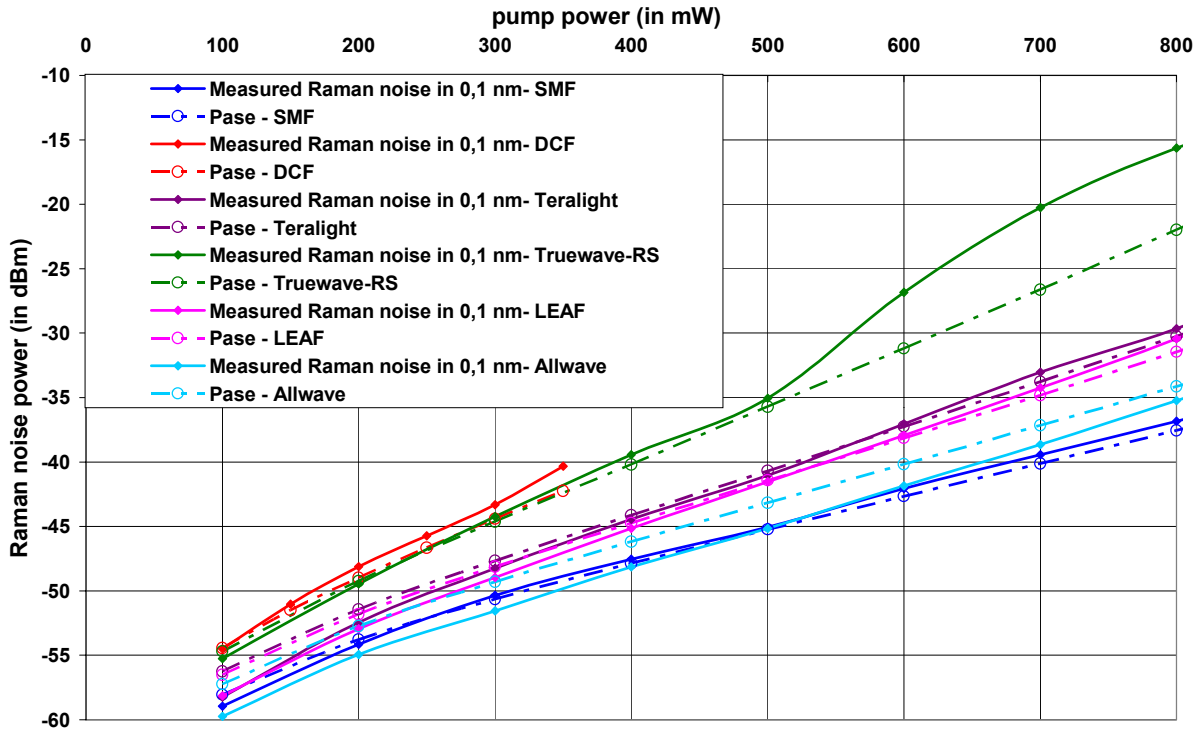

Figure 2. 19. Raman noise power in 0,1 nm as a function of backwards Raman pump power for different fibre types after a span of 100 km. Comparison between experimental (plain lines) and numerical (broken lines) results.

Using this modelling, we can, for example, study the evolution of signal and noise power in a span. In the following example, we consider a span of 100 km of SMF. We would like to achieve a 20 dB Raman on/off gain. Therefore, from Figure 2. 18, the pump power should be a little less than 700 mW.

In order to observe an evolution of the OSNR between the input and the output of the fibre, we should consider a relatively high OSNR at the emission as the Raman noise, in the case of backward pumping with 700 mW pump power, is estimated to -43 dBm only. In the following figure, we have represented the evolution of signal and noise power with an emission OSNR of 50 dB in three different cases:

- Backwards Raman amplification is considered only with a pump power of 670 mW.
- Forwards Raman amplification is considered only with a pump power of 670 mW.
- Forwards and backwards Raman amplification are considered with respective pump powers of 200 and 470 mW

In all cases, the Raman on/off gain is equal to 20 dB and is compensating for the fibre loss. We can see that the noise power accumulated in the backwards amplification case is greater than in the forwards amplification case. As a matter of fact, in the forwards amplification case, Raman amplification occurs mostly at the beginning of the fibre when Raman pump power is still high and therefore, spontaneous emission occurs at the beginning of the fibre and undergoes the attenuation of the fibre. At the opposite, in the case of backwards amplification, spontaneous emission occurs at the end of the fibre and is less influenced by the attenuation of the fibre. That's why we observe a difference between noise powers at the end of the fibre. Bidirectional Raman amplification corresponds to a medium case. We can outline that, if the noise power is less important in the case of forwards amplification, the signal power reaches a maximum power, which is greater than the fibre injection signal power (for example 10 dBm in Figure 2. 20) and this is an important counterbalance in terms of non-linear effects occurring in transmission.

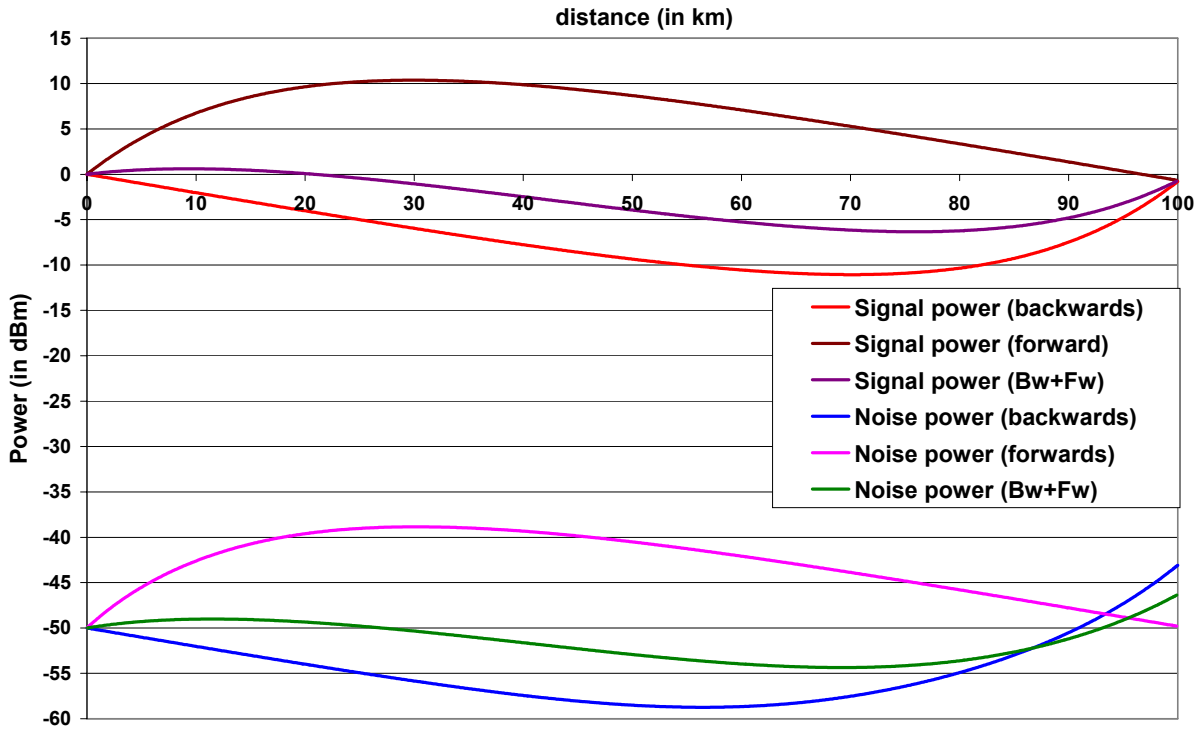

Figure 2. 20. Signal and Noise powers evolutions in three Raman amplification cases.

Unfortunately, this simple case is very restrictive and does not apply if using several Raman pumps where we should also take into account pumps interactions [7]. This matter is particularly important because a single Raman pump provides a flat amplification over 1 THz. In order to transmit several channels, we need to obtain a flat gain profile over the whole signal bandwidth and therefore use several Raman pumps [14,15] or even second-order Raman pumping [16].

In the frame of distributed amplification, the noise figure concept has to be adapted. At the opposite of a lumped amplifier where the amplification part is distinct from the attenuating part (constituted by fibre), a distributed amplifier includes both attenuation due to fibre loss and signal amplification due to Raman power conversion. In order to compare these two types of amplifiers, we introduce the equivalent noise figure as described in Figure 2. 21.

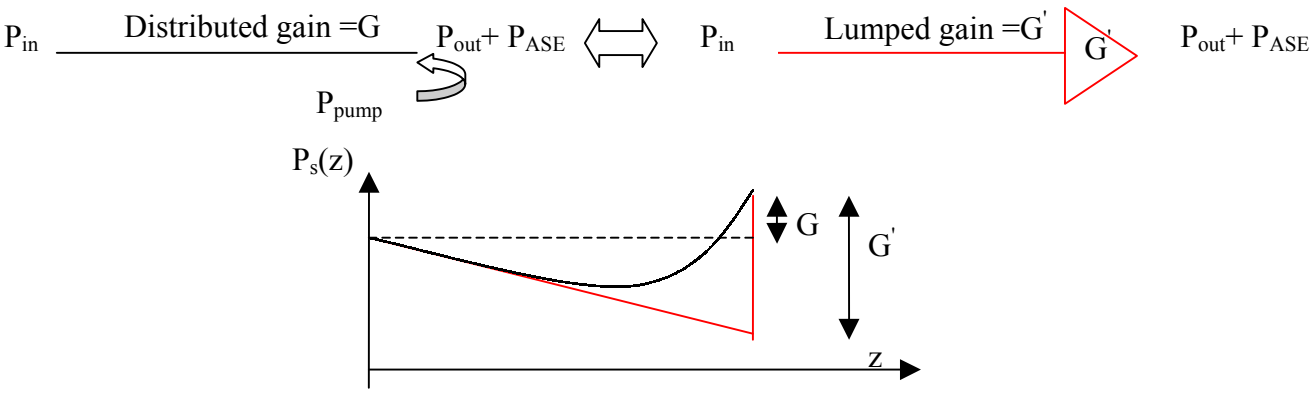

Figure 2. 21: evolution of signal power in cases of lumped and backward distributed amplifications.

If the loss coefficient of the fibre is α (in dB/km) and its length is L (in km) then: $G_{dB}' = G_{dB} + \alpha L$ where G' is the Raman gain or on/off gain expressed in dB.

The equivalent noise figure is defined by:

$$NF_{éq} = \frac{1+\frac{P_{ASE}}{h\nu\Delta\upsilon}}{10^{\frac{G'}{10}}} = \frac{1+\frac{P_{ASE}}{h\nu\Delta\upsilon}}{10^{\frac{G}{10}}.10^{\frac{\alpha.L}{10}}} = \frac{NF}{NF_{\substack{fibre\ \ only}}}$$

where P_{ASE} is the ASE noise power. NF_{eq} is the noise figure of a virtual lumped amplifier placed at the end of inline fibre and which noise power is the same than the Raman amplifier.

Indeed, we understand that ASE noise is attenuated by fibre attenuation whereas it is not the case for the equivalent configuration of lumped amplifier (see Figure 2. 21). The equivalent noise figure model does not induce an OSNR degradation but an improvement in terms of noise figure linked to the use of a distributed amplification scheme rather than a lumped one. For this reason, the equivalent noise figure can be either positive or negative.

In this chapter, we have studied Raman amplification and seen that its use is advantageous compared to lumped amplification because it induces a smaller amount of noise. As a matter of fat, it can also be used as a complement of lumped erbium amplification [17]. For transmission over long spans, we have seen that the degradation due to noise is critical. The use of Raman amplification may then be particularly interesting [18].

Conclusion: the optical line.

In this chapter, we have seen how the design of the line could influence the noise issue. Considering transmission at 160Gbit/s bit rate, it is obvious that the penalty is unacceptable in terms of OSNR when the OSNR on the output becomes lower than 25 dB and so, this helps us to determine the minimum signal power to be injected in inline fibre for a given transmission reach (see Figure 2. 16 and Figure 2. 17). We also became aware of the importance of the span length (and consequently of the gain of inline amplifiers) as we studied 3 different cases (see Figure 2. 17). At last, we have seen the basics of Raman amplification. We will see its application in some transmission examples.

5 Example of studies: some scenarios for transmission at 160 and 40 Gbit/s

In this part, we will consider a transmitter, an optical line and a preamplifier placed just before the photodiode:

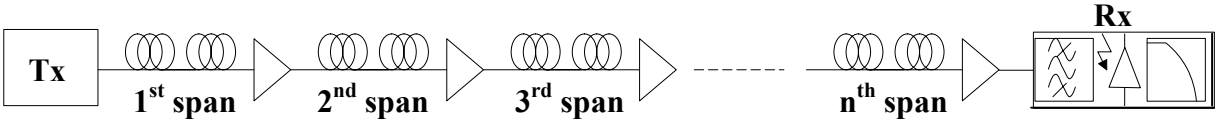

Figure 2. 22: Scheme of the considered transmission line.

The optical line will be constituted by the repetition of n spans made of:

- A positive dispersion fiber characterized by its dispersion D_+, its length L_+ and its attenuation α_+ in dB/km.
- A negative dispersion fiber characterized by its dispersion D_-, its length L_- and its attenuation α_- in dB/km.

For the receiver, we will consider:

- The optical filter with a bandwidth of B_0.
- The quantum efficiency η of the photodiode.
- The bandwidth Be of the electrical filter placed just after the photodiode.

Insertion losses will be neglected.

We consider a sufficiently high signal power so that the signal-ASE beat noise predominates. Under these conditions, an expression of the Q factor is:

$$Q^2 \approx \frac{OSNR.B_{ref}}{B_e}$$

If the signal power after the emitter is $P_{s\text{-}input}$ and the noise spectral density N_i, the signal power in front of the receiver is:

$$P_S = P_{S-input}.10^{-\frac{n}{10}.(\alpha_+.L_+ + \alpha_-.L_- - G)}$$

where α_+, α_-, L_+ and L_- are attenuation coefficients and lengths of inline fibre (+ index) and dispersion compensating fibre (- index). We note T the transmission factor of a span:

$$T = 10^{-\frac{1}{10}.(\alpha_+.L_+ + \alpha_-.L_- - G)}$$

In the same way, if we assume the noise spectral density to be constant in B_o, the noise power in front of the optical receiver in the optical bandwidth B_o is:

$$P_B = M.B_0.\left(T^n.N_i + N_{ASE}.\frac{1-T^{n+1}}{1-T}\right) \text{ if } T \neq 1$$

$$P_B = M.B_0.\left(N_i + N_{ASE}.n\right) \text{ if } T = 1$$

where N_i is the spectral density of noise per state of polarization at the emitter output.

These two relations implicitly assume that the amplified spontaneous emission power spectral density is the same for all inline amplifiers and is equal to N_{ASE}. In the following, we give another relation for general cases.

The transmission distance is $D = n.L_+$. The mean OSNR in front of the receiver can be expressed as:

$$OSNR = \frac{P_S}{2.M.P_B}.\frac{B_o}{B_{ref}}$$

Injecting the expressions of signal and noise powers in this expression, we obtain:

$$OSNR = \left(\frac{P_{s-input}.T^n.\frac{1}{2}}{B_O.[N_i.T^n + N_{ASE-1}.T^{n-1} + ... + N_{ASE-(n-1)}.T + N_{ASE-n}]}\right).\frac{B_0}{M.B_{ref}}$$

Finally, we have the general relation:

$$Q^2 \approx \frac{1}{M.B_e}.\frac{P_{s-input}.T^n.\frac{1}{2}}{[N_i.T^n + N_{ASE-1}.T^{n-1} + ... + N_{ASE-(n-1)}.T + N_{ASE-n}]}$$

where $N_{ASE-i} = h.\nu.G_i.n_{eq-i}$.

If we assume all the amplifiers to be the same on the optical line and thus all the $N_{ASE\text{-}i}$ to be equal, we have the relation:

$$Q^2 \approx \frac{1}{B_e}.\frac{P_{s-input}.T^n.\frac{1}{2}}{M.[N_i.T^n + N_{ASE}.\frac{T^{n+1}-1}{T-1}]} \text{ if } T \neq 1$$

$$Q^2 \approx \frac{1}{(1+\frac{N_{ASE-end}.B_O}{G_{end}.P_B})}.\frac{P_{s-input}.\frac{1}{2}}{M.B_e.[N_i + N_{ASE}.n]} \text{ if } T = 1$$

Numerical application:

On the output of the transmitter, we have a 10 Gbit/s signal:

- P_S=3 dBm (or mean power P_{mean}= 0 dBm).
- OSNR=35 dB.

The optical line is composed of the alternation of:

- Positive dispersion fiber: L_+=80 km, α_+=0,2 dB.km^{-1}.
- Negative dispersion fiber: L_-=15,110 km, α_-=0,6 dB.km^{-1}.
- Optical amplifiers: G= $\alpha_+.L_+ + \alpha_-.L_-$ or G = 25,06 dB and NF = 4 dB.

The receiver is constituted by:

- A photodiode with efficiency η=1
- An electrical filter with a bandwidth B_e=7 GHz.

The OSNR will be estimated in 0,1 nm (i.e. 12,5 GHz).

We are going to estimate the quality factor as a function of the number of spans n:

- The input signal power is: $P_{S\text{-}input}$=3 dBm, i.e. 2 mW.
- The noise spectral density per state of polarization on the output of the emitter is:
  $N_i = P_S./(2.M.B_{ref}.10^{OSNR/10}) = 1{,}26.10^{-14}$ mW.Hz^{-1} because M=2.
- The noise spectral density added on the output of each in line amplifier per state of polarization is:
  $N_{ASE} = h.\nu.G.n_{eq}$ with n_{eq}= (NF-1/G)/2=1.256 so: $N_{ASE} = 5{,}08.10^{-14}$ mW.Hz^{-1}.

Numerical application gives us:

- n=1 → Q² ≈30,4 dB
- n=10 → Q² ≈21,4 dB
- n=30 → Q² ≈16,7 dB

In order to compare these results, we will make the same numerical approach considering a 40 Gbit/s signal instead of 10 Gbit/s:

- Spectral densities of noise remain the same.
- B_e becomes 32 GHz.

Numerical application gives:

- n=1 → Q² ≈24,4 dB
- n=5 → Q² ≈18,3 dB
- n=10 → Q² ≈15,4 dB

At last, we can also estimate this relation for a bit rate of 160 Gbit/s:

- n=1 → Q² ≈18,4 dB
- n=2 → Q² ≈15,9 dB

- n=3 → Q² ≈14,3 dB

In order to consider a more realistic scenario, we now consider that the amplification is enabled by double-stage erbium amplifiers with the following scenario. The input signal power is set to 3 dBm, the attenuation of inline fibre is still 16 dB considering a span length of 80 km. It is then followed by an erbium doped fibre amplifier which output power is equal to -1 dBm and so its gain is 12 dB. The dispersion compensating fibre length is still 15,1 km which produces an attenuation of 9 dB. It is followed by an erbium doped fibre amplifier which gain is set to 13 dB as described in the following figure.

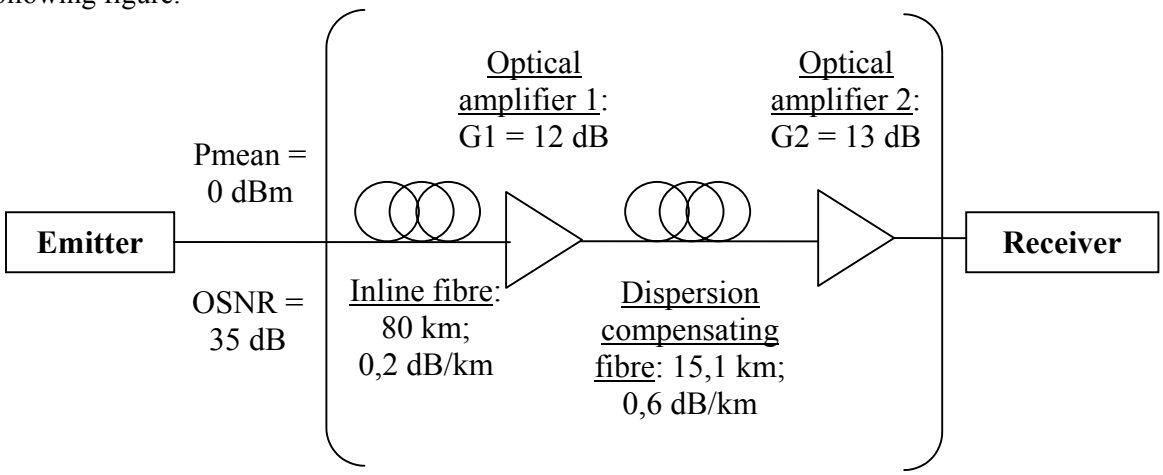

Figure 2. 23: scenario for double-stage amplification.

The optical signal to noise ratio at the emitter output is set to 35 dB. The receiver is composed of an optical filter (bandwidth B_o=2xBit Rate), a photodiode (efficiency η=1) and an electrical filter (bandwidth B_e = 0,7xBit Rate).

The added density of noise per span per state of polarization is:

$$N_{ASE} = h.\nu.\left(G_1.G_2 n_{eq-1}.10^{-\frac{\alpha_{-}.L_{-}}{10}} + G_2.n_{eq-2} \right)$$

où $10^{-\frac{\alpha_{-}.L_{-}}{10}}$ is the attenuation in the dispersion compensating fibre. Assuming a noise factor NF=4 dB for each amplifier, we can deduce:

$$n_{eq-1} = (NF-1/G_1)/2=1.224 \text{ and } n_{eq-2} = (NF-1/G_2)/2=1,231$$

Numerical application gives:

$$N_{ASE} = 9,37.10^{-15} \text{ mW.Hz}^{-1}$$

The spectral density of noise per state of polarization at the emission is still:

$$N_i = \frac{P_S}{2.M.OSNR_{Tx}.B_{ref}} = 1,26.10^{-14} \text{ mW.Hz}^{-1}$$

Assuming the signal-ASE beat noise to be preponderant upon others, we can estimate the quality factor. On the following figure, we can see the evolution of the quality factor for 10, 40 and 160 Gbit/s as a function of distance:

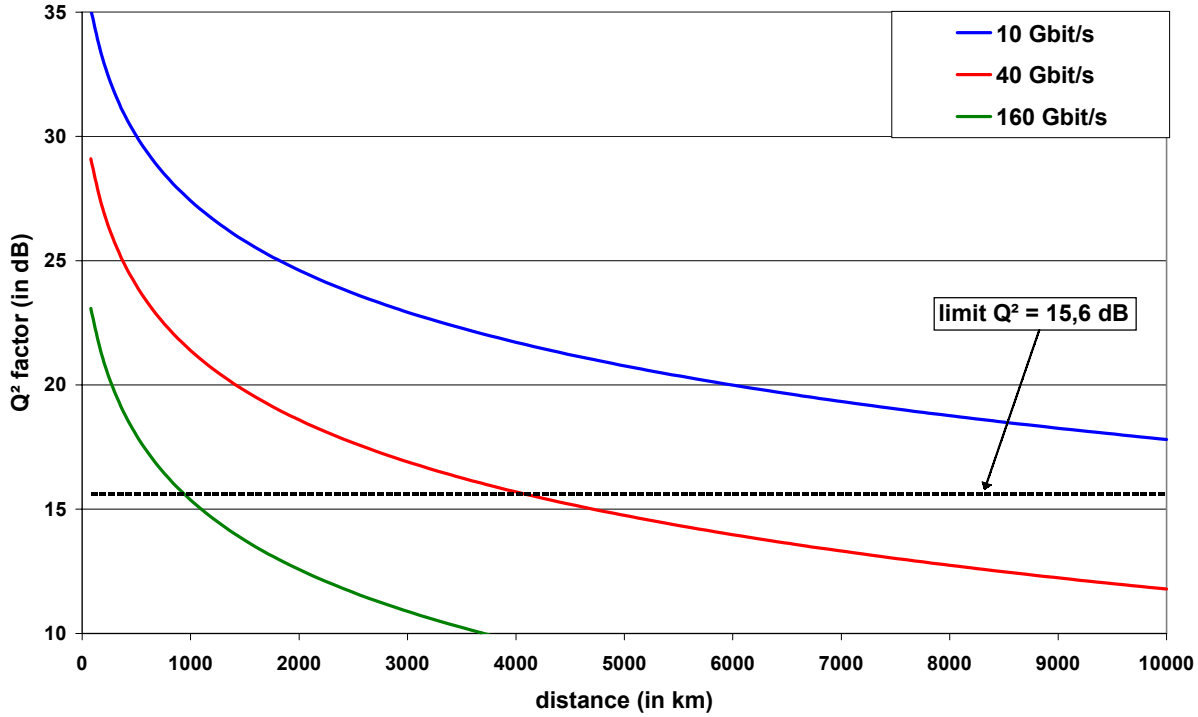

Figure 2. 24: evolution of Q factor versus distance with a mean power of 0 dBm and an emission OSNR=35 dB.

6 Conclusion: optical noise and power analysis

In order to conclude this noise study and to see the real issue it represents, we will simulate all noise effects and estimate the quality factor at 160 Gbit/s for two distinct scenarios. In a first time, amplification is enabled by double stage erbium amplifiers which gains compensate for the loss of the fibre line just before. In a second time, amplification is provided by Raman amplification in the inline fibre with a 20 dB on/off gain and an erbium amplifier compensating for the attenuation in the dispersion compensation fibre.

We first consider SMF as inline fibre (D=17 ps/nm/km) with a span length of 100 km. On Figure 2. 25 are plotted the evolution of the linear Q factor for several injection powers (in solid line for double stage EDFAs and dashed line for hybrid amplification).

With these results, we are now able to predict the impact of noise in an optical transmission system at 160 Gbit/s. We can express this prediction by the statement that, in order to make a transmission on a target reach, and with a choice of amplification scenario, the optical power launched into the fibre should be greater than a certain value. For example, if we want to achieve a transmission on 400 km, the optical power should be more than 0 dBm for a double-stage erbium amplifier scenario or more than -6 dBm for an hybrid scenario as described before.

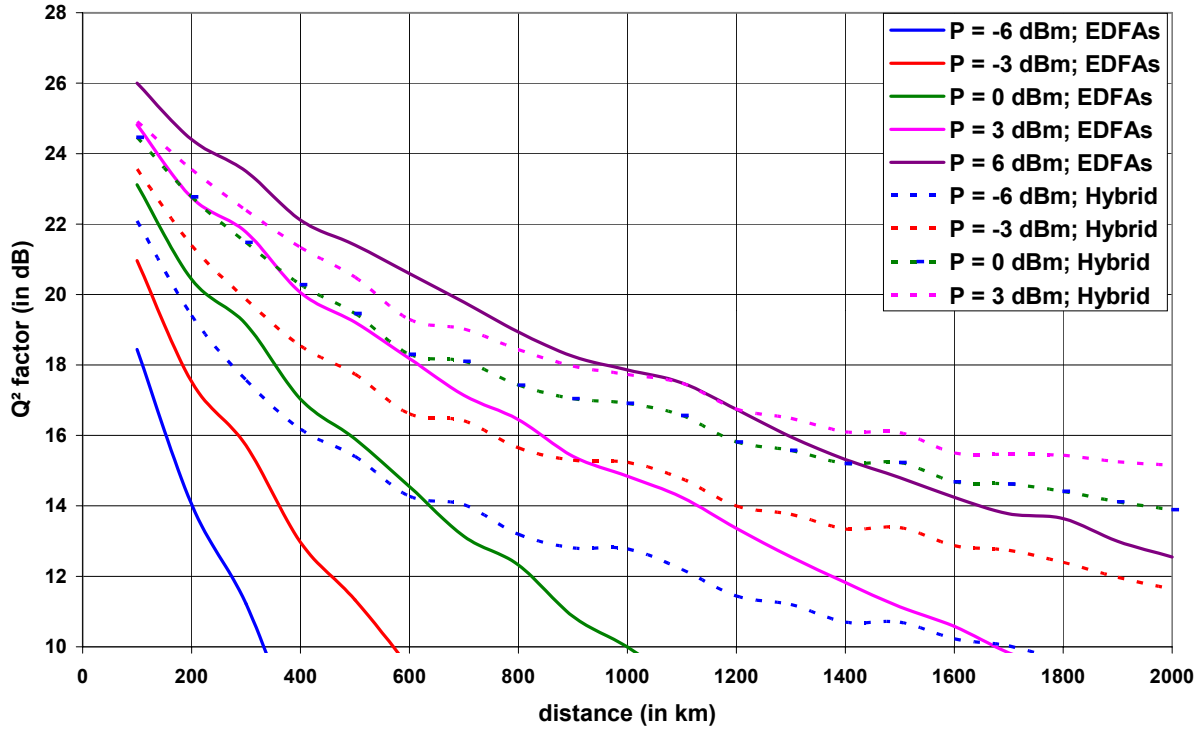

Figure 2. 25: Evolution of linear Q factor versus distance. Span length is 100 km and inline fibre is SSMF.

Such minimum injection powers allowing target reaches are given in the following table for the two considered scenarios. In this case, the span length is set to 100 km and the fibre type is SSMF, which dispersion is 17 ps/nm/km.

Target reach	200	400	600	1000	1500	2000
Min. power for erbium scenario in dBm	-1	2	3	6	7	9
Min. power for hybrid scenario in dBm	-8	-5	-3	-1	1	2

Table 2. 5: minimum injection powers in inline fibre as a function of target reach and amplification scenario for a span length of 100 km of SSMF.

Similar results can be shown for a span length of 80 and 120 km as following.

Target reach	240	400	640	1040	1520	2000
Min. power for erbium scenario in dBm	-3	-1	1	3	5	6
Min. power for hybrid scenario in dBm	-9	-7	-5	-2	-1	0

Table 2. 6. Minimum injection powers in inline fibre as a function of target reach and amplification scenario for a span length of 80 km of SSMF.

Target reach	240	480	600	1080	1560	2040
Min. power for erbium scenario in dBm	2	5	6	9	11	12
Min. power for hybrid scenario in dBm	-5	-2	-1	2	3	5

Table 2. 7: minimum injection powers in inline fibre as a function of target reach and amplification scenario for a span length of 120 km of SSMF.

Similar results can be shown for different fibre types such as LEAF (D=4 ps/nm/km). Indeed, as the inline fibre dispersion is lower, the length of DCF module, which compensates the dispersion after each span, is smaller and the attenuation is also smaller. Thus, the gain of the erbium amplifiers is reduced, which impacts the amount of amplified spontaneous emission noise. The following tables give the minimum injection powers into LEAF fibre in order to make a transmission on a target reach and depending the span length.

Target reach	200	400	600	1000	1500	2000
Min. power for erbium scenario in dBm	-2	1	3	5	7	8
Min. power for hybrid scenario in dBm	-10	-7	-5	-3	-1	0

Table 2. 8: Minimum injection powers in inline fibre as a function of target reach and amplification scenario for a span length of 100 km of LEAF.

Similar results can be shown for a span length of 80 and 120 km as following.

Target reach	240	400	640	1040	1520	2000
Min. power for erbium scenario in dBm	-4	-2	0	2	4	5
Min. power for hybrid scenario in dBm	-12	-10	-8	-6	-4	-3

Table 2. 9: Minimum injection powers in inline fibre as a function of target reach and amplification scenario for a span length of 80 km of LEAF.

Target reach	240	480	600	1080	1560	2040
Min. power for erbium scenario in dBm	2	5	6	9	10	11
Min. power for hybrid scenario in dBm	-7	-4	-3	0	1	2

Table 2. 10: Minimum injection powers in inline fibre as a function of target reach and amplification scenario for a span length of 120 km of LEAF.

7 References

1. "Erbium-doped fiber amplifiers: principles and applications", E. Desurvire, Wiley-Interscience publication.
2. "The noise figure of optical amplifiers", H.A. Haus, Photonics Technology Letters, Vol. 10, N° 11, November 1998, pages 1602-1604.
3. "160 Gbit/s error-free demultiplexing by ultrafast optical gate monolithically integrating photodiode and electroabsorption modulator", Kodama, S. et al, Electronics Letters , Vol. 38, N°24, 21 Nov. 2002, Pages 1575-1576.
4. "Clock recovery and demultiplexing performance of 160-gb/s OTDM field experiments", Turkiewicz J.P. et al, Photonics Technology Letters, IEEE , Vol.16 , N°6 , June 2004, pages 1555-1557.
5. "Dependence of optically preamplified receiver sensitivity on optical and electrical filter bandwidths – Measurement and simulation", Pfennigbauer M., Photonics Technology Letters, Vol. 14, N°6, June 2002, pages 831-833.
6. "Noise and intersymbol-interference properties of OTDM and ETDM receivers", M.M. Strasser et al, Photonics Technology Letters, Vol. 16, N°1, January 2004, pages 248-250.
7. "Pump interactions in a 100 nm bandwidth Raman amplifier", H. Kidorf et al, Photonics Technology Letters, Vol. 11, N°5, May 1999, pages 530-532.
8. "Lightwave systems with optical amplifiers", N.A. Olsson, Journal of lightwave technology, Vol. 7, N°7, July 1989.
9. "Fibre Raman amplifier properties for applications to long-distance optical communications", Aoki Y., Optical and Quantum Electronics, Vol. 21, S89-S104, 1989.
10. "Impact of the fiber type and non-linear management over the performance of a 16x40 Gb/s DWDM transmission system", Pincemin E., Non-Linear Guided Waves conference, 28-31/03/04, Toronto, Canada.
11. "Gain saturation in fiber Raman amplifiers due to stimulated Brillouin scattering", Foley B., Journal of lightwave technology, Vol. 7, N°12, December 1989, pages 2024-2030.
12. "Effects of Raman noise and double Rayleigh backscattering on bidirectionally Raman-pumped systems at constant fibre nonlinearity", Essiambre R.-J., 27th European Conference on Optical Communication 2001, Vol. 2 , 30 Sept.-4 Oct. 2001, Pages:108 – 109
13. "Experimental validation of DRS impact on transmission systems at 2.5, 10 and 40 Gbit/s", Dibon C. et al, European Conference on optical communication, Copenhagen, Denmark, Paper 3.1.4
14. "Optimal design of flat-gain wide-band fiber Raman amplifiers", V.E. Perlin et al, Journal of Lightwave Technology, Vol. 20, N°2, February 2002, pages 250-254.
15. "Comparison of engineering scenarios for Nx160 Gb/s WDM transmission systems." Cuenot B.; Photonics Technology Letters, IEEE , Volume: 15 , Issue: 6 , June 2003, Pages:864 – 866
16. "Optimization of pumping schemes for 160 Gbit/s single-channel Raman amplified systems", Z. Xu et al, Photonics Technology Letters, IEEE , Vol.16 , N°1 , January 2004, pages 329-331.
17. "Experimental comparison of all-Raman and Raman/EDFA hybrid amplifications using 40 Gbit/s-based transmissions over 400 km TW-RS fibre", Y. Zhu et al, Electronics Letters, Vol. 38, N° 16, 1st August 2002, pages 893-895.
18. "40 Gbit/s RZ unrepeatered transmission over 252 km SMF using Raman amplification", M. Gunkel et al, Optical Fiber Communication Conference and Exhibit, 2001. Optical Fiber communication Conference, March 17-22 2001, Anaheim, California ,Volume: 2 , 2001, Pages:TuU3-1 - TuU3-3 vol.2

Analysis of propagation effects

1 First approach of transmission effects

The propagation of an electromagnetic field E(z,t) in a fibre is governed by Schrödinger equation [1,2]:

$$\frac{\partial E}{\partial z}+i\frac{\beta_2}{2}\frac{\partial^2 E}{\partial t^2}-\frac{\beta_3}{6}\frac{\partial^3 E}{\partial t^3}-i\gamma\left|E\right|^2E+i\gamma_R E\frac{\partial\left(\left|E\right|^2\right)}{\partial t}+\gamma_S\frac{\partial\left(\left|E\right|^2E\right)}{\partial t}+\frac{\alpha}{2}E=0$$

where β_2 (in ps^2/km) and β_3 (in ps^3/km) are related to the dispersion in the fibre. D (in ps/nm/km), the local dispersion of the fibre, and S (in $ps/nm^2/km$), the local dispersion slope of the fibre, are related to these parameters by the following relations:

$$\beta_2=-\frac{\lambda^2}{2\pi.C}.D$$

$$\beta_3=\left(\frac{\lambda}{2\pi.C}\right)^2.\left(\lambda^2.S+2.\lambda.D\right)$$

γ is the non linear coefficient denoting Kerr effects. γ_R and γ_S are non-linear coefficients related to stimulated Raman scattering and self-steepening non-linear effects. When there are no non-linear effects ($\gamma = \gamma_r = \gamma_S = 0$) and when the third-order dispersion is not considered ($\beta_3 = 0$), solutions of this equation can be found using the Fourier method and it can be shown that gaussian pulses are a family of solutions to this equation [1].

1.1 Modelling of transmission effects

The complete solution of this equation does not have a simple analytical expression and we can only approximate it under certain conditions. The aim of this introduction chapter is to explain what were the different methods I have used.

A common method used in numerical simulations is called split-step Fourier method. We can understand it when decomposing the Schrödinger equation under two distinct terms when writing:

$$\frac{\partial E}{\partial z}=\left(-i\frac{\beta_2}{2}\frac{\partial^2 E}{\partial t^2}+\frac{\beta_3}{6}\frac{\partial^3 E}{\partial t^3}-\frac{\alpha}{2}E\right)+\left(i\gamma\left|E\right|^2E-i\gamma_R E\frac{\partial\left(\left|E\right|^2\right)}{\partial t}-\gamma_S\frac{\partial\left(\left|E\right|^2E\right)}{\partial t}\right)$$

The first term represents linear transmission effects (dispersion and attenuation) and the second tem represents non linear effects. The split-step Fourier method gives an approximate solution to this equation by assuming that these two kinds of effects (linear and non-linear) do not interact over a small distance. It is then possible to describe the evolution of an optical field over this small distance by a two-steps rule: at first, non linearities are considered alone in time domain whereas in a second step, dispersive and attenuation effects are applied in spectral domain to the resulting solution of the first step. This method is massively used in numerical simulation tools in order to fasten the resolution of differential equations. Moreover, it is the case of the software I have used for the optical transmission simulations in my research studies and mainly VPI TransmissionMaker and Matlab.

Another method we have used is related to an approximation of the solution of this equation by an ansatz function [2,3,4]. This method refers to the collective variable theory. To simplify calculation, the ansatz function is Gaussian with the form:

$$E(z,t) = X_1.e^{-\frac{(t-X_2)^2}{X_3^2}}.e^{i.\left(\frac{X_4}{2}.(t-X_2)^2+X_5.(t-X_2)+X_6\right)}$$

We therefore can link these parameters to the pulse peak power X_1^2 (in W), the pulse temporal position X_2 (in ps), the full-width-at-half-maximum $X_3.\sqrt{2.\ln(2)}$ (in ps), the chirp X_4 (in ps^{-2}), the frequency deviation X_5 (in ps^{-1}), and the phase X_6 (in radians).

Along this chapter dealing with linear and non-linear effects, I will use several times the results given by the collective variable theory as it gives a very simple understanding of propagation based effects. In a few words, we first introduce its basics in order to have a good understanding of its limits: the collective variable theory can be used to investigate effects that are implemented in the non-linear Schrödinger equation (or in any phenomena governed by differential equation) but it cannot be used to study statistic effects such as polarization mode dispersion. The limits of application of this theory to the case of fibre transmission remains in the stability of the ansatz function: considering linear effects, Agrawal has shown [1] that gaussian functions were solution of the linear differential equations but non-linearities induce degradation which affects the gaussian shape of the pulse.

While using this theory, the gaussian shape is conserved whatever the importance of non-linear effects which are considered as small perturbations. That's why it cannot be used when these non-linear perturbations are too strong. In the case of a single optical pulse, the application of the collective variable theory leads to the following differential equations ($\dot{X}_i = \frac{\partial X_i}{\partial z}$) [2,3]:

$$\dot{X}_1 = -\frac{1}{2}.\alpha.X_1 + \frac{1}{2}.(\beta_2 - \beta_3.X_5).X_1.X_4$$

$$\dot{X}_2 = -\beta_2.X_5 + \beta_3.\left(\frac{1}{2.X_3^2} + \frac{X_5^2}{2} + \frac{X_3^2.X_4^2}{8}\right) + \frac{3}{2.\sqrt{2}}.\gamma_S.X_1^2$$

$$\dot{X}_3 = -(\beta_2 - \beta_3.X_5).X_3.X_4$$

$$\dot{X}_4 = -(\beta_2 - \beta_3.X_5).\left(\frac{4}{X_3^4} - X_4^2\right) - \frac{\sqrt{2}.X_1^2.(\gamma - \gamma_S.X_5)}{X_3^2}$$

$$\dot{X}_5 = \frac{\sqrt{2}.\gamma_R.X_1^2}{X_3^2} + \frac{\gamma_S.X_1^2.X_4}{\sqrt{2}}$$

$$\dot{X}_6 = \beta_2.\left(\frac{1}{X_3^2} - \frac{X_5^2}{2}\right) + \beta_3.\left(\frac{X_5^3}{3} + \frac{X_3^2.X_4^2.X_5}{8} - \frac{X_5}{2.X_3^2}\right) + \frac{X_1^2.(5.\gamma + \gamma_S.X_5)}{4\sqrt{2}}$$

Equation 3. 1. Differential equations for parameters of the ansatz function.

From these equations , we can derive a program computing the evolution with z of the collective variables X_1, X_2, X_3, X_4, X_5, X_6. Knowing the values of the collective variables at a given position z and setting a sample length dz for the propagation into the fibre, we can calculate the values of the collective variables for every position $z = n \times dz$. Such an algorithm is simple to elaborate because the increment $\dot{X}_i = \frac{\partial X_i}{\partial z}$ is easy to compute but it is better for more precision to calculate this evolution with the Runge-Kutta method implemented in Matlab sofware.

In Figure 3. 1, we have represented the evolution in a linear regime ($\gamma = \gamma_R = \gamma_S = 0$) of chirp versus pulse width (i.e. X_4 as a function of X_3) for different initial pulse widths and on 80 km of SMF

fibre. On this graph, lines represent the calculation results through the collective variable method whereas dots represent these same calculation results through the split-step Fourier transform method. We can first notice the very good similarity between these results concerning pulse chirp and width evolutions. A second remark to be made concerns the broadening of the pulse due to fibre dispersion.

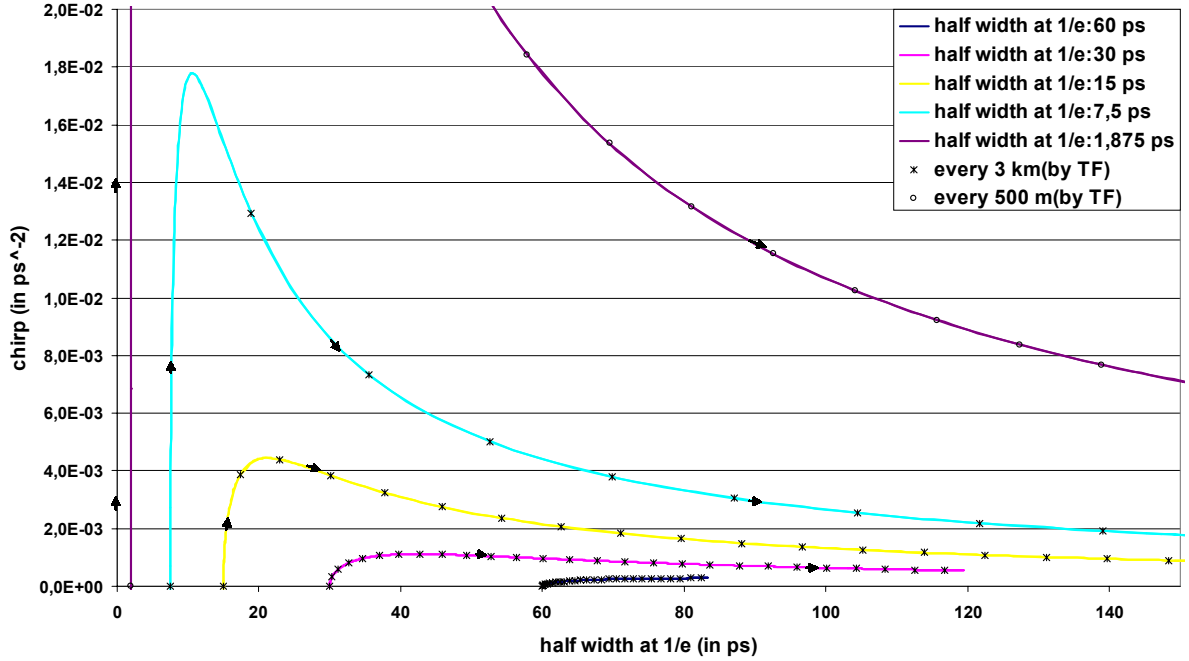

Figure 3. 1. Evolution in a linear regime of chirp X_4 versus the pulse width X_3 for different initial pulse widths on 80 km of SMF.

We see on this graph that the final pulse width after 80 km of SMF fibre are higher as the initial pulse width is small. Indeed, the final pulse width after 80 km of SMF fibre is given by the relation [1]:

$$\frac{T_1}{T_0} = \sqrt{1+\left(\frac{z}{L_D}\right)^2} = \sqrt{1+\left(\frac{z\times|\beta_2|}{T_0^{\,2}}\right)^2}$$

where T_0 (respectively T_1) is the half width at 1/e in intensity at z=0 (respectively at z km) of the pulse and is related to the collective variable X_3 by the relation $X_3(z=0) = T_0.\sqrt{2}$. We can now compare the final pulse width for different bit rates and 80 km of SMF ($|\beta_2| = 21{,}667$ ps²/km):

- At 10 Gbit/s, with T_0=24 ps (corresponding to FWHM=40 ps): $\frac{T_1}{T_0} = 3{,}1$.
- At 40 Gbit/s, with T_0=6 ps (corresponding to FWHM=10 ps): $\frac{T_1}{T_0} = 48{,}1$.
- At 160 Gbit/s, with T_0=1,5 ps (corresponding to FWHM=2,5 ps): $\frac{T_1}{T_0} = 770{,}4$.

At 160 Gbit/s, it means that the pulse width after 80 km of fibre is bigger than 1 ns. Due to dispersion, the pulse broadens so rapidly that it will be expanded on more than 700 time bits after 80 km of SMF fibre. It is very important to understand this point because it will be the driver for intrachannel pulses interactions which play a fundamental role in 160 Gbit/s transmissions. As a matter of fact, the broadening of all pulses in the 160 Gbit/s sequence induces pulse interaction giving rise to intrachannel non-linear effects known as intrachannel four-wave mixing and intrachannel cross-phase modulation.

1.2 Tolerance to dispersion in linear propagation

The following criterion is defined for tolerance: the dispersion tolerance is calculated for a relative variation of the pulse width of 10 % compared to the width of the transmitted pulse. In the linear case, the dispersion tolerance is obvious because we know the variation law for the width:

$$\sqrt{1+\left(\frac{L}{L_D}\right)^2} = 1.1 \Leftrightarrow L = L_D.\frac{\sqrt{21}}{10}$$

where L_D is the dispersion length ($L_D = \frac{T_0^2}{\beta_2}$).

From this relation, knowing the dispersion of DCF (|D|=90ps/nm/km), the dispersion tolerance is:

$$Tolerance = \pm\frac{T_0^{\,2}}{|\beta_2|}.\frac{\sqrt{21}}{10}.|D_{DCF}| = \pm T_0^{\,2}.\frac{\sqrt{21}}{10}.\frac{2\pi.C}{\lambda^2}$$

For example, we have:

- At 10 Gbit/s: T_0=30 ps, Tolerance = ± 323.6 ps/nm (7200 m of DCF)
- At 40 Gbit/s: T_0=7.5 ps, Tolerance = ± 20.2 ps/nm (450 m of DCF)
- At 160 Gbit/s: T_0=1.875 ps, Tolerance = ± 1.3 ps/nm (30 m of DCF)

On the following figure, we represented a pulse for different levels of cumulated dispersion in order to visualize the deformation caused by dispersion.

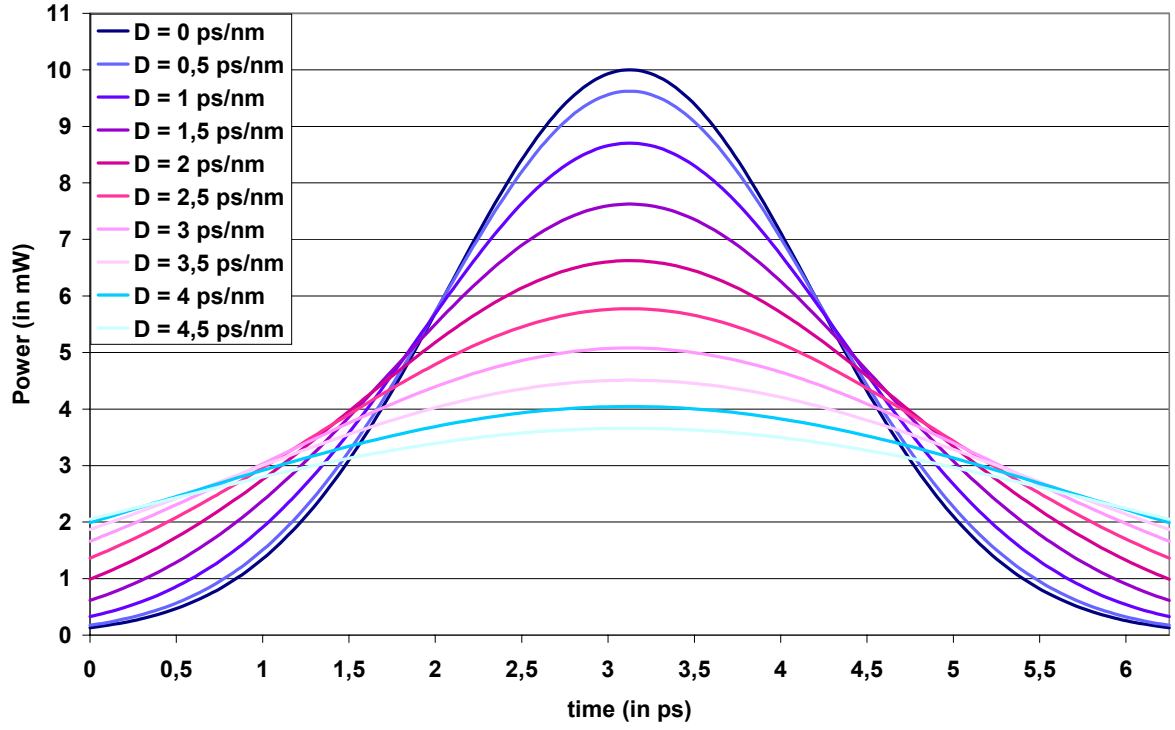

Figure 3. 2. Visualization of pulse deformation due to cumulated dispersion (initial pulse width: 2,5 ps).

As we have seen, the dispersion tolerance is very low. Furthermore, considering the temperature dependence of chromatic dispersion, we can show that the problem is even more complex. As a matter of fact, the variation of dispersion with temperature is expressed by the relation:

$$\frac{dD}{dT} = \frac{1}{4}\left(\lambda - \frac{\lambda_0^{\,4}}{\lambda^3}\right)\frac{dS_0}{dT} - \frac{S_0\lambda_0^{\,3}}{\lambda^3}\frac{d\lambda_0}{dT} \approx \frac{d\lambda_0}{dT}.R$$

where S_0 is the dispersion slope at λ_0 (wavelength where the dispersion D is equal to zero) and R is equal to $-\frac{S_0\lambda_0^{\ 3}}{\lambda^3}$. The first term can be generally neglected [5]. Vorbeck has shown [6] that a variation of ±10 degree is not critical for 40 Gbit/s transmission up to 900 km. For 160 Gbit/s systems, the dispersion variation is comparable to the dispersion tolerance even for 100 km and so, tunable dispersion compensation is needed. As a matter of fact, the cumulated dispersion variation can be expressed by the following relation:

$$\Delta D.L \approx \left(\frac{d\lambda_0}{dT}.R\right).\Delta T.L$$

where L is the transmission distance and ΔT is the temperature variation. With the example of NZ-DSF fibre, the coefficient $\frac{d\lambda_0}{dT}.R$ is nearly equal to -0,0025 ps/nm/km/°C. Assuming no temperature variation for the dispersion compensating fibre (as it is placed inside the location sites and thus less dependent on temperature variations), we obtain the following figure showing cumulated dispersion variation as a function of the transmission distance for three different temperature ranges:

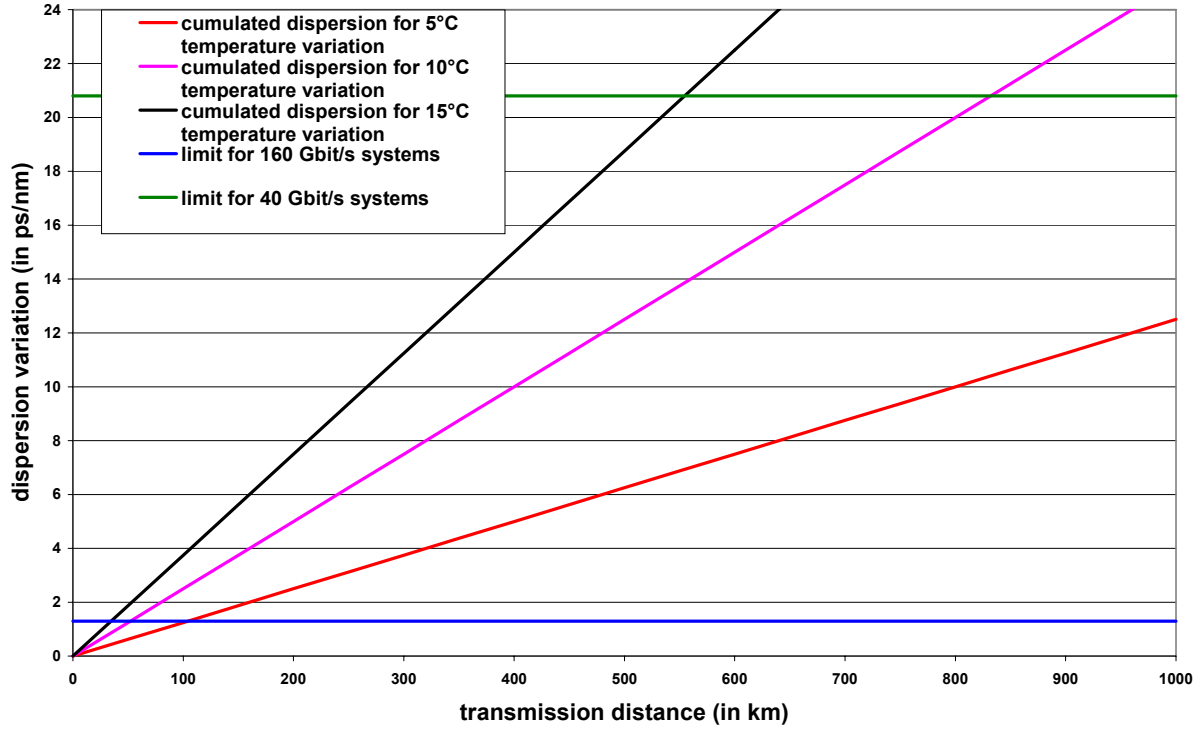

Figure 3. 3. Effects of temperature variation on dispersion variation.

At last, we would like to mention the power penalty resulting from the dispersion variation in order to highlight its importance. The variation of cumulated dispersion induces a variation of the peak power of the pulses as we have:

$$P_{peak} = \frac{P_0}{\sqrt{1+\left(\frac{z}{L_D}\right)^2}}$$

Consequently, we can define a power penalty in dB by:

$$Power\_penalty = 10.\log\left(\frac{P_{peak}}{P_0}\right) = -5.\log\left(1+\left(\frac{z}{L_D}\right)^2\right)$$

$$Power\_Penalty = 10.\log\left(\frac{P_{peak}}{P_0}\right) = -5.\log\left(1+\left(\frac{\lambda^2.Cumulated\_Dispersion^2}{2.\pi.C.T_0^{\ 2}}\right)^2\right)$$

For a 2,5 ps initial pulse width, the power penalty for some values of cumulated dispersion is displayed in Table 3. 1:

Cumulated dispersion in ps/nm	Power Penalty in dB
0	0
1	- 0,6
2	- 1,8
5	- 4,8

Table 3. 1. Power penalty as a function of cumulated dispersion.

We see that this penalty is already high but we also need to remind that, as a consequence of the pulse width increase, the peak power decreases but it will also result in overlapping between pulses and interferences between symbols. The suppression of this impairment is highly desirable and this is the reason why an important task for the emerging of such high bitrate systems consists in the development of devices for tunable dispersion compensation [7].

1.3 Effects of dispersion slope in linear propagation

For a positive pulse chirp (X_4>0), the fibre dispersion is responsible for pulse broadening in positive dispersion fibre and pulse compression in negative dispersion fibre. If the pulse chirp is negative, it is exactly the opposite. Each fibre has its own characteristics as displayed in Table 1.2. The dispersion slope characterizes the linear evolution of the dispersion with frequency.

In a general way, we have the relation:

$$\beta(\omega) = \beta_0 + \beta_1.(\omega-\omega_0) + \frac{1}{2}\beta_2.(\omega-\omega_0)^2 + \frac{1}{6}\beta_3.(\omega-\omega_0)^3 + \ldots$$

This implies that when considering several channels transmission, the dispersion is not the same for adjacent channels and consequently, the compensation of this dispersion may not be perfect for all channels.

For example, if we want to transmit 9 channels spaced by 400 GHz: transmitting on one span of 100 km SMF (D = 17 ps/nm/km; S = 0,058 ps/nm²/km) only, the inline fibre dispersion is fully compensated for the central channel by DCF (D = -90 ps/nm/km; S = -0,45 ps/nm²/km). On the first channel (whose spacing from the central channel is 12,8 nm or 1,6 THz), the cumulated dispersion is:

$$Cumulated\_Dispersion = (17-0{,}058.*12{,}8).100 + (-90+0{,}45*12{,}8).(100.\frac{17}{90})$$

$$Cumulated\_Dispersion = 34{,}56 \text{ ps/nm}$$

This value is about 25 times greater than the tolerance for a 2,5 ps pulse width. Thus, we see that this characteristic of fibre has a great repercussion on optical communications systems as, even if the first order dispersion is compensated for the central channel, it is not the case over the complete signal bandwidth. In fact, per channel compensation is needed if the dispersion and the dispersion slope are not both compensated by the dispersion compensation fibre. This characteristic is inherent to high bit rate systems only as the dispersion tolerance is proportional to the square of the pulse width, i.e. basically to the inverse square of the bit rate. Of course, in order to avoid per channel dispersion compensation, the dispersion slope of DCF is chosen in order to compensate the one of inline fibre but, as we have seen in the previous chapter, the tolerance is so small that it is difficult to do so.

Even when first order dispersion is fully compensated for a channel, the cumulated dispersion slope impacts the pulse shape and especially at high bit rate as 160 Gbit/s. Thus, the higher order dispersion is responsible for the oscillations near the trailing edge of the pulse [1]. On the following figure, we have estimated the degradation due to cumulated dispersion slope with respect to the Eye Opening Factor parameter at 160 Gbit/s and we also show how a pulse is corrupted for a cumulated slope dispersion of 1 ps/nm².

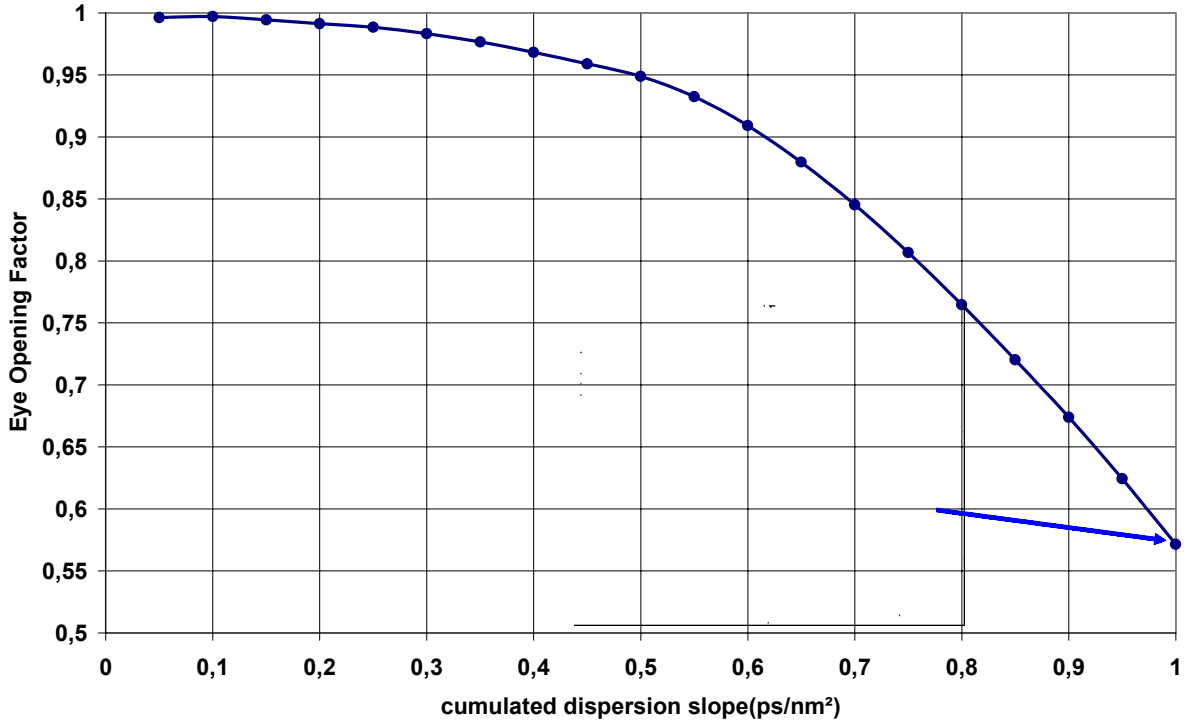

Figure 3. 4. Eye Opening Factor as a function of cumulated dispersion slope for a pulse width of 2,5 ps and visualization of the pulse shape with a cumulated dispersion slope of 1 ps/nm².

It is then possible to estimate the penalty from these results. For example, a cumulated dispersion slope of 0,75 ps/nm² is responsible for an eye opening factor of 0,8 which means that the penalty is around 1 dB, i.e. -10log(0,8). When transmitting on 100 km of SMF (D=17 ps/nm/km; Dslope=0,058 ps/nm²/km) and compensating fibre dispersion with classical DCF (D=-90 ps/nm/km; Dslope= -0,45 ps/nm²/km), the residual dispersion slope is:

$$Cumulated\_Dispersion\_slope = (100 \times 0{,}058) + (-0{,}45).(100.\frac{17}{90}) = -2{,}7 \text{ ps/nm}^2$$

We therefore realize the importance of compensating both dispersion and dispersion slope in order to optimize the transmission system at 160 Gbit/s.

Dispersion slope also has another repercussion in our study and even with a unique channel transmission: indeed, the spectral width is so high that dispersion is varying for frequency components of the pulse. The deformation caused by this effect is described by Agrawal [1] with the relation of the pulse width evolution:

$$\frac{\sigma}{\sigma_0} = \sqrt{\left(1 + \frac{C.\beta_2.z}{T_0^{\,2}}\right)^2 + \left(\frac{\beta_2.z}{T_0^{\,2}}\right)^2 + \left(1 + C^2\right)\left(\frac{\beta_3.z}{2.T_0^{\,3}}\right)^2}$$

where C is the pulse chirp. From this equation, we can estimate the importance of β_3 and the error made on the broadening of the pulse when it is not taken into account:

$$\Delta\sigma = \sqrt{\frac{\left(1+\frac{C.\beta_2.z}{T_0^{\,2}}\right)^2 + 2.\left(\frac{\beta_2.z}{T_0^{\,2}}\right)^2 + \left(2+C^2\right).\left(\frac{\beta_3.z}{2.T_0^{\,3}}\right)^2}{\left(1+\frac{C.\beta_2.z}{T_0^{\,2}}\right)^2 + 2.\left(\frac{\beta_2.z}{T_0^{\,2}}\right)^2}}$$

$$\Delta\sigma = \sqrt{1+\frac{\left(2+C^2\right).\left(\frac{\beta_3.z}{2.T_0^{\,3}}\right)^2}{\left(1+\frac{C.\beta_2.z}{T_0^{\,2}}\right)^2 + 2.\left(\frac{\beta_2.z}{T_0^{\,2}}\right)^2}}$$

At 160 Gbit/s, with a chirp-free pulse (C=0) with an initial pulse width of 2,5 ps (i.e. T_0=1,5 ps) and considering SMF fibre, this ratio is:

$$\Delta\sigma = \sqrt{1+\frac{7{,}402.10^{-4}.z^2}{1+185{,}46.z^2}} \approx 1{,}000002$$ when z is typically some kilometres.

$$\Delta\sigma \approx 1$$ when z is around some metres.

Even for LEAF fibre, this ratio is comprised between 1 and 1,000042.

This means that dispersion slope doesn't affect much the broadening of the pulse at 160 Gbit/s and that its effect can be neglected compared to dispersion and especially when investigating interaction with other effects. However, we have seen that it should be taken into account when considering the entire transmission system as the tolerance for cumulated dispersion slope is only 0,75 ps/nm². For this last reason, an important issue for the future of high bitrate optical communications is the efficiency of devices which compensate the dispersion slope [8,9].

2 Non-linear effects study

In order to lower the complexity of the problem, we will distinctly consider all non linear effects. This chapter considers the case of a single channel transmission and therefore, the impact of inter-channel non linear effects is not investigated.

We first focus our attention on the non-linear terms to understand their meanings. If we assume the electromagnetic field to be a sum of several electromagnetic fields:

$$E = u_0 + u_1 + u_2 + ... + u_n$$

Then, the development of the last term in Schrödinger equation is:

$$\gamma.|E|^2.E = \gamma.|u_0 + u_1 + u_2 + ... + u_n|^2.(u_0 + u_1 + u_2 + ... + u_n)$$

$$\gamma.|E|^2.E = \gamma.\left[(u_0 + u_1 + ... + u_n).(u_0 + u_1 + ... + u_n)^*\right](u_0 + u_1 + ... + u_n)$$

$$\gamma.|E|^2.E = \left(\sum_{j=0}^{n}\gamma.|u_j|^2.u_j^{\,*}\right) + \left(2.\gamma.\sum_k |u_k|^2.\left(\sum_{j\neq k} u_j\right)\right) + \left(\gamma.\sum_{\substack{l,m,n \\ n\neq l \\ n\neq m}} u_l.u_m.u_n^{\,*}\right)$$

The first term in the right side of the equation represents self-phase modulation. The second term represents cross-phase modulation and the last term represents four-wave mixing. In the next chapters, we will consider these effects independently if it is possible in order to quantify their impact on the transmission.

2.1 Intrachannel non linear effects

2.1.1 Self-phase modulation

The first non-linear effect to be studied here is self-phase modulation. This effect is due to the nonlinearity occurring in the fibre as its impact depends on γ, the non-linear coefficient of the fibre. If we consider this non-linear effect as a small perturbation to the gaussian model (according to the perturbation theory [2,3]), collective variable theory enables to see how self phase modulation impacts the parameters of the optical pulse. If we do not consider Raman scattering nor self-steepening effect, the evolution of the pulse chirp X_4 is ruled by the following differential equation:

$$\dot{X}_4 = -(\beta_2 - \beta_3 . X_5)\left(\frac{4}{X_3^4} - X_4^2\right) - \frac{\sqrt{2}.X_1^2.\gamma}{X_3^2}$$

As a result, self phase modulation is responsible for the apparition of a non-linear chirp as can be seen in the last term of the differential equation ruling the evolution of the pulse chirp.
Additionally, the evolution of the pulse width is described by the following equation:

$$\dot{X}_3 = -(\beta_2 - \beta_3 . X_5).X_3 . X_4$$

We see that its impact is proportional to the peak power of the pulse(X_1^2) and inversely proportional to the square pulse width. This non-linear chirp is responsible for a modified evolution of the pulse chirp and consequently of the pulse width compared to the linear regime. The following graph shows the influence of self-phase modulation on the pulse width ratio (final pulse width/initial pulse width) when varying the input power and the inline fibre dispersion. Non-linear effects are not modelled in DCF in order to focus on inline fibre. We consider erbium amplification, the span length is set to 100 km and the transmission is made on 3 spans. Cumulated dispersion is compensated after each span. The fibre effective area is set to 80 μm^2:

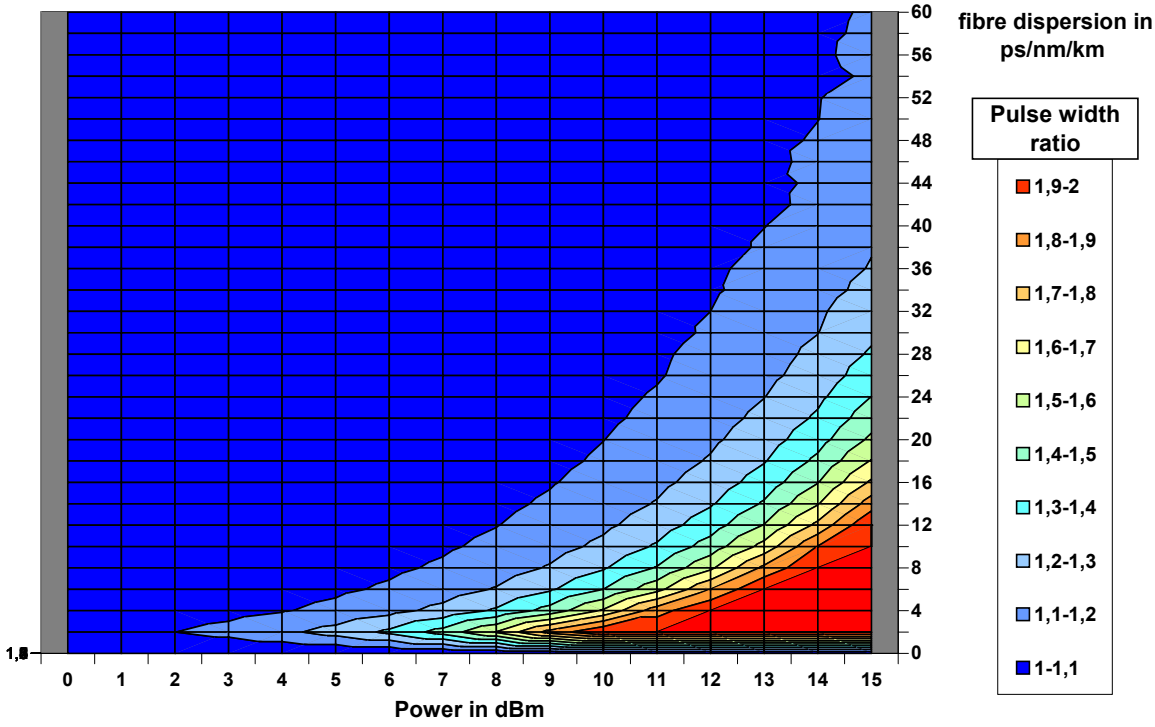

Figure 3. 5. Ratio of a pulse width after and before transmission over 3 spans of 100 km of fibre as a function of the inline fibre dispersion and the optical power (initial pulse width=2,5 ps).

We see that this effect is critical when the dispersion of the inline fibre is small and/or when the input power is high. Therefore, in the design of the transmission systems at 160 Gbit/s or higher, we should take into account the restrictions.

A way to lower the impact of self-phase modulation is to use pre-dispersion. As a matter of fact, we have seen that the impact of this non-linear effect is proportional to the peak power of the

pulse and inversely proportional to the square pulse width. Using a slight pre-dispersion, we can both lower the peak power and increase the pulse width.

This solution is investigated in the following graphs where we simulate the propagation of a pulse in 3 spans of 100 km for various injection powers and for dispersion fibre values set to 4, 8 and 17 ps/nm/km. Non-linear effects are not modelled in the predispersion fibre as the injection power into it can be sufficiently low and an optical amplifier can be placed between the predispersion fibre and the beginning of the line. Predispersion value ranges from -300 ps/nm to + 300 ps/nm. At the beginning of each span, the cumulated dispersion is equal to the predispersion value. Cumulated dispersion is totally compensated after the last span.

We have seen in the precedent chapter that, in order to obtain reach a transmission distance of 1000 km using double stage erbium amplifiers with 100 km span length, the injection power into the inline fibre should be at least 6 dBm. A common criterion is to consider that pulse width variation should be less than 10 %. These results show that if no predispersion (and no post-dispersion) is used, only SMF fibre dispersion (D = 17 ps/nm/km) is high enough to guarantee a small effect of self-phase modulation. For other fibres, self-phase modulation is responsible for a too strong variation of the pulse width and pre-dispersion (associated with post-dispersion) should then be used in order to limit its impact.

The deformations caused by self-phase modulation vary depending the amount of pre dispersion and the injection power for each inline fibre dispersion value. For zero pre dispersion, we obtain an increased impact of this non-linear effect inducing a strong variation of the pulse width. However, this increase of the pulse width due to a non-linear chirp can be compensated by an additional compensation. In that case, the total cumulated dispersion in front of the receiver will not be equal to zero.

With slightly negative pre dispersion, this effect is still present for high injection power. Indeed, at the beginning of the inline fibre, the pulse narrows and then broadens again because of accumulated dispersion. At zero cumulated dispersion, the peak power is high enough and the pulse width is small enough so that self-phase modulation induces deformation. At the opposite, for positive pre dispersion, the pulse is always broadening in the inline fibre and so the impact of self phase modulation is reduced.

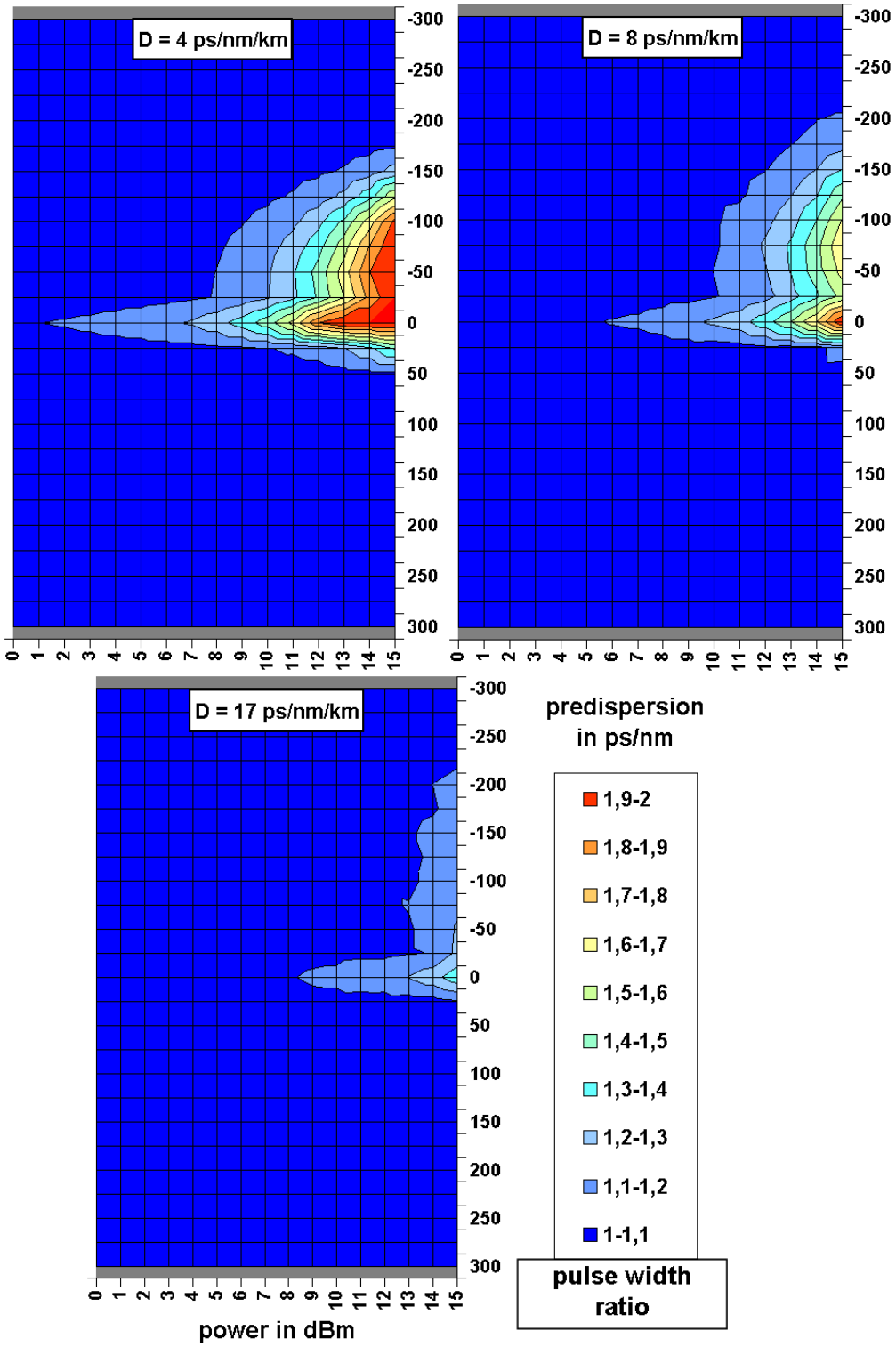

Figure 3. 6. Ratio of a pulse width after and before transmission on 3x100 km as a function of pre dispersion and input power for 3 different inline fibre dispersion values. The residual dispersion per span is zero.

As a conclusion to the impact of self phase modulation, we have seen that self phase modulation needs to be taken into account in high bit rate systems design as it directly impacts the pulse width variation. We have seen that high dispersion fibres were preferable to avoid this non linear effect. However, using predispersion, it is possible to lower the impact of this effect. Of course, other techniques [10] exist to reduce this impairment but in this study, we will mainly focus our attention on the use of dispersion management.

For example, if we want to achieve a transmission over 10 spans of 100 km of LEAF (D=4 ps/nm/km), we have seen in the previous chapter relative to noise studies that we need a minimum injection power of 4 dBm. With such a power level, self-phase modulation impacts the transmission and the pulse width variation is already more than 10 % after the third span (see Figure 3. 5). Using a slight predispersion, for example 50 ps/nm, we can lower this modification so that the variation is below 10 % as it can be seen on Figure 3. 6.

2.1.2 Intrachannel four-wave mixing

Intrachannel four-wave mixing is due to the interaction of two or three pulses. It appears in the non-linear term of Schrödinger equation under the form $\gamma . \sum_{\substack{l,m,n \\ n \neq l \\ n \neq m}} u_l . u_m . u_n^*$ where γ is the non-linear coefficient of the fibre and u_i is the electromagnetic field of the i^{th} pulse. It is responsible for the apparition of ghost pulses [11,12] which interfere with the original signal. Indeed, for zero cumulated dispersion, these ghost pulses are located within the middle of time bits and thus, the superposition with the original signal gives rise to amplitude jitter.

To have an idea of the degradations caused by this non-linear effect, we observe the pulses deformation caused by a propagation of 2 adjacent pulses through the following optical line:

- 1 km of SMF inducing a dispersion of 17 ps/nm(α=0,2 dB/km).
- 50 km DSF characterized by a dispersion of 0 ps/nm/km(α =0,2 dB/km).
- 189 m of DCF inducing a dispersion of -90 ps/nm(α =0,6 dB/km).

This example of transmission helps us to understand the importance of interaction effects. In this case, we only consider two pulses but the zero dispersion value of DSF fibre causes the pulse not to broaden. Therefore, interaction effects are maximized. All intrachannel non-linear effects are considered here but we focus on the effect on intrachannel four-wave-mixing. On the following diagrams, we observe the pulses after the optical line. We remark the apparition of the ghost pulses in the neighbouring time bits of initial pulses.

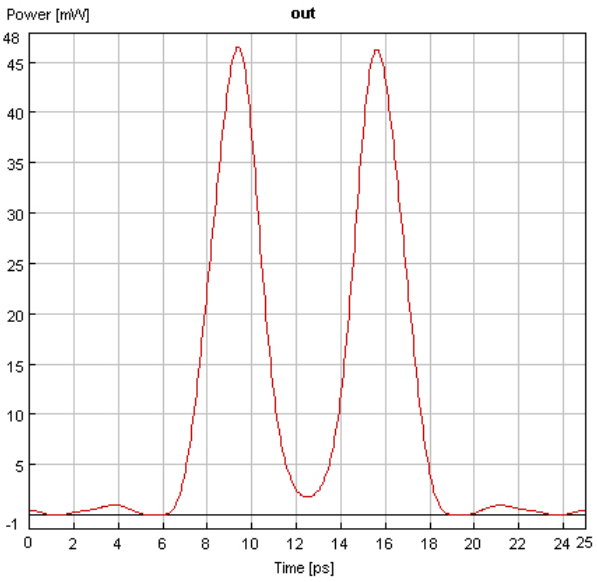

Figure 3. 7. Deformation of 2 pulses in 50 km DSF: apparition of ghost pulses in the neighbouring time bits due to intrachannel four-wave-mixing.

In the case of many pulses, every interaction between 2 or 3 pulses gives rise to a ghost pulse which means that this phenomena is extremely important as, during the transmission over 80 km of SMF, the pulse width increases by a factor greater than 700. Furthermore, all ghost pulses do not have the same energy as we can easily understand that the pulse ghost created by the interaction of three

neighbour pulses has a greater energy than the other ghost pulses because of the dispersion [12]. When looking to the eye diagram, ghost pulses with small or high energy can be seen which result in amplitude jitter.

On the following figure, we can visualize optical eyes after transmission of a Pseudo-Random Binary Sequence (PRBS). The line is constituted by spans of 100 km of SMF perfectly compensated by DCF. Double-stage erbium amplification is used but noise issues are not considered. The input power into SMF is set to 6 dBm. The optical eyes are displayed after transmission on 1, 3, 6 and 10 spans. All intrachannel non linear effects are modelled.

We first see that the main degradation of the pulse comes from amplitude jitter revealing the importance of intrachannel four-wave mixing. When examining the optical eyes, we see that the amplitude jitter of marks appears almost immediately whereas amplitude jitter of spaces is visible after the sixth span only.

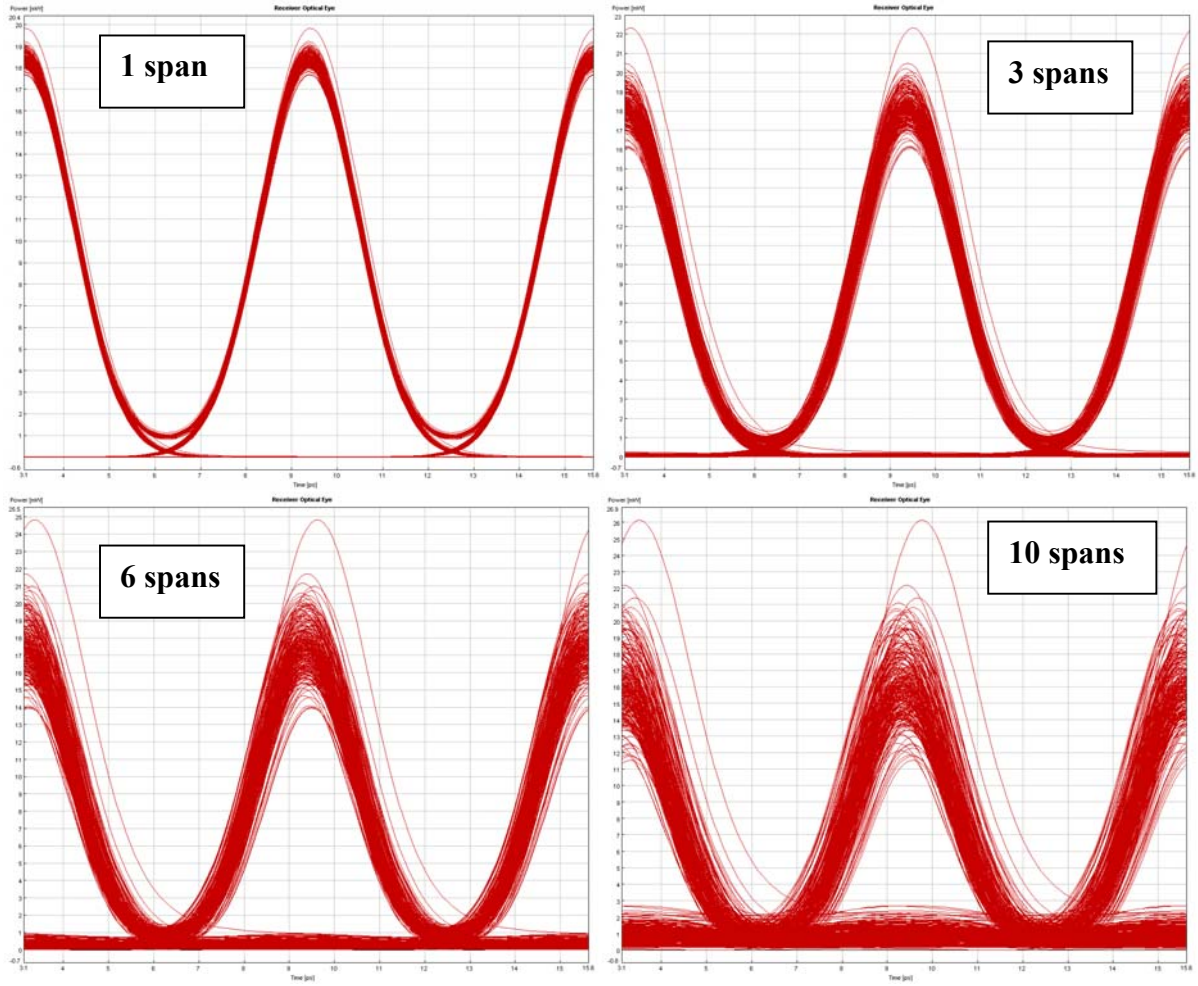

Figure 3. 8. Deformation of pulses of a PRBS sequence: rising of amplitude jitter of marks and spaces due to intrachannel four-wave mixing.

It is possible to estimate the standard deviation of marks and spaces due to this intrachannel four-wave-mixing non-linear effect. In the following figure, these standard deviations are represented as a function of the number of spans. We remark that the sum of the standard deviations of marks and spaces is linear with the number of spans [12].

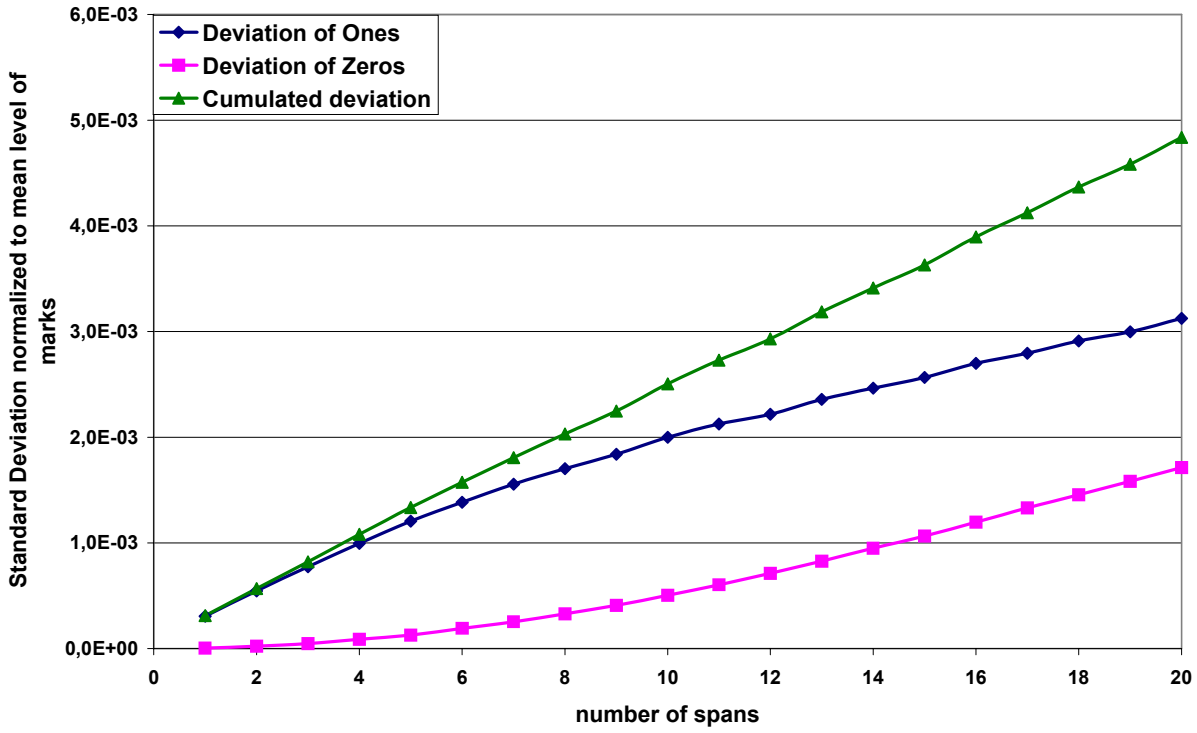

Figure 3. 9. Evolution of the standard deviation of marks and spaces due to intrachannel four-wave mixing.

In the following, we will study how phase modulation can reduce this impairment. We will then be able to determine the most efficient phase modulation for minimizing intrachannel four-wave-mixing [13,].

In the case of gaussian pulses, we can achieve a full description of these interactions. Numbering pulses depending their initial location time bit, we can show that the creation of a ghost pulse is due to the overlap of pulses {l,m,n}[11,12]. Its time location for zero cumulated dispersion is $t = (m + n - l).T$ [11,12] where T is the value of the time bit. This ghost pulse is also gaussian shaped but its width is larger by $\sqrt{3}$ from original pulses width [15]. Its phase is $\varphi(m,n,l) = \varphi_m + \varphi_n - \varphi_l$ [11-16] where φ_i is the phase of the pulse numbered i. The energy of this ghost pulse (normalized to the energy of the initial pulse) is a function of power evolution, map dispersion, span length, initial parameters of the pulses and indexes m and n [11,12]. The exact solution of this function will not be represented here, we will note it $\Delta W(z) = |Q_{m,n}|.z$ as this function is linear with z. The electric field in the middle of the ghost pulse is proportional to $\sqrt{|Q_{m,n}|.z}.e^{i.\varphi(m,n,l)}$. In the case of a random sequence of bits, the ghost pulse located at t=0 is gaussian and its energy growth normalized to z is given by the following equation:

$$\frac{\Delta W(z)}{z} = \left| \sum_{n=-N/2}^{N/2} \sum_{m=-N/2}^{N/2} b_{m+n}.b_m.b_n.\sqrt{|Q_{m,n}|}.e^{i.\varphi(m,n,m+n)} \right|^2$$

where b_k is binary representation of the bit located in $t = k.T$, equal to 0 or 1 with a probability of ½. For a given bit sequence, we can calculate the complex term inside the module and represent it in a complex scale. We will represent the contributions for 5000 random bit sequences on figure 3, where we compare the case of a two-steps phase modulation of 0,65π at 40 GHz to standard RZ modulation. The transmission is made over one span of 100 km of SMF which is perfectly compensated by DCF. The number of bit taken into account is N=100.

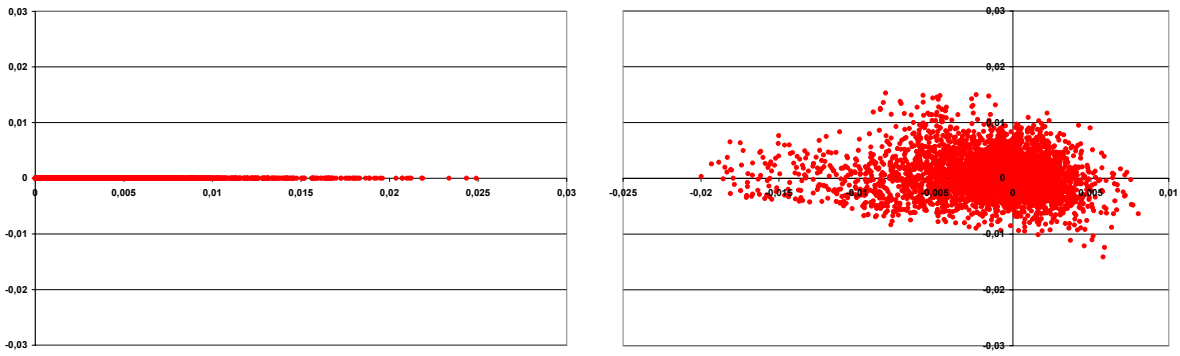

Figure 3. 10. Representation on a complex scale of the resultant ghost pulse electromagnetic field for different random data sequences for classic RZ modulation (left) and phase modulation of 0,65π at 40 GHz (right).

On these graphs, we can see that the points are scattered. It means that depending on the bit sequence, the contribution at t=0 does not have the same energy. We can also understand this scattering as a variance of the contributions to each bit implying an amplitude jitter on eye diagram on marks and spaces. From these series of points, we can deduce statistical variances and compare different phase modulations.

In Table 3. 2, format Modul.1. corresponds to a phase modulation of 0.65π at 40 GHz [16,17]. Format Modul.2 corresponds to a phase modulation in 4 steps spaced by 90 degrees ($\varphi = 0, \frac{\pi}{2}, \pi, \frac{3.\pi}{2} \ldots$). In order to easily compare the impact of intrachannel four-wave mixing for different phase modulations, we normalize these variances to the variances of return-to-zero format as shown in table 1.

Modulation format	RZ	CSRZ	Modul. 1	Modul. 2
Normalized variance on marks	1	0,61	0,50	0,57
Normalized variance on spaces	1	0,40	0,71	0,49

Table 3. 2. Normalized variances on marks and spaces for different modulation formats.

A phase modulation, as Modul. 1 or Modul. 2, added to the original pulse sequence would allow the diminution of amplitude jitter. We verified this influence by the simulation of a transmission of PRBS sequence with an erbium amplification scenario on 10x100 km. The optical power injected in the standard single mode fibre is set to 6 dBm and we compare the Eye Opening Factor. This high optical power reinforces the importance of intrachannel non linear effects and the high dispersion of the fibre enables to consider only intrachannel four-wave mixing. Furthermore, intrachannel cross-phase modulation is not sensitive to phase modulation. These simulation results, displayed in Table 3. 3, are in agreement with the theoretical results we obtained from the time-domain theory.

Modulation format	RZ	CSRZ	Modul. 1	Modul. 2
Eye opening factor: mean value	0,770298	0,84065	0,816465	0,808686

Table 3. 3. Eye opening factor after transmission on 10 spans of 100 km of SMF for different modulation formats.

Thus, we show that, considering erbium amplification, RZ modulation is not advantageous in terms of intrachannel four-wave mixing whereas phase modulations such as CSRZ or formats Modul.1 and Modul.2 allow the diminution of this impairment and significantly increase the transmission quality. Other phase modulations have been demonstrated as potential candidates for the reduction of intrachannel four wave mixing [18] but the ones we have studied may be the easiest phase

modulations to implement on a real system. Other techniques can be used to minimize intrachannel four-wave-mixing [19] but phase modulation may be one of the possibilities at 160 Gbit/s bit rate because of the separation of neighbouring bits on different OTDM lines.

2.1.3 Intrachannel cross phase modulation

Intrachannel cross phase modulation is due to the interaction of pulses. The result of this interaction is the apparition of a frequency perturbation similar to a Raman shift. This frequency perturbation, combined with chromatic dispersion) results in timing jitter because of the time position dependence towards frequency (see second equation of Equation 3. 1). Using collective variable theory with a model of two gaussian optical pulses, we can describe the perturbation caused by intrachannel cross phase modulation. This calculation is detailed in Annex 1.

To estimate the importance of this phenomena, we will make the following simulation: two pulses (peak power set to 235 mW, FWHM=2,5 ps) will be propagated into an optical line made of 160 m of SMF(D=17 ps/nm/km; α=0,2 dB/km), X km of DSF (D=0 ps/nm/km; α=0,2 dB/km) and 30 m of DCF(D=-90 ps/nm/km; α=0,6 dB/km) where X vary from 1 to 20 km as plotted on the following figure.

The time spacing between the two bits is initially set to 6,25 ps (value of the time bit). The first of the following figures shows the two pulses before and after the linear broadening by 160 m of SMF whereas the second figure shows the two pulses at the input and at the output of the line (here, with 10 km of DSF):

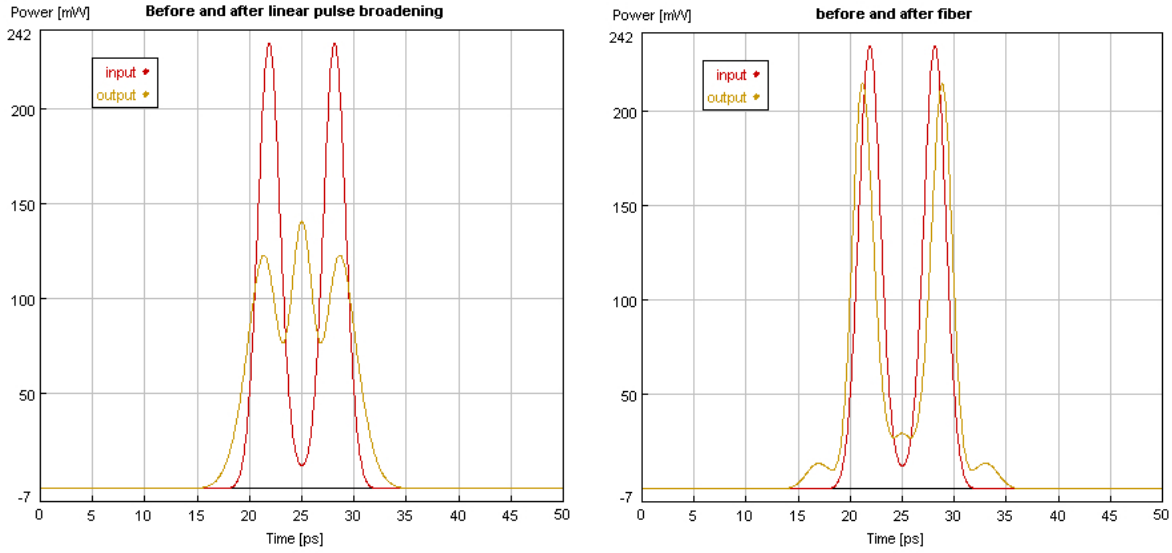

Figure 3. 11. Optical pulses before (in red on both figures), after pulse broadening in 160 m of SMF (in yellow on left figure) and after propagation in 160 m of SMF, 10 km of DSF and 30 m of DCF (in yellow on right figure).

We see that, due to pulse broadening, optical pulses are overlapping. Because of the zero dispersion in DSF fibre, this overlapping is maximized and consequently, Kerr non linear effects are strong. We remark the presence of small pulses in the neighbouring time bits of initial ghost pulses. These ghost pulses are due to intrachannel four-wave-mixing. This apparition of energy is responsible for the decrease of the peak power as it can be seen on the right figure between red and yellow traces. We also notice the presence of intrachannel cross phase modulation due to the timing jitter we observe on this figure: the bit spacing slightly increases from 6,25 ps to 7,625 ps.

In Figure 3. 12, we have represented the time spacing between the two bits as a function of X, i.e. the DSF length. We notice that the time spacing between neighbour pulses increases less and less quickly as the fibre length increases. Two reasons may be given for this fact. As a matter of fact, the attenuation in the DSF fibre results in lower optical peak powers and less non-linear effects. The optical peak power is reduced by 4 dB after 20 km. Furthermore, intrachannel four-wave-mixing

process is also occurring in the DSF fibre. This last process is responsible for an energy exchange between pulses and, in this case, a decrease of the optical peak power of initial pulses (due to the energy transfer to the ghost pulses). That's why we have also represented in Figure 3. 12 the evolution of the normalized peak power (without pulse broadening and optical losses but only non-linear effects) of initial pulses. This decrease of the peak power denotes intrachannel four-wave-mixing impairment and its effects are relatively high since the optical peak power is reduced by 1 dB after 20 km.

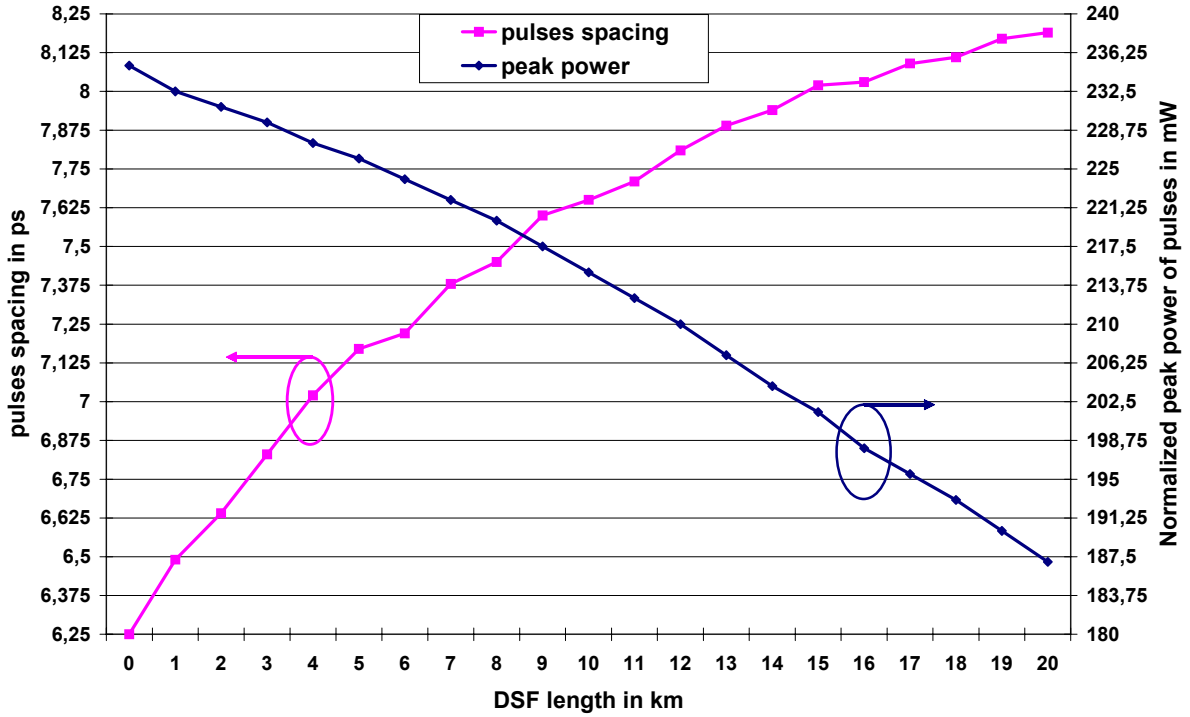

Figure 3. 12. Transmission over DSF fibre: Evolution of the pulses spacing (in pink) as a consequence of intrachannel cross phase modulation. Evolution of the normalized peak power (for zero cumulated dispersion and without optical losses) as a consequence of intrachannel four-wave-mixing.

In this case, the impact of intrachannel cross-phase modulation is important as the time deviation represents more than 10 % of the time bit after only a few kilometres of transmission but we need to precise that this design is not representative of a transmission experiment. As a matter of fact, the inline fibre dispersion is not equal to zero for a usual transmission, which reduces the interaction between two bits. At the opposite, the dispersion is responsible for the pulse broadening, inducing the interaction of pulses distant from many time bits. This can be represented by the two following diagram explaining the impact of intrachannel four-wave mixing and intrachannel cross-phase modulation [19,21]:

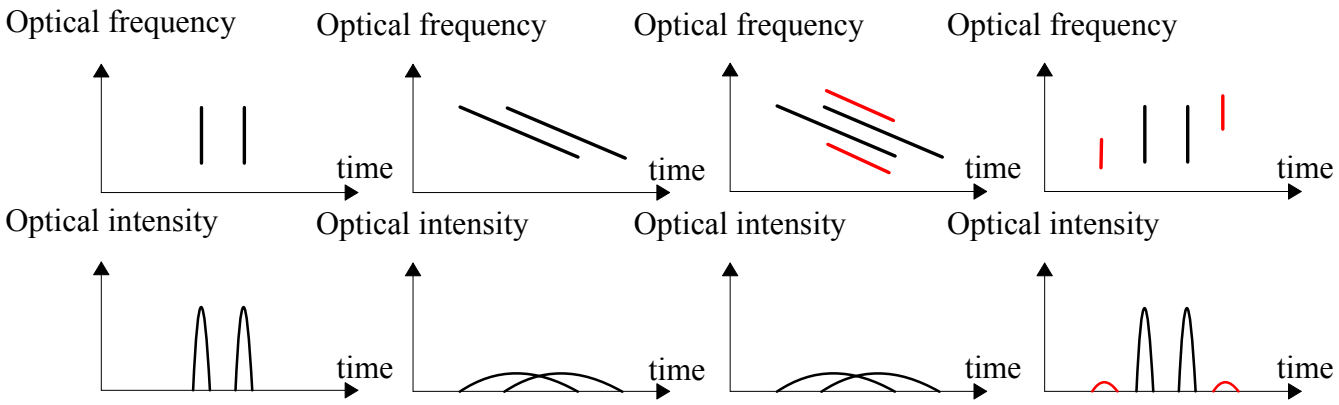

Figure 3. 13. Physical impact of intrachannel four-wave mixing.

The impact of intrachannel four-wave mixing can be understood through the following steps:

- On the left column of the figure, pulses are narrow and temporally distinct. The cumulated dispersion is zero.
- On the second column from the left, with the effect of pulse broadening due to inline fibre dispersion, the two pulses now overlap each other. If we define as f_+ and f_- the frequency components of each pulse, we can see than in the overlapping time area, signal components of frequency f_+ and f_- are interacting through non linear effects.
- In particular, four-wave mixing occurs and we obtain an energy transfer with the creation of frequency components at the frequencies $f_1 = 2.f_+ - f_-$ and $f2 = 2.f_- - f_+$. These frequency components are represented in red in the top of the third column.
- With the effect of , these perturbation signals are temporally shifted as can be seen in the last column on the right. For zero cumulated dispersion, they are centred in the time bit.

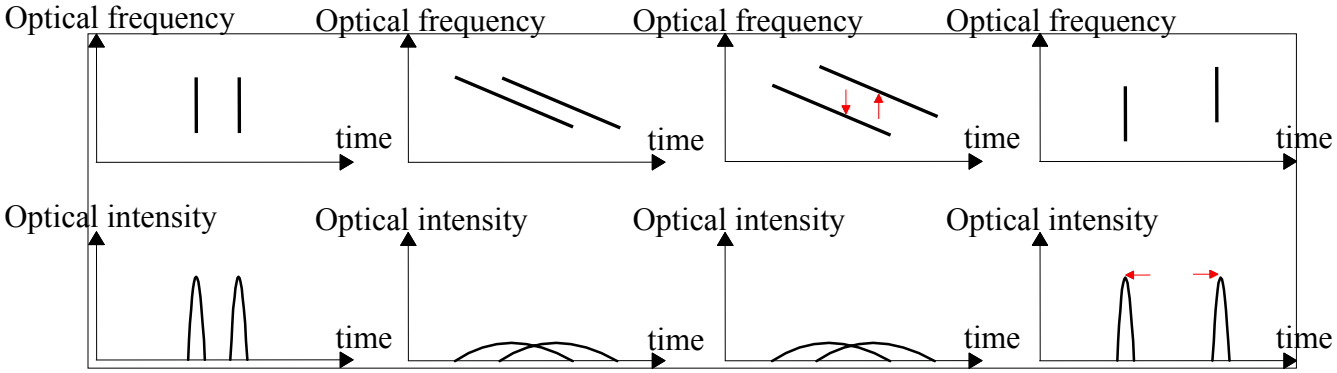

Figure 3. 14. Physical impact of intrachannel cross-phase modulation.

The impact of intrachannel cross-phase modulation can be understood through the following steps:

- On the left column of the figure, pulses are narrow and temporally distinct. The cumulated dispersion is zero.
- On the second column from the left, with the effect of pulse broadening due to inline fibre dispersion, the two pulses now overlap each other. If we define as f_+ and f_- the frequency components of each pulse, we can see than in the overlapping time area, signal components of frequency f_+ and f_- are interacting through non linear effects.
- In this case, cross-phase modulation occurs and we obtain a phase modulation, i.e. a frequency modulation or a frequency deviation, which is here represented by the red arrows on the third column from the left.
- The signal components are now shifted in frequency and, due to the dispersion compensation, this frequency deviation is converted into temporal deviation. This temporal deviation is not the same for all pulses depending on the degree of non linearities. This explains the apparition of timing jitter, represented in red in the top of the third column.

2.1.4 Coexistence of intrachannel four-wave-mixing and intrachannel cross phase modulation

The impact of inline fibre dispersion towards the relative importance of intrachannel cross-phase-modulation compared to intrachannel four-wave-mixing can be observed through the following simulation. A PRBS sequence of 1024 bits is transmitted into 4 spans of 100 km which is perfectly compensated after each span. The inline fibre dispersion is set to +1 ps/nm/km or +17 ps/nm/km. Effective areas are the same. Optical power is set to +6 dBm at the input of inline fibre. Noise is not

considered and amplification is enabled by ideal 2-stage erbium amplifiers. The optical eye diagrams in front of the receiver are shown on the following figure.

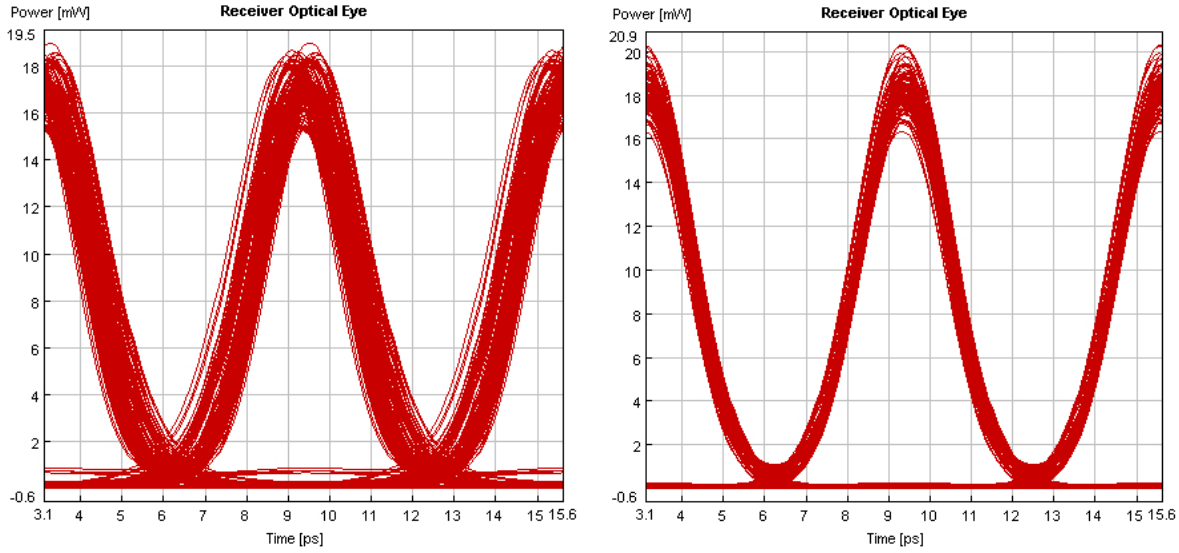

Figure 3. 15. Optical eyes after transmission over 4 spans of 100 km of fibre with D = 1 ps/nm/km(on the left) or D = 17 ps/nm/km (on the right).

We clearly see the presence of timing jitter on the first eye diagram, corresponding to an inline fibre dispersion of 1 ps/nm/km, whereas amplitude jitter is the most significant degradation on the second eye diagram, corresponding to an inline fibre dispersion of 17 ps/nm/km. This reveals that intrachannel cross-phase modulation is to be taken into account for low dispersion but it can be neglected when the dispersion is high [22].

Another important aspect for the validity of the simulations concerns the number of bits to be taken into account in the simulation. It is a crucial parameter for the estimation of intrachannel non-linear effects. Indeed, we have seen that using 100 km of SMF with an initial pulse width of 2,5 ps, the pulse is broadening up to 960 times and so, there are interactions between this pulse and other pulses in a few hundreds neighbouring bits. On the following tables, we have estimated the relative standard deviation of marks (which is characteristic of intrachannel four-wave mixing) and the timing jitter (which is characteristic of intrachannel cross phase modulation) as a function of the sequence length used in the simulation. For each sequence length, the simulation was run 50 times using a different sequence in order to calculate the mean value and the variance for each serial. The optical fibre is in the first case a low dispersion fibre (D = 1 ps/nm/km) and in the second case, a high dispersion fibre (D = 17 ps/nm/km). Optical amplification is enabled by double-stage erbium amplifiers and noise is not considered here. Statistical parameters such as relative standard deviation and timing jitter are reported in Table 3. 4 and Table 3. 5:

Number of bits in the sequence:	64	128	256	512	1024	2048	4096
Mean relative standard deviation in mW	0,0465	0,0483	0,0482	0,0472	0,0474	0,0478	0,0480
Variance of the Rel. Stand. Dev. in mW²	2,87E-05	2,57E-05	1,11E-05	4,97E-06	1,86E-06	4,93E-07	2,00E-07
Mean Jitter in ps	0,4702	0,3812	0,2919	0,3014	0,2842	0,2879	0,2900
Variance of jitter in ps²	0,1521	0,0422	0,0020	0,0052	0,0004	0,0002	0,0001

Table 3. 4. Estimation of the impact of non-linear effects as a function of the sequence length for 4 spans of 100 km with D=1 ps/nm/km and P=6 dBm.

Number of bits in the sequence:	64	128	256	512	1024	2048	4096
Mean relative standard deviation in mW	0,0476	0,0522	0,0542	0,0547	0,0530	0,0530	0,0530
Variance of the Rel. Stand. Dev. in mW²	1,67E-04	1,27E-04	9,00E-05	3,94E-05	9,43E-06	6,20E-06	2,57E-06
Mean Jitter in ps	0,3135	0,2619	0,2139	0,2211	0,1849	0,1717	0,1700
Variance of jitter in ps²	0,1006	0,0398	0,0197	0,0100	0,0040	0,0020	0,0010

Table 3. 5. Estimation of the impact of non-linear effects as a function of the sequence length for 4 spans of 100 km with D=17 ps/nm/km and P=6 dBm.

These figures first confirm that timing jitter is dominant when the dispersion is low (0,29 ps compared to 0,17 ps using a 2^{12} PRBS sequence) whereas the standard deviation is the main degradation when the dispersion is high (0,053 compared to 0,048) which reinforces the importance of intrachannel cross phase modulation when the dispersion is low.

If we define an error ratio margin of 5 % on these estimations, we see that we need at least 1024 bits in order to obtain a sufficient precision. Of course, this number of bits to be taken into account in the simulation mainly depends on the importance of dispersion and non-linearity but in the second of these two cases (P = 6 dBm and D = 17 ps/nm/km), the conditions are inducing enough non-linearities so that it can be representative of all other scenarios.

In the following, we have estimated the impact of these intrachannel non linear effects by measuring the eye opening factor as a function of the inline fibre injection power, the number of spans and the inline fibre dispersion. The span length is set to 100 km in all cases. Results are displayed in the following figure for injection powers of 2, 6 and 10 dBm. Effective areas are respectively 80, 65 and 72 µm² for SMF, Teralight and Leaf fibre types.

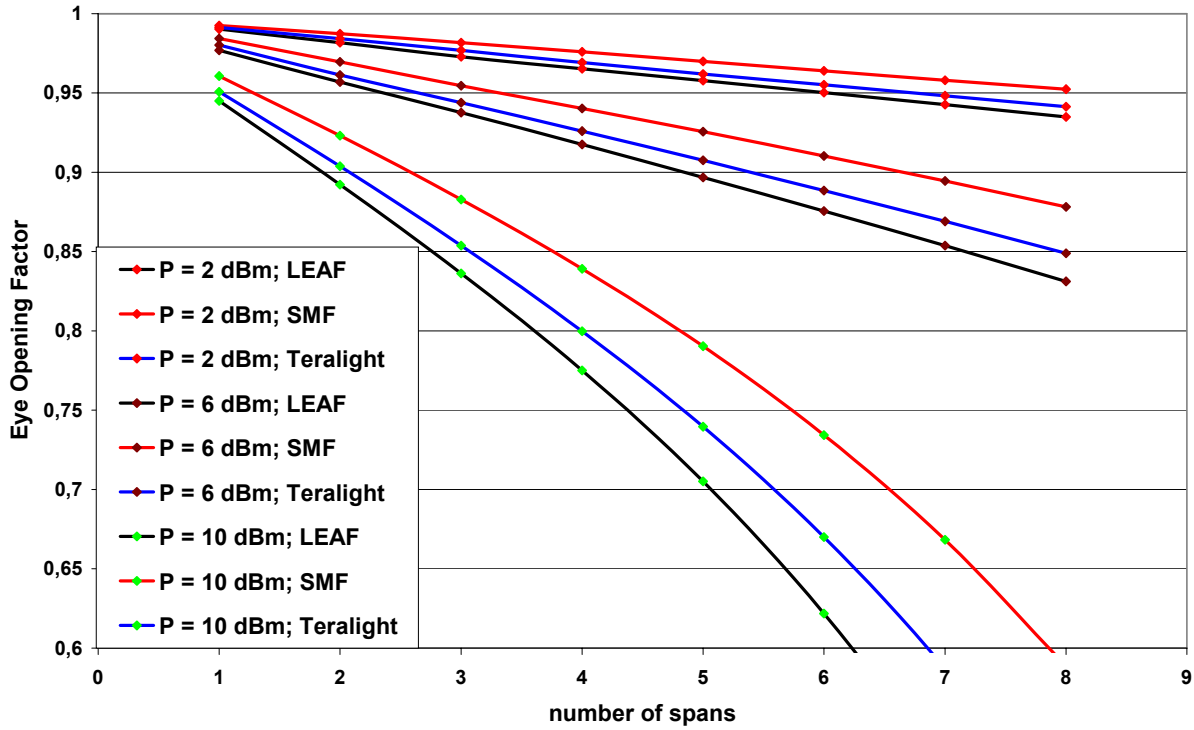

Figure 3. 16. Eye opening factor versus number of spans for different signal powers and different types of fibre.

If we define that the eye opening factor should be greater than 0,9 then we can extract from these data the maximum injection signal power as a function of the number of spans and fibre type:

Number of spans of 100 km	LEAF	Teralight	SMF
3 spans	8	8	8
4 spans	6	6	8
5 spans	4	6	6
6 spans	4	4	6
7 spans	4	4	4

Table 3. 6. Maximum signal power (in dBm) depending number of spans and fibre type.

2.1.5 Stimulated Raman scattering and self-steepening effect

From collective variable theory, we know that a Gaussian pulse is perturbed by stimulated Raman scattering and self-steepening effects. These two effects impact the pulse parameters and especially the temporal position, the chirp and the frequency offset (the pulse phase X_6 is also affected but it does not have any repercussion for classical communication systems, except when information is encoded into the difference of phase as DPSK).

$$\dot{X}_2 = -\beta_2 . X_5 + \beta_3 . \left(\frac{1}{2 . X_3^{\,2}} + \frac{X_5^{\,2}}{2} + \frac{X_3^{\,2} . X_4^{\,2}}{8} \right) + \frac{3}{2.\sqrt{2}} . \gamma_S . X_1^{\,2}$$

$$\dot{X}_4 = -\left(\beta_2 - \beta_3 . X_5\right) . \left(\frac{4}{X_3^{\,4}} - X_4^{\,2} \right) - \frac{\sqrt{2} . X_1^{\,2} . \left(\gamma - \gamma_S . X_5\right)}{X_3^{\,2}}$$

$$\dot{X}_5 = \frac{\sqrt{2} . \gamma_R . X_1^{\,2}}{X_3^{\,2}} + \frac{\gamma_S . X_1^{\,2} . X_4}{\sqrt{2}}$$

We can comment these three equations by evaluating the importance of non-linear terms due to Raman scattering and self-steepening compared to linear contributions.

Concerning the frequency offset X_5, its evolution is only dependant of these two non-linear effects. It is quite difficult to compare these two contributions when looking at this equation. However, the contribution of self-steepening is zero at z=0 since the chirp X_4 is zero. From there, chirp increase very quickly in the first few tens metres whereas the pulse width does not vary a lot (see Figure 3. 1) so during these few tens metres, the impact of self steepening on the frequency offset should rise. After that, the chirp should decrease and the pulse width should increase very quickly thus reducing the impact of Raman scattering (which is inversely proportional to the pulse width). Of course, both of these effects are dependant on the peak power X_1^2 which is decreasing with attenuation and dispersion. In order to visualize the relative part of each of these effects, we have launched simulations with Raman scattering and including self-steepening or not. The frequency offset after one span of 80 km of SMF is shown as a function of the input signal power on Figure 3. 17. We remark that the contributions of Raman scattering and self-steepening are almost of the same order of magnitude but Raman scattering most impacts the frequency offset than self-steepening effect. We also see on this graph that this frequency offset is typically a few MHz which has nearly no impact on the transmission.

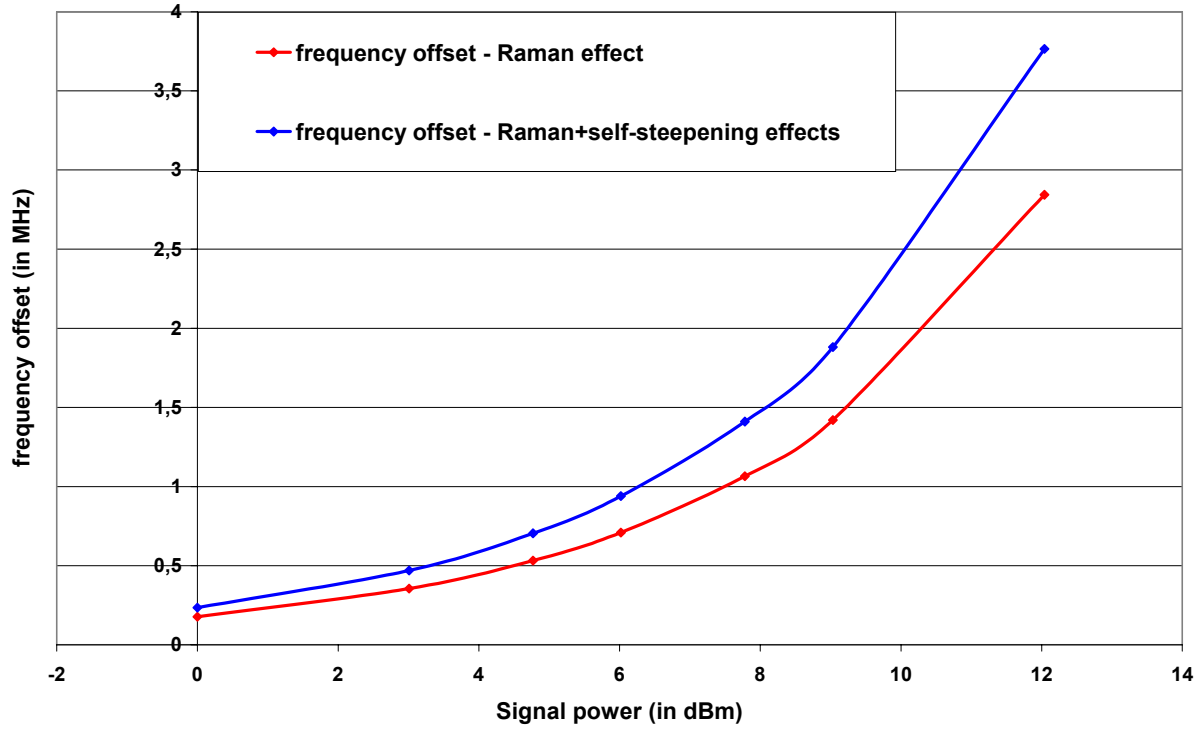

Figure 3. 17. Frequency shift due to Raman scattering and self-steepening effects after 80 km SMF versus injected signal power.

We can now discuss about the importance of self-steepening concerning the variation of chirp and temporal position as we know that the frequency offset value is around some MHz. Concerning the chirp evolution, we have to compare γ to $\gamma_S \times X_5$ and β_2 to $\beta_3 \times X_5$. For SMF fibre, we have:

- $\gamma = 1{,}312$ W^{-1}.km^{-1} and $\gamma_S = \dfrac{\gamma}{2\pi.\dfrac{C}{\lambda}}$ =1,078.10^{-15} s.W^{-1}.km^{-1}, with X_5 typically a few MHz, we obtain $\gamma_S.X_5 \approx 10^{-9}$ W^{-1}.km^{-1} which is high upon γ.
- β_2 = - 21,667 ps².km^{-1} and $\beta_3.X_5 \approx 10^{-7}$ ps².km^{-1} which can be neglected upon β_2 as X_5 is typically a few MHz.

This means that the chirp variation due to Raman scattering and self steepening effect is minor compared to non-linear chirp due to Kerr effect.

Concerning the temporal offset X_2, self-steepening impacts its evolution in direct (non-linear term in X_2 evolution equation) and indirect ways (by the combination of 2nd and third order dispersion and the impact of self-steepening on chirp and frequency offset). However, since the frequency offset appears at the very beginning of the fibre, we can deduce that this frequency offset does not impact the temporal position as far as dispersion and dispersion slope is compensated at the end of the line. It means that as far as non-linear effects are occurring when the cumulated dispersion and dispersion slope are zero, then the frequency offset due to Raman scattering and self steepening effects does not impact the temporal position via dispersion. We can therefore try to estimate the direct non-linear contribution of self-steepening to the evolution of the temporal position. For SMF fibre and for an optical power of 6 dBm and a full width at half maximum of 2,5 ps, the optical peak power is equal to X_1^2 = 11,3 mW at the input. Numerical application gives:

- $\frac{3}{2\sqrt{2}}.\gamma_S.X_1^2 \approx 10^{-5}$ ps.km^{-1} which means that even if non-linear effects were occurring during a few kilometres, the temporal offset is about five orders of magnitude less than picoseconds.

Self-steepening effect can thus be considered as a minor degradation.

2.1.6 Identification of major transmission effects in a single channel transmission

In the previous chapters, we have seen that non linear effects occurring in the transmission fibre were leading to severe degradations for the signal. After having studied independently these effects, we have seen that self-phase modulation, intrachannel four-wave mixing and intrachannel cross-phase modulation were the main degrading effects whereas stimulated Raman scattering, self-steepening could be ignored.

Fibre dispersion

In the following, we will try to minor the impact of these three non-linear effects in order to improve the transmission distance. We have already seen that inline fibre dispersion is a key factor since it influences pulses dispersion and thought self-phase modulation but also pulse overlapping.

In Figure 3. 16, we have investigated the impact of non-linear effects (mainly self-phase modulation, intrachannel four-wave mixing and cross-phase modulation) with various inline fibre dispersion of 4, 8 and 17 ps/nm/km corresponding to classical transmission fibres. In Table 3. 6, we deduced the maximum signal power to be injected in the transmission fibre depending the number of spans and the fibre dispersion. We remark that for a given optical power (same colour of dots), degradations are higher when inline fibre dispersion is low. For this reason, transmission on high dispersion fibre is preferable. However, due to this high dispersion, the cumulated dispersion will be more important and will require a longer dispersion compensation fibre inducing more attenuation. In this chapter, noise is not considered but this issue will be investigated in the following chapter where we considerate a global WDM system.

Regarding intrachannel non-linear effects, a fibre dispersion of 17 ps/nm/km is most advantageous compared to 4 and 8 ps/nm/km. In Figure 3. 18, the inline fibre dispersion varies from 4 to 1000 ps/nm/km whereas the signal power is set to 4 dBm at the input of inline fibre. Due to this high dispersion value, the number of bits taken into account in the simulation is set to 2^{16}. The Eye Opening Factor is measured after 3 spans of 100 km. Amplification is still enabled by double stage erbium amplifiers and noise is not considered.

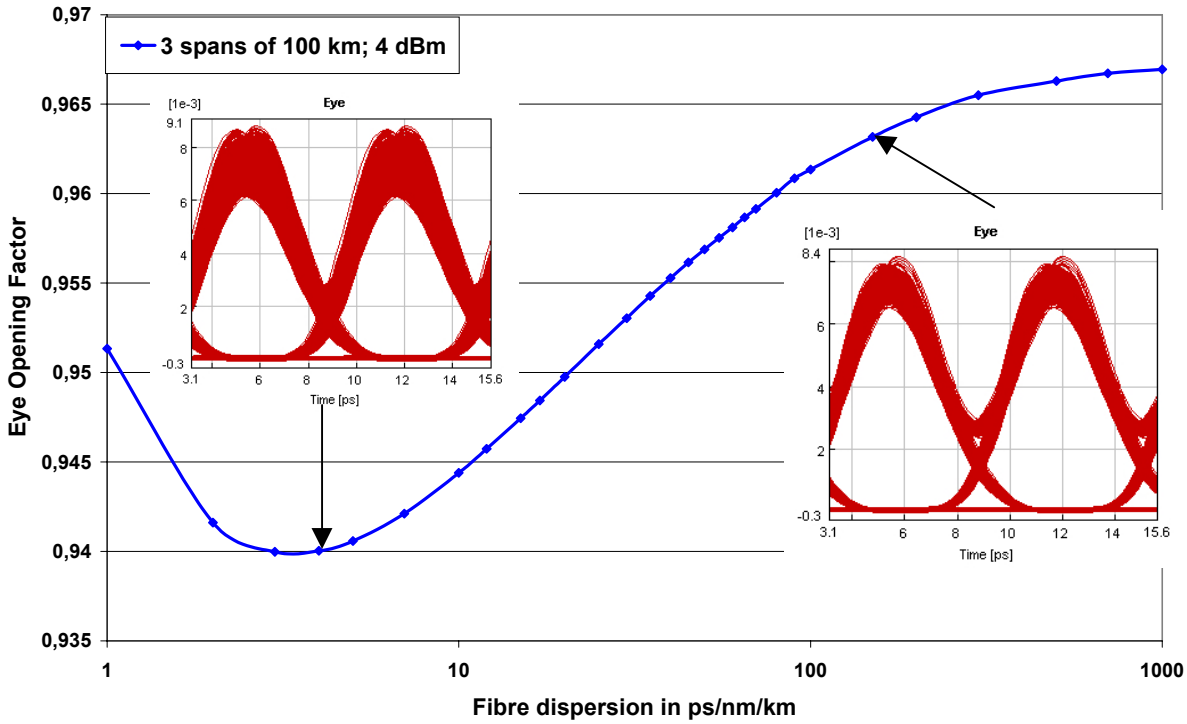

Figure 3. 18. Eye Opening Factor versus inline fibre dispersion after 3 spans of 100 km and for an injection signal power of 4 dBm. Electrical eyes for dispersion values of 5 and 200 ps/nm/km.

We first remark that impairments appear under the form of timing jitter (for low fibre dispersion for example) and amplitude jitter (for high fibre dispersion for example). Amplitude jitter only appears on the marks as the transmission is made over 3 spans only (see Figure 3. 9).

We here notice that the penalty on the eye opening factor is the largest for a dispersion value around 4 ps/nm/km. We obtain a reduction of non linear effects for either smaller or higher dispersion values. For low dispersion values, pulses do not broad quickly and thus, the overlapping is weak but the energy taken into account in the Kerr effects is high because of the low dispersion. For high dispersion, pulses broad a lot while propagating in the fiber and there are a lot of interactions but as a consequence, optical powers involved in non-linear effects are low. Between these two extremes, we obtain a significative amount of overlapping and optical power resulting in strong degradation. Similar results have been shown for different bit rates and a comparison can be made in terms of non linear effects between SSMF fibre at 40 Gbit/s and NZDSF fibre at 160 Gbit/s [23].

We see that the curve has an asymptotic tendency reaching a maximum value around 0,974 when inline fibre dispersion is greater than 50 ps/nm/km. However, this effect is counterbalanced when we take noise into account noise. When inline fibre dispersion is high, the DCF length is also high and the induced attenuation rises. The possible use of higher-order-mode module enables to compensate large values of dispersion and reduces optical losses compared to classic dispersion compensation modules [24].

Duty cycle

Up to now, we haven't considered the influence of the pulse width. In the equation obtained by the collective variable theory, we have shown that the non-linear chirp due to self-phase modulation is inversely proportional to the square pulse width. We now investigate the influence of this parameter on the impact of self-phase modulation, four-wave mixing and cross-phase modulation. We therefore consider an optical line made of 3 spans of 100 km SSMF perfectly compensated after

each span. The emitter is characterized by a various duty cycle between 0,2 and 0,8 and the signal power at the input of the inline fibre is also varying between -4 and 12 dBm. Noise issues are not considered. The Eye Opening factor is measured after detection.

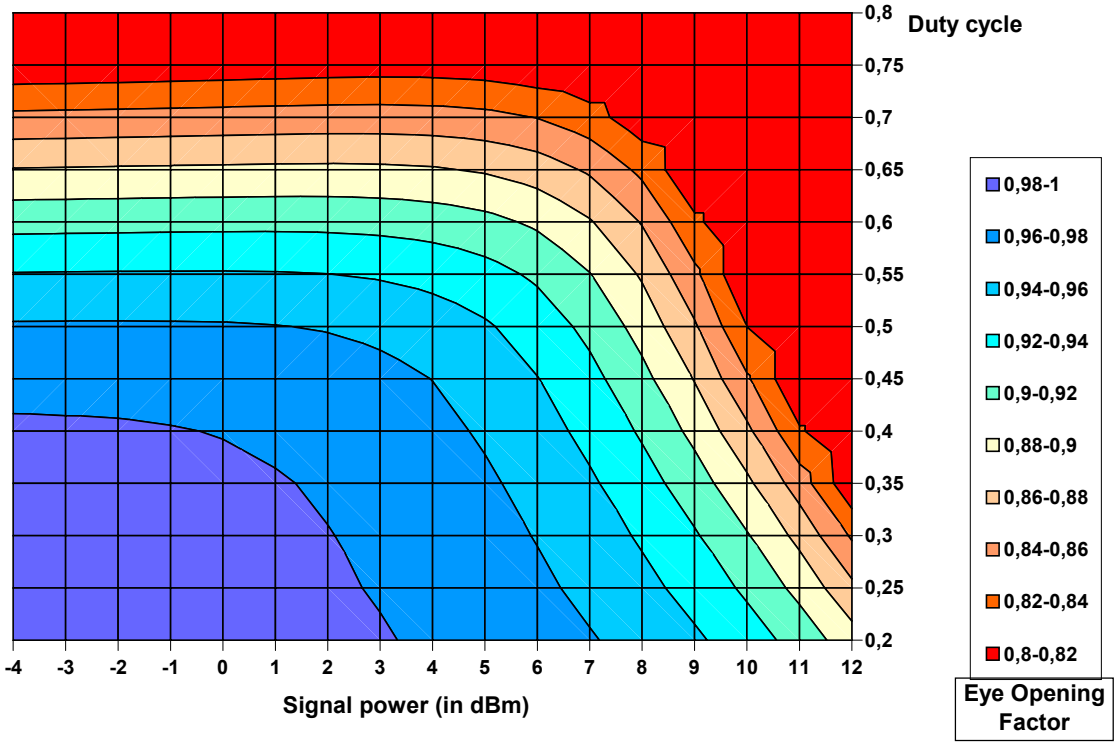

Figure 3. 19. Eye opening factor after 3 spans of 100 km SSMF with perfect compensation

On this figure, we first remark that a duty cycle greater than 0,6 is not suitable since the crosstalk between adjacent bits is degrading the quality even without non-linear effects. For a lower duty cycle, we notice that the tolerance to non-linear effects is higher in terms of signal power. However, if the duty cycle is low, it means that the pulse width is low and consequently, the spectrum width will be high reinforcing noise impact, inter-channel non linear effects and spectrum overlapping for a given spectral efficiency. As a matter of fact, most of the simulations have been performed considering a duty cycle of 0,4 making a good compromise between the optical spectrum width and inter-symbol-interference due to time crosstalk. However, it is possible to increase the duty cycle when we consider an OTDM-based transmission. In that case, the pulse width can reach up to 5 ps and the OTDM-demultiplexing device enables to avoid inter-symbol-interference because of the time gating small width.

2.2 Interchannel non linear effects

Due to the transmission of several channels in the same optical fibre using WDM multiplexing, non linear effects appear due to the collision of optical pulses. In the same way that intrachannel four wave mixing and cross-phase modulation is due to the collision of pulses of the same channel, inter-channel four wave mixing and inter-channel cross phase modulation is due to the collision of optical pulses from different channels as shown in Figure 3. 20 and Figure 3. 21.

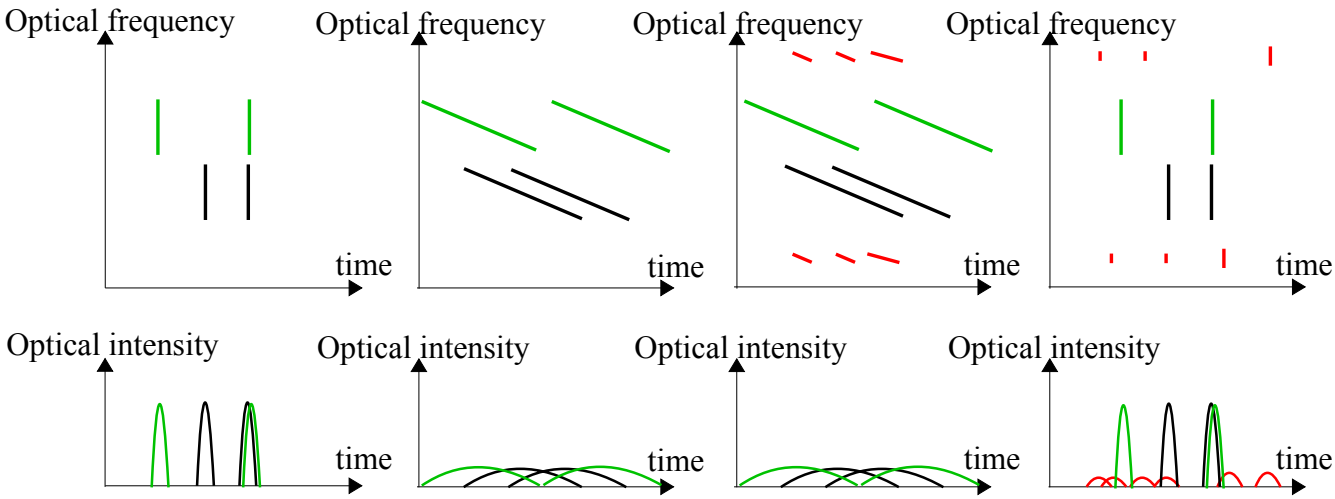

Figure 3. 20. Collision of pulses with several channels and apparition of frequency components due to inter-channel four-wave mixing.

The impact of inter-channel four-wave mixing can be understood through the following steps:

- On the left column of the figure, pulses from a same channel are narrow and temporally distinct but pulses from two different channels may overlap. The cumulated dispersion is zero.
- On the second column from the left, with the effect of pulse broadening due to inline fibre dispersion, pulses overlap each other. In particular, we observe an overlapping between pulses from two distinct channels.
- In this case, inter-channel four-wave mixing occurs and we obtain a transfer of energy. Two frequency components appear. If we define as f_1 and f_2 the channel frequencies, the frequency components created by inter channel four wave mixing are $f_3 = 2.f_1-f_2$ and $f_4=2.f_2-f_1$.

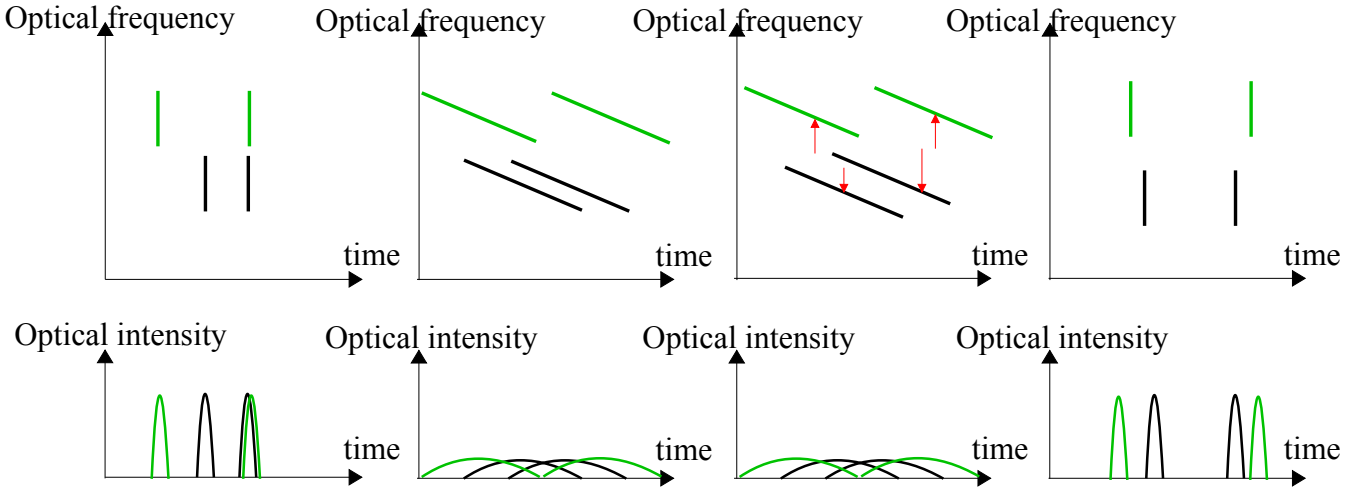

Figure 3. 21. Collision of pulses with several channels and apparition of timing jitter due to inter-channel cross-phase modulation.

The impact of inter-channel cross phase modulation can be understood through the following steps:

- On the left column of the figure, pulses from a same channel are narrow and temporally distinct but pulses from two different channels may overlap. The cumulated dispersion is zero.

- On the second column from the left, with the effect of pulse broadening due to inline fibre dispersion, pulses overlap each other. In particular, we observe an overlapping between pulses from two distinct channels.
- In this case, inter-channel four-wave mixing occurs and we obtain a phase modulation, i.e. a frequency deviation. This frequency deviation may not be the same for all pulses from the same channel.
- With the effect of dispersion, this frequency shift is converted into time shift. As the effect is not the same for all pulses in a same channel, a timing jitter appears.

In order to quantify the impact of these non linear effects, we simulate the transmission of 3 channels over 5 spans of 100 km of SMF (or LEAF) with various channel spacing and channel powers. Detection is made after each span and the eye opening factor is measured for the central channel. Amplification is enabled by double-stage erbium amplifiers but noise is not considered. WDM demultiplexing is enabled by a sharp trapezoidal filter (bandwidth of 300 GHz). The three following graphs show these simulation results for three different channel spacing, i.e. 300, 350 and 400 GHz. For each channel, the duty cycle is set to 0,4 and the channel power ranges from 0 to 6 dBm. The plain lines correspond to a unique transmission channel whereas dash lines correspond to a WDM transmission. The horizontal dash line corresponds to the eye opening factor measured without transmission (in back to back configuration).

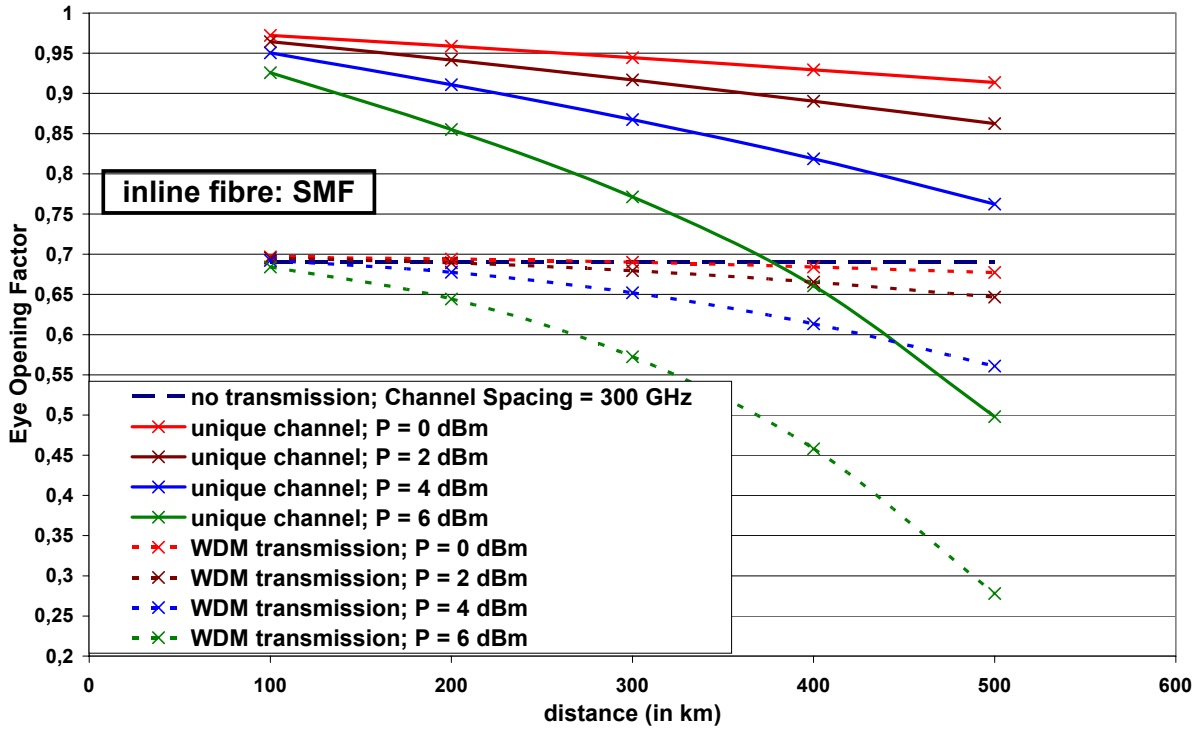

Figure 3. 22. Eye Opening factor for a channel spacing of 300 GHz(duty cycle =0,4). Comparison of the impact of intrachannel and inter channel non linear effects.

On this graph, we can see the impact of wavelength division multiplexing since the eye opening factor is significantly reduced but this is not due to inter channel non linear effects as the eye opening factor is already altered in the back to back configuration. The degradation is thus due to spectrum overlapping. In the case of a WDM system, the eye opening factor is lower than 0,7. This means that the channel spacing is not large enough. Solutions to reduce the penalty would be to increase the channel spacing and/or to consider a higher duty cycle.
On the following graph, we represented the optical spectrum before WDM demultiplexing and the optical eye after WDM demultiplexing in back to back case.

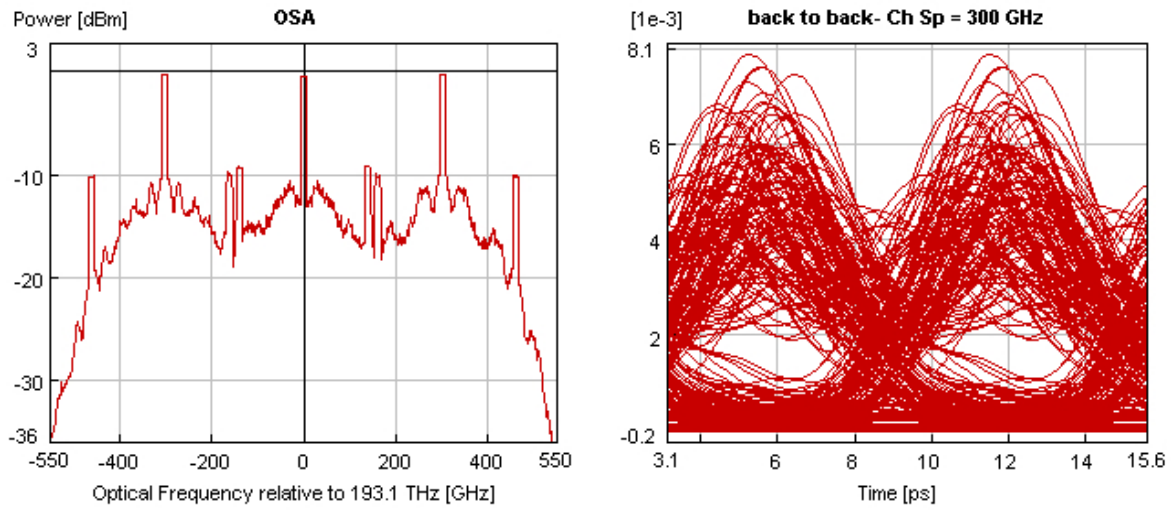

Figure 3. 23. Left: Spectrum of WDM signal with 300 GHz channel spacing. Right: Corresponding eye diagram of the central channel after demultiplexing.

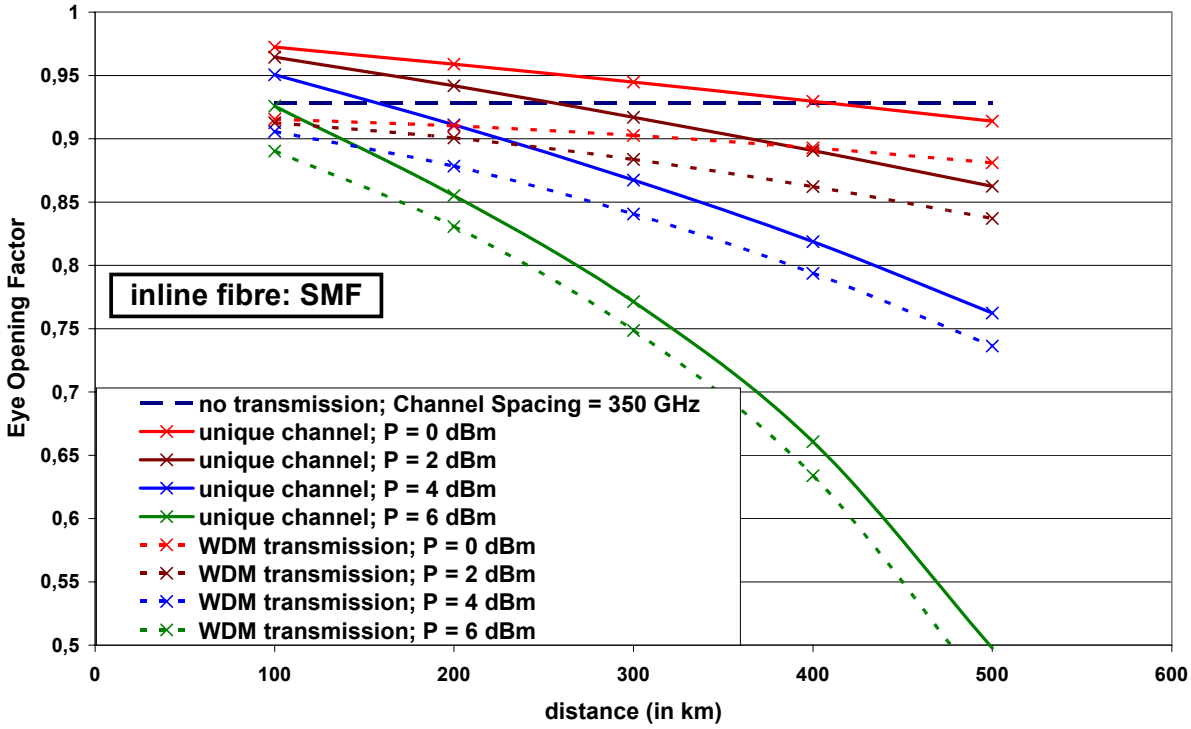

Figure 3. 24. Eye Opening factor for a channel spacing of 350 GHz (duty cycle = 0,4). Comparison of the impact of intrachannel and inter channel non linear effects.

On this graph, we can see that the degradation due to spectrum overlapping is less important than in the previous case and we can compare the eye opening factor for a unique channel and for a WDM transmission. We can see that for this channel spacing of 350 GHz, the eye opening factors measured for WDM transmission are roughly comparable to those obtained for a single channel transmission. Evolutions of the eye opening factor in the cases of a WDM system and of a unique channel are very similar and the offset between

We remark that in this case, the eye opening penalty due to WDM multiplexing is low as there's no more spectral crosstalk. Furthermore, we remark that the influence of inter-channel non linear effects can be neglected compared to the influence of intrachannel non-linear effects. As a

matter of fact, due to the high dispersion of pulses at 160 Gbit/s and reinforced by the high dispersion of SSMF fibre, intrachannel non-linear effects are exacerbated. That's why we have also consider the comparison between single channel transmission and WDM transmission over 5 spans of 100 km of LEAF. We can observe these results on Figure 3. 26 where we still remark the importance of intrachannel non-linear effects beyond inter-channel non-linear effects.

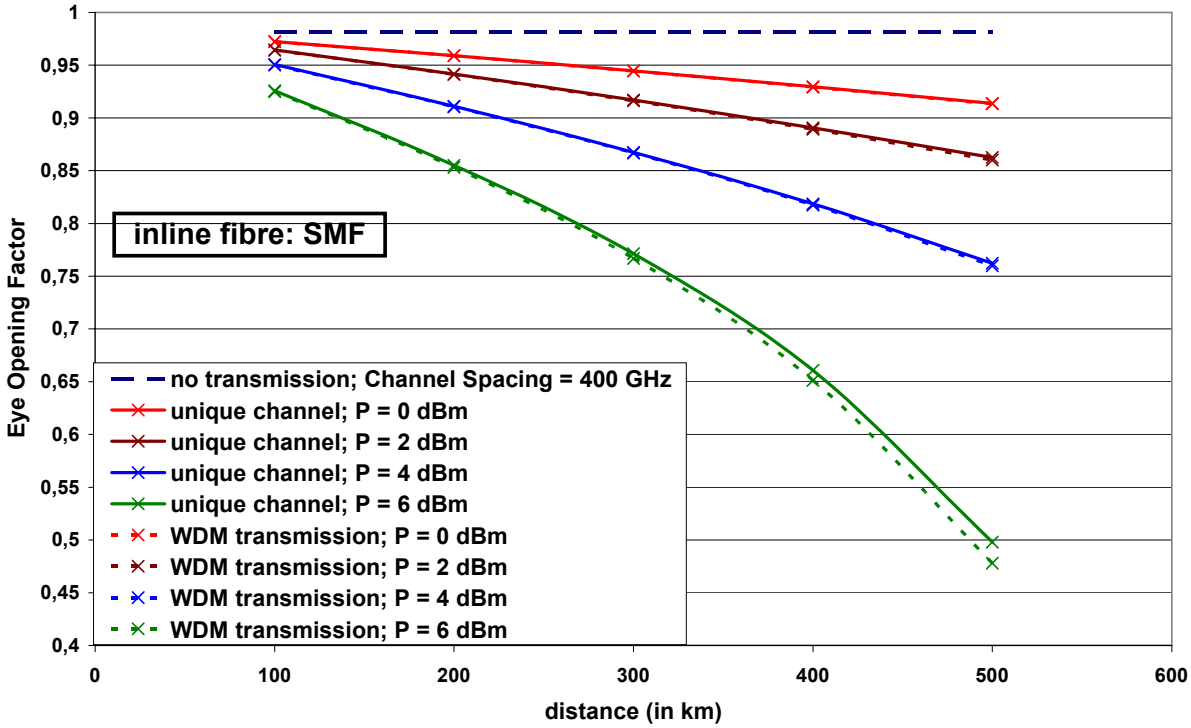

Figure 3. 25. Eye Opening factor for a channel spacing of 400 GHz (duty cycle = 0,4). Comparison of the impact of intrachannel and inter channel non linear effects.

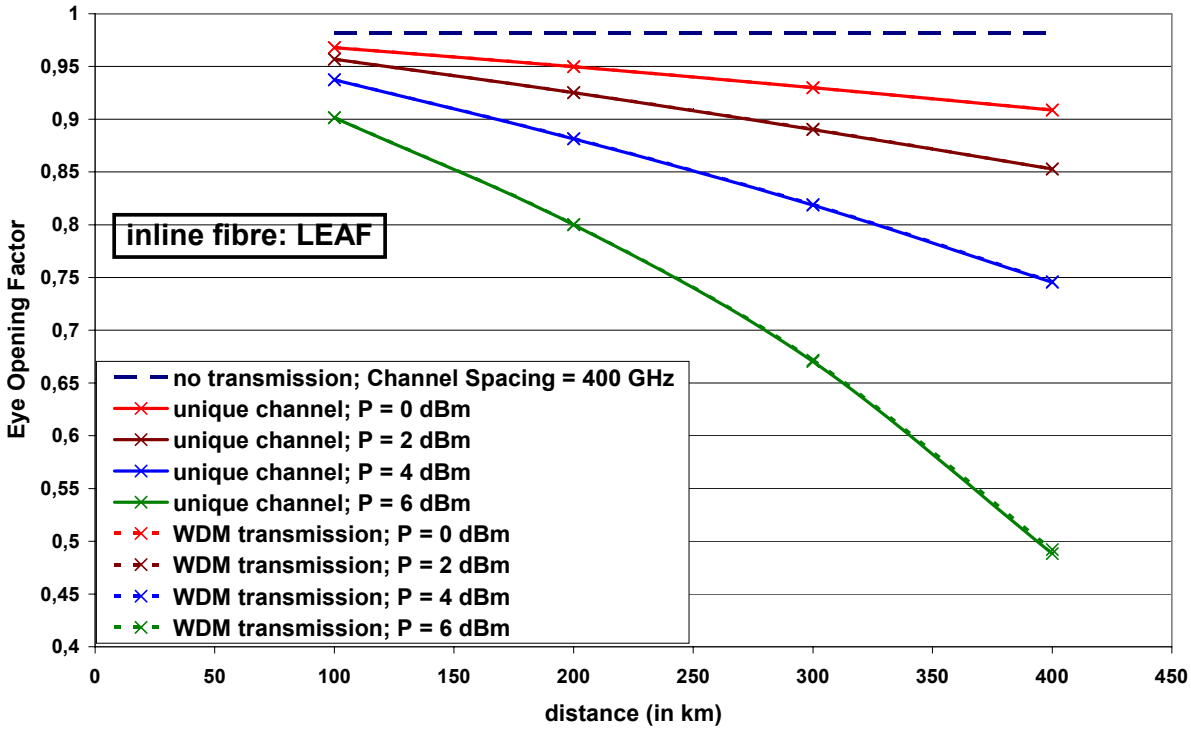

Figure 3. 26. Eye Opening factor for a channel spacing of 400 GHz (duty cycle = 0,4). Comparison of the impact of intrachannel and inter channel non linear effects.

We now investigate the importance of Raman scattering in order to evaluate the importance of this effect. Due to Raman effect, a power transfer occurs from high to low frequency channels. In the following example, we consider a transmission over 6 spans of 70 km of SSMF. Amplification is enabled by double stage erbium amplifiers but noise is not considered in a first step. The emitter is constituted by 8 OTDM channels at the bit rate of 171,2 Gbit/s. For simulation studies, there are almost no difference between 160 Gbit/s and 171,2 Gbit/s but this last bitrate has been considered because of the addition of FEC overhead. In Figure 3. 27, we can visualize the impact of this effect through the comparison of optical spectrums after the emission and at the reception.

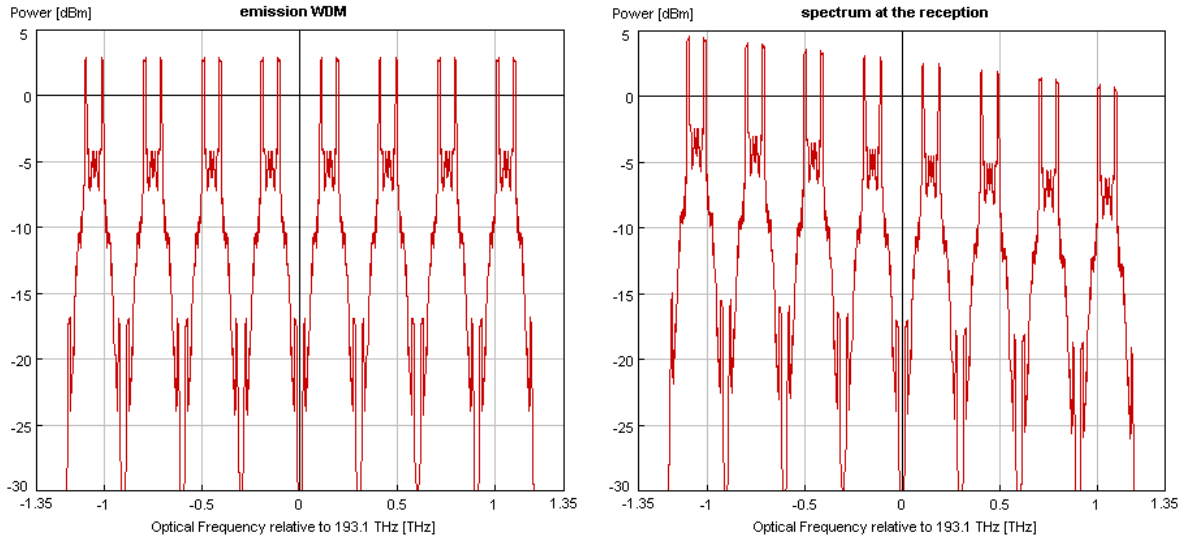

Figure 3. 27. Optical spectrums of a WDM multiplex at the emission (left) and after 420 km (right). Impact of intraband Raman scattering for a channel power of 8 dBm.

We clearly see the impact of this effect in the difference of powers between signal channels. We can therefore measure the impact of this effect by measuring the power range (difference of power between the first and the last channels) as a function of the channel power and distance. In the following graph, we report these results for a channel power of 5 and 8 dBm and with two configurations: each channel is constituted by four tributaries at 42,8 Gbit/s which are temporally multiplexed and these four tributaries are either crossed in polarization or they have the same state of polarization.

We see that for a given channel power, the Raman power transfer is maximal when the tributaries have the same state of polarization but the range after 420 km is only 1,4 dB. This value seems high but we should remember that in these simulations, the fibre attenuation is assumed to be the same and the gain of erbium amplifiers is assumed to be flat over the whole signal bandwidth.

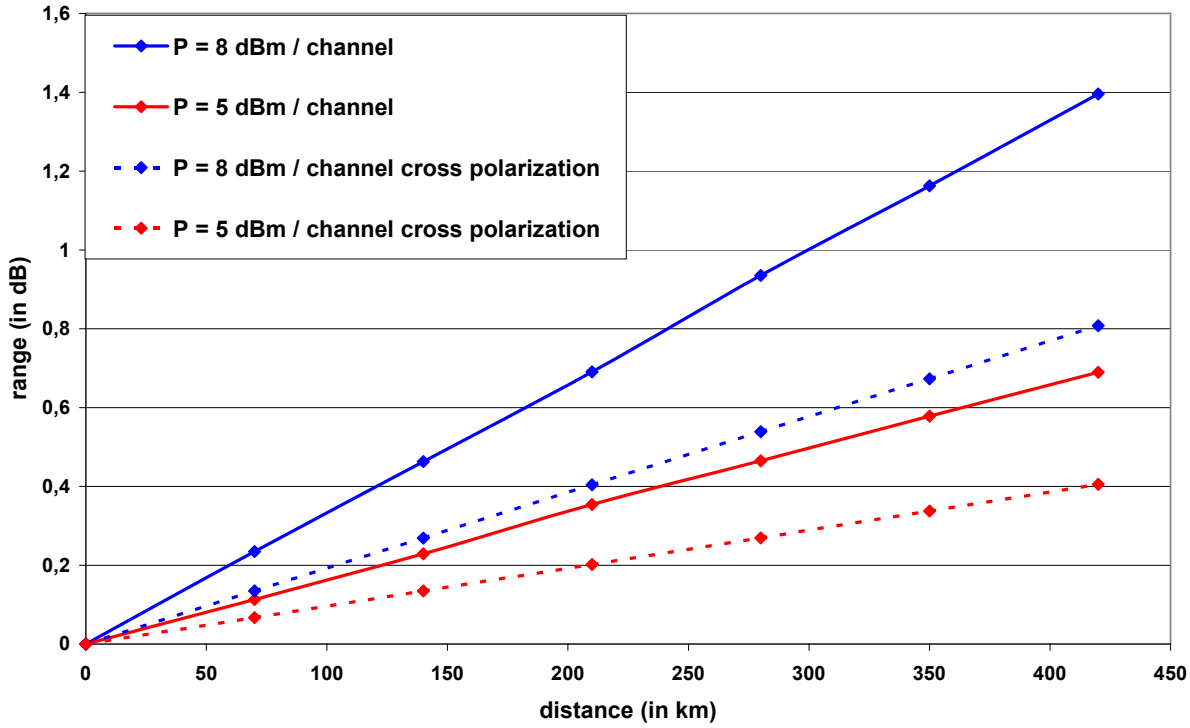

Figure 3. 28. Power range versus distance for a WDM transmission of 8 channels resulting from Raman power transfer.

On the following figure, you can visualize the WDM spectrum after 420 km in the case of single-state polarization and 8 dBm per channel. On the left, we only visualize the effects of Raman power transfer. Noise bins are represented in the bottom of the figure and we can see that the spectral density of noise is nearly flat over the whole spectral inducing a maximal difference of OSNR of 1,4 dB between low and high frequency channels. On the right, the same simulation takes into account the frequency variation of the attenuation in SMF and DCF-type fibres and also the variation of gain in the whole bandwidth. We can see that the power range in this case is a lot higher than in the precedent case: after 420 km, it is estimated to 17 dB.

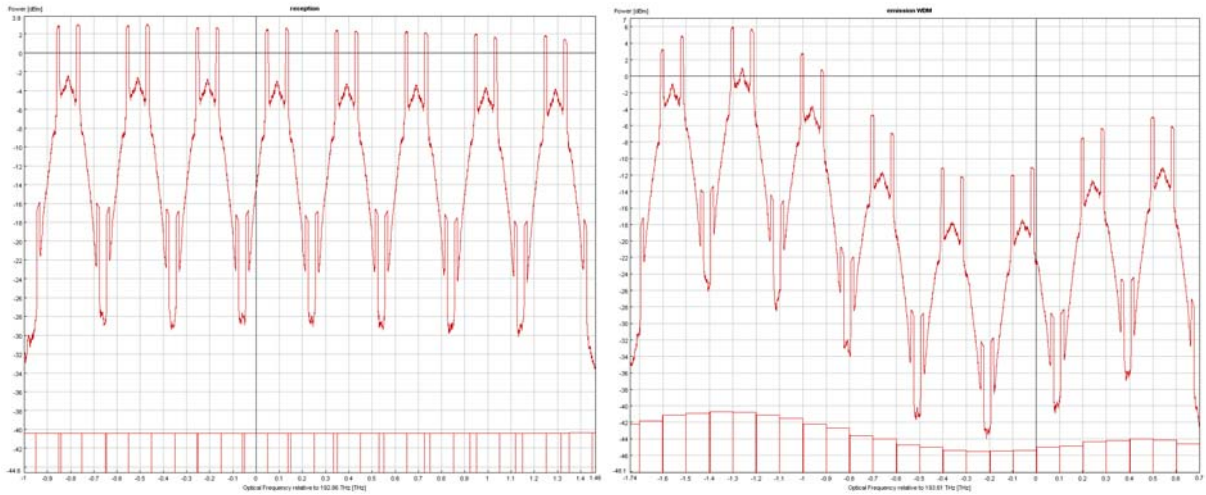

Figure 3. 29. Optical spectrums after 420 km assuming flat gain and attenuation (left) or with real dependence of attenuation and gain (right).

We have therefore shown that the Raman power transfer between signal channels could be neglected compared to other effects inducing a frequency dependent power variation as attenuation and amplifier gain.

Conclusion

This study has shown that the influence of inter-channel non linear effects could be neglected in the design of 160 Gbit/s WDM transmission systems. As a matter of fact, the impact of inter channel four-wave mixing and cross-phase modulation is very low compared to intrachannel four-wave mixing and cross-phase modulation. The important fact concerning the introduction of WDM for the quality of the transmission can thus be understood in two points:

- Firstly, the channel spacing is to be chosen carefully as a function of the spectral width (or duty cycle) as we have seen at the beginning of this chapter.
- Secondly, optical demultiplexing, which is enabled by optical filtering at the end of the transmission line and just before the receiver, should be carefully designed as a function of the signal spectrum.

3 Dispersion management at 160 Gbit/s

3.1 Introduction and first results

In the previous chapters, we have investigated the different propagation effects in order to identify the physical effects responsible of the signal degradation. We have seen that this degradation is mostly due to intrachannel non-linear effects (and mainly intrachannel four-wave mixing). We have identified how the impact of these effects could be reduced using a phase modulation for example. We have seen that using a lower duty cycle, we could increase the channel power but the channel spacing is also to be increased due to a larger spectral width. In the following, we consider dispersion management in order to reduce intrachannel non-linear impairments.

We first consider a lumped amplification scenario as schemed in figure 2. The propagation is considered to be linear in the pre and post dispersion fibres. The post-dispersion fibre is designed so that accumulated dispersion at the receiver is zero because of the very small dispersion tolerance at 160 Gbit/s (±2 ps/nm for a pulse width of 2,5 ps with a 10% variation tolerance on pulse width). The receiver is made of an optical filter, a photodiode and an electrical filter. The Eye opening Factor is then measured.

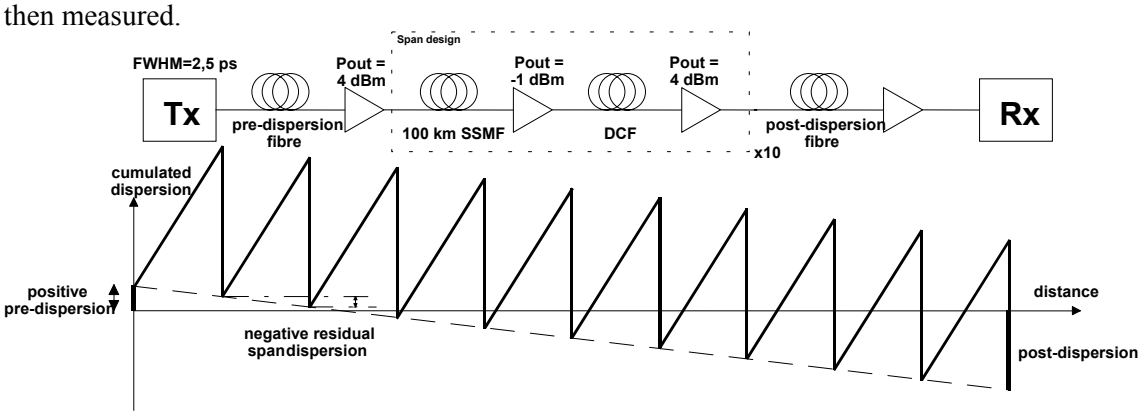

Figure 3. 30. Up: Scheme of the transmission line with lumped amplification scenario.
Down: Evolution of the cumulated dispersion with distance (in this case, positive pre-dispersion and negative residual span dispersion).

Results are plotted on Figure 3. 31 where pre-dispersion ranges from –4300 to +1250 ps/nm and residual span dispersion ranges from –500 to +500 ps/nm. We consider the cases of an RZ modulation.

From this figure, we see that for 0 ps/nm residual span dispersion, a positive pre-dispersion induces penalty whereas a slightly negative pre-dispersion (around -150 ps/nm) is advantageous. Indeed, in this last case, pulse overlapping occurs at the beginning of inline fibre but quickly decreases due to SSMF local dispersion and finally increases when cumulated dispersion becomes positive. Thus, intrachannel four-wave mixing is reduced since it appears in the beginning of the inline fibre (when optical power is high) and in the case of pulse overlapping.

Generally, it appears that a negative residual span dispersion, i.e. an over compensation of dispersion, is valuable for reducing intrachannel non-linear effects. This may be explained by the fact that cumulated dispersion is then slightly negative at the beginning of inline fibre, which reduces pulse overlapping and intrachannel four-wave mixing. We particularly remark an interesting area for which the impact of these effects is optimally reduced [25,26]. This area corresponds to an effective compromise to minimize pulse overlapping, i.e. obtain a slightly negative cumulated dispersion, in the beginning of the inline fibre over a maximum number of spans. For this reason, this compromise shouldn't be altered by the modification of the modulation format or the amplification choice.

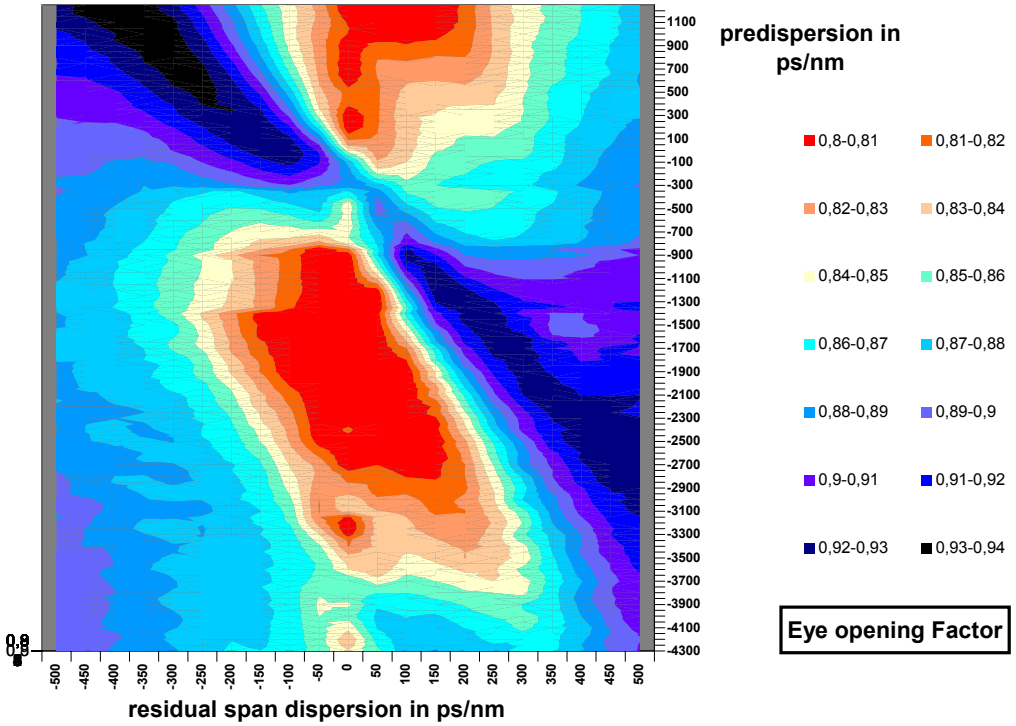

Figure 3. 31. Eye opening factor after 10 spans of 100 km of SSMF with lumped amplification as a function of pre-dispersion and residual span dispersion.

Similar results [28] can be obtained using a different modulation format (DPSK) and/or a different amplification configuration (hybrid amplification with Raman pumping in inline fibre and erbium amplification compensating for DCF loss). These results show that this choice of pre-dispersion and residual span dispersion is not dependant of the amplification choice or modulation format. Indeed, this is logical since intrachannel non-linear effects due to pulse overlapping are mainly dependant on cumulated dispersion and channel power.

For this same reason, we expect this compromise to change if modifying the span length or the inline fibre dispersion. We should now consider a negative pre-dispersion and a positive inline residual dispersion rather than a positive pre-dispersion and a negative inline residual dispersion because the additional attenuation induced by this dispersion is less in this first case. In the following example, we consider a transmission over 6 spans of 70 km of SSMF.

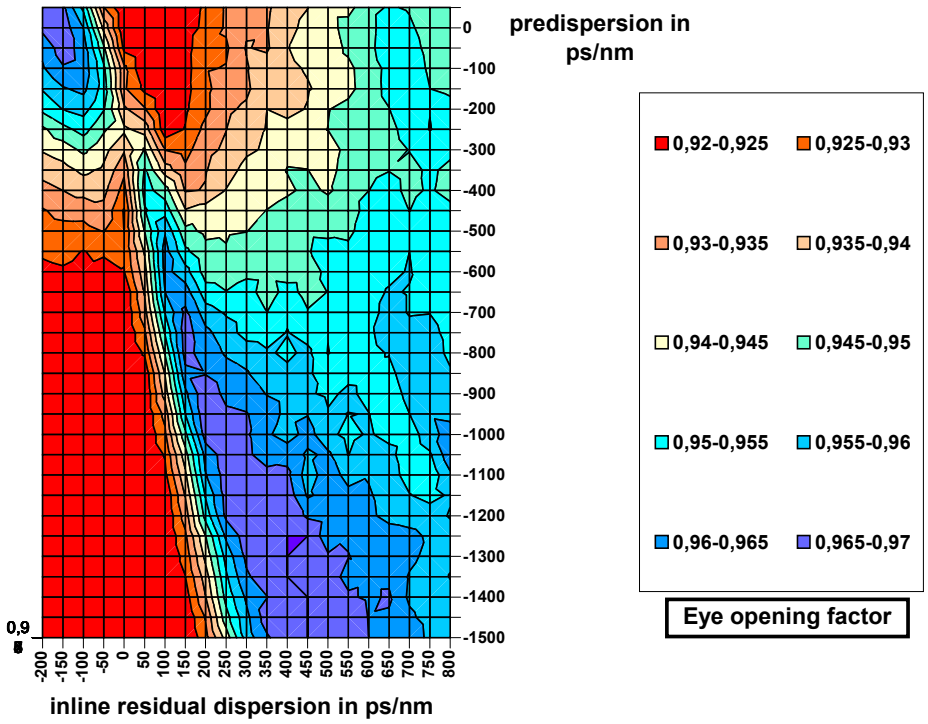

Figure 3. 32. Eye opening factor after 6 spans of 70 km of SSMF with lumped amplification as a function of pre-dispersion and residual span dispersion.

We remark that for an advantageous area, the eye opening factor rises up to 0,96 instead of 0,92 using no pre-dispersion and a perfect compensation after each span(inline residual dispersion = 0 ps/nm). Even if this diagonal area is conserved with a different link configuration, the optimal choice of dispersion management has now changed: setting the pre-dispersion to -1000 ps/nm, the optimal inline residual dispersion per span is 150 ps/nm in the first case (transmission over 10 spans of 100 km) whereas it is 225 ps/nm in the second case (transmission over 6 spans of 70 km).

3.2 Analytic expression for the reduction of non-linear interactions

Rules have been introduced [25,26,27] in order to design efficient dispersion maps for transmission at 40 Gbit/s. This rule is based on the conservation of energy. Trying to minimize the phase modulation induced by self-phase modulation, he obtains the following relation between optimal pre-dispersion and residual span dispersion:

$$D_{pre-dispersion} = -\frac{N-1}{2}.D_{residual/span} - \frac{D_{fibre}}{\alpha_{fibre}}$$

where $D_{pre\text{-}dispersion}$ and $D_{residual/span}$ are the values of pre-dispersion and residual dispersion per span, N is the number of spans, D_{fibre} and α_{fibre} are the dispersion and attenuation coefficients of inline fibre. We immediately recognize the definition of a straight line, which is coherent with the results obtained by numerical simulations. For example, using 6 spans of 70 km of SSMF, the values of D_{fibre} and α_{fibre} are respectively 17 ps/nm/km and 0,046052 km^{-1}. Numerical applications give:

- With $D_{residual/span}$ = 0 ps/nm, we obtain: $D_{pre-dispersion} = -\frac{17}{0,046052} \approx -369$ ps/nm.
- With $D_{residual/span}$ = 300 ps/nm, we obtain:

$$D_{pre-dispersion} = -2,5.300 - \frac{16}{0,046052} \approx -1097 \text{ ps/nm}.$$

These results are in agreement with those obtained on Figure 3. 32. However, we notice a small shift between numerical results and these predicted values. This rule can consequently be used at 160 Gbit/s in order to give a hint on optimal values. As a matter of fact, this rule is based on the reduction of self-phase modulation effect [26] but does not consider intrachannel four-wave mixing and intrachannel cross-phase modulation. These last two effects are due to the collision of pulses (which is due to the broadening of these pulses with dispersion). In the Schrödinger equation, the last term representing non-linear effects can be expanded under the form:

$$\gamma.|E|^2.E = \left(\sum_{j=0}^{n}\gamma.|u_j|^2.u_j^*\right) + \left(2.\gamma.\sum_k |u_k|^2.\left(\sum_{j\neq k} u_j\right)\right) + \left(\gamma.\sum_{\substack{l,m,n\\ n\neq l\\ n\neq m}} u_l.u_m.u_n^*\right)$$

Assuming Gaussian pulses, the Gaussian shape is maintained in the linear transmission and we consider non-linear effects as a small perturbation. The electromagnetic field of a pulse in the transmission fibre after z km is thus described by:

$$E(t,z) = \frac{E_0.e^{-\frac{\alpha}{2}.z}}{\sqrt{1+\frac{\lambda^4}{\pi^2.C^2}\left(D_{fibre}.z + D_{pre-dispersion}\right)^2}} e^{-\frac{t^2}{T_0^2.\left(1+\frac{\left(D_{fibre}.z+D_{pre-dispersion}\right)^2.\lambda^4}{\pi^2.C^2.T_0^2}\right)}}$$

The first term $E_0.e^{-\frac{\alpha}{2}.z}$ represents the reduction due to fibre attenuation. The term with the square root can be considered as the diminution of intensity due to the pulse broadening. At last, the exponential term symbolizes the Gaussian shape and the broadening due to dispersion. Considering three different pulses centered in t = 0, t = -T_b and t = T_b (T_b is the time bit), we have:

$$E(t,z) = \frac{E_0.e^{-\frac{\alpha}{2}.z}}{\sqrt{1+\frac{\lambda^4}{\pi^2.C^2}\left(D_{fibre}.z + D_{pre-dispersion}\right)^2}} \sum_{k=-1,0,1} e^{-\frac{(t-k.T_b)^2}{T_0^2.\left(1+\frac{\left(D_{fibre}.z+D_{pre-dispersion}\right)^2.\lambda^4}{\pi^2.C^2.T_0^2}\right)}}$$

In order to evaluate the importance of non-linear effects, we can define a hybrid factor noted ovlp which represents the amount of the non-linear perturbation in the Schrödinger equation:

$$ovlp(t,z) = \left|\gamma.|E|^2.E\right| = \gamma.|E|^3$$

The computation of this ratio can be achieved when considering a transmission with dispersion management:

$$OVLP = \int_{z=0}^{z=L}\int_{t=-\infty}^{t=+\infty} ovlp(t,z).dt.dz = \int_{z=0}^{z=L}\int_{t=-\infty}^{t=+\infty} \gamma.|E|^3.dt.dz$$

Using a numerical-based calculation and considering a transmission over 5 spans of 100 km of SMF (D = 17 ps/nm/km; α=0,2 dB.km^{-1}; γ=1,312 rad.W^{-1}.km^{-1}) compensated by DCF (D = -90 ps/nm/km; α=0,6 dB.km^{-1}; γ=3,93 rad.W^{-1}.km^{-1}). In order to better visualize the impact of dispersion management, we represented the logarithm of this value while predispersion and residual dispersion vary from -500 to +500 ps/nm. The following figure compares the results: on the left, we represented the logarithm of the overlapping factor as a function of predispersion and residual dispersion. On the right, we represented the eye opening factor obtained from numerical simulations. On these two graphs, we also represented the straight line (in red) giving the optimal predispersion as a function of

the residual dispersion [25]. On the right figure, we clearly see the presence of a transverse area where non-linear effects are reduced. This area is predicted by the rule mentioned before but numerical results also show an unexpected rupture in this transverse area when the predispersion value is between -150 and -400 ps/nm. We also observe this break on Figure 3. 31 and Figure 3. 32 for different transmission cases. This break also appears on the left figure when we consider pulse overlapping but for values of predispersion between 200 and -300 ps/nm. We also remark some unexpected results concerning the overlapping factor for extreme values of predispersion and/or residual dispersion: for example, for positive values of residual dispersion and predispersion, we obtain a small overlapping factor but this is due to our modelling which only includes three pulses. Including more pulses would allow us to solve this problem but the computation time would increase.

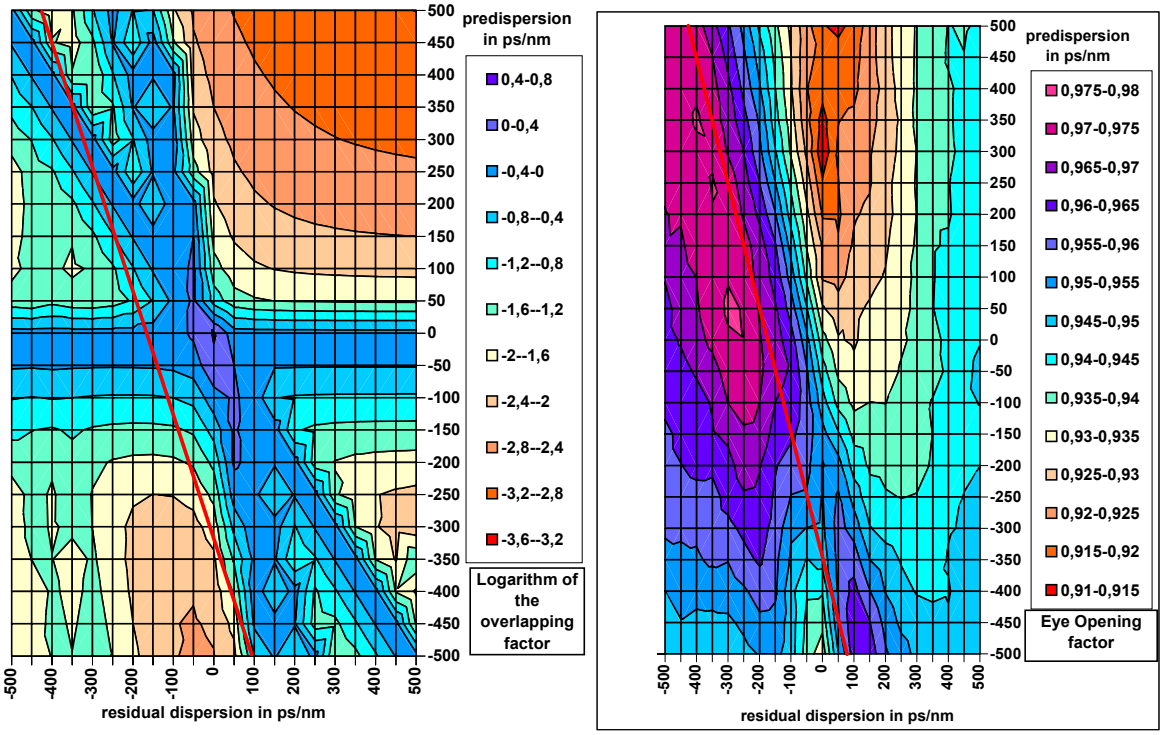

Figure 3. 33. Comparison of the overlapping factor (analytic estimation) and the eye opening factor (numerical result) after 5 spans of 100 km of SSMF as a function of pre-dispersion and residual span dispersion. Red line corresponds to analytical rule in [26]

These two figures show us that considering dispersion management as a way to reduce non-linear effects is valuable if both self-phase modulation and interaction effects (intra-channel four-wave mixing and cross-phase modulation) are considered. We have seen in the beginning of this study of non-linear effects that self phase modulation mainly occurred because of simultaneous high peak power and low pulse width but reciprocally, it is not efficient to broaden pulses (using a pre-dispersion fibre) as a too large broadening will result in pulses interactions and intra-channel non linear effects.

3.3 Simple physical analysis of the non linear effects dependence on cumulated dispersion

In order to well understand this compromised approach, we have first studied how intrachannel four-wave-mixing could be reduced using predispersion. We first consider a transmission over only one span of 100 km of SSMF. Cumulated dispersion is perfectly compensated by DCF. A pre-dispersion fibre with a varying value is used in order to shift the predispersion. Non linear effects are not considered in DCF and in the predispersion fibre. Noise issues are not considered. On Figure 3.

34, we represented the standard deviation for three different injection powers as a function of pre-dispersion.

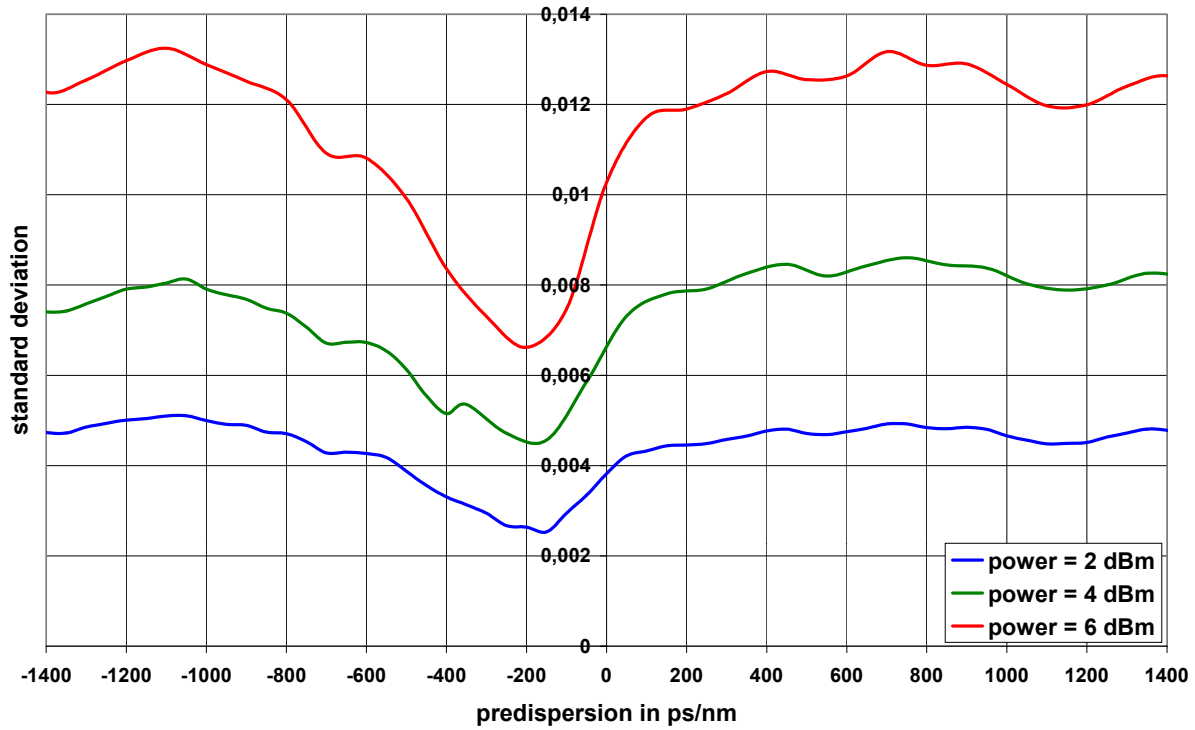

Figure 3. 34. Impact of intrachannel four-wave mixing versus predispersion after transmission over one span of 100 km of SSMF.

We can clearly see the reduction of intra-channel four-wave-mixing for a pre-dispersion value slightly greater than -200 ps/nm. We highlight the fact that this optimum value is not coherent with the rule mentioned above at 40 Gbit/s as, for a transmission over one span, we obtain:

$$D_{pre-dispersion} \approx -\frac{D_{fibre}}{\alpha_{fibre}} \approx -369 \text{ ps/nm}$$

We now would like to investigate the dependence of this value with regards to the duty cycle, i.e. the pulse width. We consider the same transmission scheme (1 span of 100 km of SSMF). Results are displayed on Figure 3. 35. We remark that this optimal value is not altered by the variation of the pulse width as the optimum value of -200 ps/nm is preserved when the duty cycle increases from 0,1 to 0,4.

On Figure 3. 36, we represented the evolution of the standard deviation versus predispersion considering different fibre lengths from 60 to 100 km. We clearly see that the optimal predispersion value does not change with this parameter.

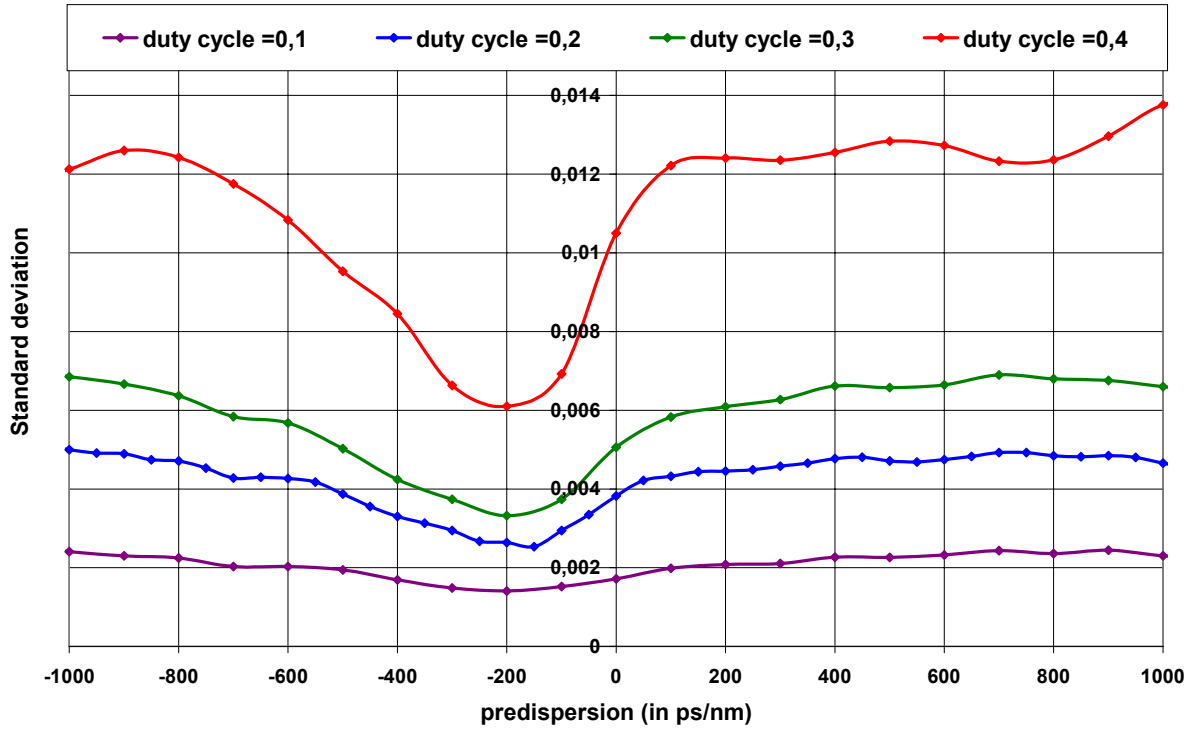

Figure 3. 35. Impact of intrachannel four-wave mixing versus predispersion for various pulse widths. Transmission over one span of 100 km of SSMF.

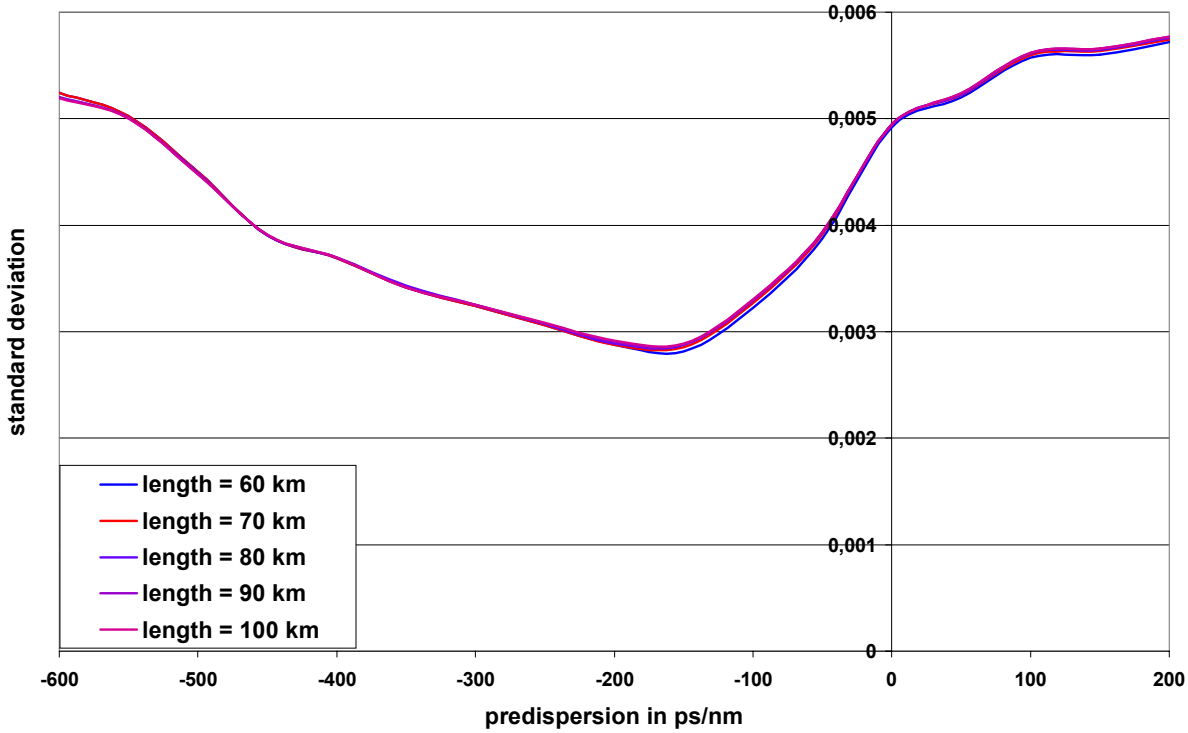

Figure 3. 36. Impact of intrachannel four-wave mixing versus predispersion for various span lengths. Transmission over one span of SSMF.

At last, on Figure 3. 37, we can see the evolution of the standard deviation versus predispersion for two different inline fibre dispersions, i.e. 4 and 17 ps/nm/km corresponding to Leaf and SSMF fibre types. This time, we notice that the optimum predispersion value is shifted from -200

ps/nm to roughly -50 ps/nm. We can understand this dependence when we consider that, in order for intra-channel four-wave-mixing to occur, a sufficient broadening of the pulse is necessary. The pulse broadening depends on the inline fibre dispersion as we have the following relation between the pulse width T(z), i.e. after z km, and the initial pulse width T_0:

$$\frac{T(z)}{T_0} = \sqrt{1 + \frac{\left(D_{fibre}.z + D_{pre-dispersion}\right)^2.\lambda^4}{\pi^2.C^2.T_0^2}}$$

If the fibre dispersion changes, reducing the pulse broadening at the beginning of the fibre in order to decrease the amount of overlapping implies to reduce the pre-dispersion by the same factor. For example, if the fibre dispersion is 17 ps/nm/km and if the pre-dispersion is set to -200 ps/nm/km then in the first ten kilometres of transmission, the pulse shortens up to its initial width whereas using a fibre dispersion of 4 ps/nm/km and the same pre-dispersion value, the pulse broadening nearly doesn't change in the first ten kilometres.

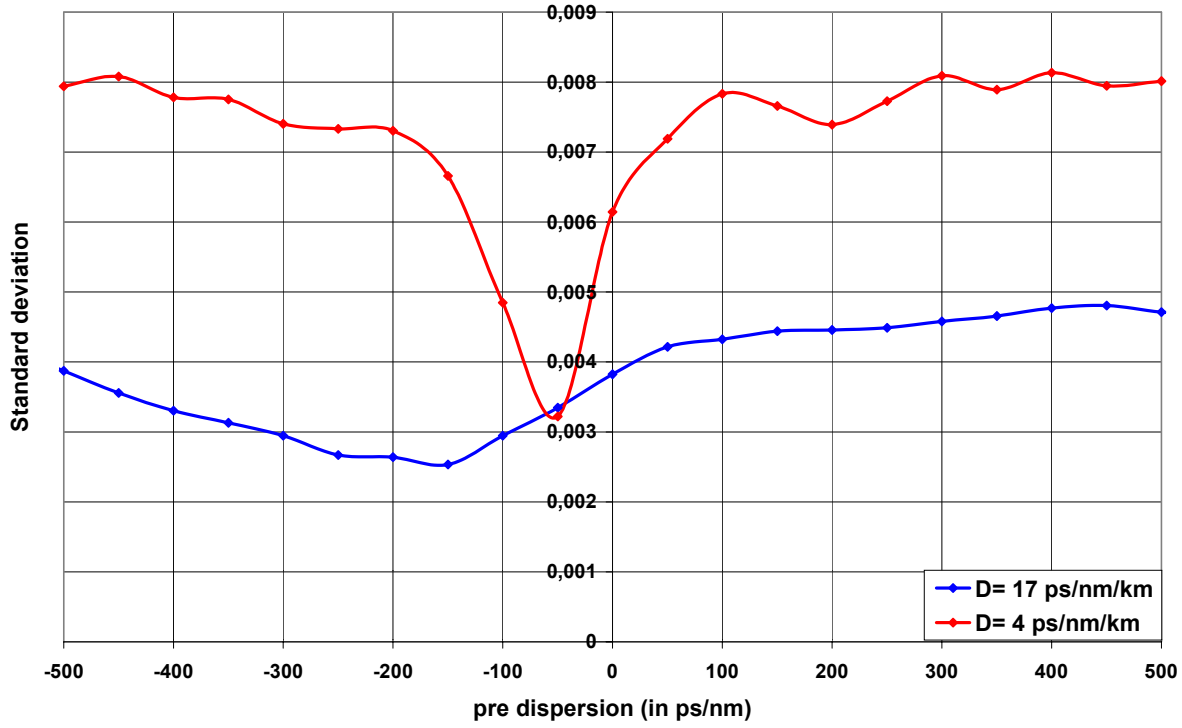

Figure 3. 37. Impact of non linear distortion versus predispersion for two different fibre dispersions.

These results on the minimization of intra-channel four-wave mixing can also be applied to the case of intra-channel cross phase modulation as these two effects are due to pulse interactions, which we reduce here by the use of pre-dispersion. As a consequence of these results, it is possible to reduce these two effects when the cumulated dispersion at the beginning of a span holds between -200 and -150 ps/nm in the case of SMF and around -50 ps/nm in the case of LEAF.

3.4 Engineering rule for the design of high bitrate WDM dispersion map

Concerning self-phase modulation, we can estimate that, if the initial pulse width is 2,5 ps, a predispersion of -150 ps/nm broadens this pulse up to 120 times its initial width. It is therefore clear that the self-phase modulation has nearly no impact in the beginning of the transmission. After 9 km, the cumulated dispersion is approximately zero and consequently, the pulse width is minimal implying self-phase modulation but the power reduction due to the propagation in the first kilometres (around 2 dB for 9 km) limits the self-phase modulation effect.

This small analysis concerning the compromise between pulse overlapping and high peak power has enabled us to understand the impact of dispersion management and its use to increase the signal quality. The following rules can be expressed:

- In order to reduce self-phase modulation, the cumulated dispersion should not be equal to zero when the mean power is high.
- In order to reduce intra-channel four-wave mixing and cross phase modulation, pulse overlapping should be reduced when the mean power is high. This can be achieved by setting the cumulated dispersion at the beginning of a transmission span between -200 and -150 ps/nm in the case of SMF (D = 17 ps/nm/km). The optimum cumulated dispersion at the beginning of the span is proportional to the fibre dispersion.

We can therefore qualitatively evaluate the efficiency of a dispersion management with regards to the importance of intrachannel non linear effects. As an example, we consider a transmission over 6 spans of 100 km of SSMF. We consider two different dispersion schemes: the first one uses neither pre-dispersion nor residual span dispersion. The second dispersion scheme is defined by a pre-dispersion of -1000 ps/nm and a residual span dispersion of 210 ps/nm. In Figure 3. 38 and Figure 3. 39, we represented the evolution of cumulated dispersion (in ps/nm), pulse width (in ps), mean power (in dBm) and peak power (in mW) for these two dispersion maps. Cumulated dispersion and pulse width are affected to the y-axis on the left whereas mean and peak powers are affected to the y-axis on the right. The fringe below the figure represents the incidence of non linear effects. Blue colour symbolizes intrachannel four-wave-mixing and red colour symbolizes self-phase-modulation.

As we have already mentioned, the incidence of self-phase modulation is due to a high peak power and a small pulse width. As an arbitrary criterion, we will consider that this non linear effect occurs if the cumulated dispersion is equal to zero and if the peak power is greater than 2 mW.

With a similar criterion, we will consider the incidence of intrachannel four wave mixing (and/or cross phase modulation) when the cumulated dispersion does not hold between -200 and -150 ps/nm and when the mean power is greater than 2 dBm. We need to precise that even if the cumulated dispersion at the beginning of the span is between these two values, pulse overlapping occurs and therefore impairments appear (ghost pulses due to intrachannel four wave mixing for example) even if there are less impairments than when using no-predispersion. Consequently, even if there is no blue colour in the fringe, it means that intrachannel four wave mixing is minimized but not cancelled as it can be seen on Figure 3. 34, Figure 3. 35, Figure 3. 36 and Figure 3. 37.

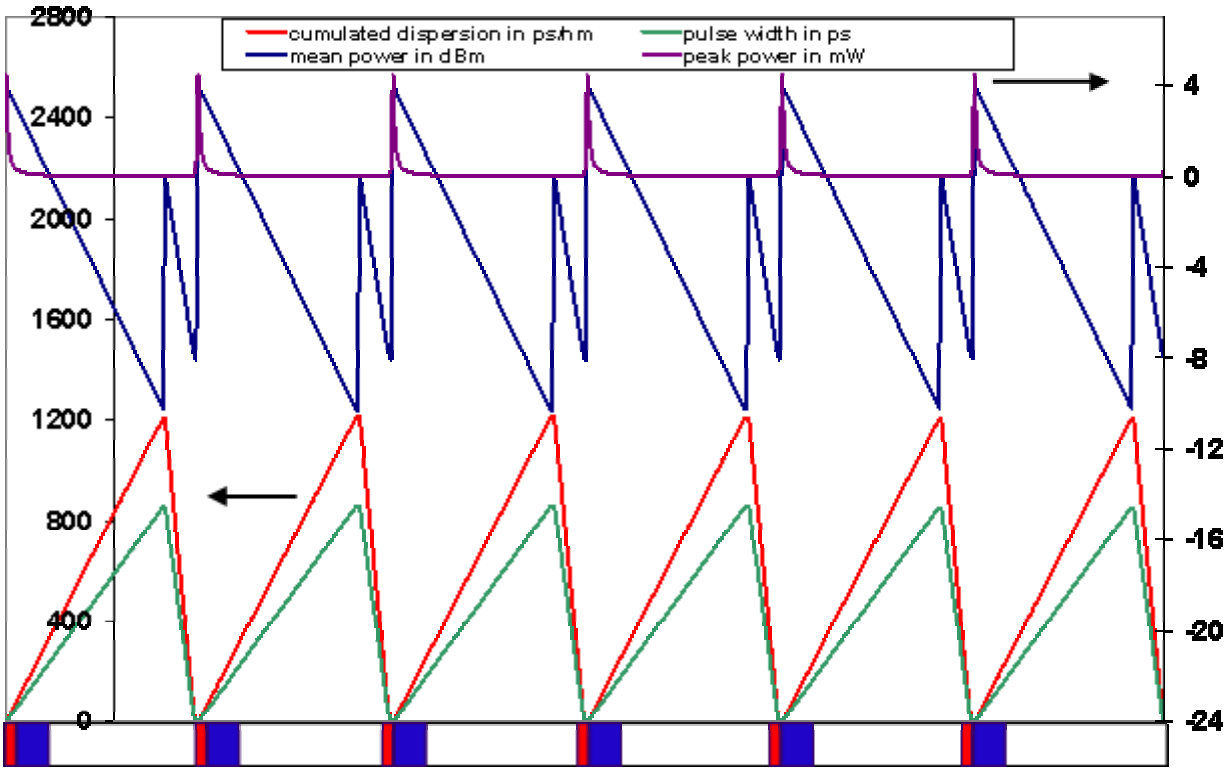

Figure 3. 38. Intrachannel non linear effects in transmission over 6 spans of 100 km of SSMF with a classic dispersion map (no predispersion, no residual dispersion). Blue colour: intrachannel four wave mixing; Red colour: self phase modulation.

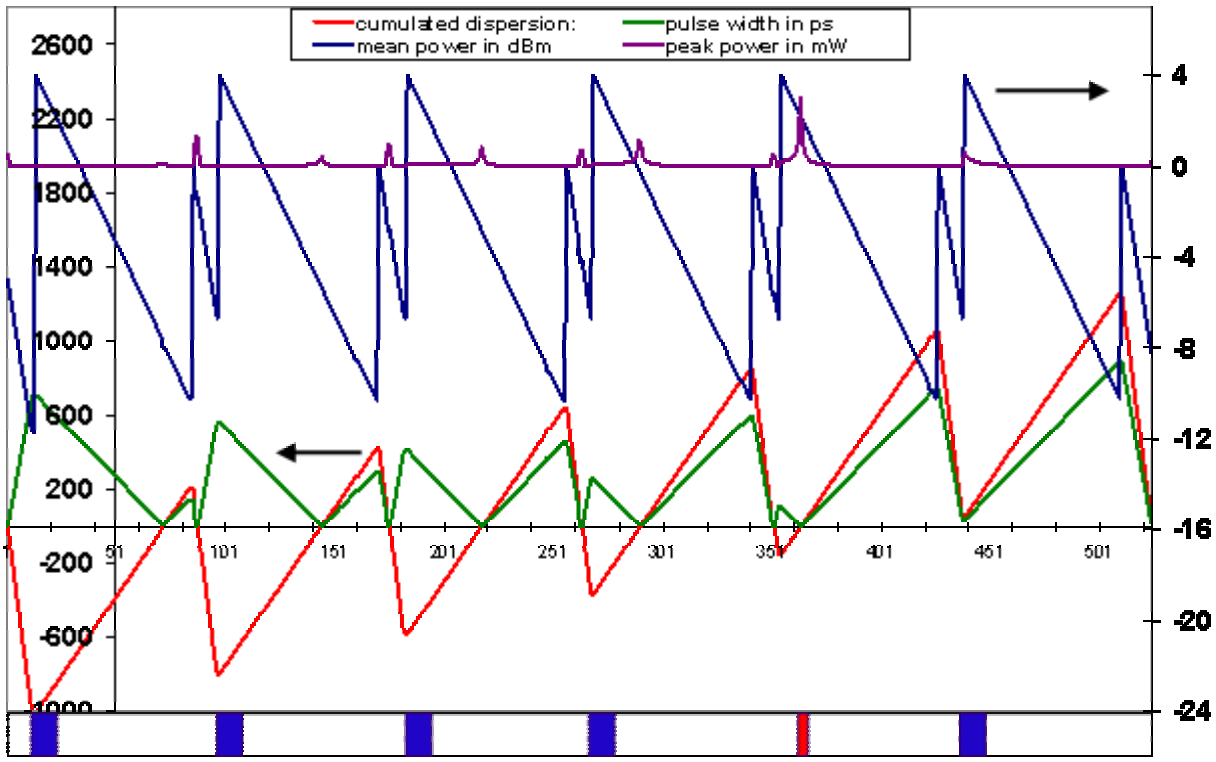

Figure 3. 39. Intrachannel non linear effects in transmission over 6 spans of 100 km of SSMF with an optimized dispersion map. Blue colour: intrachannel four wave mixing; Red colour: Self phase modulation.

We clearly see that we limit the happening of self-phase modulation with the second dispersion scheme. Furthermore, at the beginning of the 5th span, the cumulated dispersion is around -160 ps/nm. From the analysis that we have led, we know that intrachannel effects will be reduced in the beginning of this span.

With this simple rule for the design of the dispersion map, we can also choose to reduce intra-channel four-wave mixing over the transmission by considering a predispersion of -175 ps/nm and a zero residual dispersion per span as depicted on Figure 3. 40. With the same criterion than before, we remark that self-phase modulation will probably degrades the transmission quality at the beginning of each span. A solution to avoid this effect would be to reduce the injection power into inline fibre and the OSNR reduction could be compensated by the use of backwards Raman pumping.

In order to verify these results, we made numerical simulations of transmission over 6 spans of SSMF corresponding to these three dispersion schemes. In these simulations, noise issues were not considered. They only included a single-channel transmission. The eye opening factor is measured after detection. On Figure 3. 41, we display the evolution of the eye opening factor for the three dispersion schemes as a function of the injected signal power into inline fibre. We clearly see the improvement due to the change of dispersion map. Considering an eye opening factor of 0,9, we observe a difference larger than 2 dB between classic and optimized dispersion map.

On Figure 3. 42, we have represented the three electrical eyes in the case of 0 dBm inline fibre injection power. We can clearly see the reduction of standard deviation for marks in the two special designed dispersion maps.

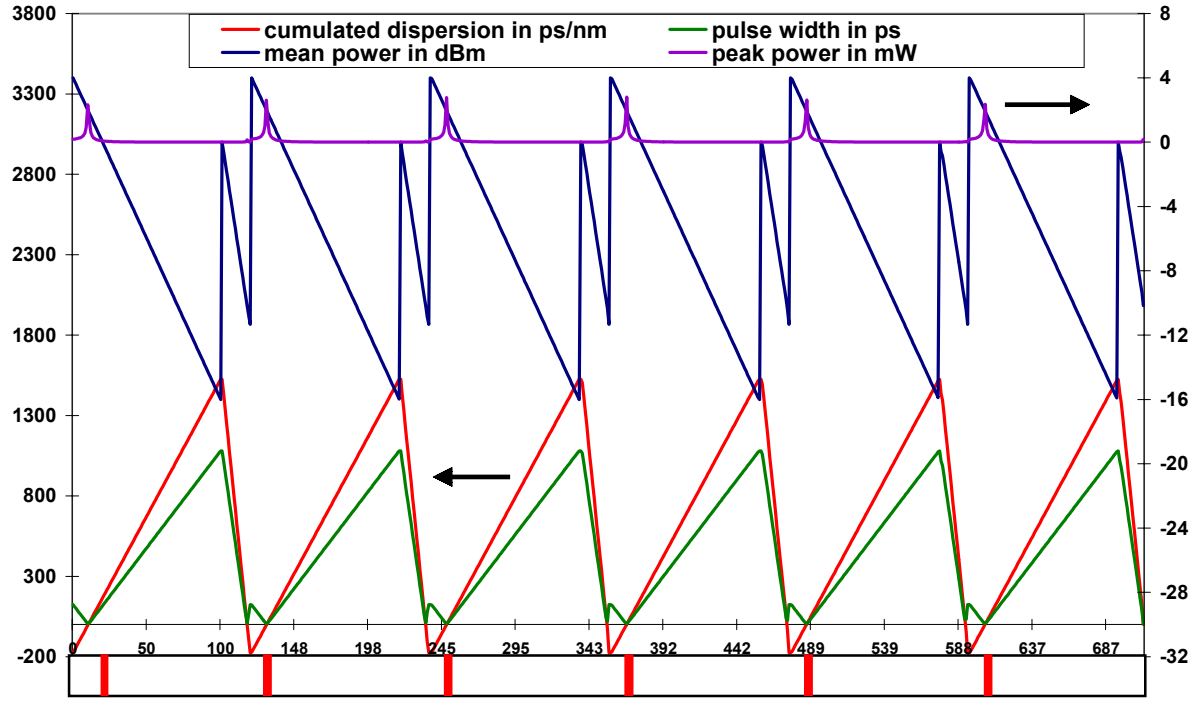

Figure 3. 40. Intrachannel non linear effects in transmission over 6 spans of 100 km of SSMF with a predispersion of -175 ps/nm and no residual dispersion per span.
Blue colour: intrachannel four wave mixing; Red colour: Self phase modulation.

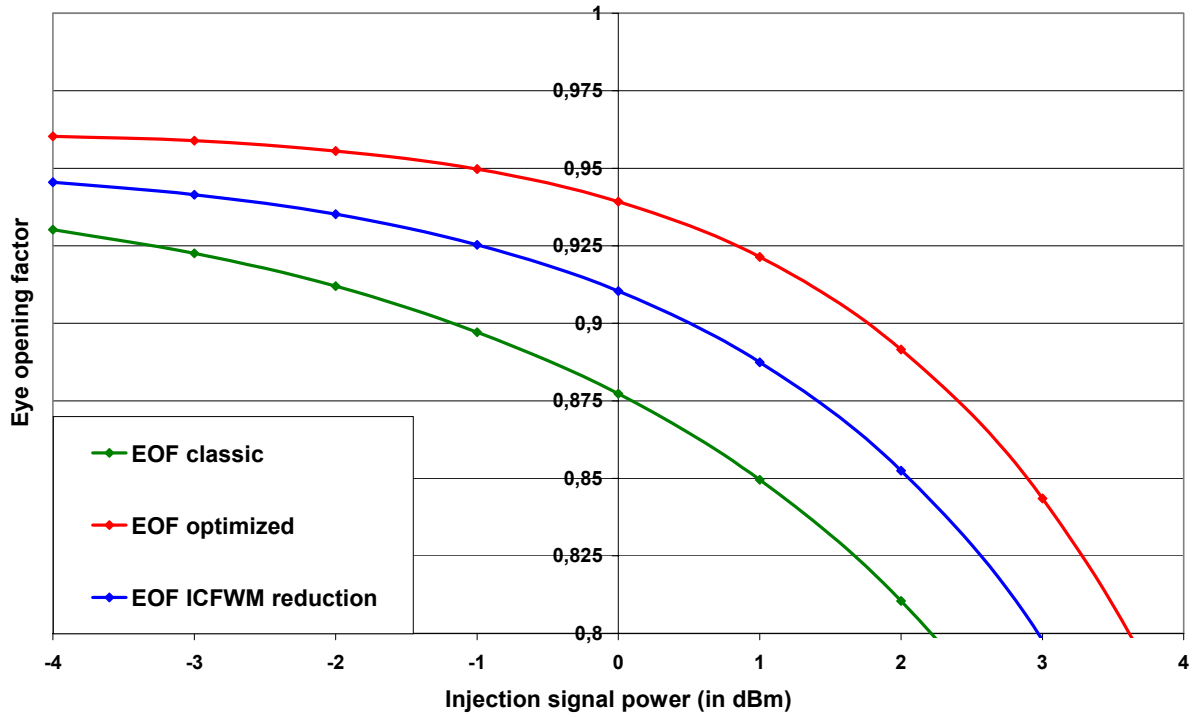

Figure 3. 41. Evolution of the eye opening factor (EOF) for the three distinct dispersion schemes as a function of the inline fibre injection power.

As predicted, we can observe the improvement from the classic dispersion map to the two other dispersion maps. We can also notice the difference between the dispersion map that reduces intrachannel four-wave-mixing and the optimized dispersion map: a broadening of the pulses, due to self phase modulation, can be clearly seen in the first case as the crosstalk between adjacent bits is more significant.

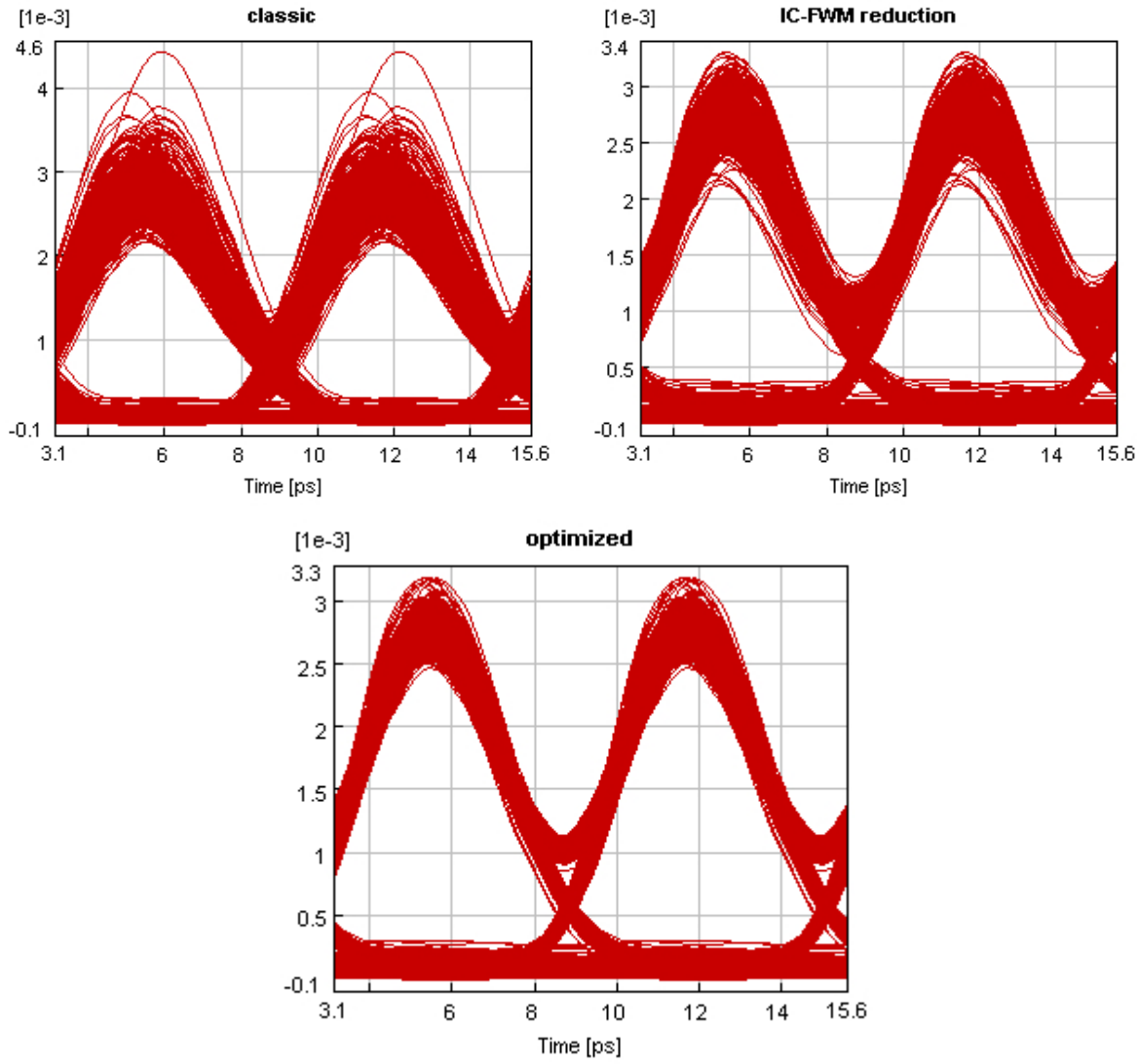

Figure 3. 42. Electrical eye obtained for the three distinct dispersion schemes after transmission over 6 spans of 100 km of SSMF.

We would like to point out that we have studied the use of dispersion management in order to reduce intrachannel non linear effects as they are preponderant in most of the 160 Gbit/s per channel transmission cases. However, with this optimization for a single channel, we can wonder if this choice of dispersion map is still efficient for every single channel transmitted. As a matter of fact, dispersion slope of fibre changes the dispersion values of predispersion and/or residual dispersion per span. In the last transmission case where we considered a transmission over 6 spans of 100 km of SSMF, an optimized dispersion map was obtained using a pre-dispersion of -1000 ps/nm and a residual dispersion per span of 210 ps/nm. We shall here consider classical values for SMF and DCF such as 17 and -90 ps/nm/km for dispersion and 0,08 and -0,45 ps/nm²/km for dispersion slope.

If the DCF lengths are adjusted so that these values are matched for the central wavelength at 1550 nm and if we consider a transmission of 9 channels with a channel spacing of 400 GHz (3,2 nm) then for the extreme channel, we have:

- Pre-dispersion: $-1000-\frac{1000}{90}.(0{,}45).(4.3{,}2)=-1064$ ps/nm
- Residual dispersion: $(1700-1490)+(\frac{1700}{17}.0{,}08.4.3{,}2-\frac{1490}{90}.0{,}45.4.3{,}2)=217$ ps/nm

These values do not differ a lot from the initial values as the relative deviation is 6% for pre-dispersion and 3% for residual dispersion and so, we can consider that the non linear effects reduction will be effective for the whole WDM multiplex.

At last, I would like to mention that the optimum value we have found for cumulated dispersion at the beginning of the span enables us a very quick and simple design of a dispersion map in order to minimize intrachannel non-linear effects whatever the considered transmission. For example, we consider a 160 Gbit/s WDM transmission with the following link:

- One span of 80 km of SSMF (D=17 ps/nm/km).
- One span of 120 km of SSMF (D=17 ps/nm/km).
- Two spans of 70 km of Leaf (D=4 ps/nm/km).
- One span of 90 km of Teralight (D=8 ps/nm/km).
- One span of 50 km of SSMF (D=17 ps/nm/km).

We have shown that, in order to reduce intrachannel four-wave mixing, the cumulated dispersion at the beginning of the span should be between -200 ps/nm and -150 ps/nm for SSMF. We can choose to set it to -175 ps/nm. We have also shown that this value is proportional to the inline fibre dispersion of the following span. Therefore, in the case of Leaf and Teralight, the cumulated dispersion should be respectively -41 and -82 ps/nm. The dispersion map (cumulated dispersion) is represented on the following graph where we can also visualize the evolution of mean power, pulse width and peak power. However, the occurring of a high peak power shortly after the beginning of each span induces self phase modulation impairment.

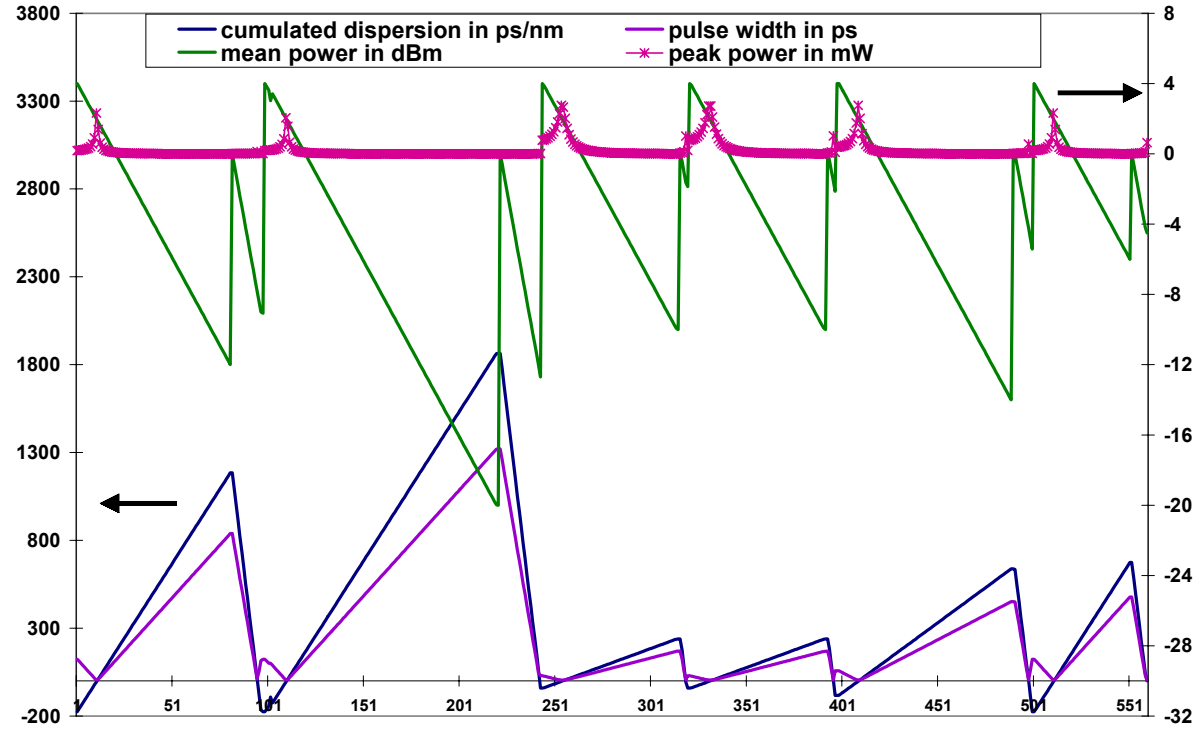

Figure 3. 43. Evolution of parameters for the designed dispersion map reducing intrachannel . Transmission over 480 km with various fibre types.

Conclusion

We have seen that with an adequate design of the dispersion map, the impact of intrachannel non-linear effects could be reduced. We will use this modelling in a next chapter in order to take into account the influence of noise in the dispersion management design. From a technical point of view, it is obvious that dispersion management is a key solution for the design of very high bit rate transmission systems. In this part, we only investigated the case of a singly periodic dispersion map but it is also possible to design more complex dispersion maps. However, these solutions present a lot

of disadvantages for practical considerations [29]. Of course, thanks to the progress in research, all problems will be solvable in the future and dispersion management appears to be one of the simplest ways to reduce nonlinear impairments.

4 References

1. Nonlinear Fiber Optics, Govind P. Agrawal, Academic Press Inc., 1989.
2. « Collective variable theory for optical solitons in fibers», P. Tchofo Dinda et al., Physical review E., vol. 64, June 2001, p. 016608.
3. « A collective variable approach for dispersion-managed solitons», P. Tchofo Dinda et al., Journal of Physics A, vol. 34, Issue 10, June 2001, L103-L110.
4. « Hamiltonian equations for multiple-collective-variable theories of nonlinear Klein-Gordon equations: A projection-operator approach», R. Boesch, P. Stancioff et C. R. Willis, Physical Review B, Volume 38, Number 10(1988), p. 6713
5. « Temperature dependence of chromatic dispersion in various types of optical fibers.», Kato T., Optical Fiber Communication Conference, 2000 , Volume: 1 , 7-10 March 2000, Pages:104 - 106 vol.1
6. « Dispersion and dispersion slope tolerance of 160-Gb/s systems, considering the temperature dependence of chromatic dispersion.», Vorbeck, S., Photonics Technology Letters, IEEE ,Vol. 15 , Issue: 10 , Oct. 2003, Pages:1470 – 1472
7. « 160 Gbit/s adaptive dispersion equalizer using a chirp monitor with a balanced dispersion configuration.», Inui T. et al., European Conference on optical communication, September 21-25 2003, Rimini, Italy.
8. « Tunable dispersion slope compensator based on chirped FBGs with temperature distribution for 160 Gbit/s.», Wakabayashi, A., Optical fiber communication conference, March 23-28 2003, Atlanta, Paper MF27.
9. « Tunable dispersion slope compensator with a chirped fiber grating for 160 Gbit/s RZ transmissions.», Matsumoto, S.; Optical fiber communication conference, March 23-28 2003, Atlanta, Paper TuD4
10. « Compensation of intra-channel nonlinearities in 40 Gbit/s pseudo-linear systems using optical phase conjugation», A. Chowdhury et al., Optical fiber communication conference, March 2004, Los Angeles, PDP32.
11. « Intrachannel pulse interactions in dispersion-managed transmission systems: energy transfer», M. J. Ablowitz, Optics Letters, vol. 27, Nb 3 (Feb. 2000), p. 203
12. « Resonant intrachannel pulse interactions in dispersion-managed transmission systems », M. J. Ablowitz, IEEE Journal of Selected Topics in Quantum Electronics, vol. 8, Nb 3 (May/June 2002), p. 603
13. «Phase modulation schemes for improving intra-channel nonlinear tolerances in 40 Gbit/s transmission»,J. Martensson et al, Optical Fiber communication conference, March 23-28 2003, Atlanta, Paper FE5.
14. «Influence of bitwise phase changes on the performance of 160 Gbit/s transmission systems», S. Randel et al, European Conference on optical communication, September 8-12 2002, Copenhagen, Denmark, Paper P3.31.
15. «Analysis of intrachannel nonlinear effects in highly dispersed optical pulse transmission », A. Mecozzi, IEEE Photonics Technology Letters, vol. 12, Nb 4 (April 2000), p. 392
16. « Suppression of nonlinear effects by phase alternation in strongly dispersion managed optical transmission », P. Johannisson, Optics Letters, vol. 27, Nb 12 (June 2002), p. 1073
17. « Suppression of intrachannel four-wave mixing by phase modulation at one quarter of bit rate», J. Martensson et al. , Electron. Lett. 38, 1463 (2002)
18. « Suppression of intrachannel four-wave mixing induced ghost pulses in high-speed transmissions by phase inversion between adjacent marker blocks», X. Liu et al, Optics Letters, Vol. 27, N°13, 1st July 2002.
19. « Intrachannel four-wave-mixing in dispersion managed RZ Systems», S. Kumar, Photonics Technology Letters, 8th August 2001, Vol. 13, N°8, page 800-802.
20. « Influence of inter bit four wave mixing in optical TDM transmission», I. Shake et al. , Electronics Letters, 6th August 1998, Vol. 34, N°16, page 1600-1601.

21. « Pulse-overlapped dispersion-managed data transmission and intrachannel four-wave mixing», P.V. Mamyshev et al. , Optics Letters, 1st November 1999, Vol. 24, N°21, pages 1454-1456.
22. « Impact of fiber chromatic dispersion in high-speed TDM transmission systems», Konrad, B.et al, Journal of Lightwave Technology, Vol. 20 , Issue 12 , Dec. 2002, Pages:2129 – 2135
23. «Optimum fiber dispersion in high-speed TDM Systems», Konrad B.; Photonics Technology Letters, IEEE , Volume: 13 , Issue: 4 , April 2001, Pages:299 – 301
24. «Comparison of engineering scenarios for Nx160 Gb/s WDM transmission systems. », Cuenot B.; Photonics Technology Letters, IEEE , Volume: 15 , Issue: 6 , June 2003, Pages:864 – 866
25. «Numerical optimization of pre and in-line dispersion compensation in dispersion managed systems at 40 Gbit/s», Y. Frignac et al, Proc. OFC 2002, Anaheim, March 17-22 2002, page(s): 612-613
26. «Enhanced analytical engineering rule for fast optimization of dispersion maps in 40 Gbit/s based transmission systems», Y. Frignac et al, Proc. OFC 2004, Los Angeles, March 2004, Paper TuN3.
27. «Reduction of Intrachannel Nonlinear Distortion in 40 Gbit/s based WDM transmission over standard Fiber», R.I. Killey et al, Photonics Technology Letters, IEEE , Volume: 12 , Issue: 12 , December 2000, Pages:864 – 866
28. «Dispersion map influence in 160 Gbit/s single channel transmission», Cuenot B., Non Linear Guided Waves conference 2004, 28-31/03/04, Toronto, Canada.
29. «Dispersion managed spans in terrestrial routes: technical advantages and practical considerations», A. Judy., Optical fiber communication conference 2003, March 23-28 2003, Atlanta, Paper TuS1.

Statistical effects in propagation

1 Birefringence in fibre and the coarse step method

In this chapter, we focus on physical effects induced by polarization mode dispersion and its impact on 160 Gbit/s transmission systems. The effect of polarization mode dispersion can be understood by considering the two axes of polarization in the fibre, which we will define as X and Y. Slow and fast polarization axes can be observed as the speed of light is not the same depending its polarization. Consequently, at the end of the fibre, the power launched in the X polarization is delayed from the power launched in the Y polarization as shown in the following figure [1,2].

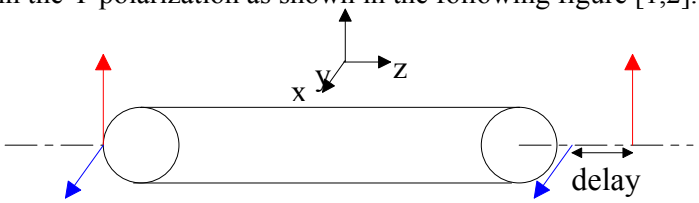

Figure 4. 1. Principle of delay between fast and slow axis of polarization.

In order to illustrate this impact, we consider a gaussian pulse with a full width at half-maximum of 2,5 ps. We assume that this pulse is launched into the fibre in the state of polarization X+Y which means that half of the power propagates on the X axis and half of the power on the Y axis. The injected light beam is then coupled on 2 propagation modes. After propagation, there is a delay between the propagation on the X and the Y axes. The shape of this originally gaussian pulse is shown in the following figure for various delays:

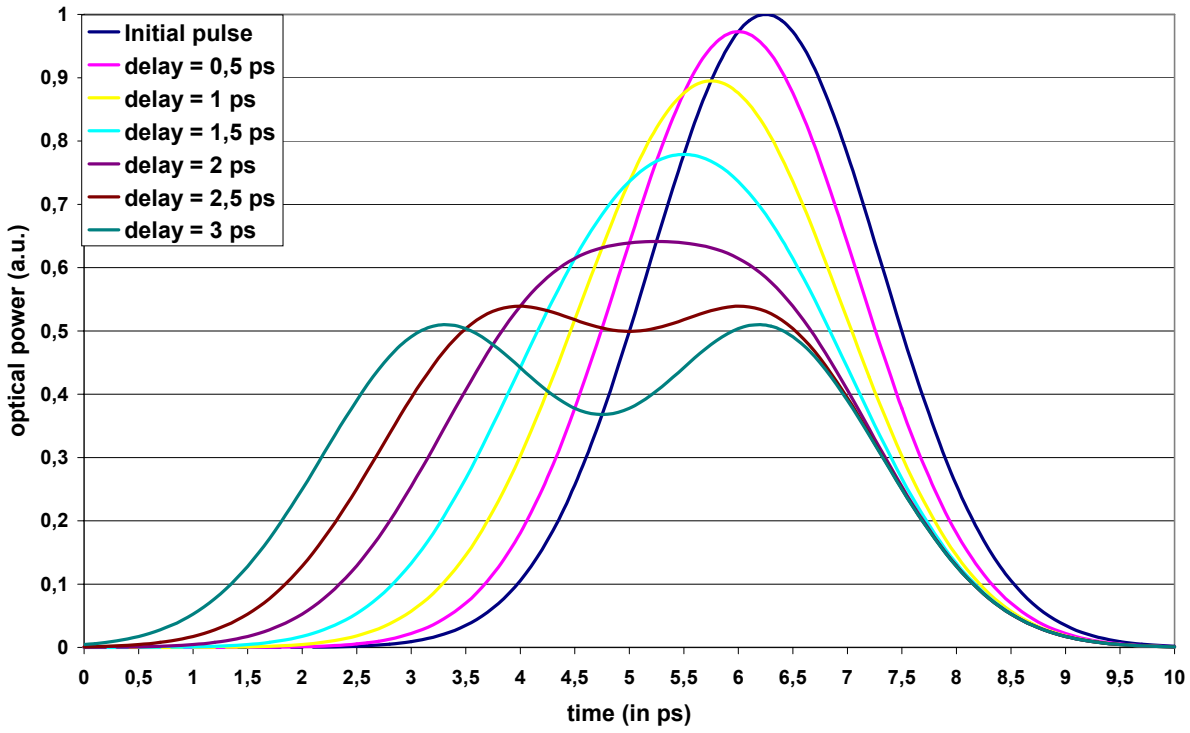

Figure 4. 2. Deformation of the pulse shape for various delays between X and Y polarization axes for an initial pulse with the polarization X+Y.

If we neglect inter-symbol-interference due to pulse broadening, we can estimate the penalty on the optical peak power due to a differential group delay between the two polarizations:

Delay in ps	0	0,5	1	1,5	2	2,5	3
Peak power penalty in dB	0	-0,1	-0,5	-1,1	-1,9	-2,7	-2,9

Table 4. 1. Penalty on optical peak power for a pulse launched into a birefringent fibre with the polarization X+Y as a function of the DGD between the two polarizations.

This peak power penalty holds between 0 and -3 dB as the pulse splits into two pulses when the delay increases. Basically, this would not be a problem as we could imagine that the optical power is launched in a certain state of polarization near an axis of polarization. This problem becomes more complex when we know that fast and slow polarization axes are only constant during a short length of fibre, typically around some hundreds of metres. As a matter of fact, the following characteristics of fibre should be taken into account in order to model polarization mode dispersion [1,2]:

- The fibre is constituted by the juxtaposition of several short pieces of fibre. In each piece of fibre, fast and slow polarization axes are remaining the same.
- There is a scattering of the polarization axes between two consecutives pieces of fibre, which means that the polarization axes are changing from a piece of fibre to the following one.
- The delay between fast and slow polarization axes is such that the sum of the delays, i.e. the DGD or differential group delay, is a random variable following a maxwellian distribution as shown in the following figure.

The differential group delay probability density function is [3]:

$$\rho(x) = \frac{32.x^2}{\pi^2.\langle x\rangle^3}.\exp\left(-\frac{4.x^2}{\pi.\langle x\rangle^2}\right)$$

where x is the DGD expressed in ps and so <x> is the mean DGD also defined as PMD.
The distribution of DGD for different values of PMD between 1 and 4 ps is given by Figure 4. 3.

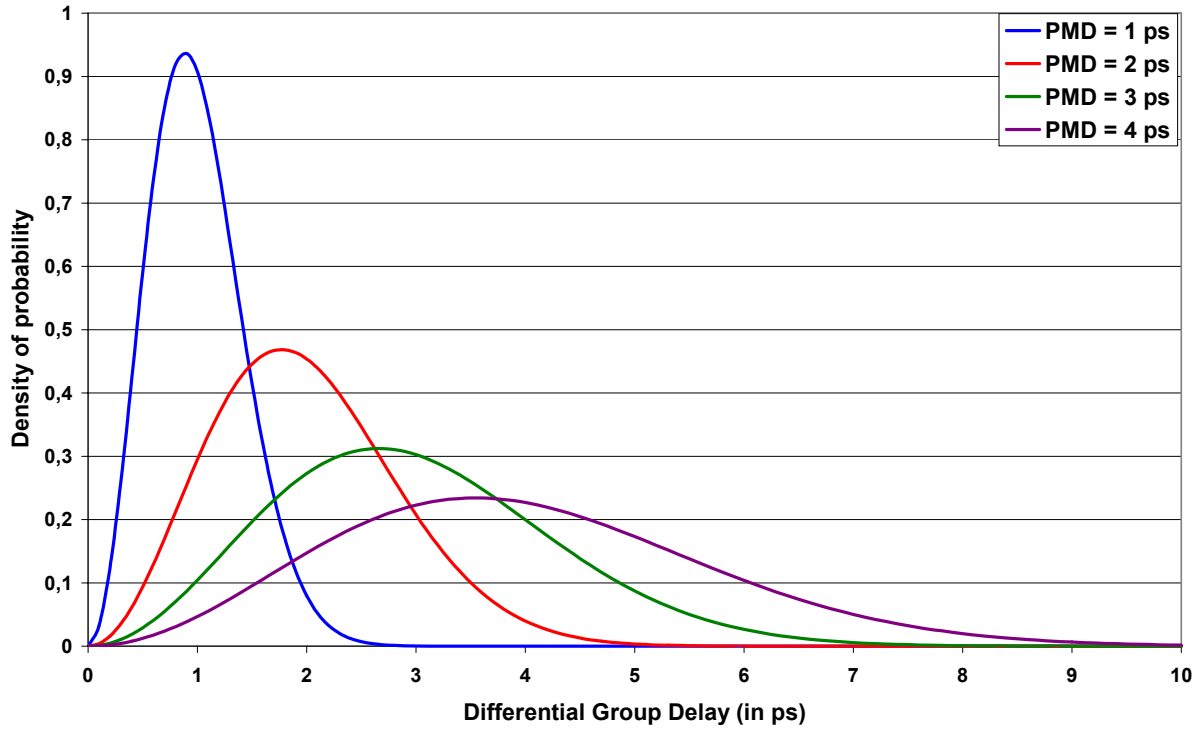

Figure 4. 3. Distribution of the DGD for different values of PMD (from 1 to 4 ps).

Considering this model, we understand that the impact of PMD has to be considered through a statistic approach. Furthermore, the problem of this physical phenomena is that the computation time to represent it is really high as high degradations (for high values of the DGD) are very rare. However, several mathematical techniques can be used to speed up the calculation of the outage probability [4,5,6]. In the following example, we consider the case of a transmission over 100 km of fibre. In this simulation with VPI Transmission Maker, noise issues and non-linear effects (Kerr or Raman effects) are not considered. The Eye Opening Factor is measured after 100 km for multiple runs and for different PMD values from 1 to 4 ps. The eye opening factor is estimated after detection and electrical filtering and the cumulated density of probability is estimated considering the entire serial of runs.

For more visibility and for smaller values of accumulated PMD over the transmission, it is necessary to observe these results with a logarithmic scale on the y axis. Actually, these results have been obtained with 1000 runs so it is not possible to obtain a precision more than 10^{-3} as shown in the following figure. The curve showing cumulated density of probability of Eye Opening Penalty for a PMD value of 1 ps is not visible in this graph since all results were in the range between 0 and -0,05 dB. Therefore, we should be able to compare these characteristics with those obtained in the case of an OTDM receiver.

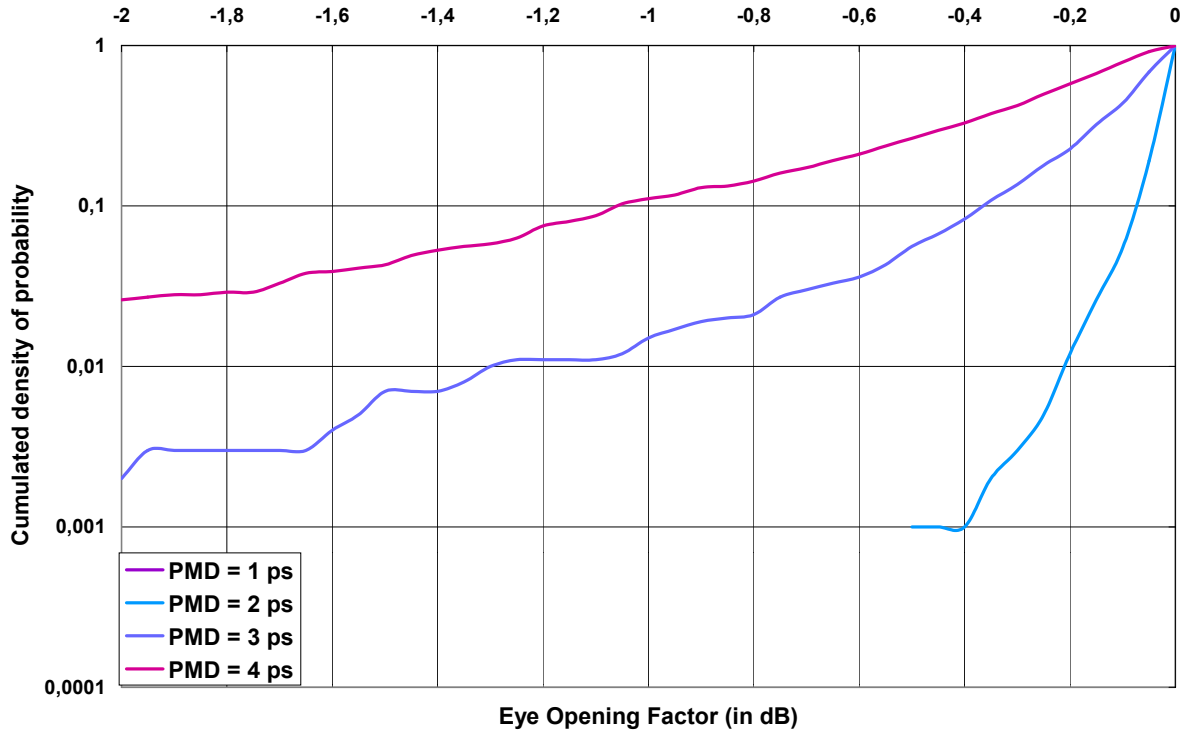

Figure 4. 4. Cumulated density of probability of EOP after 1000 runs for each PMD value.

2 Impact of optical demultiplexing on PMD aspects

We have seen in this introduction that PMD is leading to a pulse deformation which can be measured by the criteria of eye opening penalty. However, we should remember that, up to now, 160 Gbit/s transmission systems are obtained by optical multiplexing of tributaries at 10, 40 or 80 Gbit/s [9,10,11,12]. We can wonder about the tolerance to PMD in such systems. A common engineering rule is to consider that accumulated PMD should be between 10 and 15 % of the time bit if no compensation is used, less than 20 % if we use electrical mitigation and less than 30 % if PMD compensation is used [13,14,15,16].

With the use of an optical demultiplexing, the pulse shape is affected. In this chapter, we will consider the following system characteristics in order to investigate the impact of optical demultiplexing with regards to PMD. The emission is made by optically multiplexing four tributaries at 40 Gbit/s each. The pulse width is set to 2,5 ps (duty cycle = 0,4). The reception is constituted by an optical demultiplexing from 160 Gbit/s to 40 Gbit/s: this functionality is obtained through the use of optical modulators as shown in the introduction of this document. Each modulator is driven by an electrical clock at 40 GHz and electrical pulse is gaussian and its width is also 2,5 ps. After demultiplexing, the detection is enabled by a photodiode followed by an electrical Bessel filter (which bandwidth is set to 0,7 times the tributary bit rate, i.e. 28 GHz).

In order to investigate PMD effects only, we will not take into account noise issues nor Kerr effects. The optical line length is set to 100 km. The Eye Opening factor is investigated for multiple runs and for different PMD values from 1 to 4 ps. The following graph shows the cumulated density of probability of the eye opening factor considering the entire serial of runs as a function of the eye opening factor.

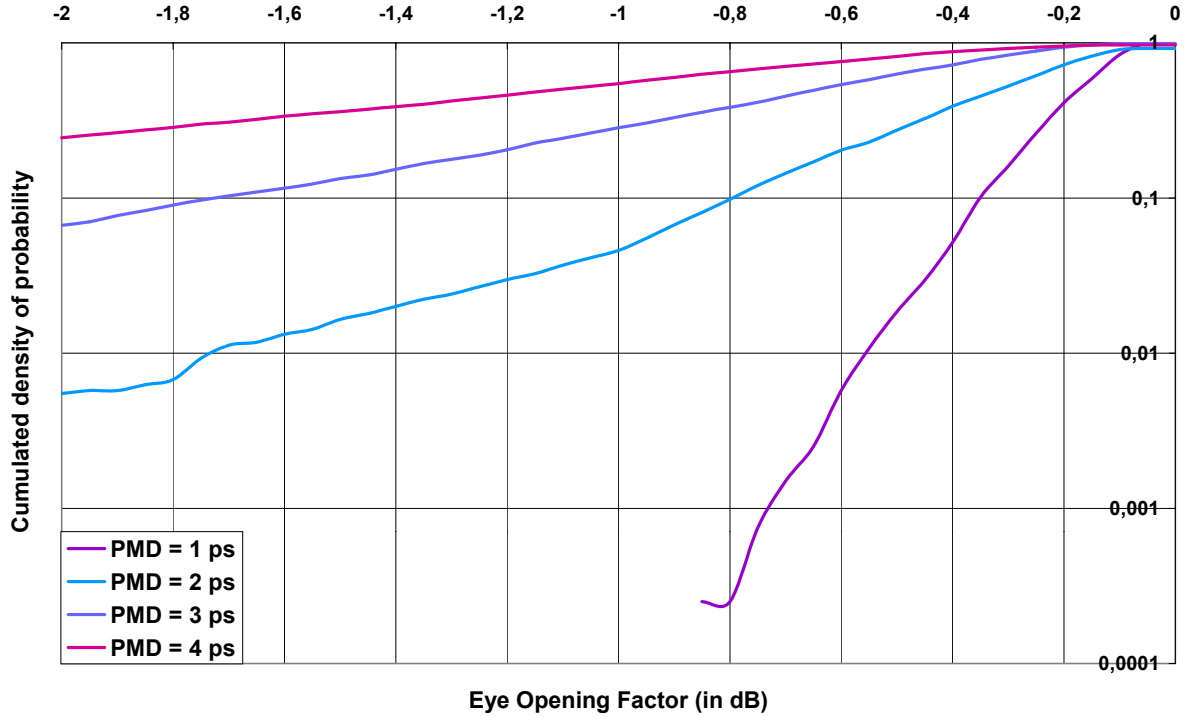

Figure 4. 5. Probability of EOP after 1000 runs for each PMD value with optical demultiplexing.

These results are to be compared with those obtained in the previous section when the receiver is directly operating at 160 Gbit/s (see Figure 4. 4). We can see that degradations due to PMD are higher in this case since the curve obtained for a PMD value of 1 ps is now visible. On this graph, a precision better than 10^{-3} is obtained even if there are still 1000 runs but this is because each run gives 4 estimations of the eye opening (one for each tributary). This can be clearly understood because of the optical demultiplexing from 160 to 40 Gbit/s. After the shape deformation due to PMD, the optical signal at 160 Gbit/s is injected in an electro absorption modulator. The output optical signal is a function of the input optical signal following the relation:

$$E_{out}(t) = E_{in}(t).\sqrt{E_{elec}(t)}$$

for a chirp free modulator where $E_{elec}(t)$ is the electrical signal.

The electrical signal is here assumed to be an electric clock at 40 GHz with gaussian pulses of 2,5 ps width. The relation between the optical input and output power is:

$$P_{out}(t) = P_{in}(t).data_{elec}(t) = P_{in}(t).\left(A.e^{-\left(\frac{t}{\left(\frac{FWHM}{2.\sqrt{\ln(2)}} \right)} \right)^2} \otimes \sum_k \delta\left(t - 4.k.T_b\right) \right)$$

where FWHM is the full width at half maximum which value is 2,5 ps and T_b = 6,25 ps.

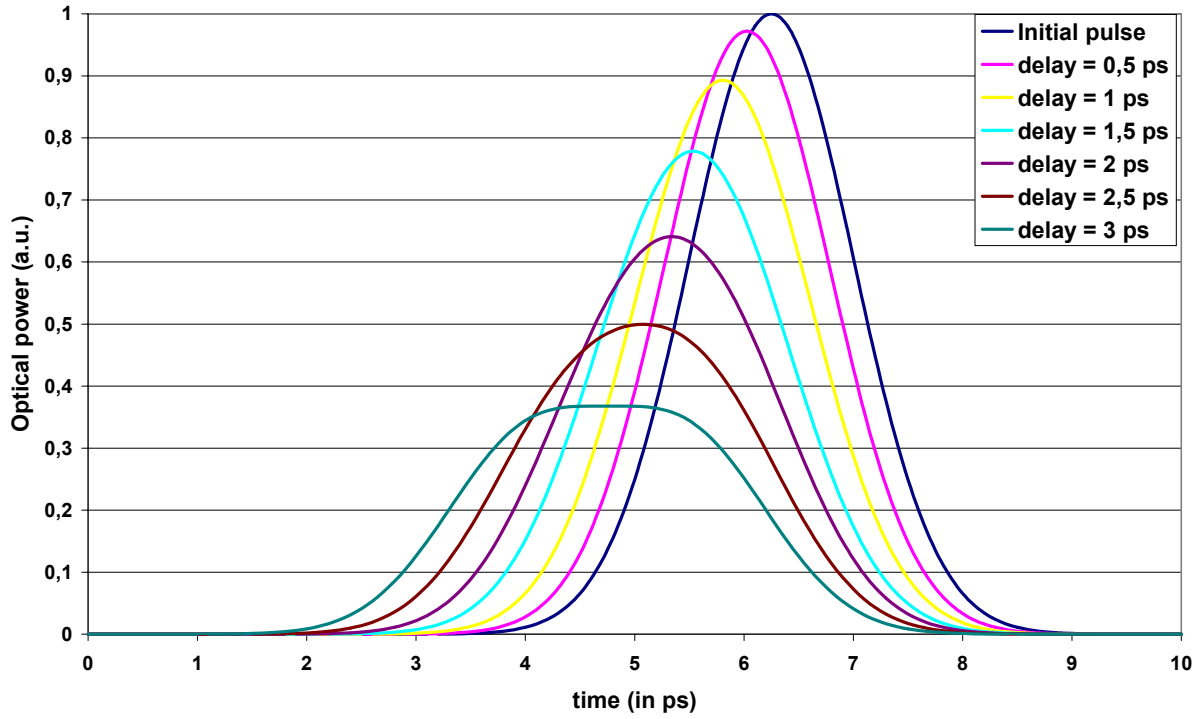

Figure 4. 6. Deformation of the pulse shape for various delays between X and Y polarization axes for an initial pulse with the polarization X+Y followed by optical demultiplexing.

Comparing these results with those on Figure 4. 2, we see that due to the time gating with the gaussian electrical pulse, the gaussian shape of the optical pulse is not maintained whereas it was the case without the OTDM demultiplexing function. Consequently, the optical peak power penalty due to the delay is lower than -3 dB for high values of the delay as shown in the following table.

Delay in ps	0	0,5	1	1,5	2	2,5	3
Peak power penalty in dB	0	-0,1	-0,5	-1,1	-1,9	-3	-4,35

Table 4. 2. Penalty on optical peak power for a pulse launched into a birefringent fibre with the polarization X+Y as a function of the DGD between the two polarizations.

3 Modelling of PMD and relation with the quality factor

Considering the maxwellian distribution of the DGD [3], we have:

$$\rho(x) = \frac{32.x^2}{\pi^2.\langle x\rangle^3}.\exp\left(-\frac{4.x^2}{\pi.\langle x\rangle^2}\right)$$

Furthermore, the Q² factor, in dB, is a function of the DGD. It can be expressed as a function of the DGD x as it can be seen on Figure 4. 7, in the case of a signal with gaussian optical pulses (FWHM=3 ps) and an OSNR of 27 dB. In a first order approximation, we have:

$$Q^2 = k + b.x^2$$

where b<0 and consequently, the maximal value of the Q² factor (for x=0, i.e. no group delay) is k. With this case, we have the approximation:

$$Q^2 = 16{,}955 - 1{,}508.x^2$$

as the mean Q² factor without PMD is estimated to 16,955.

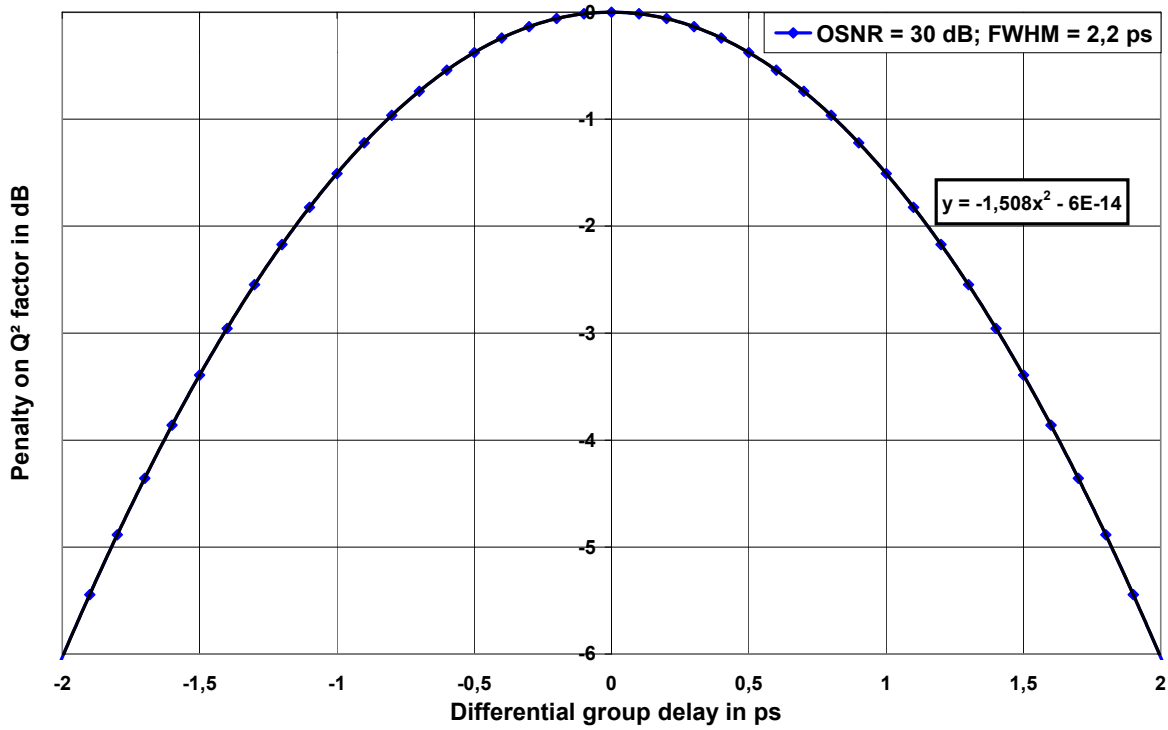

Figure 4. 7. Q² factor penalty, expressed in dB, as a function of the DGD and fit by a square profile.

As a matter of fact, it is possible to justify this polynomial fit as the Q² factor is given by:

$$Q = \frac{\mu_1 - \mu_0}{\sigma_1 + \sigma_0}$$ where Q is expressed in linear scale.

$$Q^2 = 20.\log(\mu_1 - \mu_0) - 20.\log(\sigma_1 + \sigma_0)$$ where Q² is expressed in dB.

With the effect of a differential group delay, the gaussian electromagnetic field, injected with the polarization X+Y, becomes:

$$E(t) = E_0.e^{-\frac{t^2}{2.\sigma^2}} \rightarrow E(t) = \frac{E_0}{2}\left(e^{-\frac{t^2}{2.\sigma^2}} + e^{-\frac{(t-\tau)^2}{2.\sigma^2}}\right)$$

where the last term is due to the delayed answer with a DGD equal to τ. For small values of τ (compared to the pulse width), the maximum optical power becomes:

$$P_{\max} = P(0) = {E_0}^2 \rightarrow P_{\max} = P(\frac{\tau}{2}) = {E_0}^2 e^{-\frac{\tau^2}{4.\sigma^2}}$$

Considering in a first approximation that the DGD only impacts the marks optical power, the Q² factor becomes:

$$Q^2 = 20.\log(\mu_1 - \mu_0) - 20.\log(\sigma_1 + \sigma_0) \rightarrow Q^2 = 20.\log(\mu_1.e^{-\frac{\tau^2}{4.\sigma^2}} - \mu_0) - 20.\log(\sigma'_1 + \sigma'_0)$$

Furthermore, the signal-ASE beat noise has been proved to be preponderant at high bit rate and consequently, we can make the following approximation:

$$\sigma'_1 + \sigma'_0 \approx \sigma'_{S-ASE}$$

This quantity is proportional to the square root of the signal power and the difference between Q² factors before and after is:

$$\Delta Q^2 \approx 20.\log(\frac{\mu_1.e^{-\frac{\tau^2}{4.\sigma^2}} - \mu_0}{\mu_1 - \mu_0}) - 20.\log(\frac{\sigma'_1}{\sigma_1})$$

$$\Delta Q^2 \approx 20.\log(\frac{\mu_1.e^{-\frac{\tau^2}{4.\sigma^2}} - \mu_0}{\mu_1 - \mu_0}) - 20.\log(e^{-\frac{\tau^2}{8.\sigma^2}})$$

as $\sigma'_{S\text{-}ASE}$ is proportional to $E_0.e^{-\frac{\tau^2}{8.\sigma^2}}$ and $\sigma_{S\text{-}ASE}$ is proportional to E_0.

If we now express the OSNR as a function of μ_1 and μ_0, we obtain:

$$\frac{\mu_1}{\mu_0} = \frac{2.OSNR.B_{ref}}{B_0}$$

The difference between Q² factors can thus be written:

$$\Delta Q^2 \approx 20.\log(\frac{\left(\frac{2.OSNR.B_{ref}}{B_0}\right).e^{-\frac{\tau^2}{4.\sigma^2}} - 1}{\left(\frac{2.OSNR.B_{ref}}{B_0}\right) - 1}) - 20.\log(e^{-\frac{\tau^2}{8.\sigma^2}})$$

If we develop the exponential term to the first order, assuming $\frac{\tau^2}{8.\sigma^2} < \frac{\tau^2}{4.\sigma^2} << 1$, this expression becomes:

$$\Delta Q^2 \approx 20.\log(1 - \frac{\left(\frac{2.OSNR.B_{ref}}{B_0}\right).\frac{\tau^2}{4.\sigma^2}}{\left(\frac{2.OSNR.B_{ref}}{B_0}\right) - 1}) - 20.\log(1 - \frac{\tau^2}{8.\sigma^2})$$

The same assumption leads to:

$$\Delta Q^2 \approx -20.\frac{\left(2.OSNR.B_{ref}\right).\frac{\tau^2}{4.\sigma^2}}{2.OSNR.B_{ref} - B_0}) + \frac{2{,}5.\tau^2}{\sigma^2}$$

For σ = 1,5 ps, i.e. FWHM = 2,5 ps, numerical applications give:

- $\Delta Q^2 \approx -1{,}204.\tau^2$ for an OSNR of 25 dB.
- $\Delta Q^2 \approx -1{,}134.\tau^2$ for an OSNR of 30 dB.
- $\Delta Q^2 \approx -1{,}120.\tau^2$ for an OSNR of 35 dB.
- $\Delta Q^2 \approx -1{,}113.\tau^2$ for an OSNR of 40 dB.

For σ = 1,32, i.e. FWHM = 2,2 ps and an OSNR of 30 dB corresponding to Figure 4. 7, the penalty is $\Delta Q^2 \approx -1{,}469.\tau^2$ while numerical results give a variation of Q² factor with the relation $Q^2 = 16{,}955 - 1{,}508.\tau^2$. The difference between the two coefficients, i.e. -1,469 and -1,508, is not very large as the DGD magnitude is only some ps. For example, with a DGD of 1,5 ps, the polynomial fit of numerical results predicts: $Q^2 = 16{,}955 - 1{,}508.(1{,}5)^2 \approx 13{,}6$ dB while this analytical rules predicts: $Q^2 = 16{,}955 - 1{,}469.(1{,}5)^2 \approx 13{,}6$ dB. The difference is lower than 0,1dB which is not significant and proves the validity of this analysis.

The distribution of the Q² factor, denoted f(Q²), can thus be expressed as:

$$f(Q^2)dQ^2 = \rho(x)dx = \frac{32.x^2}{\pi^2.\langle x\rangle^3}.\exp\left(-\frac{4.x^2}{\pi.\langle x\rangle^2}\right)dx$$

Furthermore, the polynomial dependence of the Q² factor versus the differential group delay is $Q^2 = k + b.x^2$ as it can be seen on Figure 4. 7. As a result, we can express dQ²:

$$dQ^2 = 2.b.x.dx = 2.b.\sqrt{\frac{(Q^2)_{dB} - k}{b}}dx$$

The expression of $f(Q^2)$ is thus given by:

$$f(Q^2) = \frac{32.(Q^2 - k)}{b\pi^2.\langle x\rangle^3}.\exp\left(-\frac{4.(Q^2 - k)}{b\pi.\langle x\rangle^2}\right).\frac{1}{2.\sqrt{b}.\sqrt{Q^2 - k}}$$

$$f(Q^2) = \frac{16.\sqrt{k - Q^2}}{|b|^{\frac{3}{2}}.\pi^2.\langle x\rangle^3}.\exp\left(-\frac{4.(k - Q^2)}{|b|\pi.\langle x\rangle^2}\right)$$

The mean value of the DGD can be noted as the PMD value: $\langle x\rangle = PMD$.

$$\log(f(Q^2)) = \left(\log\left(\frac{16.\sqrt{k}}{|b|^{\frac{3}{2}}.\pi^2.PMD^3}\right) - \frac{4.k}{\ln(10).|b|\pi.PMD^2}\right) + \left(\frac{4.Q^2}{\ln(10).|b|\pi.PMD^2}\right) + \frac{1}{2}\log\left(1 - \frac{Q^2}{k}\right)$$

Derivating this expression with Q², the result is:

$$\frac{d(\log(f(Q^2)))}{dQ^2} = \frac{4}{\ln(10).|b|\pi.PMD^2} - \frac{1}{2.(k - Q^2)}$$

When Q² is small, the last term tends to $-\frac{1}{2.k}$. For small values of Q², the logarithm of the distribution of Q² is a straight line and the slope is equal to:

$$\frac{d(\log(f(Q^2)))}{dQ^2} = \frac{4}{\ln(10).|b|\pi.PMD^2} - \frac{1}{2.k}$$

Reciprocally, for high values of Q² factor, corresponding to a low value of the DGD, the tendency of the distribution is:

$$f(Q^2) \approx \frac{16.\sqrt{k-Q^2}}{|b|^{\frac{3}{2}}\pi^2.PMD^3}.\left(1-\frac{4.(k-Q^2)}{|b|\pi.PMD^2}\right) = \frac{16.\sqrt{k-Q^2}}{|b|^{\frac{3}{2}}\pi^2.PMD^3} + o\left(\sqrt{k-Q^2}\right)$$

On the following figure, we have represented the evolution of $\log(f(Q^2))$ as a function of Q². The optical signal with full-width-at-half-maximum of 2,5 ps is transmitted in a 3x100 km link. The total PMD is 0,866 ps and an OSNR of 28dB is estimated at the receiver. On this figure, we have also represented the results obtained numerically with 5000 runs.

As we can see, a very good approximation of numerical results by this modelling (red and green curves) is obtained. In particular, we remark that curve shapes for small and high values of Q² factor are the same. The probability of high values of the Q² factor is underestimated. This may be due to the insufficient precision of the original modelling of Q² factor versus DGD.

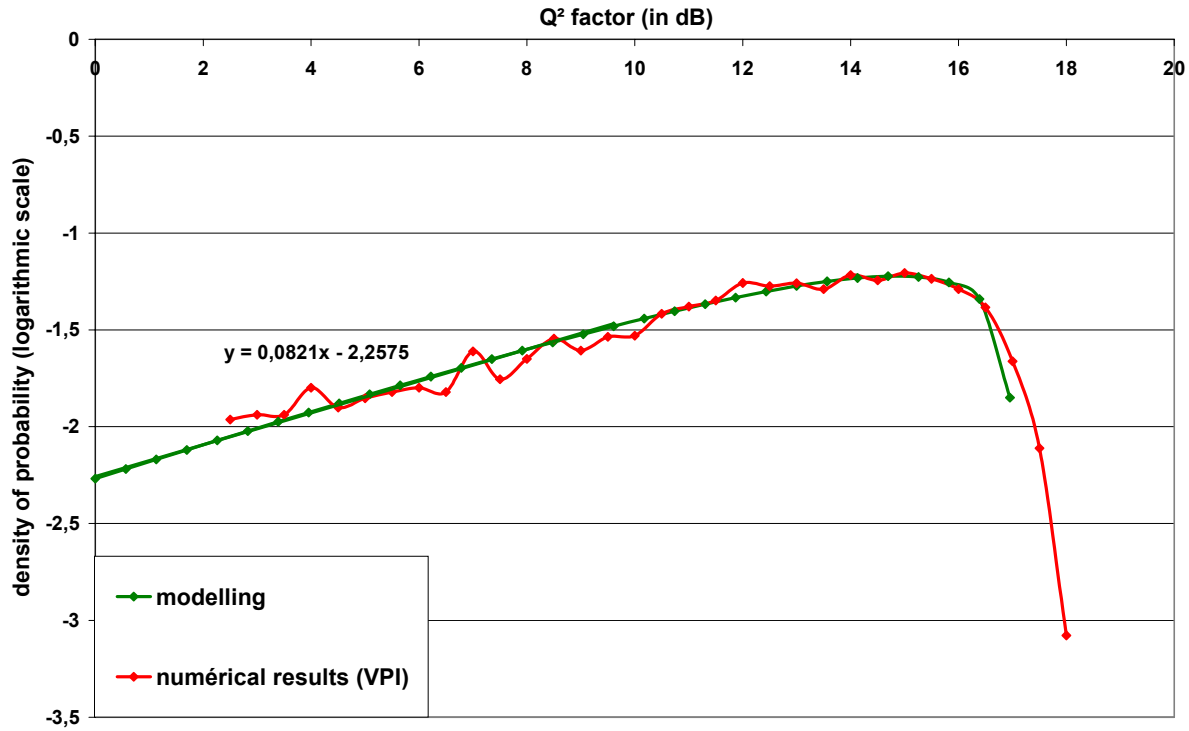

Figure 4. 8. Density of probability of Q² factor represented in logarithmic scale. Comparison between numerical results and analytic estimation.

This simple model enables a good prediction of the Q² factor density of probability. We have seen that in a first approximation, only three parameters are sufficient to obtain this prediction: the pulse width, the OSNR in front of the receiver and the PMD of the link. The maximal Q² factor, i.e. without PMD, can be deduced from the OSNR at the receiver.

On the following figure, we study some simple cases to study the dependence to these parameters. On the left, the PMD of the link is changed from 0,75 ps to 1,25 ps for a full-width-at-half maximum of 2,5 ps. On the right figure, the PMD of the link is set to 1 ps but the full-width-at-half-maximum is changed from 2 to 3 ps.

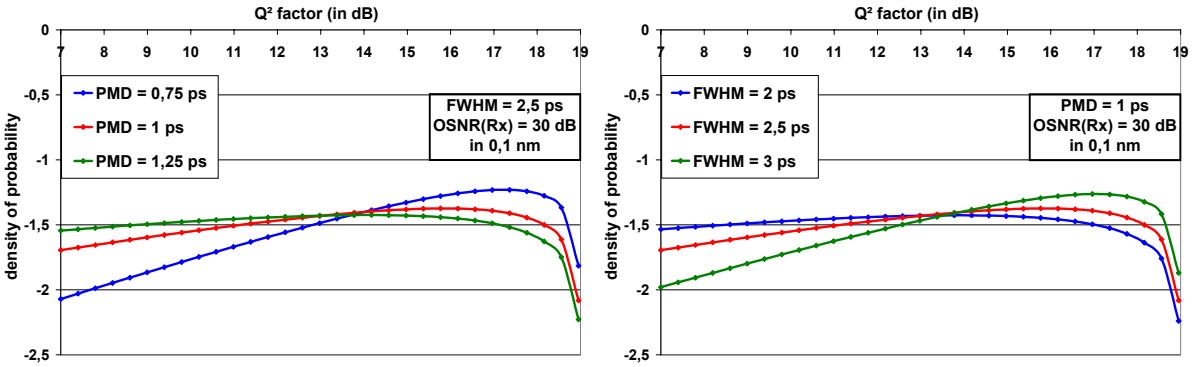

Figure 4. 9. Density of probability of Q² factor represented in logarithmic scale. Evolution with PMD (left) and with FWHM (right).

4 Conclusion

We have seen in this chapter how polarization mode dispersion effects were degrading the optical signal and how they impact on the transmission quality. We have seen that, due to the maxwellian distribution of the differential group delay, a great number of iterations (more than 10^3) had to be taken into account in order to model bad quality cases. However, a simple analytical approach based on the deformation of a Gaussian pulse with a self-delayed answer enables the prediction of the density of probability.

As we have seen in the introduction of this document, PMD is the most limiting effect at 160 Gbit/s since the tolerance is very small. For example, we have seen that with a typical G652 fibre characterised by a PMD value of 0,2 ps/$\sqrt{km}$, the estimated maximum reach is only 60 km with respect to a criteria of 25% of the time bit. It means that the majority of transmission links are not suitable for transmission at 160 Gbit/s. The aim of research in the PMD theme is now to enable PMD compensation at high bit rate [17,18,19].

5 References

1. "PMD emulators and signal distortion in 2.48-Gb/s IM-DD lightwave systems", Prola, C.H. et al, Photonics Technology Letters, IEEE , Volume: 9 , Issue: 6 , June 1997, Pages:842 – 844
2. "Polarization Mode Dispersion", Chapter 15 in Optical Fiber Telecommunications IVB, Herwig Kogelnik et al, Tingye Li and Ivan Kaminow (Eds.), Academic Press, San Diego, pp. 725-861, 2002.
3. "On differential group-delay statistics for polarization-mode dispersion emulators", Djupsjobacka, A., Lightwave Technology, Journal of , Volume: 19 , Issue: 2 , Feb. 2001, Pages 285 – 290
4. "Multiple importance sampling for first- and Second-order polarization-mode dispersion", S. Fogal et al, Photonics Technology Letters, Vol. 4, N°19, September 2002, pages 1273-1275
5. "Computation of the outage probability due to the polarization effects using importance sampling.", I.T. Liima et al, Paper TU17, Optical Fiber Communication Conference 2002, Anaheim, USA
6. "Numerical implementation of the Manakov-PMD equation with precomputed M(ω) matrices", M. Eberhard et al, Paper MC 3, Non-Linear Guided Waves conference 2004, Toronto, Canada.
7. "Optimum fiber dispersion in high-speed TDM systems", Konrad, B. et al, Photonics Technology Letters, IEEE , Volume: 13 , Issue: 4 , April 2001, Pages:299 - 301
8. "Performance comparison of 4Nx40 Gb/s and Nx160 Gb/s transmission systems", Hodzic A, Konrad B, Randel S, Petermann K. Technical University of Berlin, Germany, P3.24, ECOC 2002, Copenhagen, Denmark
9. "1-Tb/s (6/spl times/170.6 Gb/s) transmission over 2000-km NZDF using OTDM and RZ-DPSK format", Gnauck, A.H. et al, Photonics Technology Letters, IEEE , Volume: 15 , Issue: 11 , Nov. 2003, Pages 1618 – 1620
10. "Single Channel 160 Gbit/s (40 Gbit/s x 4) 300 km - Transmission Using EA Modulator based - OTDM Module and 40 GHz External - Cavity Mode-locked", LD Murai H et al, Oki Electric Industry Co., Ltd., Japan. NEC Corporation, Japan, ECOC 2002, Copenhagen, Denmark
11. "Advanced 160 Gbit/s OTDM system based on wavelength transparent 4 /spl times/ 40 Gbit/s ETDM transmitters and receivers", Lach, E. et al, Optical Fiber Communication Conference and Exhibit, 2002. OFC 2002 , 17-22 March 2002, Anaheim, USA, Pages:2 – 4
12. "Clock recovery from 160 Gbit/s data signals using phase-locked loop with interferometric optical switch based on semiconductor optical amplifier", Yamamoto, T. et al, Electronics Letters ,Volume: 37 , Issue: 8 , 12 Apr 2001, Pages:509 – 510
13. "Operation of digital optical transmission system with minimal degradation due to polarisation mode dispersion", Bulow, H., Electronics Letters , Volume: 31 , Issue: 3 , 2 Feb. 1995, Pages:214 – 215
14. "System outage probability due to first- and second-order PMD", Bulow, H., Photonics Technology Letters, IEEE ,Volume: 10 , Issue: 5 , May 1998, Pages:696 – 698
15. "Extension of polarization-mode dispersion limit using optical mitigation and phase-shaped binary transmission", Stéphanie Lanne et al, Paper ThH3, Optical Fiber Communication Conference 2000, Baltimore, USA
16. "Is PMD compensation really useful?", M. Eiselt et al, Paper MF113, Optical Fiber Communication Conference 2003, Atlanta, USA
17. "Long-term automatic PMD compensation for 160 Gbit/s RZ transmission", Westlund, M. et al, Electronics Letters , Volume: 38 , Issue: 17 , 15 Aug 2002, Pages:982 – 983
18. "Adaptive PMD compensation in a 160 Gb/s RZ transmission system using eye monitor feedback", Buchali F et al, Paper 7.1.3, European Conference on Optical Communications 2002, Copenhagen, Denmark
19. "Optical and Electronic PMD compensation", H. Bülow et al, Paper ThP1, Optical Fiber Communication Conference 2003, Atlanta, USA

Validation and discussion

In this chapter, we aim at the validation of the above explanation and method for the optimisation of 160 Gbit/s per channel transmission systems. That's why we should take into account all physical effects together. Consequently, we will define some key parameters and engineering rules in order to maximize the transmission reach. This modus operandi will be applied to the design and optimization of engineering scenarios for 2 typical transmission lines. At last, the simulation studies performed for the preparation of the field trial are presented and compared to the experimental results.

1 General modelling of a WDM transmission system

In the previous chapter, we have investigated the impact of possibly limiting physical effects for 160 Gbit/s transmission systems. We have determined the minimum optical signal to noise ratio in order to obtain a good signal quality (BER=10^{-9}). From there, we deduced the minimum injection signal power as a function of the span attenuation and number of spans. We have outlined the very small tolerance of such transmission systems to dispersion. We should also remember that intrachannel non linear effects are preponderant compared to interchannel non linear effects for usual systems. Especially, intrachannel four-wave mixing, intrachannel cross-phase modulation and self-phase modulation are degrading the signal quality. At last, we have seen that polarization mode dispersion effects were degrading the signal quality because of the birefringence of the transmission fibre. The conclusions derived from these studies are summarized in the following table.

Name of physical effect	Impact	Reason	Limit
Optical noise	Errors in detection	Due to the presence of optical amplifiers	OSNR = 28,6 dB in 0,1 nm at 160 Gbit/s
Ways of optimisation: Increase injection power, use of Raman or hybrid amplification, reduce optical losses			
Dispersion	Broadening of the pulse	Due to fibre dispersion	± 2 ps/nm for a pulse width of 2,5 ps [1]
Ways of optimisation: Devices for dispersion compensation.			
Dispersion slope	Dissymmetry of the pulse	Due to fibre dispersion and large signal bandwidth	± 6 ps/nmm² for a pulse width of 2,5 ps [1]
Ways of optimisation: Devices for dispersion slope compensation.			
Self phase modulation	Inducing a non linear chirp and a broadening of the pulse by the effect of dispersion	Due to small pulse width and high peak power	Expressed as a maximum injection power.
Ways of optimisation: Reduce injection power. Adjust predispersion.			
Intrachannel FWM	Apparition of ghost pulses inducing amplitude jitter.	Due to pulse overlapping and mostly for high dispersion fibre (D>8 ps/nm/km)	Expressed as a maximum injection power.
Ways of optimisation: Reduce injection power. Consider dispersion management and/or phase modulation.			
Intrachannel XPM	Modulation of the phase of the pulse resulting in timing jitter	Due to pulse overlapping and mostly for low dispersion fibre (D<8 ps/nm/km)	Expressed as a maximum injection power.
Ways of optimisation: Reduce injection power. Consider dispersion management.			

Gordon-Haus jitter	Modulation of the phase of the pulse resulting in timing jitter	Due to the presence of noise	Expressed as a maximum injection power.
Ways of optimisation: Reduce optical noise and/or signal power.			
Raman effect	Frequency shift of the signal inducing a dispersion impact	Due to the delayed Raman response of the fibre and small pulse width	
In practical, this effect is not restricting over typical transmission distances			
Raman power transfer	Power transfer from upper to lower signal frequencies	Due to high signal mean power and Raman pumping	
In practical, this effect is not significative compared to frequency dependant attenuation			
Self steepening	Asymmetric spectral broadening and time shape	Spectral dependence of the non linear coefficient	
In practical, this effect is not restricting for typical 160 Gbit/s transmissions.			
Interchannel FWM	Apparition of frequency components	Due to pulse overlapping (pulses from different channels)	
In practical, this effect is not restricting compared to intrachannel non linear effects.			
Interchannel XPM	Modulation of the phase of the pulse resulting in timing jitter	Due to pulse overlapping (pulses from different channels)	
In practical, this effect is not restricting compared to intrachannel non linear effects.			
PMD	Propagation delay between polarization components.	Due to birefringence effects in fibre.	14 % of the time bit (i.e. 0,875 ps) [4]

Table 5. 1. Summary of degrading effects over the transmission.

2 First case study: long haul transmission

2.1 Introduction

We now would like to apply these rules to an example in order to validate this approach. That's why we will consider a transmission over 3 spans of 100 km. The choice of the fibre is to be made between SMF, Teralight and LEAF. The aim of this example is to determine the physical parameters of the transmission. That's why we will examine all physical aspects described above and compare them with a complete simulation of the transmission.

We see in this table that the impact of non-linear effects depends on the signal power. For example, we have seen that using no pre-dispersion and exact inline compensation, self-phase modulation impacts the broadening of the pulse. For a transmission over 300 km, the maximum injection power regarding SPM effect is:

- 4 dBm for LEAF fibre (D = 4 ps/nm/km).
- 6 dBm for Teralight fibre (D = 8 ps/nm/km).
- 8 dBm for SMF fibre (D = 17 ps/nm/km).

Regarding the importance of intrachannel four-wave mixing and intrachannel cross phase modulation, the maximum injection power for a transmission over 300 km is:

- 8 dBm for LEAF, Teralight or SMF fibre.

Regarding the impact of PMD, the limit is set to 14 % of the time bit (i.e. 0,875 ps). However, we also have to take into account the PMD of dispersion compensating fibre and optical amplifiers.

It implies that the PMD coefficient of the fibre should be less than:

$$\text{PMD\_coeff\_max} = \sqrt{\frac{\left(0{,}875^2 - \left(0{,}08.\sqrt{\frac{300.17}{90}}\right)^2\right)}{300}} = 0{,}036\ \text{ps}/\sqrt{km}$$

where DCF fibre is characterized by a PMD coefficient of 0,08 ps/$\sqrt{km}$ and where we have not taken into account PMD brought by amplifiers.

This is probably the strongest requirement because this figure indicates that inline fibre is a very good fibre. Consequently, we should raise the signal power in order to gain an OSNR margin.

2.2 Noise analysis

Results from noise studies indicate that, whatever the fibre type, the inline fibre injection power should be greater than 0 dBm in order to obtain an OSNR of 28,6 dB at the reception. Actually, these results do not take into account noise present at the emission. The following calculation gives the OSNR at the reception as a function of the OSNR at the emission in the case of 3 spans of 100 km.

The optical loss of a span is: $T_1 = 10^{-\frac{0,2*100}{10}}$ =0,01 or -20 dB where we consider a typical attenuation of 0,2 dB/km.

The optical loss of the DCF fibre is: $T_2 = 10^{-\frac{0,6*100*D}{10*90}}$ where D is the dispersion of the inline fibre and where we consider a typical attenuation of 0,6 dB/km so we have:

- T_2 = 0,54 or -2,66 dB for LEAF
- T_2 = 0,29 or -5,33 dB for Teralight
- T_2 = 0,074 or -11,33 dB for SMF

We will consider that the gain of erbium amplifiers is the same in the first and in the second stage. All amplifiers are characterized by a noise figure of 4,5 dB. Consequently, we have:

- $G_1 = G_2 = \frac{1}{\sqrt{T_1.T_2}}$ depends on inline fibre type: 11,34 dB in the case of LEAF, 12,66 dB in the case of Teralight and 15,66 dB for SMF.

The added density of noise per span is:

$$N_{ASE\_span} = h\nu.\left(G_1.G_2 n_{eq-1}.T_2 + G_2.n_{eq-2}\right) = h\nu.n_{eq}\left(\frac{1}{T_1} + G_2\right)$$

where $n_{eq} = n_{eq-1} = n_{eq-2} = \frac{\left(NF_1 - \frac{1}{G_1}\right)}{2}$ is 1,37 in the case of LEAF, 1,38 in the case of Teralight and 1,40 in the case of SMF. The numerical application is:

- N_{ase_span}= 2,00.10^{-14} mW.Hz^{-1} in the case of LEAF.
- N_{ase_span}= 2,09.10^{-14} mW.Hz^{-1} in the case of Teralight.
- N_{ase_span}= 2,45.10^{-14} mW.Hz^{-1} in the case of SMF.

The density of noise at the emission is:

$$N_{ASE\_Tx} = \frac{P_S}{2.B_{ref}.10^{\frac{OSNR\_Tx}{10}}}$$

where Ps is the signal power (the mean signal power is Ps/2!) and OSNR_Tx is the emission OSNR.

Consequently, the density of noise at the reception is:

$$N_{ASE} = N_{ASE\_Tx} + 3.N_{ASE\_span}$$

We can thus express the OSNR at the reception as a function of the mean signal power <P> and the emission OSNR:

$$OSNR\_Rx = \frac{\langle P \rangle}{N_{ASE}} . \frac{1}{B_{ref}}$$

$$OSNR\_Rx)_{dB} = 10.\log_{10}\left(\frac{\langle P \rangle}{\frac{\langle P \rangle}{B_{ref}.10^{\frac{OSNR\_Tx}{10}}} + 3.N_{ASE\_span}} . \frac{1}{B_{ref}} \right)$$

We know that in order to obtain a good signal quality (BER<10^{-9}), the OSNR is to be greater than 28,6 dB (or 724, 43). We can thus determine the minimum signal power as a function of the emission OSNR:

$$\langle P \rangle > 724{,}43.\left(\frac{\langle P \rangle}{10^{\frac{OSNR\_Tx}{10}}} + 3.N_{ASE\_span}.B_{ref} \right)$$

$$\langle P \rangle > \frac{\langle P \rangle}{10^{\frac{OSNR\_Tx-28{,}6}{10}}} + 2173{,}29.N_{ASE\_span}.B_{ref}$$

$$P_{\min} = \frac{2173{,}29.N_{ASE\_span}.B_{ref}}{1-10^{\frac{28{,}6-OSNR\_Tx}{10}}}$$

The following table gives some numerical applications of the minimum injection power depending on the emission OSNR and the fibre type:

OSNR_Tx\fibre type	LEAF	Teralight	SMF
35 dB	0,7 mW or -1,5 dBm	0,74 mW or-1,3 dBm	0,86 mW or -0,6 dBm
40 dB	0,58 mW or -2,4 dBm	0,61 mW or -2,1 dBm	0,72 mW or -1,4 dBm
45 dB	0,55 mW or -2,6 dBm	0,58 mW or -2,3 dBm	0,68 mW or -1,6 dBm

Table 5. 2. Minimum signal power for a transmission over 3 spans of 100 km depending the emission OSNR.

We see that the variations are not very important when varying the fibre type or the emission OSNR. This is due to the fact that, in this example, the considered OSNRs are very good. For example, if the emission OSNR is only 30 dB, the minimum signal powers are:

- <P> = 1,96 mW or 2,9 dBm in the case of LEAF.
- <P> = 2,06 mW of 3,15 dBm in the case of Teralight.
- <P> = 2,42 mW or 3,8 dBm in the case of SMF.

We can here observe a strong variation (nearly 5,5 dB of variation for the minimum signal power in the case of SMF for a variation of the emission OSNR from 30 to 45 dB).

2.3 Intrachannel non linear effects.

In order to estimate the impact of intrachannel non linear effects, we investigate the evolution of the Q factor after 3 spans of 100 km (SMF, Teralight or LEAF) when varying the channel power.

Polarization effects are not considered for the moment. Optical filtering is enabled by a trapezoidal filter with a zero-dB bandwidth of 300 GHz (i.e. 2,4 nm) and a sharp slope (-60 dB at 325 GHz bandwidth). The OSNR at the emission is set to 40 dB. Two series of simulations are considered: the first one will consider erbium doped fibre amplifiers with equal gain on each stage whereas, in the second one, the gain of the first amplifier will be adjusted so that the input power in the DCF module is 0 dBm. A variable optical attenuator will also be included in the inter-stage so that the total loss between the two amplifiers is equal to 11,3 dB (which is the value of the DCF attenuation compensating for 100 km of SMF). This last case better corresponds to real systems.

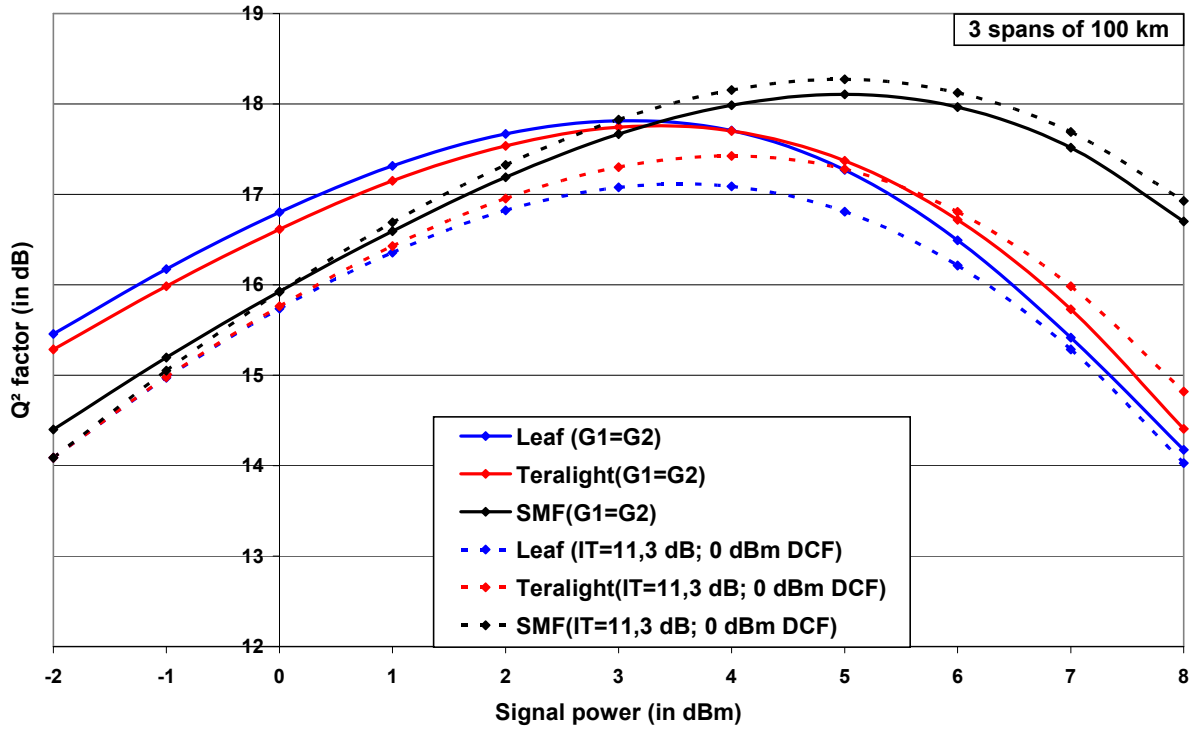

Figure 5. 1. Q² factor versus signal power for a unique channel transmission over 3 spans of 100 km and for various types of fibre.

We can understand these results in the following way: for low signal powers (less than 3 dBm), optical noise is the predominant degrading effect. This degradation is stronger in the case of SMF than in the case of LEAF because of the required length of DCF fibre compensating for inline fibre. At the opposite, when the signal power increases, signal degradation is mostly due to intrachannel non-linear effects. We observe a strong difference between SMF and other fibre types. This is due to the fact that dispersion and mainly effective areas are not the same for these three fibre types. As we have seen in the previous part of this document, when increasing the dispersion, intrachannel non-linear effects are decreasing and that's why the signal power can be increased in the case of SMF. As a conclusion to this graph, we cannot observe a predominance of one fibre type among the others as the Q² values are almost the same. The choice of a fibre type clearly has an impact on the relative importance of noise and non linear effects so this clearly determines the optimal injection power into inline fibre (difference of 2 dB between SMF and other fibres).

In the second serial of simulation, the inter-stage losses are equal for SMF, Teralight and Leaf. Consequently, we obtain the same Q² factor for low signal powers, i.e. when noise is the predominant degrading effect. Once again, SMF fibre shows the best performance towards intrachannel non-linear effects and we obtain 1 dB difference between optimal injection power. We can see a strong decrease of the mean Q² factor for Teralight and Leaf fibres for low signal power. This is due to the more important amount of noise in this second scenario. Consequently, the optimal injection power is shifted up of 1 dB for these two fibre types.

2.4 Impact of fibre dispersion

With this example of compromise between noise and non-linear effects, we can also wonder about the optimal dispersion of the inline fibre in this case if effective areas were the same. That's why following simulations consider a variation of inline fibre dispersion up to 20 ps/nm/km. The attenuation of inline fibre is set to 0,2 dB/km. Dispersion compensating fibre (attenuation of 0,6 dB/km) is used after each span, matching for exact compensation of inline fibre dispersion. The gain of each erbium amplifier is set to half the total gain of double stage EDFA. Results are plotted in the next figure.

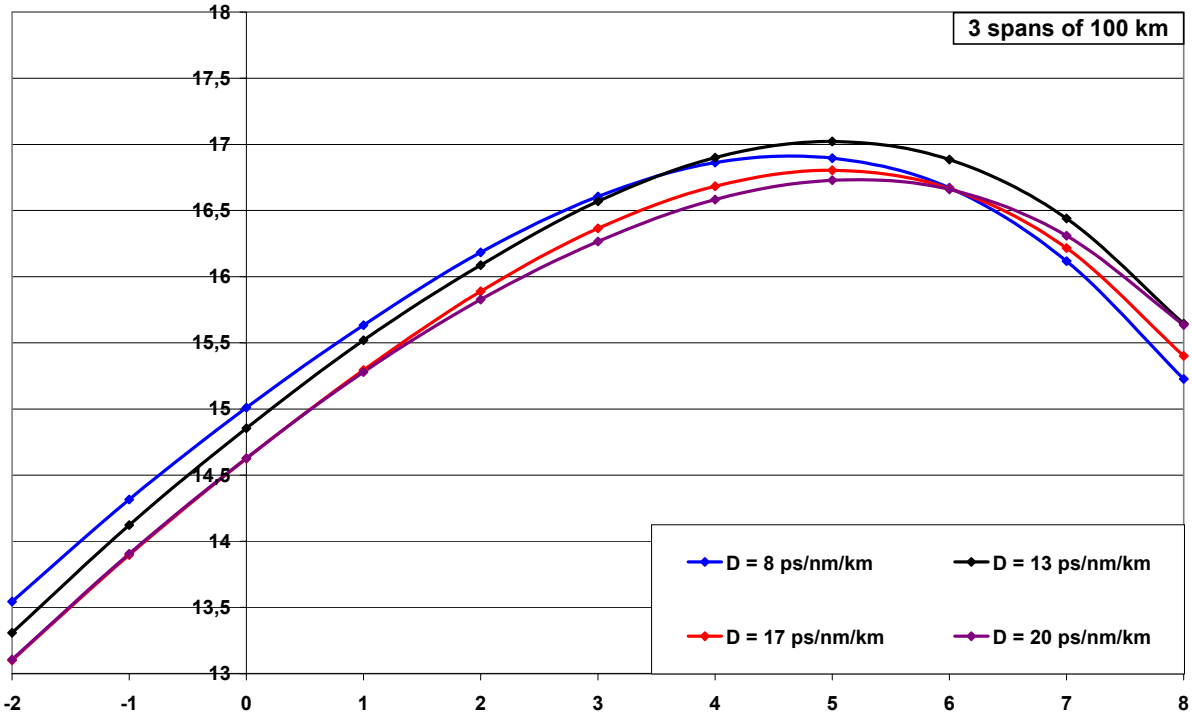

Figure 5. 2. Q² factor versus signal power for a unique channel transmission over 3 spans of 100 km and various inline fibre dispersion.

We have to be aware that the difference between the blue curve (corresponding to D = 8 ps/nm/km) on this figure and the red curve on the previous figure (corresponding to Teralight fibre) is due to the fact that, in this last case, the inline fibre effective area is set to 80 µm² whereas it is set to 50 µm² in the case of Teralight fibre. We remark that the best quality factor corresponds to an inline fibre dispersion of 13 ps/nm/km and a channel power of 5 dBm. For low signal powers, noise is the predominant degrading effect and that's why small inline fibre dispersions are preferable because they require a small length of DCF and thus less attenuation. For high signal powers, non linear effects are predominant and we have seen in the previous chapter that intrachannel non-linear effects were higher for small dispersion values. A compromise has to be made on this dispersion choice between these two effects and the best choice is, in this case of transmission over 3 spans of 100 km, to choose a dispersion value between 8 and 17 ps/nm/km. However, we notice that the difference between Q² factors for dispersion values of 8, 13 and 17 ps/nm/km and for a signal power of 5 dBm (corresponding to the optimal injection power) is less than 1 dB. Even thought the precision of the estimation of the Q² factor is good as these simulations were performed with 1024 bits using 32 samples per bit, it is not possible to tell with certitude that the choice of 13 ps/nm/km for inline fibre dispersion would lead to the best results. In this transmission case, we notice that the dispersion change has a relatively low impact on the signal degradation. It means that the amount of non linear effects is not that important in this case. It's quite remarkable to see that these differences between optimal powers when changing fibre types are not dependant on the dispersion value.

2.5 Impact of fibre effective area

On the following graph, we investigate the Q² value in the same transmission case of 3 spans of 100 km. The inline fibre dispersion value is set to 17 ps/nm/km but the effective area is varying from 40 to 150 µm².

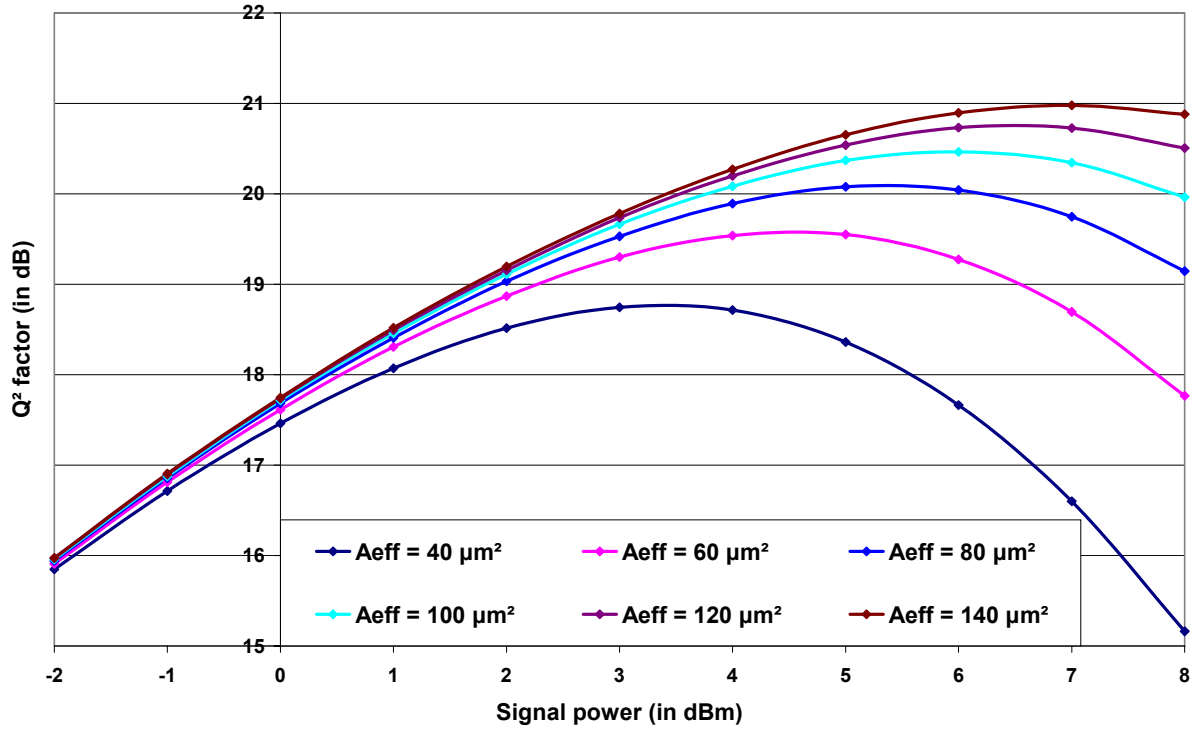

Figure 5. 3. Q² factor versus signal power for a unique channel transmission over 3 spans of 100 km. Inline fibre dispersion is set to 17 ps/nm/km but its effective area is varying from 40 to 140 µm².

We here see the great importance of the impact of this parameter as the effective area of the inline fibre influences the amount of non-linear effects. It is directly related to the non-linear coefficient γ (describing non-linear perturbation in the Schrödinger equation) by:

$$\gamma = \frac{n_2 . \omega_0}{C . A_{eff}}$$

where n_2 is the non-linear index (equal to $2{,}6.10^{-20}$ m²/W for most fibres), C is the light speed, ω_0 is the light frequency and A_{eff} is the effective area of the fibre. This difference between the three fibre types explains the evolution of Q factors versus signal powers shown in Figure 5. 1. The small advantage of SMF over Leaf and Teralight is not only due to the higher dispersion of SMF fibre but also to its higher effective area.

2.6 Use of a hybrid amplification scheme

We now would like to investigate the use of Raman pumping in order to evaluate its gain for such a transmission. Inline fibre is SSMF. Thought, we consider an hybrid transmission scheme described as follows.

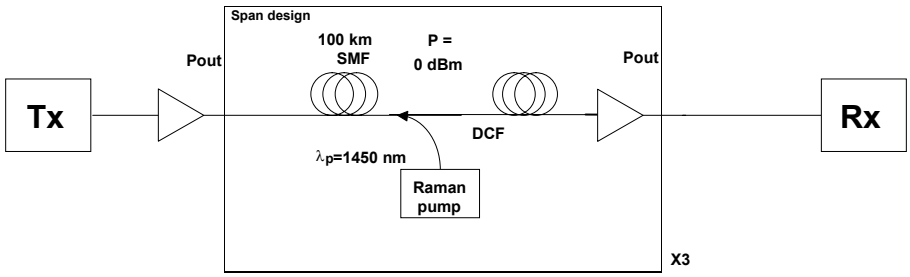

Figure 5. 4. Scheme of the optical line with hybrid amplification choice for transmission over 3 spans of 100 km of SSMF.

Raman pump is providing a gain so that the DCF input power is 0 dBm. The validation of the chosen Raman pump power has been made by comparing it to experimental values:

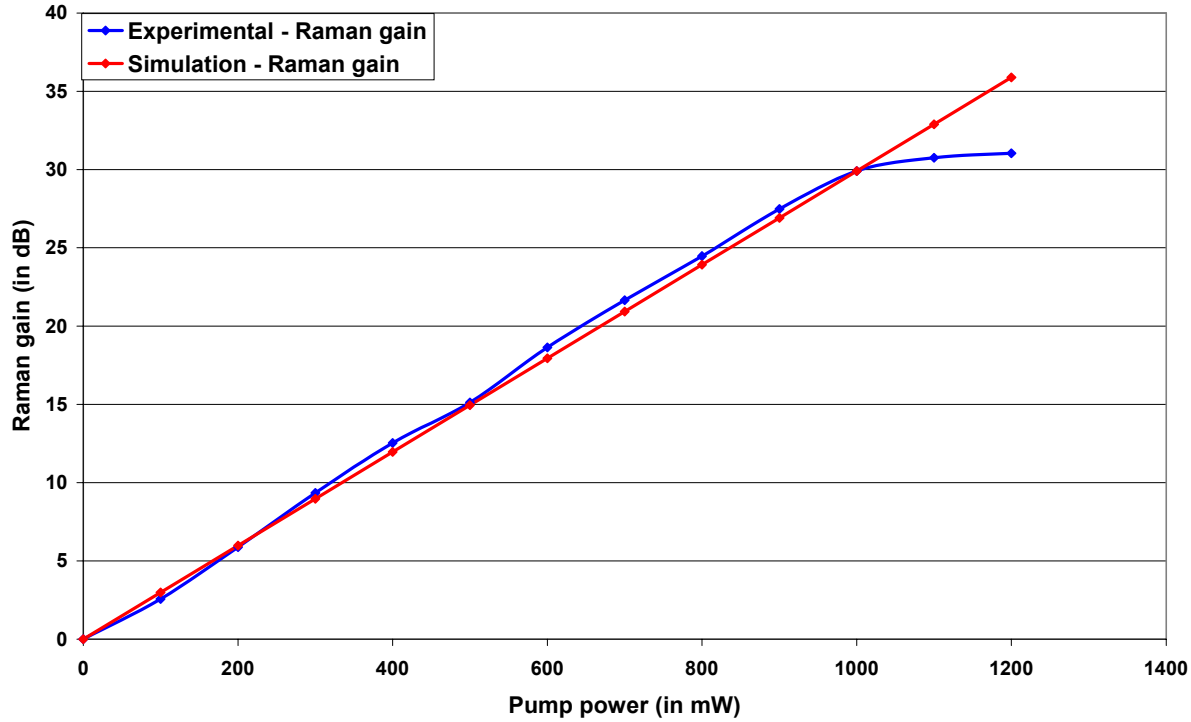

Figure 5. 5. Raman gain (in dB) as a function of pump power (in mW). Comparison of simulation and experimentation values.

We can see that these values perfectly match except for high Raman pump power where there is a saturation phenomena. In simulation cases, the Raman gain is always less than 30 dB.

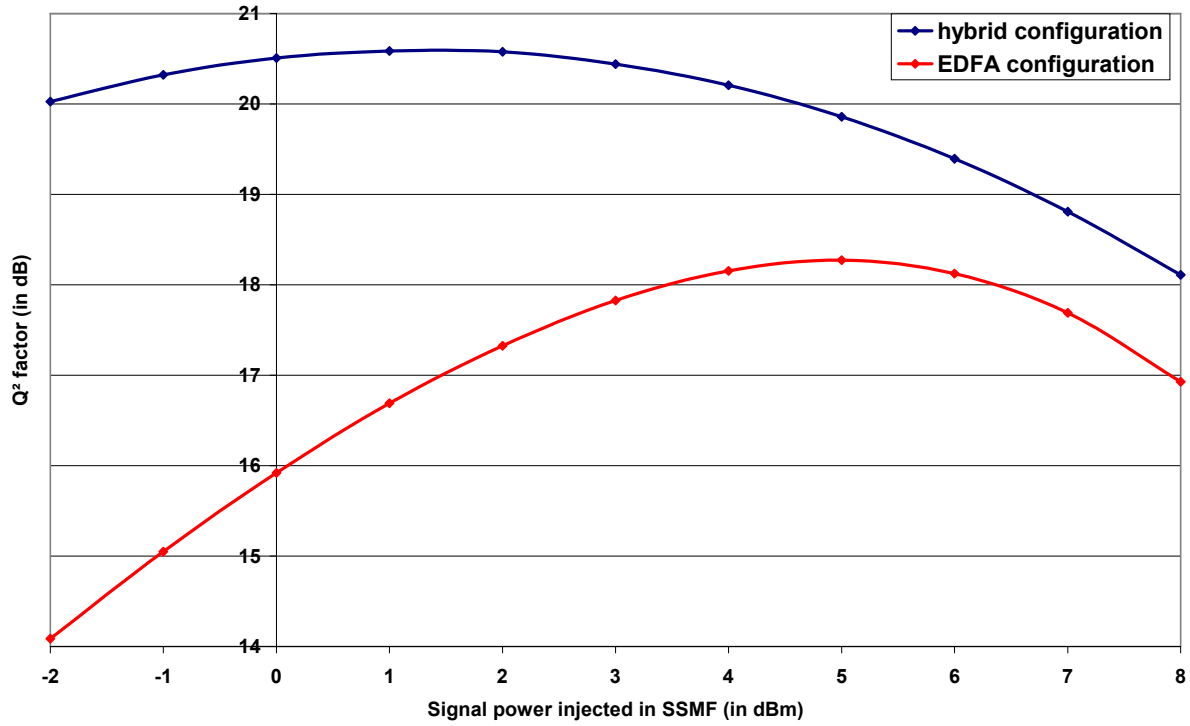

Figure 5. 6. Evolution of Q² factors for transmission over 3x100 km of SMF as a function of injected signal power for hybrid and erbium amplification.

We can see that the optimal power is shifted to 2 dBm in the case of hybrid amplification because of the reduction of noise. This reduction leads to the reduction of non-linear effects and enables the increase of the Q² factor. In the case of a 2 dBm injection power, the Raman gain is set to 18 dB which means that the Raman pump is around 580 mW. This way, the Raman noise is equal to $P_{ASE\text{-}Raman} \approx$ -42,5 dBm in 0,1 nm ($N_{ASE\text{-}Raman} = 4{,}49.10^{-15}$ mW.Hz^{-1}) and so the added density of noise per span is:

$$N_{ASE\_span} = N_{ASE-Raman}.T_2.G_2 + h\nu.G_2.n_{eq-2}$$

For SSMF, the values of T_2 and G_2 are -11,3 dB and 13,3 dB. For this value of amplifier gain, we have:

$$n_{eq\text{-}2} = \frac{\left(NF_2 - \frac{1}{G_2}\right)}{2} \approx 1{,}386$$

Numerical application gives:

$$N_{ASE\_span} = 4{,}49.10^{-15}.1{,}585 + 1{,}279.10^{-16}.21{,}38.1{,}386 \approx 1{,}09.10^{-14}\ \text{mW.Hz}^{-1}$$

Considering an emission OSNR of 40 dB, the output OSNR is:

$$OSNR\_Tx = 10.\log_{10}\left(\frac{\langle P\rangle}{\frac{\langle P\rangle}{B_{ref}.10^{\frac{OSNR\_Tx}{10}}} + 3.N_{ASE\_span}}.\frac{1}{B_{ref}}\right) \approx 34{,}46 \quad dB$$

In the case of erbium amplification, the OSNR value is estimated to 34,08 dB when the inline fibre injection power is set to 5 dBm. Consequently, Raman amplification enables a 3 dB power reduction.

3 Second case study: very long haul transmission

3.1 Noise analysis

We now would like to consider a long haul transmission over 8 spans of 80 km. Inline fibre is not determined. As in the previous example, we will try to define the parameters of the transmission in order to enable a good quality of the transmission.

The first thing to consider in the transmission scenario concerns noise aspects. The inline fibre injection power is to be such that:

$$P_{\min} = \frac{8.10^{\frac{28,6}{10}}.N_{ASE\_span}.B_{ref}}{1-10^{\frac{28,6-OSNR\_Tx}{10}}}$$

where N_{ASE_span} is the added density of noise per span. Using double stage erbium amplifiers (NF=4,5 dB for each amplifier), we have:

$$N_{ASE\_span} = h\nu.\left(G_1.G_2 n_{eq-1}.T_2 + G_2.n_{eq-2}\right)$$

where G_1 and G_2 are the gain of erbium amplifiers and T_2 is the attenuation of the DCF module. In the case of SMF (D = 17 ps/nm/km), this attenuation is equal to:

$$T_2 = 80.\frac{17}{90}.(-0,6) = \text{-9,06 dB or 0,124}$$

In a first time, we will consider that G_1=G_2=12,53 dB and so, $n_{eq-1} = n_{eq-2} = 1,38$. Thus, we have the following numerical application:

$$N_{ASE\_span} = 1,279.10^{-16}.1,38.(320,6.0,124 + 17,9) = 1,02.10^{-14}\ \text{mW.Hz}^{-1}$$

Depending the emission OSNR, the minimum signal power to be injected into inline fibre is:

OSNR_Tx	Minimum signal power
30 dB	2,68 mW or 4,3 dBm
32 dB	1,36 mW or 1,4 dBm
36 dB	0,9 mW or -0,47 dBm
40 dB	0,78 mW or -1 dBm

Table 5. 3. Minimum signal power depending the emission OSNR for a transmission over 8 spans of 80 km of SMF.

3.2 Impact of fibre dispersion

In order to estimate the impact of intrachannel non-linear effects, we investigate the variation of Q² factor with the signal power. On the following figure, we compare these evolutions for different inline fibre dispersions from 1 ps/nm/km to 21 ps/nm/km. We can see on this figure that the best results are obtained for the lowest inline fibre dispersion and for an optical power of 2 dBm injected in each span. This means that the quality of the signal is here much influenced by the amount of noise (which is lower for low dispersion fibres) than by the amount of non-linear effects (which is higher for low dispersion fibres). As a matter of fact, we notice that the optimal power value is always increasing with inline fibre dispersion due to the reduction of non-linear effects. This effect is counterbalanced by the noise accumulation which increases with inline fibre dispersion. However, the reduction of non-linear effects is not sufficient to improve signal quality by increasing the injected power except for the cases corresponding to an inline fibre dispersion of 13 and 17 ps/nm/km. Nevertheless, we should remember that the values of effective areas of inline fibre were here all equal to 80 µm² and that it is not the case of real available fibres. It is yet interesting to compare this analysis with the similar analysis that has been made for the transmission over 3 spans of 100 km and where the optimal inline fibre dispersion was 13 ps/nm/km.

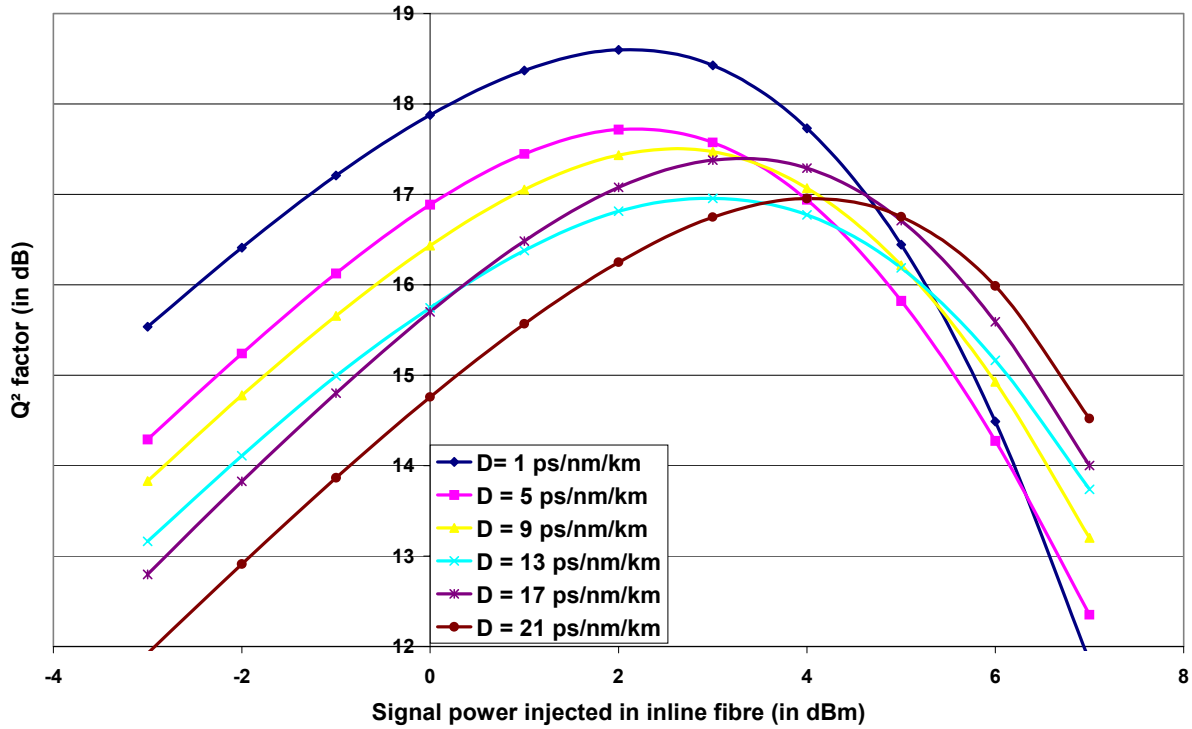

Figure 5. 7. Q² factor versus signal power for a unique channel transmission over 8 spans of 80 km and various inline fiber dispersion.

3.3 Modelling of the transmission with real fibres

In order to model the transmission over 8 spans of 80 km, we now incorporate the physical parameters of three commercially available fibres. In the following graph, we study the evolution of the Q factor with the signal power for three available fibres (SMF, Teralight and Leaf). In a first simulation, the amplifiers are still considered with the same gain whereas, in a second simulation, the input DCF power is set to 0 dBm and the inter-stage loss is set to 9 dB. As a matter of fact, an injection power of 0 dBm into DCF fibre is limiting the occurring of non-linear effects. The 9 dB value of the inter-stage loss is equal to the attenuation of the DCF fibre compensating for 80 km of SMF fibre. This way, if inline fibre type is Leaf, the inter-stage is constituted by 3,73 km of DCF (inducing an attenuation of 2,2 dB) and an optical attenuator with 6,8 dB loss. This last case better corresponds to what happens in real systems.

Looking to the results plotted in Figure 5. 8, we can see that in the first simulation (for equal gain amplifiers), this long reach transmission enhances the impact of noise as seen in the comparison of the three continuous lines for small signal powers. For example, for an SMF injection power of -2 dBm, we can see a difference of 2 dB between Leaf and SMF fibre. If we neglect the influence of non-linear effects in fibre, this means there is a difference of 2 dB between optical-signal-to-noise ratios at the output. As the signal power increases, this difference is counter-balanced by the impact of non-linear effects and the optimal Q values are roughly equal for the three fibre types but for different optimal signal powers (1 dBm for LEAF and Teralight, 3 dBm for SMF).

If we now compare the evolution of dotted lines, we have to remember that for a given signal power, the amount of noise is the same for the three fibre types. It implies that, in the absence of non-linear effects, the OSNRs are all equal and consequently, the Q factors are equal. When the signal power increases, the impact of intrachannel non-linear effects is higher for low dispersion and small effective area fibres. This is a significant difference between SMF and Leaf resulting in a 1 dB difference between optimal Q values. Another remarkable point is the difference between the two simulation series: for SMF fibre, we obtain nearly 0,5 dB difference between optimal Q values. This is

mostly due to the reduction of noise. For the first serial and for SMF fibre type (the inter-stage loss is 9 dB), the spectral density of ASE noise added after each span is:

$$N_{ASE\_span} = 1{,}02.10^{-14}\ \text{mW.Hz}^{-1}\ \text{as calculated before.}$$

In the case of an injection power of 0 dBm into DCF, the optimal injection signal power into inline fibre is 2 dBm. It means that the signal power before the first amplifier is equal to -14 dBm. Consequently, the first amplifier gain is 14 dB whereas the second amplifier gain is 11,06 dB. The spectral density of ASE noise added after each span is then:

$$N_{ASE\_span} = h\nu.\left(G_1.G_2 n_{eq-1}.T_2 + G_2.n_{eq-2}\right)$$

$$N_{ASE\_span} = 1{,}279.10^{-16}.1{,}38.\left(320{,}6.0{,}124 + 12{,}76\right) = 9{,}27.10^{-15}\ \text{mW.Hz}^{-1}$$

The spectral densities of noise at the end of the line are thus:

$$N_{ASE} = N_{ASE\_Tx} + 8.N_{ASE\_span}$$

$$N_{ASE-1} = 1{,}26.10^{-14} + 8.1{,}02.10^{-14} = 9{,}42.10^{-14}\ \text{mW.Hz-1 in the first case.}$$

$$N_{ASE-2} = 1{,}26.10^{-14} + 8.9{,}27.10^{-15} = 8{,}67.10^{-14}\ \text{mW.Hz-1 in the second case.}$$

The difference between these two values (N_{ASE-1}/N_{ASE-2}) is 0,35 dB which implies the same difference between OSNRs and between Q² factors.

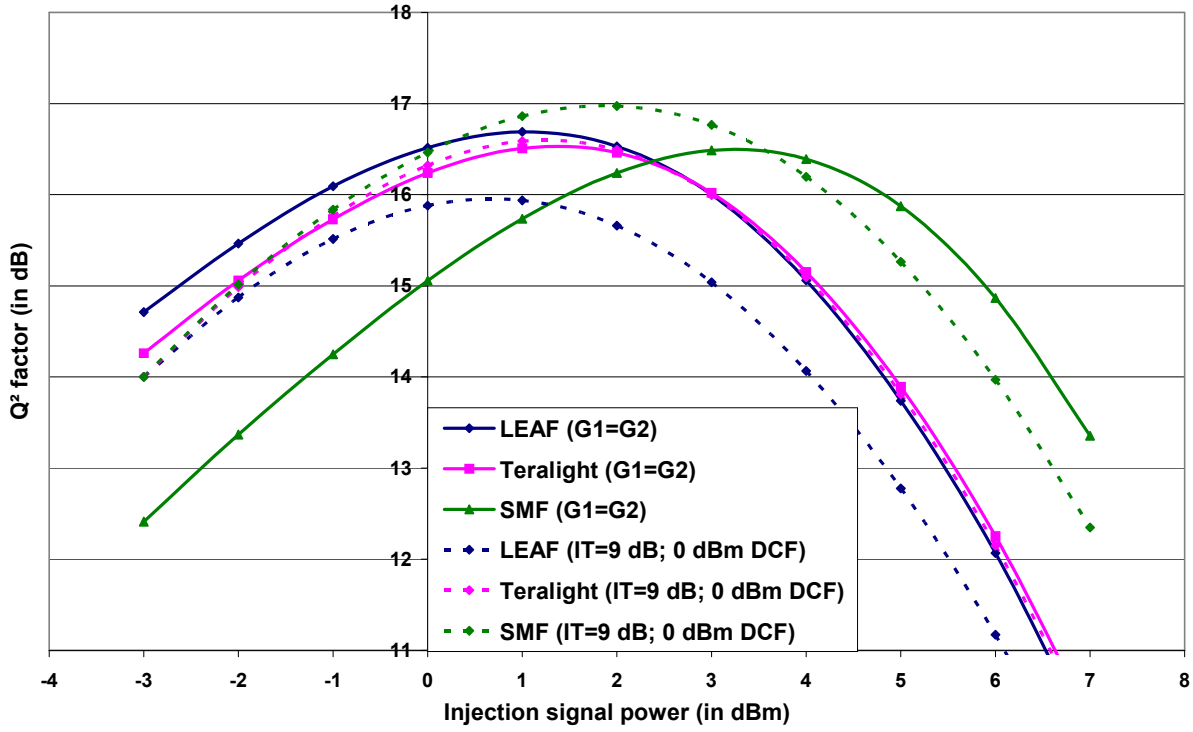

Figure 5. 8. Q² factor versus signal power for a unique channel transmission over 8 spans of 80 km with three fibre types and 2 simulation types (continuous lines: equal gain amplifiers; dotted lines: more realistic amplifiers)

These last results give advantage to the choice of SMF fibre for a transmission over 8x80 km with double stage erbium amplifiers.

3.4 Use of dispersion management

We now try to reduce the impact of intrachannel non-linear effects by dispersion management. That's why we use a pre-dispersion of -1000 ps/nm and a residual dispersion per span equal to 175 ps/nm. The residual dispersion per span has been chosen according to the following rule [2,3]:

$$D_{inline,residual} = \frac{D_{pre-dispersion} - \frac{D_{fibre}}{\alpha_{fibre}}}{-0,5.(N_{span}-1)}$$

$$D_{inline,residual} = \frac{-1000 + \frac{17}{0,2.\ln(10)}}{-0,5.7} \approx 175 \text{ ps/nm}$$

The improvement of the Q² factor can be observed in the following figure: the optimal SMF injection power improves from 2 to 4 dBm and the mean Q² factor increases from 17 to 18,8 dB. On the same figure, we have represented the evolution of Q² factors in the case of WDM transmission. We note that there's no degradation due to spectral crosstalk as the difference between Q² factors for low signal powers is weak (<0,5 dB). We see that the optimal Q factor is obtained for a signal power of 3 dBm per channel and we roughly obtain the same Q² factor in the WDM case than in the single channel case. Therefore, the penalty due to inter-channel non-linear effects can be neglected in the preparation of such a transmission.

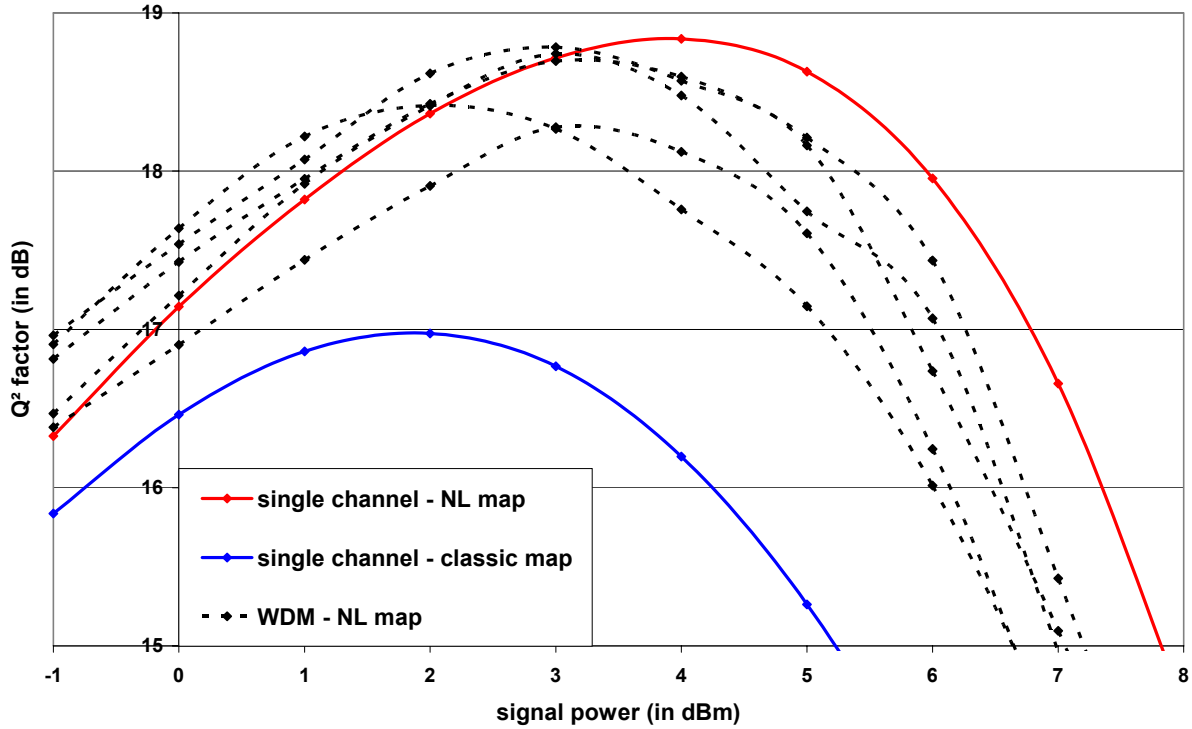

Figure 5. 9. Q² factor versus signal power for a unique channel transmission over 8 spans of 80 km of SSMF with a classic dispersion map (in blue) and with an improved dispersion map (in red). Case of a WDM transmission for the improved dispersion map.

We now investigate the choice of a hybrid amplification. Backwards Raman pumping is used in inline fibre and the pump power is adjusted so that the DCF input power is 0 dBm. The inter-stage loss is set to 9 dB and is constituted by DCF and possibly by an optical attenuator. An erbium amplifier enables the compensation of this attenuation. The scheme of the line is shown in the following figure.

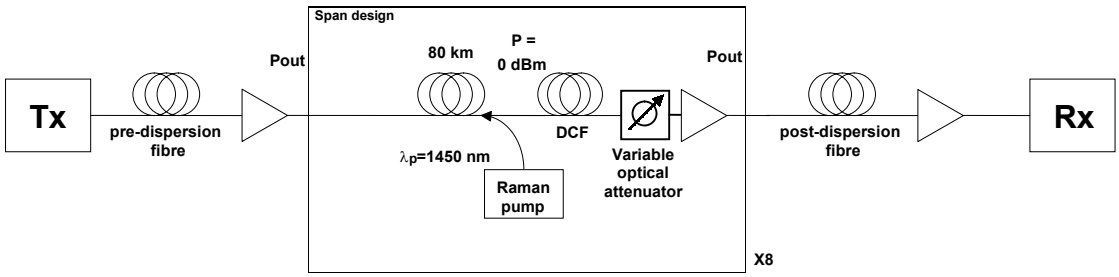

Figure 5. 10. Scheme of the optical line with hybrid amplification choice for transmission over 8 spans of 80 km.

In a first time, the transmission will be made over a classic map so there will not be any pre-dispersion nor post-dispersion fibres. The total loss of DCF and the variable optical attenuator is equal to 9 dB. The Q² factor is displayed for the three usual fibre types on the following graph when varying the inline fibre injection power. In a second time, we investigate the evolution of Q² factor using an optimized dispersion map. This map consists of a pre-dispersion of -1000 ps/nm. The residual dispersion per span is given by:

$$D_{inline,residual} = \frac{D_{pre-dispersion} - \frac{D_{fibre}}{\alpha_{fibre}}}{-0{,}5.\left(N_{span} - 1\right)}$$

Numerical application gives:

- $D_{inline,residual}$ = 175 ps/nm for SMF.
- $D_{inline,residual}$ = 236 ps/nm for Teralight.
- $D_{inline,residual}$ = 260 ps/nm for Leaf.

The injection power is varying from -6 to 7 dBm and the Q² factor is estimated as a measure of the signal quality.

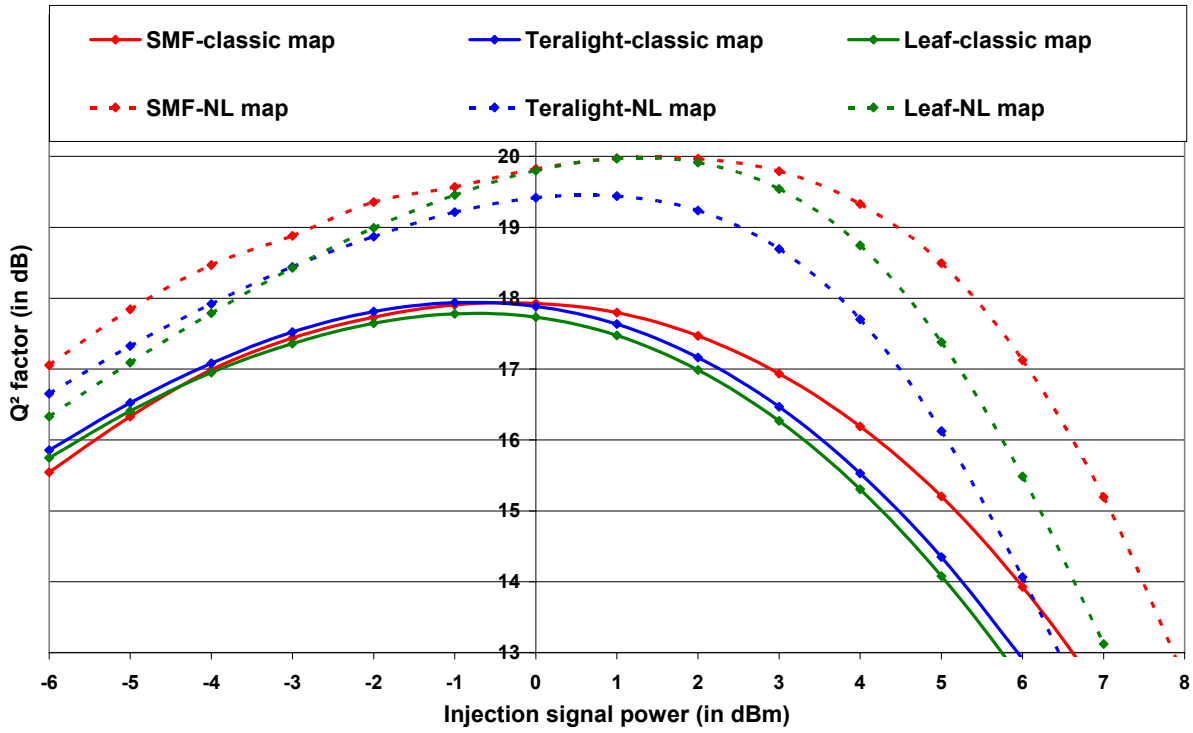

Figure 5. 11. Q² factor versus injection signal power in hybrid amplification transmission over 8 x 80 km with three usual fibre types and two types of dispersion management.

In this graph, we can first compare the evolution of Q² factor versus injected signal power with a classic dispersion map and for the three fibre types. For low signal power, the difference between obtained values is quite tight which means there is no advantage of a fibre type over the others. Increasing the signal power, we obtain the optimal Q² factor between -1 and 0 dBm whatever the fibre type. Beyond this value, non-linear effects decrease the signal quality. These effects are more important in Leaf and Teralight fibre due to inline dispersion and effective area, as already shown. The difference between these three results and those obtained when using dispersion management are quite important: the optimal signal power is now between 1 and 2 dBm. This 2 dB improvement is also reflected on the Q² factor as we nearly obtain 20 dB for the Q² factor instead of 18 dB. Once again, differences between the three fibre types are minor. For low signal power, differences are due to the different attenuations of the post-dispersion fibre. The last erbium amplifier (just before the receiver) compensated this attenuation. The post-dispersion values and the corresponding attenuation (or amplifier gain) are:

- For SMF:

$$D_{post\text{-}dispersion} = -(-1000 + 8 \,.\, 175) = 400 \text{ ps/nm}$$

$$\text{Attenuation} = \frac{400.0{,}6}{90} = 2{,}66 \text{ dB}$$

- For Teralight:

$$D_{post\text{-}dispersion} = -(-1000 + 8 \,.\, 236) = 888 \text{ ps/nm}$$

$$\text{Attenuation} = \frac{400.0{,}6}{90} = 5{,}92 \text{ dB}$$

- For Leaf:

$$D_{post\text{-}dispersion} = -(-1000 + 8 \,.\, 175) = 1080 \text{ ps/nm}$$

$$\text{Attenuation} = \frac{400.0{,}6}{90} = 7{,}2 \text{ dB}$$

When increasing the signal power beyond 2 dBm, intrachannel non-linear effects are responsible for the decrease of the signal quality. The surprising point is the clear advantage of Leaf over Teralight. We have seen that the effect of dispersion is not predominant for the occurrence of non-linear effects (see Figure 5. 7) but the impact of inline fibre effective area is prevailing (see Figure 5. 11). This way, the advantage is given to Leaf fibre (A_{eff} = 72 µm²) compared to Teralight fibre (A_{eff} = 65 µm²). Furthermore, the analysis I have led in the reduction of intrachannel non-linear effects by the use of dispersion management has shown that a better improvement of the performances is obtained for small inline dispersion fibres.

3.5 PMD impact

After the optimization of the link in terms of noise and non linear effects, a quality factor of 20 dB is obtained using a hybrid amplification scheme and a dispersion management with Leaf fibre as inline fibre. We assume an emission OSNR of 40 dB and a mean signal power of 1,5 dBm (see Figure 5. 11). When using Raman amplification to obtain a Raman on/off gain of 16 dB, the required Raman pump power is P_p=400 mW. After 8 spans, the OSNR is estimated to 32 dB. If we assume a pulse width of 2,5 ps, we can estimate the second order factor in the relation between the quality factor penalty and the differential group delay (see section 3 of 'Statistical effects in propagation').

The following figure shows cumulated probability as a function of the quality factor for PMD values from 1 to 1,75 ps. Therefore, we see that a total PMD value of less than 1 ps is required so that the outage probability is less than 10^{-2}. This figure of 1 ps of PMD for the total link seems very difficult to obtain. Neglecting the PMD due to the dispersion compensation fibre modules and due to the EDFAs, the requirement for the linear PMD value of inline fibre is:

$$PMD < \frac{1}{\sqrt{640}} \approx 0{,}039 \quad ps/\sqrt{km}$$

This value corresponds to a good fibre in laboratory but this is not the case of most fibre types.

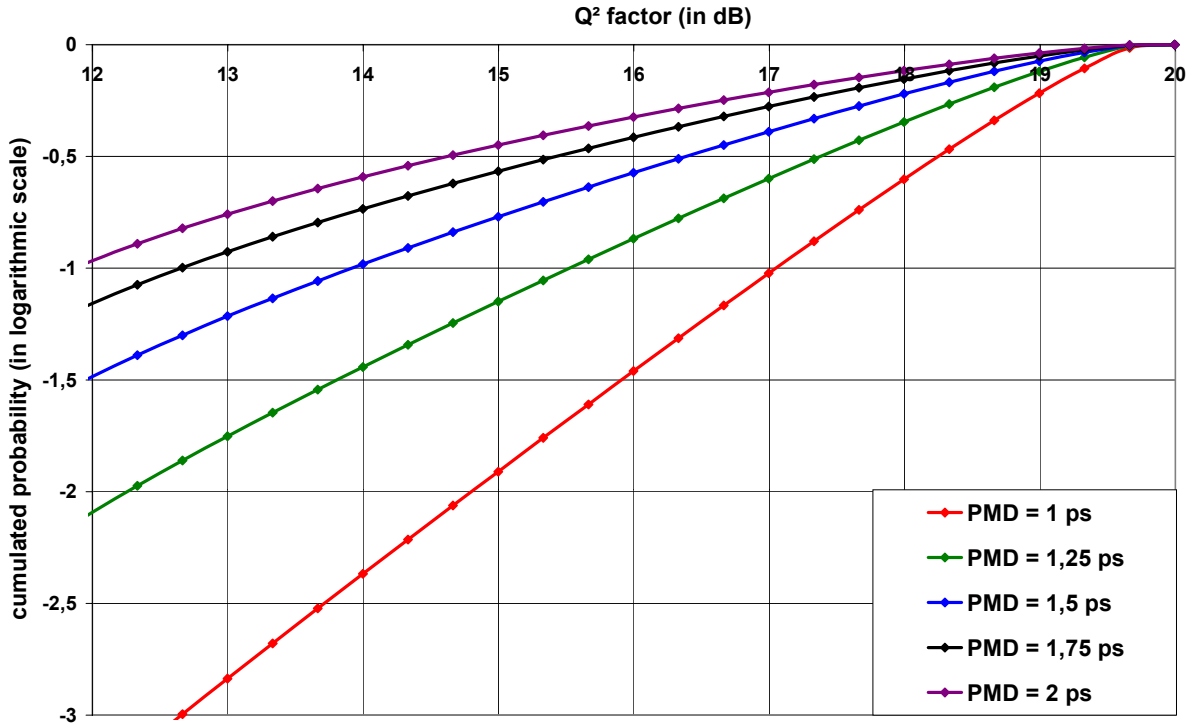

Figure 5. 12. Estimation of the cumulated probability (in logarithmic scale) as a function of the quality factor for 4 different PMD values.

3.6 Conclusion

If we want to summarize the main points of this transmission study case of 8 spans of 80 km, we can say that:

- For an emission OSNR of 40 dB, an inline fibre injection power greater than -1 dB is needed. This analytical calculation, taking into account noise consideration, assumes EDFAs with equal gain on the two stages. Non-linear effects in transmission induce nearly 2 dB penalty as a signal power of 1 dBm is required to achieve a quality factor of 15,6 dB (see Table 5. 3 and Figure 5. 8) using this configuration.
- The adjustment of the two amplifiers gains (increase the gain of the first amplifier) allows reducing the amount of noise. Consequently, the reception OSNR can be conserved when decreasing the inline fibre injection power (in order to reduce non-linear effects) as seen Figure 5. 8.
- The effects of inline fibre dispersion and effective area give advantage to SMF fibre compared to Leaf and Teralight in the erbium amplification scheme.
- Dispersion management allows the reduction of intra-channel non-linear effects and enables a 2 dB gain for the optimal injection power in the case of SMF. This gain is nearly the same for the Q² factor.
- Inter-channel non-linear effects are found to have nearly no impact as we observe only 1 dB difference between optimal injection signal powers. WDM transmission of 5 channels with 0,4 bit/s/Hz spectral efficiency over 8 spans of 80 km of SMF is investigated and a mean Q² factor of 18,5 dB is obtained for a signal power of 3 dBm per channel.
- Using an hybrid amplification scheme with backwards pumping in inline fibre, we obtain a slight improvement: the reduction of noise allows to decrease the signal power and the non-

linear effects. The optimal signal power becomes -1 dBm instead of 2 dBm and the mean Q^2 factor is shifted from 17 to 18 dB whatever the fibre type.

- Strong improvement of the quality is obtained using dispersion management in order to reduce intrachannel non linear effects and a mean Q^2 factor of 20 dB is obtained for 2 dBm signal power for SMF and Leaf fibres and slightly less for Teralight.
- Requirement for PMD seems difficult to achieve since a PMD value of 1 ps is needed for the global link.

4 Preparation of field trial experimentation

4.1 Introduction

This last part of the validation study brings together the most important study points concerning the preparation of the field trial over France Telecom network. This field trial was carried out in the frame of the TOPRATE project in order to demonstrate a Terabit/s long haul transmission. Here are some technical points concerning the transmission:

- Transmission of 8 channels from 1562,2 nm to 1545,3 nm. The channel spacing is set to 300 GHz (spectral efficiency of 0,53 bit/s/Hz).
- The channel bit rate is 172,8 GHz due to a 7 % overload for FEC encoding.
- Each channel is obtained by optical multiplexing of 42,8 Gbit/s sequences. Neighbouring bits have alternate polarization as represented on the following figure.
- The emission OSNR is 39 dB in single channel transmission and 33 dB in WDM transmission.
- Transmission over 6 spans of 70 km of G652 fibre (D = 17 ps/nm/km; α=0,2 dB.km^{-1}).
- The total PMD of the link was measured to 0,8 ps but this figure doesn't take into account the PMD due to DCF modules.

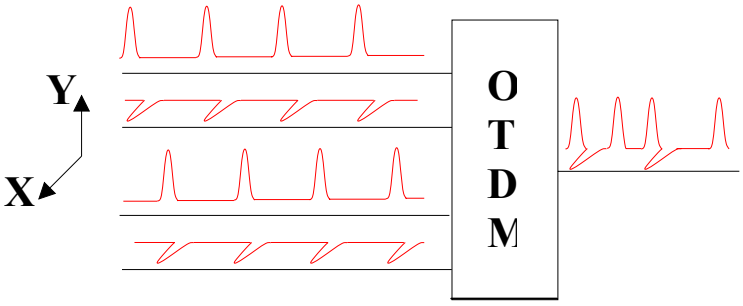

Figure 5. 13. Polarization-multiplexed OTDM lines.

Before going further in the simulations for the preparation of this field trial, we shall interest ourselves to the difference between single and alternate polarization. In order to evaluate the gain brought by alternating the polarization of neighbouring bits, we consider a transmission over 5 spans of 100 km of SSMF perfectly compensated by DCF. The emission is constituted by 4 OTDM lines at 40 Gbit/s with a full width at half maximum equal to 2,5 ps. The emission OSNR is infinite.

Amplification is enabled by double stage erbium amplifiers after each span. Each erbium amplifier is characterized by a noise figure of 4,5 dB. The injection power varies from –1 dBm to +9 dBm at the input of the inline fibre. The injection power in DCF is only 0 dBm. The Q factor is measured after optical filtering, detection and electrical filtering. Due to the impact of statistical distribution of the data sequence on intrachannel four wave mixing, the simulations are run 240 times (thus we obtain 960 measurements for the Q factor) in order to estimate correctly the statistic impact of the data sequence. The results are displayed on the following histograms.

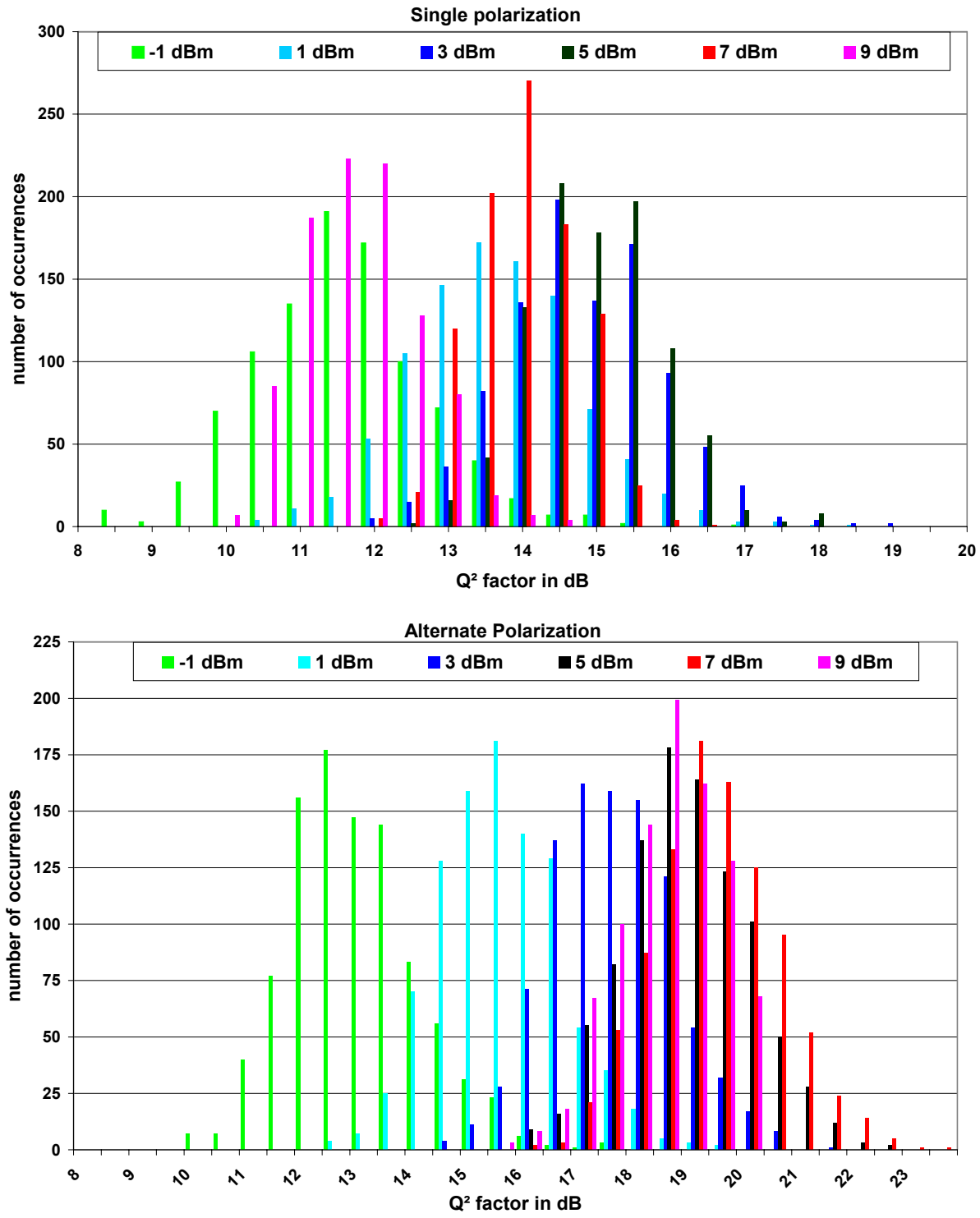

Figure 5. 14. Distribution of Q² factor after transmission over 5 spans of 100 km of SMF for various injection powers with single or alternate polarization.

We can clearly see the enhancement due to alternate polarization since, in the case of single polarization, the optimal inline fibre injection power holds between 3 and 5 dBm whereas it is delimited by 7 and 9 dBm in the case of alternate polarization. From these statistical runs, we can extract some characteristics in order to confirm this trend:

	-1 dBm; 5 spans	1 dBm; 5 spans	3 dBm; 5 spans	5 dBm; 5 spans	7 dBm; 5 spans	9 dBm; 5 spans
mean value:	12,67	15,28	17,24	18,56	19,05	18,38
variance:	1,32	1,19	1,20	1,24	1,26	1,14

Table 5. 4. Characteristics for alternate polarization (after 500 km of transmission).

	-1 dBm; 5 spans	1 dBm; 5 spans	3 dBm; 5 spans	5 dBm; 5 spans	7 dBm; 5 spans	9 dBm; 5 spans
mean value:	11,36	13,45	14,61	14,75	13,77	11,50
variance:	1,31	1,28	1,16	0,81	0,50	0,60

Table 5. 5. Characteristics for single polarization (after 500 km of transmission).

As we have already seen, intrachannel non-linear effects are preponderant in 160 Gbit/s systems due to the high dispersion of pulses. Dispersion induced collisions are resulting in timing jitter (due to cross-phase modulation) and amplitude fluctuation (due to four-wave-mixing). Polarization multiplexing enables the reduction of these deformations because of the coupling reduction between orthogonal polarization waves [5].

Apart from non-linear effects reduction during transmission, polarization-multiplexing also enables to have a larger pulse width. The Gaussian electromagnetic field of a pulse is given by:

$$E(t) = E_0.e^{-\frac{t^2}{2.T_0^2}}$$

where T_0 is the half-width at 1/e and is related to the full width at half maximum, to the duty cycle DC and to the time bit T_b by the relation:

$$FWHM = 2.T_0.\sqrt{2.\ln(2)} = DC.T_b$$

We define a crosstalk factor as the ratio of the optical power at t = 0 and t = $\frac{T_b}{2}$. If we consider a single pulse neighboured by two spaces, this ratio is:

$$r = \frac{P\left(\frac{T_b}{2}\right)}{P(0)} = e^{-\frac{T_b^2}{4.T_0^2}} = e^{-\frac{2.\ln(2)}{DC^2}}$$

If the optical pulse is neighboured by a mark, the electromagnetic field of the adjacent pulse alters the optical power. In a first approximation, we neglect the power change in the centre of the time bit (t=0). For a classic RZ pulse sequence, we have:

$$r = \frac{P\left(\frac{T_b}{2}\right)}{P(0)} = 4.e^{-\frac{T_b^2}{4.T_0^2}} = 4.e^{-\frac{2.\ln(2)}{DC^2}}$$

In case of a polarization multiplexed transmitter, this ratio is:

$$r = \frac{P\left(\frac{T_b}{2}\right)}{P(0)} = 2.e^{-\frac{T_b^2}{4.T_0^2}} = 2.e^{-\frac{2.\ln(2)}{DC^2}}$$

This crosstalk ratio is divided by two due to the use of orthogonal polarization multiplexing. Consequently, orthogonal polarization is an efficient way to reduce time crosstalk due to large pulses.

4.2 Different dispersion maps

The comparison of different dispersion maps, based on the available dispersion compensation modules for the field trial, has been made by varying the SMF injection power from -2 to 12 dBm. The DCF injection power is set to 0 dBm. This comparison has been made with a single channel transmission which is modulated in CSRZ-AP format (Alternate Polarization and CSRZ at 80 Gbit/s). The following figure depicts the different dispersion schemes. The dispersion maps named France Telecom Link 1 to 5 are based on suggestions for the field trial and the dispersion map named Lab Link corresponds to the dispersion map for the experimental preparation of the field trial.

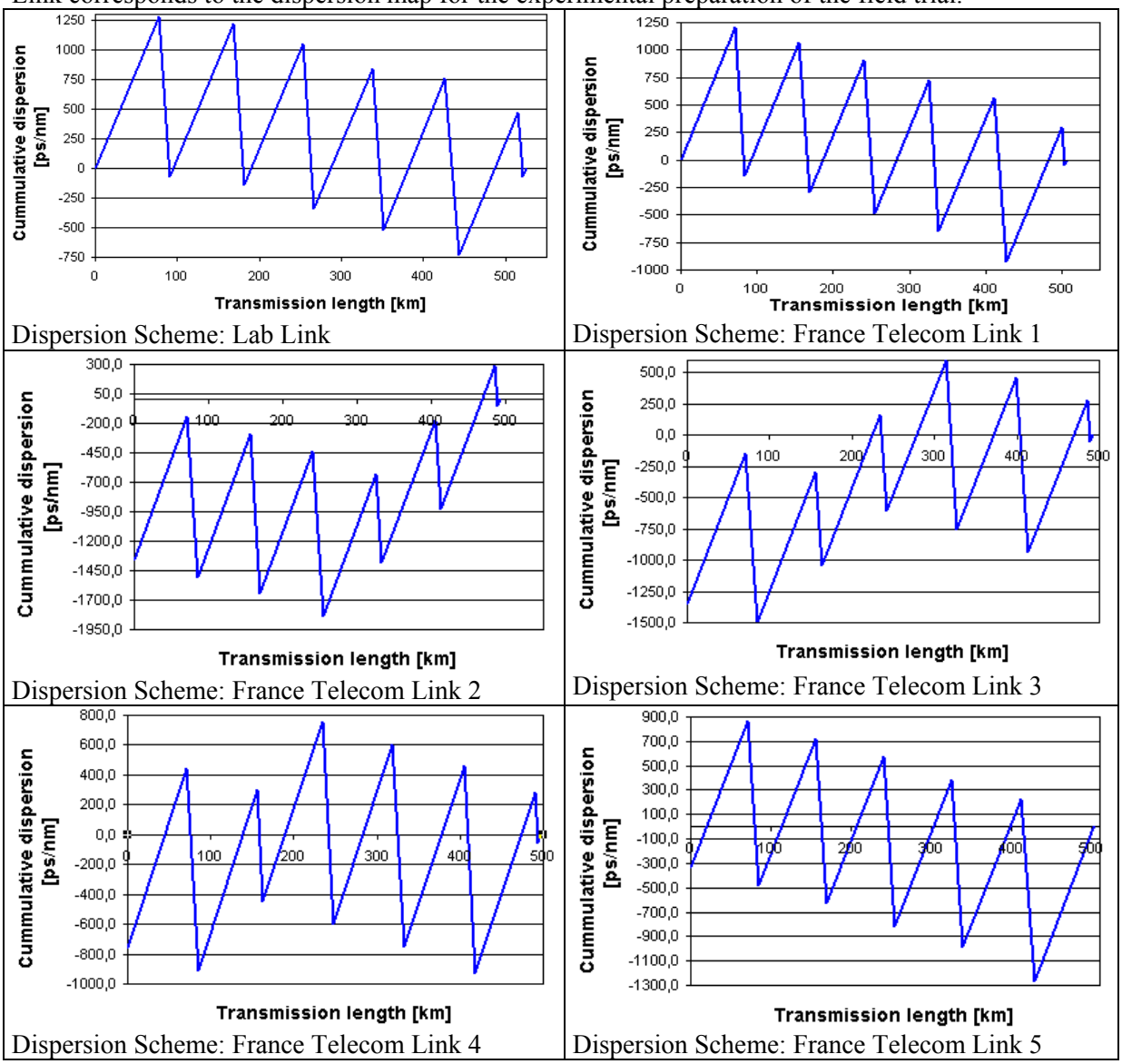

Figure 5. 15. Different dispersion compensation schemes for the France Telecom field trial.

Only single channel transmission is considered for the moment, the pulse width is set to 5 ps in all cases. Simulations have also been performed in the case of dispersion map FT link 1 with a pulse width of 4 ps. At the emission, the optical-signal-to-noise-ratio is 40 dB. Results are plotted in Figure 5. 16.

- **A clear advantage can be seen for the dispersion map named as FT link 1** compared to the other dispersion maps. This dispersion map consists of:

- No precompensation.
- Compensation of -1354 ps/nm after the 1st span.
- Compensation of -1356 ps/nm after the 2nd span.
- Compensation of -1393 ps/nm after the 3rd span.
- Compensation of -1366 ps/nm after the 4th span.
- Compensation of -1494,2 ps/nm after the 5th span.
- Compensation of -338,6 ps/nm after the 6th span and fine adjustment.

The optimal injection power per channel is around 8 dBm for FT link 1 whereas it is only 6 dBm for FT link 5 (and less for the other dispersion maps). From this first simulation we can summarize, that the dispersion schemes without predispersion show the best performance and the performance degrades with the amount of predispersion.

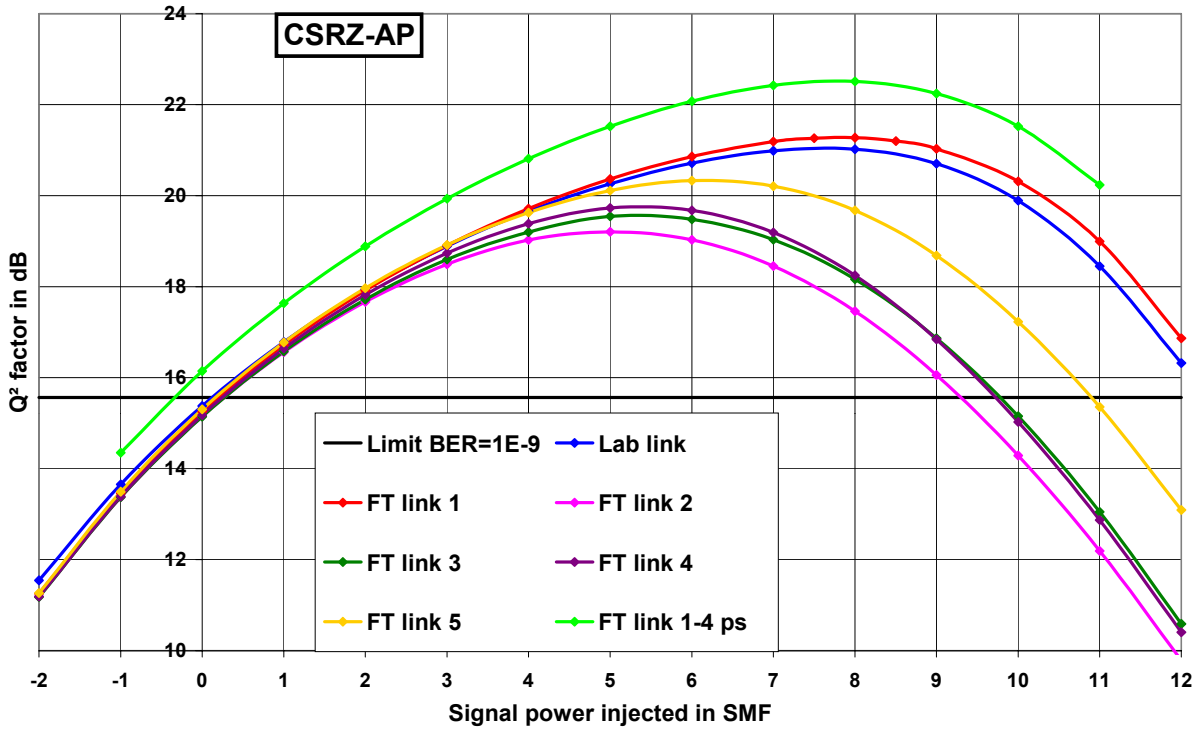

Figure 5. 16. Estimated Q² factors (in dB) when varying the injection signal power for different dispersion maps (see Figure 5. 15). The pulse width is set to 5 ps except for the last sweep. The emission OSNR is 40 dB.

- We can see that the results obtained for FT link 1 and for Lab link are nearly the same. Therefore we expect quite similar results for the lab experiments of FT link1 and the lab link. Only the slightly higher PMD values of the lab link might cause higher signal degradations during the experiment. This effect can be minimized by coupling the signal on the states of polarization of the fibre link, minimizing the impact of PMD.

4.3 Modulation format

The comparison of different modulation formats has been made in the following way:

- The dispersion map is FT link 1. We decided to investigate the effect of modulation format for this dispersion map only as the effect should be the same for other dispersion maps.
- The emission and reception are remaining the same except for the phase differences between OTDM-Tx tributaries ($\Delta\varphi$ = 0° for RZ, 90° for Pi/2-RZ and 180° for CSRZ). It means that the optical filter at the reception is the same for the 3 modulation formats.
- All formats are considered with alternate polarization.

The SMF injection power is varying from -2 to 11 dBm. Results are plotted in the following graph.

We observe a quite important difference between RZ, CSRZ and Pi/2-RZ even for low signal power (for example 0 dBm) where non-linear effects should be quite low and consequently, the signal quality should be the same. From this statement, I think that the reception might not be well adapted for all of these modulation formats and I checked this by setting the signal power to 0 dBm and turning off non-linearities in the fibre. I observed nearly 1 dB difference between CSRZ and RZ modulation formats indicating that the reception is not correctly adapted. From there, I did not consider the obtained Q^2 value as a criteria but the optimal SMF injection power (the power for which the Q value is maximal).

The optimal injection power is plotted with arrows on the graph and it is 7.5 , 8 and 8.5 respectively for RZ,CSRZ and Pi/2-RZ**.**

I would like to point out that this difference of 1 dB only between modulation formats might be due to the fact that non-linear effects have already been reduced by the choice of the dispersion map. It is possible that the same comparison with a "classic" dispersion map would have led to larger differences.

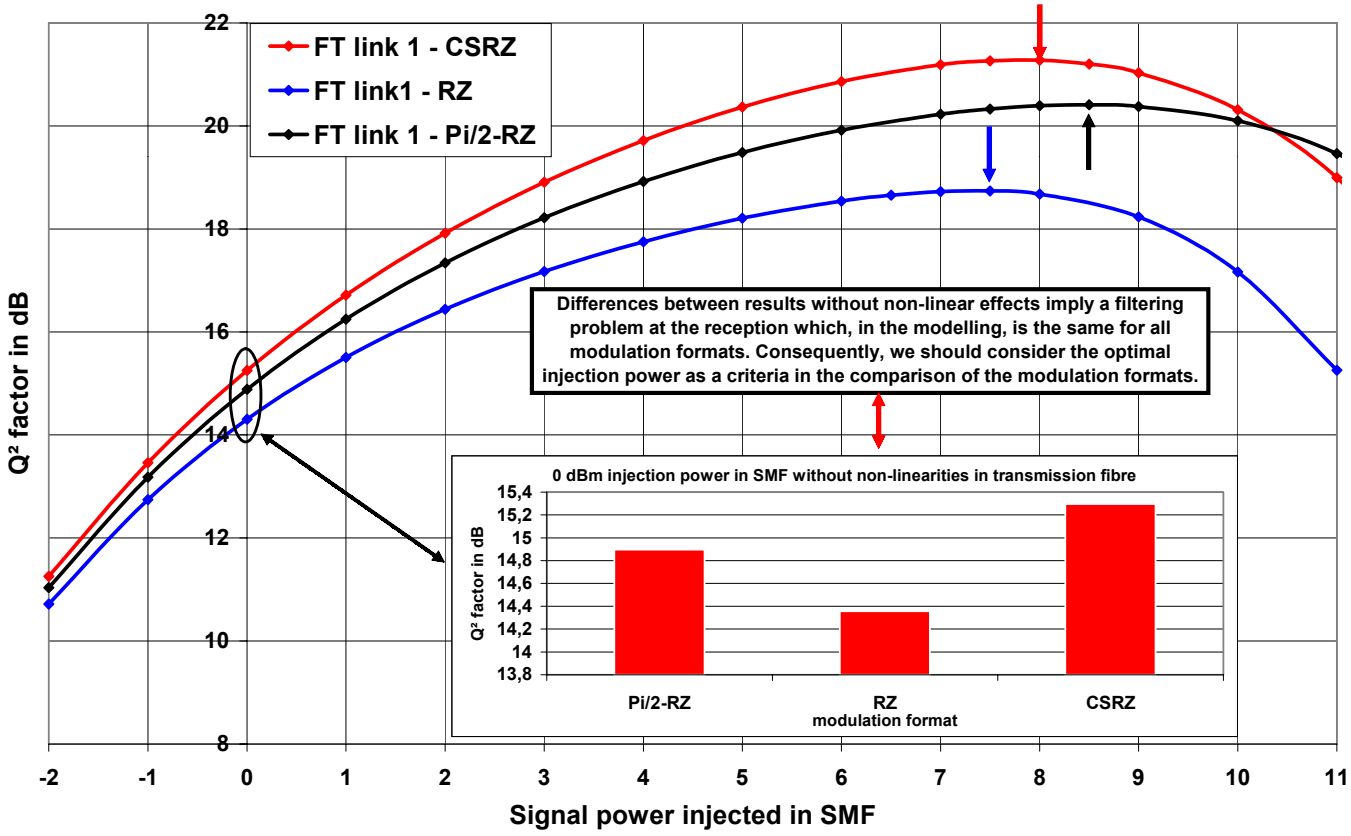

Figure 5. 17. Comparison of modulation formats and evidence of non adapted reception.

4.4 Modelling of double-stage EDFAs and additional losses

Up to now, we have always considered double-stage amplifiers constituted of two EDFAs: the first one is characterized by an output power of 0 dBm and the second one is characterized by a varying output power (from -2 to 12 dBm).
Referring to data sheets provided by Alcatel SEL for Avanex amplifiers, we have modified the modeling of double-stage erbium amplifiers in the following way:

- The first amplifier has a constant gain of 17 dB.
- It is followed by a variable attenuator and by the DCF module. The attenuation of this variable attenuator is set so that the optical power at the input of the DCF module is fixed. This power value is investigated in our simulations.
- The output power of the second amplifier is 20 dBm. In reality, it is set to 11 dBm in order to emulate the presence of 8 channels.
- It is followed by a variable attenuator so that the SSMF injection channel power varies from -2 to 11 dBm.

In the same time, we have modelled additional losses due to connectors:

- The lumped losses include the fiber losses within the offices from the basement to the patch panel and back. Furthermore the connector losses are taken into account.
- Therefore the lumped losses can be modelled by two attenuators of 2 dB. One attenuator can be set before the amplification (before the first amplifier) and one after amplification (after the second amplifier before the next SSMF).We have considered a relatively high loss for these connectors in order to investigate the worst case.

This modelling is schemed on the following figure.

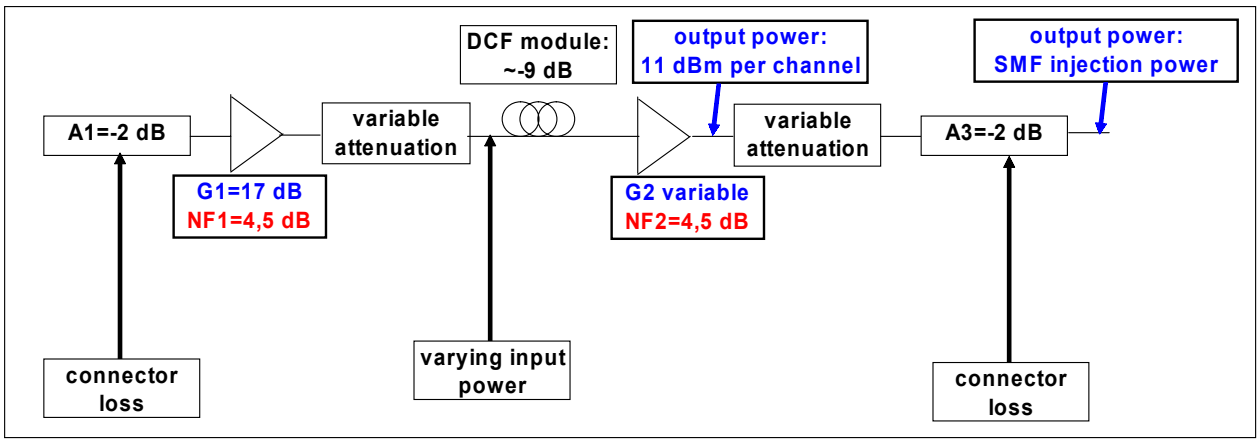

Figure 5. 18. Modelling of double-stage Erbium Doped Fibre Amplifier.

As a matter of fact, the attenuation of the spans in the field trial is varying between 14 and 17 dB.

The equivalent noise figure can be calculated as a function of the SMF injection power, as shown in the following graph in the case of 0 dBm DCF injection power. It is compared to the case of an ideal modelling of double-stage EDFAs.

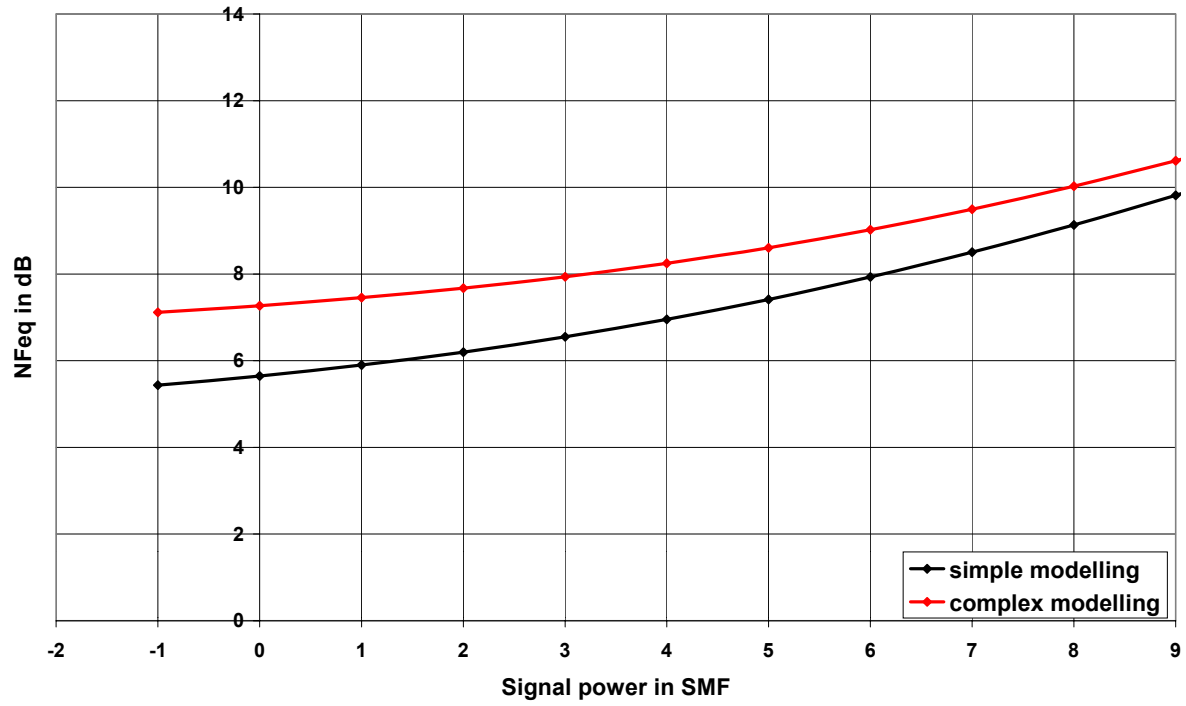

Figure 5. 19. Comparison of equivalent noise figure of double stage Erbium Doped Fibre Amplifier.

We can outline that the difference between these two modellings is minimal for high signal power. It means that the approximations we have made so far concerning the amplification stage can be accepted for high signal power. Using FT link 1 and CSRZ-AP modulation format, we have investigated the variation of the DCF injection power with this complex modelling of double stage EDFAs. DCF injection power has been varying from -3 to 4 dBm and we obtained the characteristics plotted in the following figure.

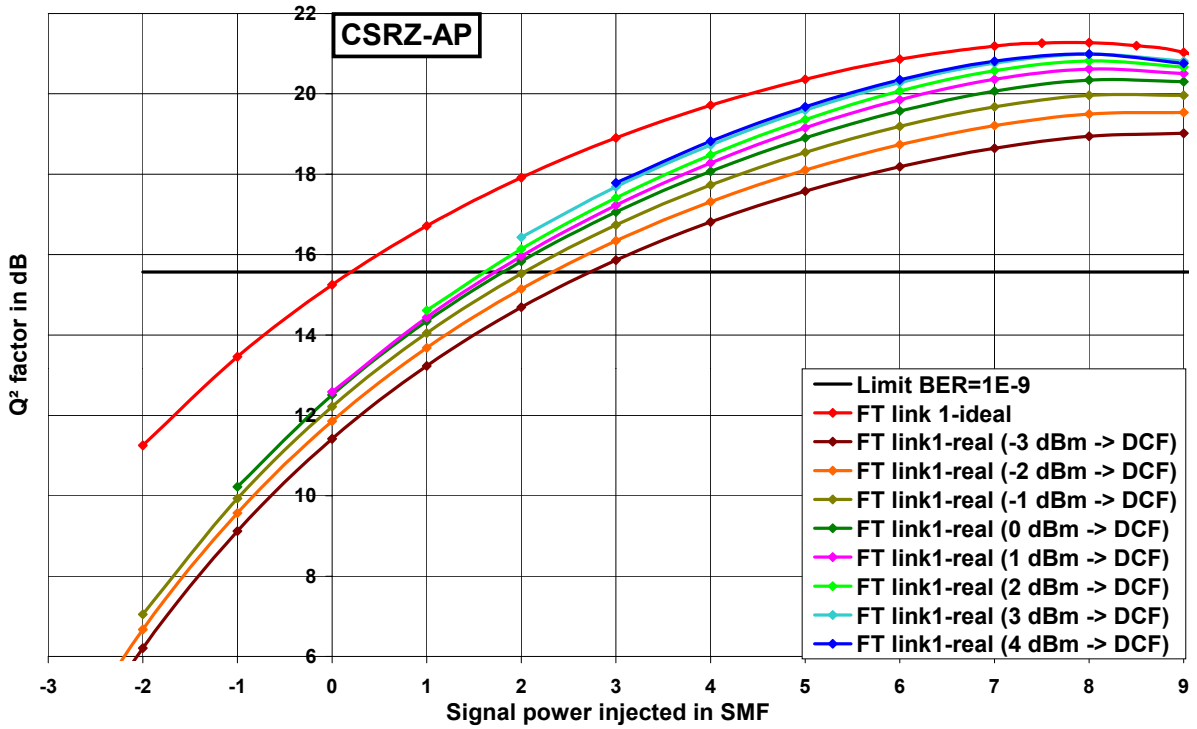

Figure 5. 20. Comparison of ideal/complex modelling of EDFAs with various DCF injection powers.

4.5 Variation of predispersion for Lab link

The impact of predispersion has been considered for the Lab Link. Results show an advantage for a slightly negative predispersion, i.e. -50 ps/nm. This optimal value should be the same for the dispersion map named FT link 1.

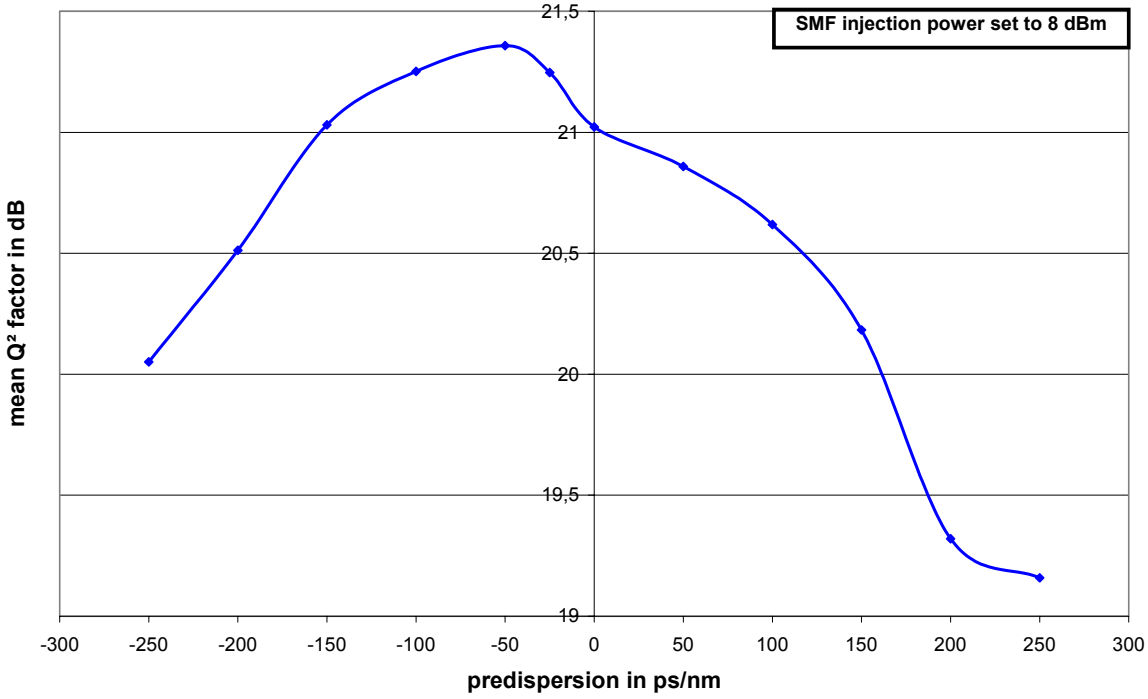

Figure 5. 21. Q² factor as a function of predispersion for 8 dBM SMF injection power.

These results are very interesting because they show a sort of symmetric behaviour with respect to -50 ps/nm, i.e. a slightly negative predispersion, minimizing the non linear interaction effects.

4.6 PMD impact

In the same way than in chapter 3.5, the estimated probability of the quality factor is estimated for several PMD values. An emission OSNR of 40 dB is assumed. For an injection channel power of 8 dBm into SMF and of 0 dBm into DCF, the spectral density of noise added after each span is:

$$N_{ASE\_span} = h\nu.\left(G_1.G_2 n_{eq-1}.T_2 + G_2.n_{eq-2}\right)$$

$$N_{ASE\_span} = 1{,}279.10^{-16}.1{,}38.\left(15{,}848 + 39{,}81\right) = 9{,}82.10^{-15}\ \text{mW.Hz}^{-1}$$

The OSNR at the reception is estimated to 30 dB. The following figure shows the variation of the cumulated probability (in logarithmic scale) as a function of the quality factor.

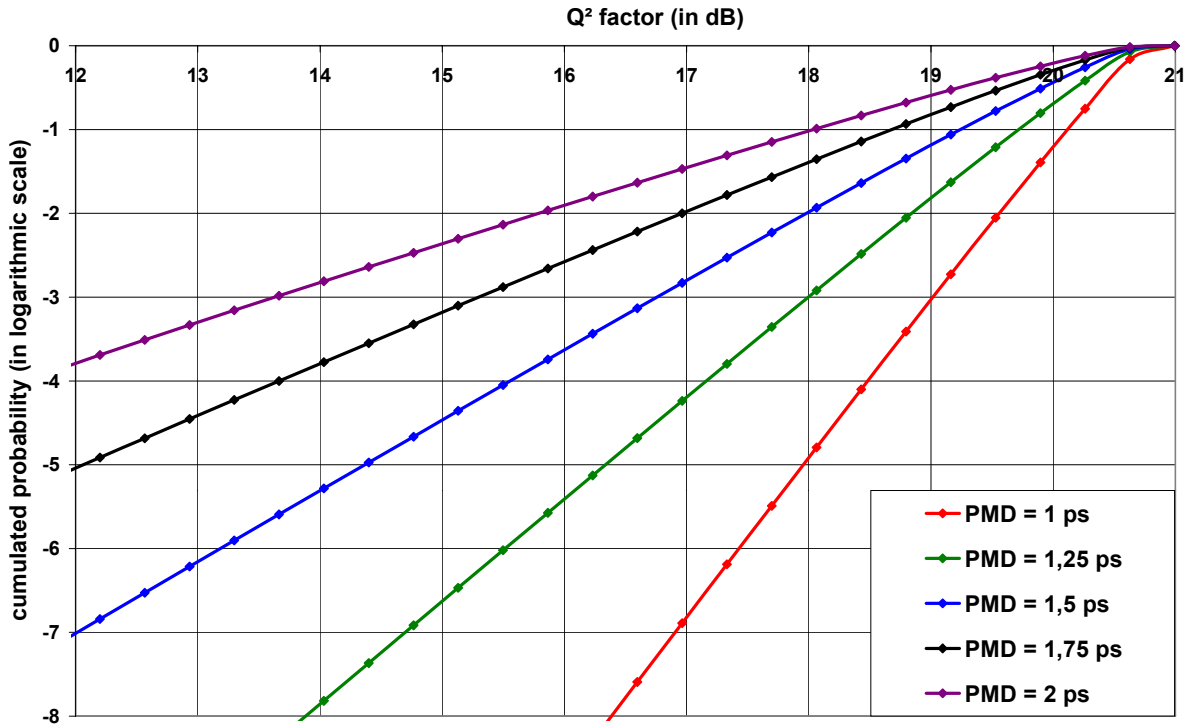

Figure 5. 22. Estimation of the cumulated probability as a function of the quality factor for total PMD values from 1 to 2 ps.

We see that the tolerance to PMD is larger in this case than in the previous case mainly because of the pulse width (equal to 5 ps in this case). The cumulated probability of the quality factor for $Q^2 \approx 16$ dB is around 10^{-2} for a total PMD value of 2 ps.

5 Conclusion

In this chapter, different transmission cases were modelled and studied in order to optimize the transmission with respect to noise and propagation effects. After a summary of the different disturbing effects, how they impact the signal, their importance and how to avoid them, three different transmission cases were studied in order to apply the rules derived from the analysis we have led. All disturbing effects were taken into account in simulations and the transmission was optimized in the three cases. The impact of dispersion management and possibly Raman amplification was found to be highly recommended in order to decrease the amount of non linear effects. In that way, transmission reaches of several hundred kilometres seem feasible using very low PMD fibres.

6 References

1. Dispersion and dispersion slope tolerance of 160-Gb/s systems, considering the temperature dependence of chromatic dispersion, *Vorbeck, S.et al,* Photonics Technology Letters, IEEE, Volume: 15 , Issue: 10 , Oct. 2003, Pages:1470 – 1472
2. «Reduction of Intrachannel Nonlinear Distortion in 40 Gbit/s based WDM transmission over standard Fiber», R.I. Killey et al, Photonics Technology Letters, IEEE , Volume: 12 , Issue: 12 , December 2000, Pages:864 – 866
3. «Enhanced analytical engineering rule for fast optimization of dispersion maps in 40 Gbit/s based transmission systems», Y. Frignac et al, Proc. OFC 2004, Los Angeles, March 2004, Paper TuN3.
4. System outage probability due to first- and second-order PMD, Bulow, H., Photonics Technology Letters, IEEE ,Volume: 10 , Issue: 5 , May 1998, Pages:696 – 698
5. "Benefits of bit-to-bit polarisation interleaving for Nx40 Gbit/s all distributed Raman amplified submarine transmission", G. Le Meur et al, Electronics Letters, 26th September 2002, Vol. 38, N°20.

Discussion: about the significance of 160 Gbit/s OTDM/WDM transmissions

1 Critical point of view and analysis of the technology

First of all, it is interesting to examine the different motivations for 160 Gbit/s bit rate studies. With the increase of the total amount of data in the past years, the channel bit rate increased from 2,5 to 10 Gbit/s. The perspective of 40 Gbit/s bit rate per channel transmission is now mature as some commercial products are available [1]. Now that the technical feasibility of 40 Gbit/s WDM transmission is sufficient, the matter of the economical interest is decisive for the introduction of 40 Gbit/s systems in the network. This economical interest appears when we consider the cost reduction of the edge equipments. For example, the cost of a 40 Gbit/s emitter should be at least less expensive than 4 emitters at 10 Gbit/s. For that reason, the supply and demand have a great part in the driving force of 40 Gbit/s bit rate. However, this explanation can not be evaluated at 160 Gbit/s because equipment are only prototypes. Furthermore, the simplicity introduced in the network because of the reduction of the number of channels may be a great advantage for the upgrade of 10 Gbit/s systems.

In this document, we have seen many technical constraints for the emergence of 160 Gbit/s systems. For example, we have seen that dispersive effects decrease the dispersion tolerance by a ratio of 16 from 40 to 160 Gbit/s. Additionally, the large bandwidth of the signal strengthens intrachannel non-linear effects such as four-wave-mixing and cross-phase modulation. Another important issue concerns polarization-mode-dispersion as its effects are dramatically decreasing the signal quality. For example, using G652D fibre with a PMD value of 0,2 ps/$\sqrt{km}$, the reach of a system decreases from 1000 km at 40 Gbit/s to 60 km at 160 Gbit/s. Moreover, we have seen that it is not possible to significantly increase the spectral efficiency from 40 to 160 Gbit/s bitrate.

These restrictions seem to reduce the interest of such high bitrate transmissions. However, this statement is to be nuanced since progress in the area of high bitrate compensation devices is currently being accomplished. For example, in the field of dispersion compensation, devices are under study in laboratory [2,3]. Concerning polarization effects, many devices are under investigation [4,5] and enable a significant reduction of the impairments. At last, we have seen that it was possible to reduce the amount of non-linear effects (by the use of dispersion management [6], modulation format [7] or phase modulation [8], polarization multiplexing [9]…). In my opinion, progress in these areas is to be continued so that 160 Gbit/s transmissions become even more worthwhile.

2 Network point of view

In order for 160 Gbit/s bit rate to be valuable, we have to think about evolution scenarios that could bring out a benefit to 160 Gbit/s bit rate. The interest for a solution is driven by the cost reduction it brings. Consequently, 160 Gbit/s transmissions are significant if they enable a cost reduction compared to lower bitrate. Therefore, the main problem about the interest of such high bitrate systems appears: how is it possible to reduce the cost of a system by increasing the bitrate?

Answering this question can be considered in a different way. As we have seen so far, there is no technical advantage of 160 Gbit/s transmissions compared to 40 Gbit/s transmissions. However, it is possible to reduce the number of functions because it is possible to share some of these functions.

For example, in the case of a transparent network using optical cross connects or switches, this means that using one 160Gbit/s channel may decrease the number of needed port by 4 for an equivalent traffic demand when compared to 40Gbit/s bitrate. This straightforward line of argument however, does not consider that 160Gbit/s channels are probably constituted of demands which may be aggregated or des-aggregated throughout their way in the network.

As a matter of fact, most functions can not cope with several wavelengths simultaneously (PMD compensation, regeneration, wavelength conversion…) while optical amplifiers such as EDFA

do. Hence using the time domain for multiplexing channels instead of the wavelength domain allows to use this function simultaneously for all different TDM channels. As we said, regeneration or PMD compensation may be shared, leading to a potential decrease in resource compared to lower bitrate. However, the system reach for such high bit rates is greatly reduced as well as the tolerances to PMD, leading to a greater need for regeneration or PMD compensation.

Up to now, we have always considered 160 Gbit/s bit rate from a transmission point of view as we considered point to point communication and the aim was to optimize the quality at the reception. In this part, we shall have a look at the opportunities with a networking point of view, i.e. with different links and nodes. We shall investigate this in the following example. We have considered a traffic demand between 6 different nodes:

- 70 Gbit/s between node 1 and node 5.
- 25 Gbit/s between node 1 and node 4.
- 40 Gbit/s between node 2 and node 5.
- 90 Gbit/s between node 2 and node 6.
- 35 Gbit/s between node 3 and node 5.

The traffic exchange is represented on the following figure. For simplicity, we only consider traffic from the left to the right of the figure. The number of node ports would be twice in a bidirectional configuration.

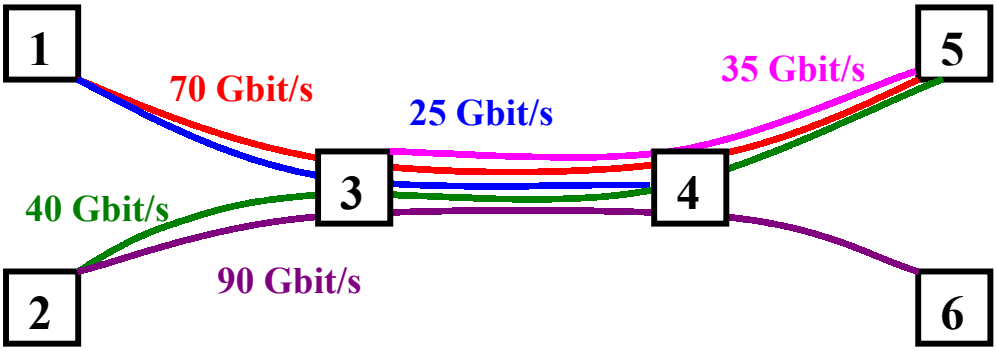

Figure 6. 1. Traffic exchange example between 6 nodes.

If we consider a first scenario with 40 Gbit/s bitrate then this traffic demand requires:

- 2 wavelengths from node 1 to node 5.
- 1 wavelength from node 1 to node 4.
- 1 wavelength from node 2 to node 5.
- 3 wavelengths from node 2 to node 6.
- 1 wavelength from node 3 to node 5.

We can also represent this demand by the minimum number of wavelengths to be allocated from one node to its neighbours:

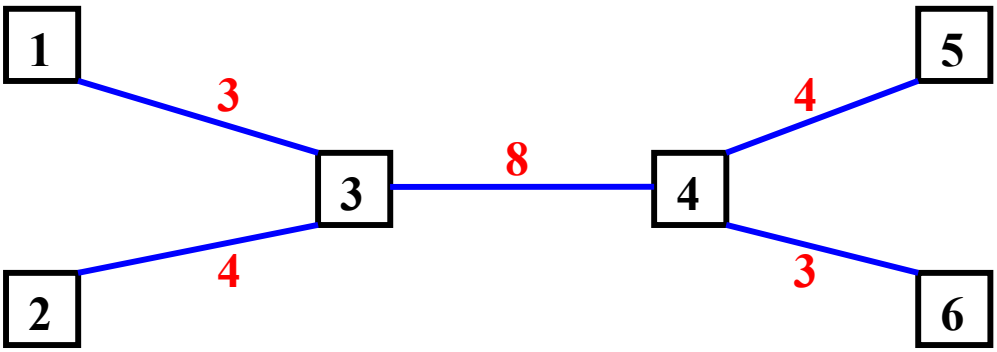

Figure 6. 2. Minimum number of wavelengths between neighbouring nodes for a 40 Gbit/s scenario.

If we consider a second scenario with 160 Gbit/s bitrate and with aggregation of 40 Gbit/s channels at the nodes then this traffic demand requires:

- 1 wavelength from node 1 to node 3.
- 1 wavelength from node 2 to node 3.
- 2 wavelengths from node 3 to node 4.
- 1 wavelength from node 4 to node 5.
- 1 wavelength from node 4 to node 6.

We can also represent this demand by the minimum number of wavelengths to be allocated from one node to its neighbours, as displayed on the following figure:

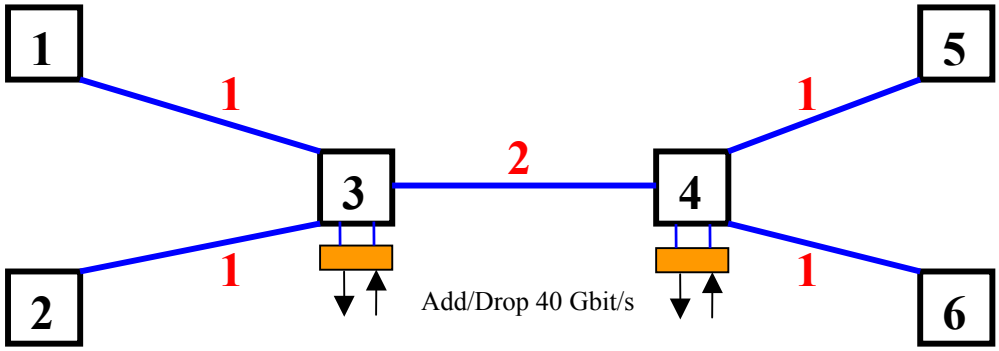

Figure 6. 3. Minimum number of wavelengths between neighbouring nodes for a 160 Gbit/s scenario with aggregation of 40 Gbit/s channels.

Therefore, we see that, using this second scenario at 160 Gbit/s with aggregated 40 Gbit/s channels, we significantly reduce the required number of wavelengths. This decrease has a great impact on the number of devices to be placed in the nodes.

For example, if we choose to regenerate the signal at each node, then we should have as many regenerators as required wavelengths. For the first scenario, it makes a total number of regenerators of 22 while this number is only 6 for the second scenario. Of course, this choice of regeneration at each node can be criticized: if a regeneration of the signal might be useful at each node in the second scenario, it is doubtful that this regeneration is also required in the first scenario at the quarter of the bitrate.

Another example would be to consider the chromatic dispersion compensation. If a device is used to perform this function at each node, the number of devices effectively decreases from 22 for the first scenario to 6 for the second scenario. We can also consider that dispersion compensation is only needed at the end of the transmission in which case the number of required devices is 8 for the first scenario and 6 for the second scenario. If the choice of regeneration was doubtful at 40 Gbit/s because of the poor degradation of the signal, it is very important to compensate dispersion even if the tolerance towards dispersion is 16 times higher at 40 Gbit/s than at 160 Gbit/s.

At last, the number of optical cross-connect ports needed at each node is displayed in the following tables for the two scenarios:

First scenario – 40 Gbit/s bitrate					Second scenario – 160 Gbit/s bitrate with aggregated 40 Gbit/s channels				
Node number	In	Out	Add	Drop	Node number	In	Out	Add	Drop
1	0	3	3	0	1	0	1	3	0
2	0	4	4	0	2	0	1	4	0
3	7	8	1	0	3	2	2	1	0
4	8	7	0	1	4	2	2	0	1
5	4	0	0	4	5	1	0	0	4
6	3	0	0	3	6	1	0	0	3

Table 6. 1. Required number of optical cross-connect ports for the two scenarios.

We remark that the number of optical cross-connect ports is decreasing from the first to the second scenario mainly because the network granularity is coarser in the second scenario. As a matter of fact, the number of transit ports is equal to the number of wavelengths arriving or leaving each node and so, this number is roughly 4 times smaller in the second scenario. For the 40 Gbit/s bitrate scenario, we remark that we have the following relation between the number of optical cross-connect ports for each node:

$$N_{in} + N_{add} = N_{out} + N_{drop}$$

This relation is no more valid in the second scenario because we consider channels aggregation at a smaller bitrate (40 Gbit/s). As a matter of fact, the number of add/drop ports is the same in both scenarios considering the same 40 Gbit/s aggregation granularity. This last statement implies that the configuration of the second scenario is more complex because of the insertion of data into another channel (using optical-time-division-multiplexing). We also note that the second scenario requires extra ports to rearrange 40 Gbit/s OTDM channels into 160 Gbit/s WDM channels.

This reduction of the number of optical cross-connect ports may be a motivation for the increase of the bitrate because it reduces the number of resources used in the network leading to more simplicity in the network.

3 Conclusion

We have therefore seen that there could be some advantages to 160 Gbit/s transmission using aggregated channels at a lower bitrate because it reduces the number of resources in the network. We can also think of the space reduction in terminal sites or a power reduction because of the decreased number of pieces of equipment.

In this study, we have focused on typical terrestrial transmissions for long haul and very long-haul reaches and we have identified the technical challenges which makes that the comparison between 40 and 160 Gbit/s bitrate is against 160 Gbit/s. However, we have also shown that the high dispersion and large effective area of SMF fibre is an advantage as it enables a reduction of non-linear effects. This is an important revelation as this fibre type is mostly used over classic telecommunication networks. As we have seen, the main problem for these transmissions is polarization-mode-dispersion effects which can be considered as proportional to the PMD value of the fibre and to the square root of the transmission distance. A solution in order to reduce the impact of PMD would be to increase the pulse width considering, for example, unusual modulation formats such as QPSK where the time bit is two times the inverse of the bitrate [10]. Last but not least, it may be interesting to consider 160 Gbit/s bitrate for smaller distances in order to avoid these impairments. For instance, short reach transmissions with high traffic demand with typical reaches up to a few tens kilometres might benefit this high bitrate because of the simplicity and space/power reduction it enables.

4 References

1. "Mintera Freshens Up Long-Haul", P. Harvey, Light Reading, http://www.lightreading.com/document.asp?site=lightreading&doc_id=41688
2. "Tunable dispersion slope compensator with a chirped fiber grating for 160-Gb/s RZ transmissions", Matsumoto, S.; Ohira, T.; Takabayashi, M.; Yoshiara, K.; Sugihara, T.; Hashimoto, T.; Matsuoka, K.; Miyazaki, T.; Kubota, F.; Optical Fiber Communications Conference, 2003. OFC 2003, Atlanta, USA.
3. "Tunable dispersion slope compensator based on chirped FBGs with temperature distribution for 160 Gbit/s", Wakabayashi, S.; Baba, A.; Moriya, H.; Wang, X.; Hasegawa, T.; Suzuki, A., OFC 2003 , Atlanta, USA.
4. "Adaptative PMD compensator in 160 Gbit/s DPSK transmission over installed fiber", S. Kieckbush, S. Ferber, H. Rosenfeldt, R. Ludwig, C. Boerner, A. Ehrhardt, E. Brinkmeyer, H.G. Weber,
5. Dynamic distortion compensation in a 160 Gb/s RZ OTDM system: adaptive 2 stage PMD compensation, Buchali, F.; Baumert, W.; Schmidt, M.; Bulow, H., OFC 2003, Atlanta, USA.
6. "Enhanced analytical engineering rule for fast optimization of dispersion maps in 40 Gbit/s-based transmission systems", Y. Frignac, J.C. Antona, S. Bigo, Paper TuN3, OFC 2004, Los Angeles, USA.
7. "Comparison of DPSK and OOK modulation format in 160 Gbit/s transmission system", S. Ferber, R. Ludwig, C. Boerner, A. Wietfeld, B. Schmauss, J. Berger, C. Schubert, G. Unterboersch, H.G. Weber, Electronics Letters , Volume: 39 , Issue: 20 , 2nd Oct. 2003.
8. "Suppression of intrachannel four-wave mixing by phase modulation at one quarter of bit rate", J. Martensson, J. Li, A; Berntson, A. Djupsjöbacka, M. Forzati, Electronics Letters, Vol. 38, N° 23, 7th November 2002.
9. "Benefits of bit-to-bit polarisation interleaving for Nx40 Gbit/s all-distributed Raman amplified submarine transmission.", G. Le Meur, E. Corbel, Electronics Letters, Vol. 38, N° 20, 26th September 2002.
10. "1.6-b/s/Hz 6.4-Tb/s QPSK-OCDM/WDM (4 OCDM × 40 WDM × 40 Gb/s) transmission experiment using optical hard thresholding", Sotobayashi, H.; Chujo, W.; Kitayama, K.; Photonics Technology Letters, IEEE , Volume: 14 , Issue: 4 , April 2002

Conclusion

The data flows transmitted by WDM (Wavelength Division Multiplexing) optical transmission systems has been constantly increasing since their appearance in the middle of the years 1990. The first developments are currently in progress among equipment suppliers for the system family of Nx40 Gbit/s. The bitrate of 40 Gbit/s by wavelength is obtained by electric temporal multiplexing (ETDM, Electrical Time Division Multiplexing) of 10 Gbit/s data. Bitrate by WDM channel higher than 40 Gbit/s (for example 160 Gbit/s) seems for the moment not easily possible if using only electric temporal multiplexing.

Optical telecommunications are currently facing the limitations in frequency of electronic devices. Thus, beyond a few tens of GHz (Gbit/s), optoelectronic transmitters are extremely difficult to realize, their performances are very bad and their cost and electric consumption are very high. The development of transmission systems using optical time division multiplexing (OTDM) associated to optical wavelength multiplexing (WDM) could constitute an alternative approach. Optical time division multiplexing makes it possible to increase the bitrate per WDM channel without increasing electronics speed. If OTDM techniques are for the moment still at the exploratory stage, European projects such as the IST TOPRATE project (Terabit/s optical transmission systems based one ultra-high channel bitrate) aim to prove the feasibility of such techniques.

In particular, the techniques of optical time multiplexing developed in TOPRATE project (based on the temporal multiplexing of 4 optical channels with 40Gbit/s) make it possible to consider WDM optical transmission systems with 160 Gbit/s by wavelength. However, the consequences in terms of engineering of these systems are still unknown. As a matter of fact, although the propagation effects at 2,5, 10 or 40 Gbit/s by wavelength also happen at 160 Gbit/s, their relative impacts are different. Moreover, the increase of the bitrate associated or not with this time multiplexing technique leads to disturbing effects which were negligible or non-existent at lower bitrates. On the other hand, temporal multiplexing could also be a benefit for the system and release some technical constraints.

The process adopted to answer these questions firstly consisted in the distinct and then coupled study of different physical phenomena. Transmission of WDM channels at 160 Gbit/s by wavelength induces many distortions and this study enabled to quantify their impacts and to define solutions to improve the signal quality.

Initially, the degradation of the signal related to the optical noise brought by the amplifiers during the amplification of the signal along the line was studied in relation with the quality factor of the transmission. The specificity of the temporal optical multiplexing was also considered because it strongly influences the choice of the detection elements of the signal (optical filter, demultiplexing, electric filter...). For instance, a 6 dB theoretical gain on the signal quality can be obtained by the use of optical temporal multiplexing of 4 optical channels. Furthermore, thanks to simple analytical models that we applied to various configurations of the transmission line, different transmission scenarios were identified for terrestrial configuration, i.e. with distance between amplifiers ranging between 80 and 120 km. In particular, the advantage of a hybrid amplification scheme, associating Raman to classical Erbium amplifications, was shown especially in the case of a transmission over long spans.

In the second time, propagation effects in fibre were identified and evaluated. Three distinct families of effects were studied separately: linear effects (deterministic), nonlinear effects in power and statistical linear effects. The first ones are related to chromatic dispersion of the optical signal during the propagation in optical fibre. In an intrinsic way, an optical signal which propagates in a medium (non empty) is subject to chromatic dispersion (variation of the group delay according to the wavelength). In an optical fibre, it results in a "spreading out" or a "compression" of the optical pulses

according to their initial characteristics. This effect is all the more important as the pulses are short (what results in a broad optical spectrum). We studied first and second order chromatic dispersion. The impact of chromatic dispersion on the engineering of the lines of transmission was also evaluated by adopting realistic approaches of constraints on the fibre environment (variations of dispersion related to the temperature for example). Given the very short tolerance towards dispersion, this last study confirmed the requirement for dynamic chromatic dispersion compensation devices.

The spectral width of the signals at 160Gbit/s is more important than at a lower bitrate. This means that the quantity of noise detected in reception is also more important. It is thus necessary to increase the signal power in order to preserve a sufficient signal to noise ratio or OSNR (Optical Signal to Noise Ratio). But when the power is high, degradations related to the nonlinear effects appear. The most preponderant nonlinear effects in power (related to the Kerr effect) and occurring during the transmission of a WDM Nx160 Gbit/s multiplex were independently analysed in order to evaluate their relative impacts. A first approach was established by the use of a method of perturbative analysis in order to understand the mechanism and the impact of the simplest effects. The simulations based on the method of Fourier with symmetrical step enabled us to confirm this approach and to complement it. The impact of self-phase modulation was thus evaluated just as that of intrachannel four-wave-mixing, intrachannel cross-phase-modulation and other non-linear effects. Intrachannel four-wave-mixing (and cross-phase-modulation in a minor way) was found to be highly disturbing. An interesting advantage of optical time multiplexing consists in the possibility to introduce a phase difference between adjacent optical pulses. The impact of the phase modulation on the quality of transmission was analysed. Results have shown that carrier-suppressed RZ modulation efficiently reduces amplitude jitter linked to intrachannel four-wave-mixing.

Thanks to this analysis, the most disturbing nonlinear effects could be identified in order to optimize the quality of transmission of a single 160 Gbit/s channel. The addition of optical signals at different frequencies (wavelengths) by the use of wavelength division multiplexing also degrades the quality of transmission. We analyzed and modelled interchannel nonlinear effects generated by considering interchannel four-wave-mixing, interchannel cross phase modulation and Raman effect. Intrachannel nonlinear effects were shown to be preponderant upon other nonlinear effects at 160 Gbit/s by wavelength.

We also modelled the impact of dispersion management on nonlinear effects. Intrachannel nonlinear effects, which are related to the overlapping of optical impulses of the same optical channel, can highly be reduced using dispersion management. In particular, we have shown that a slightly negative cumulated dispersion at the beginning of the span enhances the signal quality.

Lastly, the study of the statistical effects of polarization mode dispersion (PMD) was undertaken in the context of transmissions at 160 Gbit/s by channel. The PMD is due to birefringence of optical fibre related on the techniques of manufacture and the random constraints applied to the fibre (torsions, vibrations, temperature...). The propagation is dependent on the axes of polarization of fibre. One can model this effect by a differential group delay between the propagation times on the two principal axes of polarization, this delay following a Maxwellian distribution law. The consequence of this effect is a random deformation of the optical signal and thus a deterioration of signal quality. This effect was studied in association with the implementation of devices for temporal demultiplexing at the reception (in order to convert an OTDM 4x40 Gbit/s signal into four signals with 40 Gbit/s). We could then determine the impact of the first order polarization mode dispersion effects for the optical transmission of 160 Gbit/s data. Nevertheless, these analyses are very "expensive" in simulation time because they require a great number of simulations in order to correctly represent the statistics of polarization effects. In order to reduce this computing time, several methods are based on an artificial increase in the probability of strong degradations of the signal but these methods do not give information about the outage time of the link, i.e. fraction of time during which degradation is too large. As a consequence, we worked out a heuristic model allowing us to describe, in an entirely analytical way, the impact of the PMD on the availability. This method is extremely fast and very easy to implement in order to model the degradation of the signal related to polarization effects.

The studies of the physical phenomena were then exploited for the complete evaluation of a transmission configuration at 160 Gbit/s by channel. By using the studies results concerning the various isolated effects, we could determine the relative importance of the effects and identify the principal parameters to adjust for the optimization of WDM system transmissions. We also could confront these results with experimental achievements having taken place in laboratories.

These methods were applied to the preparation study of a field trial on the network of France Telecom. We contributed to the definition of the engineering of the transmission with an aim of optimizing the quality of the transmission. The simulation studies results are analyzed and can be put in prospect with the experimental results obtained during the field trial.

The assessment of achieved work, the optimization of engineering of transmission systems at 160 Gbit/s and the understanding of physical phenomena occurring in these systems, are achieved objectives in a satisfactory way. Lastly, we sought to draw up some prospects concerning the evolutions for the optical transmissions with very high flow. These prospects are based on technical, network or economic concepts to justify or not interest of transmission to very high flow.

Annex: collective variable theory and its applications to pulse propagation in fibre

1 Theoretical base and application to the generalized non-linear Schrödinger equation

1.1 General introduction

In order to solve the differential equation giving the evolution of a physical particle, the CV theory may be used in order to understand more clearly the physical aspects of a phenomenon.

The approach is to replace the exact solution function ψ by the introduction of new variables: $\psi = f(X) + q$ [1] where ***X*** is a vector of variables *(X_1, X_2, X_3, ... , X_n)* and *q* is not depending on the collective variable ***X***. This way, the sum *f* + *q* is an exact solution of the general dynamical problem. However, we will most commonly describe the problem by *f*. Due to this determination, *q* can be understood as a residual field or a little perturbation of the static solution f. We consider the energy of this little perturbation also called residual field energy:

$$\varepsilon = \int_{-\infty}^{+\infty} |q|^2 \, dt = \int_{-\infty}^{+\infty} |\psi - f(X)|^2 \, dt \qquad (1)$$

To ensure the stability of the function f, we need to minimize this functional ***ε***. Indeed, in case of a one-dimensional in space evolution, the number of degrees of freedom is *n+2* because of the n collective variables, the space dimension and the time. We are going to set a certain number of constraints to recover the original number of degrees of freedom. The first set of constraints will allow the collective variables to evolve only in a particular direction to minimize the functional ***ε*** during the dynamics:

$$C_j = \frac{\partial \varepsilon}{\partial X_j} = 0 \ \ (\ or \approx 0) \qquad (2)$$

Equation (1) successively implies:

$$\frac{\partial}{\partial X_j} \int_{-\infty}^{+\infty} |\psi - f|^2 \, dt = 0$$

$$\frac{\partial}{\partial X_j} \int_{-\infty}^{+\infty} (\psi - f).(\psi - f)^* \, dt = 0$$

$$\int_{-\infty}^{+\infty} (\psi - f)^* . \frac{\partial}{\partial X_j} \big((\psi - f)\big) + (\psi - f). \frac{\partial}{\partial X_j} \big((\psi - f)\big)^* \, dt = 0$$

$$\int_{-\infty}^{+\infty} \left(- q^* . \frac{\partial f}{\partial X_j} - q . \frac{\partial f^*}{dX_j} \right) dt = 0 \ \text{ because } \frac{\partial \psi}{\partial X_j} = 0$$

$$C_j = -2. \int_{-\infty}^{+\infty} \Re \left[q . \frac{\partial f^*}{dX_j} \right] dt = 0 \qquad (3)$$

This also implies that the initial values of the collective variables must be chosen correctly to satisfy to constraints (2). We then define a second set of constraints to guarantee that $C_j = 0$ (or ≈ 0) for all z:

$$\left(\dot{C}_j\right) = \frac{\partial C_j}{\partial z} = 0 \quad (\ or \approx 0) \qquad (4)$$

Equation (4) successively implies:

$$\frac{\partial^2 \varepsilon}{\partial X_j \partial z} = 0 \Leftrightarrow \frac{\partial C_j}{\partial z} = \frac{\partial}{\partial z}\int_{-\infty}^{+\infty}\left(-\frac{\partial f}{\partial X_j}.q^* - q.\frac{\partial f^*}{\partial X_j}\right)dt = 0$$

$$\frac{\partial C_j}{\partial z} = \int_{-\infty}^{+\infty}\left(-\frac{\partial^2 f}{\partial X_j \partial z}.q^* - \frac{\partial f}{\partial X_j}.\frac{\partial q^*}{\partial z} - \frac{\partial q}{\partial z}.\frac{\partial f^*}{\partial X_j} - q.\frac{\partial^2 f^*}{\partial X_j \partial z}\right)dt = 0$$

$$\frac{\partial C_j}{\partial z} = -\int_{-\infty}^{+\infty}\left(\frac{\partial f}{\partial X_j}.\frac{\partial q^*}{\partial z} + \frac{\partial f^*}{\partial X_j}.\frac{\partial q}{\partial z}\right)dt - \int_{-\infty}^{+\infty}\left(\frac{\partial^2 f}{\partial X_j \partial z}.q^* + \frac{\partial^2 f^*}{\partial X_j \partial z}.q\right)dt = 0$$

If we use the notation $< f, g >= \int_{-\infty}^{+\infty} f(t).g(t)dt$, we can write:

$$\frac{\partial C_j}{\partial z} = -\left\langle \frac{\partial f^*}{\partial X_j}, \frac{\partial q}{\partial z} \right\rangle - \int_{-\infty}^{+\infty} \frac{\partial}{\partial X_j}\left(\sum_{k=1}^{n} \frac{\partial f^*(X_1, X_2, ..., X_n)}{\partial X_k}.\frac{\partial X_k}{\partial z}\right).q + cc = 0$$

where cc stands for the complex conjugate of the expression before.

$$\frac{\partial C_j}{\partial z} = -\left\langle \frac{\partial f^*}{\partial X_j}, \frac{\partial q}{\partial z} \right\rangle - \sum_{k=1}^{n} \frac{\partial X_k}{\partial z} \int_{-\infty}^{+\infty} \frac{\partial^2 f^*(X_1, X_2, ..., X_n)}{\partial X_j \partial X_k}.q + cc = 0$$

For j=1 and 2, we have:

$$\frac{\partial C_1}{\partial z} = -\left\langle \frac{\partial f^*}{\partial X_1}, \frac{\partial q}{\partial z} \right\rangle - \sum_{k=1}^{n} \frac{\partial X_k}{\partial z} \int_{-\infty}^{+\infty} \frac{\partial^2 f^*(X_1, X_2, ..., X_n)}{\partial X_1 \partial X_k}.q + cc = 0$$

$$\frac{\partial C_2}{\partial z} = -\left\langle \frac{\partial f^*}{\partial X_2}, \frac{\partial q}{\partial z} \right\rangle - \sum_{k=1}^{n} \frac{\partial X_k}{\partial z} \int_{-\infty}^{+\infty} \frac{\partial^2 f^*(X_1, X_2, ..., X_n)}{\partial X_2 \partial X_k}.q + cc = 0$$

Thus, for any j, we can write with matrices:

$$\left[\frac{\partial C}{\partial z}\right] = \left[\frac{\partial C}{\partial X}\right].\left[\dot{X}\right] + \left[R\right] \qquad (5)$$

where $\left[\dot{X}\right] = \begin{bmatrix} \frac{\partial X_1}{\partial z} \\ \vdots \\ \frac{\partial X_n}{\partial z} \end{bmatrix}$, $\left[R\right] = \begin{bmatrix} R_1 \\ \vdots \\ R_n \end{bmatrix}$ with $R_j = -\left\langle \frac{\partial f^*}{\partial X_j}, \frac{\partial q}{\partial z} \right\rangle + cc \qquad (6)$

and $\left[\frac{\partial C}{\partial X}\right]=\begin{bmatrix} \frac{\partial C_1}{\partial X_1} & \cdots & \frac{\partial C_1}{\partial X_n} \\ \vdots & \ddots & \vdots \\ \frac{\partial C_n}{\partial X_1} & \cdots & \frac{\partial C_n}{\partial X_n} \end{bmatrix}$ with $\frac{\partial C_j}{\partial X_k}=-\left\langle \frac{\partial^2 f^*}{\partial X_j \partial X_k}, q \right\rangle + cc$ (7)

We can express $\frac{\partial C_j}{\partial X_k}$ a better way by writing:

$$\frac{\partial C_j}{\partial X_k}=\frac{\partial}{\partial X_k}\left(-\left\langle q, \frac{\partial f^*}{\partial X_j}\right\rangle + cc\right)$$

$$\frac{\partial C_j}{\partial X_k}=-\left\langle \frac{\partial q}{\partial X_k}, \frac{\partial f^*}{\partial X_j}\right\rangle - \left\langle q, \frac{\partial^2 f^*}{\partial X_j \partial X_k}\right\rangle + cc$$

Using relation $\psi = f(X) + q$, we have:

$$\frac{\partial C_j}{\partial X_k}=-\left\langle \frac{\partial(\psi - f)}{\partial X_k}, \frac{\partial f^*}{\partial X_j}\right\rangle - \left\langle q, \frac{\partial^2 f^*}{\partial X_j \partial X_k}\right\rangle + cc$$

$$\frac{\partial C_j}{\partial X_k}=-\left\langle -\frac{\partial f}{\partial X_k}, \frac{\partial f^*}{\partial X_j}\right\rangle - \left\langle q, \frac{\partial^2 f^*}{\partial X_j \partial X_k}\right\rangle + cc$$

$$\frac{\partial C_j}{\partial X_k}=2.\int_{-\infty}^{+\infty}\Re\left[\frac{\partial f}{\partial X_k}.\frac{\partial f^*}{\partial X_j}\right]dt - 2.\int_{-\infty}^{+\infty}\Re\left[q.\frac{\partial^2 f^*}{\partial X_j \partial X_k}\right]dt \quad (8)$$

From there, the second set of constraints (4) allow us to write $\left[\frac{\partial C}{\partial z}\right]=[0]$ and therefore, the evolving of the collective variables is given by:

$$[\dot{X}]=-\left[\frac{\partial C}{\partial X}\right]^{-1}.[R] \quad (9)$$

1.2 Application to pulse propagation

In the case of pulse propagation, ψ is representing the electric field and is solution of the generalized non linear Schrödinger equation [2,3]:

$$\frac{\partial \psi}{\partial z} + i\frac{\beta_2}{2}\frac{\partial^2 \psi}{\partial t^2} - \frac{\beta_3}{6}\frac{\partial^3 \psi}{\partial t^3} - i\gamma|\psi|^2\psi + i\gamma_R\psi\frac{\partial\left(|\psi|^2\right)}{\partial t} + \gamma_S\frac{\partial\left(|\psi|^2\psi\right)}{\partial t} + \frac{\alpha}{2}\psi = 0 \quad (10)$$

The ansatz function f is to be chosen so that it is a solution of the linear problem [1] (without any perturbation). That's why we will give this function a gaussian profile:

$$f(X_j, t)_{j=1..6} = X_1 e^{\frac{-(t-X_2)^2}{X_3^2}} e^{i\left(\frac{X_4}{2}(t-X_2)^2 + X_5(t-X_2)\right)} e^{iX_6} \quad (11)$$

The collective variables X_1, X_2 , X_3 , X_4 , X_5, X_6 respectively represent the pulse amplitude, temporal position, half width at 1/e, chirp, frequency shift and phase. We must remember that the true propagating field is not ψ but $\psi.e^{-i\omega t}$ because of the time variable change operated in order to obtain the generalized non-linear Schrödinger equation. Using the relation $\psi = f(X) + q$, we can write from relation (10):

$$\frac{\partial q}{\partial z} + i\frac{\beta_2}{2}\frac{\partial^2 q}{\partial t^2} - \frac{\beta_3}{6}\frac{\partial^3 q}{\partial t^3} - i\gamma|f+q|^2 q + i\gamma_R q\frac{\partial\left(|f+q|^2\right)}{\partial t} + \gamma_S\frac{\partial\left(|f+q|^2 q\right)}{\partial t} + \frac{\alpha}{2}q =$$
$$-i\frac{\beta_2}{2}\frac{\partial^2 f}{\partial t^2} + \frac{\beta_3}{6}\frac{\partial^3 f}{\partial t^3} + i\gamma|f+q|^2 f - i\gamma_R f\frac{\partial\left(|f+q|^2\right)}{\partial t} - \gamma_S\frac{\partial\left(|f+q|^2 f\right)}{\partial t} - \frac{\alpha}{2}f \quad (12)$$

From this equation, we obtain an expression for $\frac{\partial q}{\partial z}$ which we can substitute in relation (6) to obtain the expression of R_j:

$$R_j = \beta_2.\Re\left[\left\langle i\frac{\partial f^*}{\partial X_j}, \frac{\partial^2 f}{\partial t^2}\right\rangle\right] - \frac{\beta_3}{3}\Re\left[\left\langle\frac{\partial f^*}{\partial X_j}, \frac{\partial^3 f}{\partial t^3}\right\rangle\right] - 2.\gamma.\Re\left[\left\langle i.\frac{\partial f^*}{\partial X_j}, |f+q|^2.f\right\rangle\right]$$
$$+\alpha.\Re\left[\left\langle\frac{\partial f^*}{\partial X_j}, f\right\rangle\right] + 2.\gamma_R.\Re\left[\left\langle i\frac{\partial f^*}{\partial X_j}, f.\frac{\partial|f+q|^2}{\partial t}\right\rangle\right] + 2.\gamma_S.\Re\left[\left\langle\frac{\partial f^*}{\partial X_j}, \frac{\partial\left(|f+q|^2.f\right)}{\partial t}\right\rangle\right]$$
$$+\beta_2.\Re\left[\left\langle i\frac{\partial f^*}{\partial X_j}, \frac{\partial^2 q}{\partial t^2}\right\rangle\right] - \frac{\beta_3}{3}.\Re\left[\left\langle\frac{\partial f^*}{\partial X_j}, \frac{\partial^3 q}{\partial t^3}\right\rangle\right] - 2.\gamma.\Re\left[\left\langle i.\frac{\partial f^*}{\partial X_j}, |f+q|^2.q\right\rangle\right]$$
$$+\alpha.\Re\left[\left\langle\frac{\partial f^*}{\partial X_j}, q\right\rangle\right] + 2.\gamma_R.\Re\left[\left\langle i\frac{\partial f^*}{\partial X_j}, \frac{\partial|f+q|^2}{\partial t}.q\right\rangle\right] + 2.\gamma_S.\Re\left[\left\langle\frac{\partial f^*}{\partial X_j}, \frac{\partial\left(|f+q|^2.q\right)}{\partial t}\right\rangle\right]$$

(13)

Using expression (11) for f, the partial derivatives are given by:

$$\frac{\partial f}{\partial X_1} = \frac{1}{X_1}.f \qquad \frac{\partial f}{\partial X_4} = f.\frac{i}{2}(t-X_2)^2$$
$$\frac{\partial f}{\partial X_2} = f.\left((t-X_2).\left(\frac{2}{X_3^2} - i.\frac{X_4}{2}\right) - i.X_5\right) \qquad \frac{\partial f}{\partial X_5} = f.i.(t-X_2)$$
$$\frac{\partial f}{\partial X_3} = f.\frac{2(t-X_2)^2}{X_3^3} \qquad \frac{\partial f}{\partial X_6} = f.i \quad (14)$$

Furthermore, we have the values of the integrals:

$$< f, f^* >= \int_{-\infty}^{+\infty} f(t).f^*(t)dt = X_1{}^2.X_3.\sqrt{\frac{\pi}{2}}$$

$$< (t-X_2)^{2n+1}.f, f^* >= \int_{-\infty}^{+\infty} (t-X_2)^{2n+1}.f(t).f^*(t)dt = 0, n \in \mathrm{N}$$

$$< (t-X_2)^2.f, f^* >= \int_{-\infty}^{+\infty} (t-X_2)^2.f(t).f^*(t)dt = \frac{1}{4}X_1{}^2.X_3{}^3.\sqrt{\frac{\pi}{2}}$$

$$< (t-X_2)^4.f, f^* >= \int_{-\infty}^{+\infty} (t-X_2)^4.f(t).f^*(t)dt = \frac{3}{16}.X_1{}^2.X_3{}^5.\sqrt{\frac{\pi}{2}} \quad (15)$$

From now, we will work with the lowest-order approximation of the CV theory, also called 'bare approximation' [3]. This approximation consists in setting the residual field q to 0. The expression of R_j and $\frac{\partial C_j}{\partial X_k}$ is then considerably simplified from equations (8) and (13):

$$\frac{\partial C_j}{\partial X_k} = 2.\Re\left[\left\langle \frac{\partial f}{\partial X_k}, \frac{\partial f^*}{\partial X_j} \right\rangle\right] \quad (16)$$

$$R_j = \beta_2.\Re\left[\left\langle i\frac{\partial f^*}{\partial X_j}, \frac{\partial^2 f}{\partial t^2} \right\rangle\right] - \frac{\beta_3}{3}\Re\left[\left\langle \frac{\partial f^*}{\partial X_j}, \frac{\partial^3 f}{\partial t^3} \right\rangle\right] - 2.\gamma.\Re\left[\left\langle i.\frac{\partial f^*}{\partial X_j}, |f|^2.f \right\rangle\right]$$
$$+\alpha.\Re\left[\left\langle \frac{\partial f^*}{\partial X_j}, f \right\rangle\right] + 2.\gamma_R.\Re\left[\left\langle i\frac{\partial f^*}{\partial X_j}, f.\frac{\partial |f|^2}{\partial t} \right\rangle\right] + 2.\gamma_S.\Re\left[\left\langle \frac{\partial f^*}{\partial X_j}, \frac{\partial\left(|f|^2.f\right)}{\partial t} \right\rangle\right] \quad (17)$$

From equation (16) and (17), we will use relations (14) and (15) to calculate the coefficients of the matrices $\left[\frac{\partial C}{\partial X}\right]$ and $[R]$. For example, we have:

$$\frac{\partial C_1}{\partial X_1} = 2.\Re\left[\left\langle \frac{\partial f}{\partial X_1}, \frac{\partial f^*}{\partial X_1} \right\rangle\right] = 2.\Re\left[\left\langle \frac{1}{X_1}.f, \frac{1}{X_1}.f^* \right\rangle\right] = 2.X_3.\sqrt{\frac{\pi}{2}}$$

With the example of f and the generalized non-linear Schrödinger equation, matrix equation (9) is finally replaced by [3]:

$$\dot{X}_1 = -\frac{1}{2}.\alpha.X_1 + \frac{1}{2}.(\beta_2 - \beta_3.X_5).X_1.X_4$$

$$\dot{X}_2 = -\beta_2.X_5 + \beta_3.\left(\frac{1}{2.X_3{}^2} + \frac{X_5{}^2}{2} + \frac{X_3{}^2.X_4{}^2}{8}\right) + \frac{3}{2.\sqrt{2}}.\gamma_S.X_1{}^2$$

$$\dot{X}_3 = -(\beta_2 - \beta_3.X_5).X_3.X_4$$

$$\dot{X}_4 = -(\beta_2 - \beta_3.X_5).\left(\frac{4}{X_3{}^4} - X_4{}^2\right) - \frac{\sqrt{2}.X_1{}^2.(\gamma - \gamma_S.X_5)}{X_3{}^2}$$

$$\dot{X}_5 = \frac{\sqrt{2}.\gamma_R.X_1{}^2}{X_3{}^2} + \frac{\gamma_S.X_1{}^2.X_4}{\sqrt{2}}$$

$$\dot{X}_6 = \beta_2.\left(\frac{1}{X_3{}^2} - \frac{X_5{}^2}{2}\right) + \beta_3.\left(\frac{X_5{}^3}{3} + \frac{X_3{}^2.X_4{}^2.X_5}{8} - \frac{X_5}{2.X_3{}^2}\right) + \frac{X_1{}^2.(5.\gamma + \gamma_S.X_5)}{4\sqrt{2}} \quad (18)$$

We will pay attention to the fact that even if the collective variable X_5 becomes positive: the physical meaning is that the frequency shift is negative because of the term of propagation $\psi.e^{-i\omega t}$. In the same way, the chirp X_4 becomes positive but the physical chirp is negative. Thus, this modelling gives us lots of information on the evolution of a gaussian pulse. However, we have to remember that whatever deformations the field ψ will face, its approximation *f* will keep a gaussian profile.

2 Interactions with other pulses

2.1 Equations for propagation

In this chapter, we will not consider the generalized non-linear Schrödinger equation but the coupled non-linear Schrödinger equation describing the interaction between two pulses ψ_1 and ψ_2:

$$\frac{\partial \psi_l}{\partial z} + i\frac{\beta_2}{2}\frac{\partial^2 \psi_l}{\partial t^2} - i\gamma|\psi_l|^2\psi_l + \frac{\alpha}{2}\psi_l = i\gamma\left(2|\psi_l|^2.\psi_{3-l} + \psi_l{}^2.\psi_{3-l}{}^*\right) \text{ with l = 1 or 2 (19)}$$

We will therefore consider a pulse ψ_l is interacting with its neighbour ψ_{3-l} with l=1 or l=2. The important thing to understand here is that if we consider we have two pulses with 6 defined parameters for each (as in (11)), the entire pattern of two bits and its evolution is then controlled by 12 variables.

Indeed, the ansatz for this pulse propagation will be modified in order to center the time origin between the two pulses:

$$\mathrm{f}_1(\mathrm{X}_{\mathrm{j1}},\mathrm{t})_{\mathrm{j=1..6}} = X_{11}e^{\frac{-(t-X_{21})^2}{X_{31}{}^2}}e^{i\left(\frac{X_{41}}{2}(t-X_{21})^2 + X_{51}(t-X_{21})\right)}e^{iX_{61}}$$

$$\mathrm{f}_2(\mathrm{X}_{\mathrm{j2}},\mathrm{t})_{\mathrm{j=1..6}} = X_{12}e^{\frac{-(t+X_{22})^2}{X_{32}{}^2}}e^{i\left(\frac{X_{42}}{2}(t+X_{22})^2 - X_{52}(t+X_{22})\right)}e^{iX_{62}} \quad (20)$$

In a similar way from before, we will work with the lowest order approximation of this CV theory. The collective variables X_{11}, X_{21},…, X_{61}, X_{12}, X_{22}…X_{62} are solution of the system:

$$[\dot{X}] = -\left[\frac{\partial C}{\partial X}\right]^{-1}.[R] \quad (21)$$

where $R_{jl} = -\left\langle \frac{\partial f_l^*}{\partial X_j}, \frac{\partial q}{\partial z} \right\rangle + cc$ and $\frac{\partial C_{jl}}{\partial X_{km}} = 2.\int_{-\infty}^{+\infty} \Re\left[\frac{\partial f_l}{\partial X_{km}} . \frac{\partial f_m^*}{\partial X_{jl}} \right] dt$ (22)

The expression of $\frac{\partial q}{\partial z}$ is obtained from equation (19) by replacing ψ by $f+q$. Applicating the lowest order approximation, we note R_{11}, R_{21}, … , R_{61}, R_{12}, R_{22}, … R_{62} the coefficients of matrix R:

$$R_{jl} = \Re\left\langle i.\beta_2 \frac{\partial^2 f_l}{\partial t^2}, \frac{\partial f_l^*}{\partial X_{jl}} \right\rangle - 2.\gamma.\Re\left\langle i.\frac{\partial f_l^*}{\partial X_{jl}}, |f_l|^2 f_l \right\rangle + \alpha.\Re\left\langle \frac{\partial f_l^*}{\partial X_{jl}}, f_l \right\rangle$$
$$- 2.\gamma.\Re\left\langle i.\frac{\partial f_l^*}{\partial X_{jl}}, f_l^2 . f_{3-l}^* \right\rangle - 4.\gamma.\Re\left\langle i.\frac{\partial f_l^*}{\partial X_{jl}}, |f_l|^2 . f_{3-l} \right\rangle \quad (23)$$

With this notation, the matrix C can be written:

$$\left[\frac{\partial C}{\partial X}\right] = \begin{bmatrix}
\frac{\partial C_{11}}{\partial X_{11}} & \frac{\partial C_{11}}{\partial X_{21}} & \cdots & \frac{\partial C_{11}}{\partial X_{61}} & \frac{\partial C_{11}}{\partial X_{12}} & \frac{\partial C_{11}}{\partial X_{22}} & \cdots & \frac{\partial C_{11}}{\partial X_{62}} \\
\frac{\partial C_{21}}{\partial X_{11}} & \frac{\partial C_{21}}{\partial X_{21}} & \cdots & \frac{\partial C_{21}}{\partial X_{61}} & \frac{\partial C_{21}}{\partial X_{12}} & \frac{\partial C_{21}}{\partial X_{22}} & \cdots & \frac{\partial C_{21}}{\partial X_{62}} \\
\vdots & \vdots & \ddots & \vdots & \vdots & \vdots & \ddots & \vdots \\
\frac{\partial C_{61}}{\partial X_{11}} & \frac{\partial C_{61}}{\partial X_{21}} & \cdots & \frac{\partial C_{61}}{\partial X_{61}} & \frac{\partial C_{61}}{\partial X_{12}} & \frac{\partial C_{61}}{\partial X_{22}} & \cdots & \frac{\partial C_{61}}{\partial X_{62}} \\
\frac{\partial C_{12}}{\partial X_{11}} & \frac{\partial C_{12}}{\partial X_{21}} & \cdots & \frac{\partial C_{12}}{\partial X_{61}} & \frac{\partial C_{12}}{\partial X_{12}} & \frac{\partial C_{12}}{\partial X_{22}} & \cdots & \frac{\partial C_{12}}{\partial X_{62}} \\
\frac{\partial C_{22}}{\partial X_{11}} & \frac{\partial C_{22}}{\partial X_{21}} & \cdots & \frac{\partial C_{22}}{\partial X_{61}} & \frac{\partial C_{22}}{\partial X_{12}} & \frac{\partial C_{22}}{\partial X_{22}} & \cdots & \frac{\partial C_{22}}{\partial X_{62}} \\
\vdots & \vdots & \ddots & \vdots & \vdots & \vdots & \ddots & \vdots \\
\frac{\partial C_{62}}{\partial X_{11}} & \frac{\partial C_{62}}{\partial X_{21}} & \cdots & \frac{\partial C_{62}}{\partial X_{61}} & \frac{\partial C_{62}}{\partial X_{12}} & \frac{\partial C_{62}}{\partial X_{22}} & \cdots & \frac{\partial C_{62}}{\partial X_{62}}
\end{bmatrix}$$

Indeed, we can already simplify this matrix because a lot of terms are null. For example, $\frac{\partial C_{11}}{\partial X_{12}} = 2.\int_{-\infty}^{+\infty} \Re\left[\frac{\partial f_1}{\partial X_{12}} . \frac{\partial f_2^*}{\partial X_{11}} \right] dt = 0$ since X_{12} is not a variable of f_1 and X_{11} is not a variable of f_2. Consequently, the matrix $\left[\frac{\partial C}{\partial X}\right]$ is a block diagonal matrix:

$$\left[\frac{\partial C}{\partial X}\right]=\begin{bmatrix} a & 0 \\ 0 & b \end{bmatrix} \text{ with } a=\begin{bmatrix} \frac{\partial C_{11}}{\partial X_{11}} & \cdots & \frac{\partial C_{11}}{\partial X_{61}} \\ \vdots & \ddots & \vdots \\ \frac{\partial C_{61}}{\partial X_{11}} & \cdots & \frac{\partial C_{61}}{\partial X_{61}} \end{bmatrix} \text{ and } b=\begin{bmatrix} \frac{\partial C_{12}}{\partial X_{12}} & \cdots & \frac{\partial C_{12}}{\partial X_{62}} \\ \vdots & \ddots & \vdots \\ \frac{\partial C_{62}}{\partial X_{12}} & \cdots & \frac{\partial C_{62}}{\partial X_{62}} \end{bmatrix}.$$

The matrix coefficients can thus be determined. For example, we have:

$$\frac{\partial C_{41}}{\partial X_{21}}=2.\Re\left[\left\langle \frac{\partial f_1}{\partial X_{21}},\frac{\partial f^*}{\partial X_{41}}\right\rangle\right]=2.\Re\left[\left\langle f_1.\left((t-X_{21}).\left(\frac{2}{{X_{31}}^2}-i.\frac{X_{41}}{2}\right)-i.X_{51}\right),-f_1^*.\frac{i}{2}(t-X_{21})^2\right\rangle\right]$$

$$\frac{\partial C_{41}}{\partial X_{21}}=2.\Re\left[\left\langle -i.X_{51}.f_1,-\frac{i}{2}(t-X_{21})^2.f_1\right\rangle\right]=-X_{51}.\int_{-\infty}^{+\infty}(t-X_{21})^2.f_1(t).f_1^*(t)dt$$

$$\frac{\partial C_{41}}{\partial X_{21}}=-\frac{1}{8}{X_{11}}^2{X_{31}}^3X_{51}\sqrt{2\pi}$$

Thus, we obtained the expression of matrix $\left[\frac{\partial C}{\partial X}\right]$:

$$\frac{\partial C_{11}}{\partial X_{11}}=X_{31}.\sqrt{2\pi} \qquad \frac{\partial C_{31}}{\partial X_{31}}=\frac{3.{X_{11}}^2}{4.X_{31}}\sqrt{2\pi}$$

$$\frac{\partial C_{11}}{\partial X_{31}}=\frac{X_{11}}{2}.\sqrt{2\pi} \qquad \frac{\partial C_{41}}{\partial X_{21}}=\frac{{X_{11}}^2.{X_{31}}^3.X_{51}}{8}\sqrt{2\pi}$$

$$\frac{\partial C_{21}}{\partial X_{21}}={X_{11}}^2.\sqrt{2\pi}.\left(\frac{1}{X_{31}}+\frac{{X_{41}}^2{X_{31}}^3}{4}+{X_{51}}^2X_{31}\right) \qquad \frac{\partial C_{41}}{\partial X_{41}}=\frac{3.{X_{11}}^2.{X_{31}}^5}{64}\sqrt{2\pi}$$

$$\frac{\partial C_{21}}{\partial X_{41}}=\frac{{X_{11}}^2.{X_{31}}^3.X_{51}}{8}\sqrt{2\pi} \qquad \frac{\partial C_{41}}{\partial X_{61}}=\frac{{X_{11}}^2.{X_{31}}^3}{8}\sqrt{2\pi}$$

$$\frac{\partial C_{21}}{\partial X_{51}}=\frac{{X_{11}}^2.{X_{31}}^3.X_{41}}{4}\sqrt{2\pi} \qquad \frac{\partial C_{51}}{\partial X_{21}}=\frac{{X_{11}}^2.{X_{31}}^3.X_{41}}{4}\sqrt{2\pi}$$

$$\frac{\partial C_{21}}{\partial X_{61}}={X_{11}}^2.X_{31}.X_{51}\sqrt{2\pi} \qquad \frac{\partial C_{51}}{\partial X_{51}}=\frac{{X_{11}}^2.{X_{31}}^3}{4}\sqrt{2\pi}$$

$$\frac{\partial C_{31}}{\partial X_{11}}=\frac{X_{11}}{2}\sqrt{2\pi} \qquad \frac{\partial C_{61}}{\partial X_{21}}={X_{11}}^2.X_{31}.X_{51}.\sqrt{2\pi}$$

$$\frac{\partial C_{61}}{\partial X_{41}} = \frac{X_{11}{}^{2}.X_{31}{}^{3}}{8}.\sqrt{2\pi}$$

$$\frac{\partial C_{61}}{\partial X_{61}} = X_{11}{}^{2}.X_{31}.\sqrt{2\pi}$$

$$\frac{\partial C_{12}}{\partial X_{12}} = X_{32}.\sqrt{2\pi}$$

$$\frac{\partial C_{42}}{\partial X_{22}} = \frac{X_{12}{}^{2}.X_{32}{}^{3}.X_{52}}{8}\sqrt{2\pi}$$

$$\frac{\partial C_{12}}{\partial X_{32}} = \frac{X_{12}}{2}.\sqrt{2\pi}$$

$$\frac{\partial C_{42}}{\partial X_{42}} = \frac{3.X_{12}{}^{2}.X_{32}{}^{5}}{64}\sqrt{2\pi}$$

$$\frac{\partial C_{22}}{\partial X_{22}} = X_{12}{}^{2}.\sqrt{2\pi}.\left(\frac{1}{X_{32}} + \frac{X_{42}{}^{2}X_{32}{}^{3}}{4} + X_{52}{}^{2}X_{32}\right)$$

$$\frac{\partial C_{42}}{\partial X_{62}} = \frac{X_{12}{}^{2}.X_{32}{}^{3}}{8}\sqrt{2\pi}$$

$$\frac{\partial C_{22}}{\partial X_{42}} = \frac{X_{12}{}^{2}.X_{32}{}^{3}.X_{52}}{8}\sqrt{2\pi}$$

$$\frac{\partial C_{52}}{\partial X_{22}} = \frac{X_{12}{}^{2}.X_{32}{}^{3}.X_{42}}{4}\sqrt{2\pi}$$

$$\frac{\partial C_{22}}{\partial X_{52}} = \frac{X_{12}{}^{2}.X_{32}{}^{3}.X_{42}}{4}\sqrt{2\pi}$$

$$\frac{\partial C_{52}}{\partial X_{52}} = \frac{X_{12}{}^{2}.X_{32}{}^{3}}{4}\sqrt{2\pi}$$

$$\frac{\partial C_{22}}{\partial X_{62}} = X_{12}{}^{2}.X_{32}.X_{52}\sqrt{2\pi}$$

$$\frac{\partial C_{62}}{\partial X_{22}} = X_{12}{}^{2}.X_{32}.X_{52}.\sqrt{2\pi}$$

$$\frac{\partial C_{32}}{\partial X_{12}} = \frac{X_{12}}{2}\sqrt{2\pi}$$

$$\frac{\partial C_{62}}{\partial X_{42}} = \frac{X_{12}{}^{2}.X_{32}{}^{3}}{8}.\sqrt{2\pi}$$

$$\frac{\partial C_{32}}{\partial X_{32}} = \frac{3.X_{12}{}^{2}}{4.X_{32}}\sqrt{2\pi}$$

$$\frac{\partial C_{62}}{\partial X_{62}} = X_{12}{}^{2}.X_{32}.\sqrt{2\pi}$$

If we note:

$$D_k = X_{1k}{}^2.\sqrt{2\pi}.\begin{bmatrix} \frac{X_{3k}}{X_{1k}{}^2} & 0 & \frac{1}{2.X_{1k}} & 0 & 0 & 0 \\ 0 & \left(\frac{1}{X_{3k}} + \frac{X_{4k}{}^2 X_{3k}{}^3}{4} + X_{5k}{}^2 X_{3k}\right) & 0 & \frac{X_{3k}{}^3.X_{5k}}{8} & \frac{X_{3k}{}^3.X_{4k}}{4} & X_{3k}.X_{5k} \\ \frac{1}{2.X_{1k}} & 0 & \frac{3}{4.X_{3k}} & 0 & 0 & 0 \\ 0 & \frac{X_{3k}{}^3.X_{5k}}{8} & 0 & \frac{3.X_{3k}{}^5}{64} & 0 & \frac{X_{3k}{}^3}{8} \\ 0 & \frac{X_{3k}{}^3.X_{4k}}{4} & 0 & 0 & \frac{X_{3k}{}^3}{4} & 0 \\ 0 & X_{3k}.X_{5k} & 0 & \frac{X_{3k}{}^3}{8} & 0 & X_{3k} \end{bmatrix}$$

The expression of $\left[\frac{\partial C}{\partial X}\right]$ is:

$$\left[\frac{\partial C}{\partial X}\right] = \begin{bmatrix} D_1 & 0 \\ 0 & D_2 \end{bmatrix}$$

The determination of matrix R (referring to equations 21 and 22) is a little bit harder since we need to compute the non-linear terms corresponding to the integral of the products of gaussian functions f_1 and f_2 which are not centered on the same position.

$$R_{11} = \sqrt{2.\pi}.\left(\alpha.\frac{X_{11}.X_{31}}{2} + 2.\gamma.\mathrm{Im}\left(W + 2.\overline{W}\right)\right) = \sqrt{2.\pi}.\left(\alpha.\frac{X_{11}.X_{31}}{2} - 2.\gamma.\mathrm{Im}\left(W_1\right)\right)$$

where

$$W_1 = X_{11}{}^2.X_{12}.K$$

$$K = \frac{e^{\frac{1}{2}\left(-I.X_{41}.X_{21}{}^2 - 6.\frac{X_{21}{}^2}{X_{31}{}^2} - 2.\frac{X_{22}{}^2}{X_{32}{}^2} + 2.I.X_{51}.X_{21} + \frac{I.\left(X_{31}{}^2.\left((X_{21}.X_{41} - 2.X_{51}).X_{32}{}^2 + X_{22}.\left(X_{42}.X_{32}{}^2 + 2.I\right)\right) - 6.I.X_{21}.X_{32}{}^2\right)^2}{X_{31}{}^4.X_{32}{}^2.\left(X_{32}{}^2.\left(X_{41} - X_{42}\right) - 2.I\right) - 6.I.X_{31}{}^2.X_{32}{}^4} + I.X_{22}{}^2.X_{42} - 2.I.X_{22}.X_{51} - 2.I.\left(X_{61} - X_{62}\right)\right)}}{\sqrt{\frac{6}{X_{31}{}^2} + \frac{2}{X_{31}{}^2} + I.\left(X_{41} - X_{42}\right)}}$$

$$R_{21} = X_{11}{}^2\sqrt{\frac{\pi}{2}}.\left(\beta_2.\frac{X_{51}}{4.X_{31}}.\left(-4 + 3.X_{31}{}^4.X_{41}{}^2 + 4.X_{31}{}^2.X_{51}{}^2\right) + 4.\gamma.X_{11}{}^2.X_{31}.X_{51} - 32.\gamma.\mathrm{Re}\left(W_2\right)\right)$$

$$W_2 = -K.X_{11}.X_{12}.\begin{pmatrix} \left(2.i + X_{31}{}^2.X_{41}\right)\left(-2.i + X_{32}{}^2.X_{42}\right)\left(X_{21} - X_{22}\right) \\ \frac{-2.i.X_{32}{}^2.\left(4.X_{51} + X_{52}\right) + X_{31}{}^2.X_{51}.\left(-2.i + X_{32}{}^2.X_{42}\right) - X_{32}{}^2.X_{41}.X_{52}}{\left(-6.i.X_{32}{}^2 + X_{31}{}^2.\left(-2.i + X_{32}{}^2.\left(X_{41} + X_{42}\right)\right)\right)} \end{pmatrix}$$

$$R_{31} = X_{11}{}^2\sqrt{\frac{\pi}{2}}.\left(-\beta_2.X_{31}.X_{41} + \frac{\alpha.X_{31}}{2} + 32.\gamma.\mathrm{Re}\left(W_3\right)\right)$$

$$W_3 = -K.X_{11}.X_{12}.\left(\begin{array}{c} -2.X_{31}^{\ 2}.X_{32}^{\ 2} - 6.X_{32}^{\ 4} - i.X_{31}^{\ 2}.X_{32}^{\ 4}.(X_{41}+X_{42}) + X_{31}^{\ 2}.\left(-2.i + X_{32}^{\ 2}.X_{42}\right)^2.\left(X_{21}^{\ 2}+X_{22}^{\ 2}\right) \\ + X_{31}^{\ 2}.X_{32}^{\ 4}.(X_{51}+X_{52})^2 + 2.X_{22}.X_{31}^{\ 2}.X_{32}^{\ 2}.\left(-2.i + X_{32}^{\ 2}.X_{42}\right).(X_{51}+X_{52}) \\ -2.X_{21}.X_{31}^{\ 2}.\left(-2.i + X_{32}^{\ 2}.X_{42}\right).\left(X_{22}.\left(-2.i + X_{32}^{\ 2}.X_{42}\right) + X_{32}^{\ 2}.(X_{51}+X_{52})\right) \\ \hline \left(-6.i.X_{32}^{\ 2} + X_{31}^{\ 2}.\left(-2.i + X_{32}^{\ 2}.(X_{41}+X_{42})\right)\right) \end{array}\right)$$

$$R_{41} = X_{11}^{\ 2}.\sqrt{\frac{\pi}{2}}.\left(\frac{\beta_2.X_{31}^{\ 3}}{8}.\left(\frac{5}{X_{31}^{\ 2}} - X_{51}^{\ 2} + \frac{3.X_{31}^{\ 2}.X_{41}^{\ 2}}{4}\right) - \frac{\gamma.X_{11}^{\ 2}.X_{31}^{\ 3}}{2} - 16.\gamma.\mathrm{Re}(W_3)\right)$$

$$R_{51} = X_{11}^{\ 2}.\sqrt{\frac{\pi}{2}}.(2.\beta_2.X_{31}.X_{41}.X_{51} - 16.\gamma.\mathrm{Re}(W_4))$$

$$W_4 = -K.X_{11}.X_{12}.\left(\frac{(X_{21}+X_{22}).X_{31}^{\ 2}.\left(2.i + X_{32}^{\ 2}.X_{42}\right)}{\left(-6.i.X_{32}^{\ 2} + X_{31}^{\ 2}.\left(-2.i + X_{32}^{\ 2}.(X_{41}+X_{42})\right)\right)}\right)$$

$$R_{61} = X_{11}^{\ 2}.\sqrt{\frac{\pi}{2}}.\left(\beta_2.X_{31}.\left(\frac{3}{X_{31}^{\ 2}} - X_{51}^{\ 2} - \frac{X_{31}^{\ 2}.X_{41}^{\ 2}}{4}\right) - 4.\gamma.X_{11}^{\ 2}.X_{31} - 32.\gamma.X_{11}.X_{12}\,\mathrm{Im}(K)\right)$$

$\left[\frac{\partial C}{\partial X}\right]$ is a diagonal matrix and so, $\left[\frac{\partial C}{\partial X}\right]^{-1}$ is also a diagonal matrix and it can be expressed as:

$$\left[\frac{\partial C}{\partial X}\right]^{-1} = \begin{bmatrix} F_1 & 0 \\ 0 & F_2 \end{bmatrix} \text{ where } F_k = D_k^{\ -1}$$

The calculation leads to the following expression for D_k:

$$D_k = \frac{1}{\sqrt{2\pi}}.\begin{bmatrix} \frac{3}{2.X_{3k}} & 0 & \frac{-1}{2.X_{1k}} & 0 & 0 & 0 \\ 0 & \left(\frac{4.X_{3k}}{X_{1k}^{\ 2}.\left(4+X_{4k}^{\ 2}X_{3k}^{\ 4}\right)}\right) & 0 & 0 & \frac{4.X_{3k}.X_{4k}}{X_{1k}^{\ 2}.\left(4+X_{4k}^{\ 2}X_{3k}^{\ 4}\right)} & \frac{4.X_{3k}.X_{5k}}{X_{1k}^{\ 2}.\left(4+X_{4k}^{\ 2}X_{3k}^{\ 4}\right)} \\ \frac{-1}{2.X_{1k}} & 0 & \frac{2.X_{3k}}{X_{1k}^{\ 2}} & 0 & 0 & 0 \\ 0 & 0 & 0 & \frac{32}{X_{1k}^{\ 2}X_{3k}^{\ 5}} & 0 & \frac{-4}{X_{1k}^{\ 2}.X_{3k}^{\ 3}} \\ 0 & \frac{4.X_{3k}.X_{4k}}{X_{1k}^{\ 2}.\left(4+X_{4k}^{\ 2}X_{3k}^{\ 4}\right)} & 0 & 0 & \frac{4.\left(4+X_{3k}^{\ 4}.X_{4k}^{\ 2}\right)}{X_{1k}^{\ 2}.X_{3k}^{\ 3}.\left(4+X_{4k}^{\ 2}X_{3k}^{\ 4}\right)} & \frac{4.X_{3k}.X_{4k}.X_{5k}}{X_{1k}^{\ 2}.\left(4+X_{4k}^{\ 2}X_{3k}^{\ 4}\right)} \\ 0 & \frac{4.X_{3k}.X_{5k}}{X_{1k}^{\ 2}.\left(4+.X_{4k}^{\ 2}X_{3k}^{\ 4}\right)} & 0 & \frac{-4}{X_{1k}^{\ 2}.X_{3k}^{\ 3}} & \frac{4.X_{3k}.X_{4k}.X_{5k}}{X_{1k}^{\ 2}.\left(4+X_{4k}^{\ 2}X_{3k}^{\ 4}\right)} & \frac{3}{2.X_{3k}} - \frac{4.X_{3k}.X_{5k}}{4+X_{4k}^{\ 2}X_{3k}^{\ 4}} \\ & & & & & X_{1k}^{\ 2} \end{bmatrix}$$

where T_b is the time bit and $\delta\Phi = X_{61} - X_{62}$ is the phase difference between pulse number 1 and pulse number 2. Finally, we can obtain the matrix $\left[\dot{X}\right]$. We will present the first six lines first and the last six lines after. As a result, the variations of the collective variables of the first pulse (index=1) are ruled by the following differential equations:

$$\dot{X}_{11} = -\alpha.\frac{X_{11}}{2} + \frac{\beta_2}{2}.X_{11}.X_{41} + \gamma.{X_{11}}^2.\left(\frac{3}{X_{31}}.\mathrm{Im}(W_1) - \mathrm{Re}(W_3)\right)$$

$$\dot{X}_{21} = -\beta_2.X_{51} - \frac{4.\gamma.X_{31}.{X_{11}}^2}{4+{X_{31}}^2.{X_{41}}^2}.(2.\mathrm{Re}(W_2) + \mathrm{Re}(W_3) + 2.X_{11}.X_{12}.\mathrm{Im}(K))$$

$$\dot{X}_{31} = -\beta_2.X_{31}.X_{41} + \gamma.{X_{11}}^2.\left(-\frac{1}{X_{11}}.\mathrm{Im}(W_1) - \frac{4.X_{31}}{{X_{11}}^2}.\mathrm{Re}(W_3)\right)$$

$$\dot{X}_{41} = -\beta_2.\left(\frac{4}{{X_{31}}^4} - {X_{41}}^2\right) - \gamma.{X_{11}}^2.\left(\frac{\sqrt{2}}{{X_{31}}^2} - 8.\left(\frac{4}{{X_{31}}^5}\mathrm{Re}(W_3) - \frac{X_{12}.\mathrm{Im}(K)}{X_{11}.{X_{31}}^3}\right)\right)$$

$$\dot{X}_{51} = \frac{4.\gamma.{X_{11}}^2}{4+{X_{41}}^2{X_{31}}^4}.\left(2.X_{31}.X_{41}.\mathrm{Re}(W_2) + \frac{4+{X_{41}}^2{X_{31}}^4}{{X_{31}}^3}.\mathrm{Re}(W_4) + \frac{X_{31}.X_{41}.X_{51}}{X_{11}}.2.\mathrm{Im}(K)\right)$$

The differential equation expressing the variation of the phase X_{61} is not calculated here as its expression is not important in this matter. We notice that the evolution of the shift frequency (X_{51}) only depends on non-linear interactions of the pulse and its neighbour. This is due to intrachannel cross phase modulation. Combined with the second-order dispersion in the fibre, this frequency shift is responsible for a time deviation as it can be seen in the differential equation of X_{21}. The amount of this frequency shift is not the same for all pulses because they do not have the same neighbours. As a consequence, the amount of time deviation is not the same for all pulses and timing jitter appears.

The evolution of all these parameters are constituted by a non-linear term which represents the deformation induced by neighbouring pulses (terms with W_i or K). The physical explanation for these contributions lies in inter-bit non-linear effects such as intrachannel cross-phase modulation and intrachannel four-wave mixing.

3 References

1- « Hamiltonian equations for multiple-collective-variable theories of nonlinear Klein-Gordon equations: A projection-operator approach», R. Boesch, P. Stancioff et C. R. Willis, Physical Review B, Volume 38, Number 10(1988), p. 6713
2- Nonlinear Fiber Optics, Govind P. Agrawal, Quantum Electronics, Principles and Applications, p41.
3- «A collective variable approach for dispersion-managed solitons», P. Tchofo Dinda et al, Journal of Physics A: Mathematical and General, Volume 34 (2001), p. 103

Acronym list

Acronym	Definition
3R regeneration	Re-amplification, re-shaping, re-timing
ASE	Amplified Spontaneous Emission
ASK	Amplitude Shift Keying
AWG	Array Waveguide Grating
BER	Bit Error Rate
CD	Chromatic Dispersion
CSRZ	Carrier Suppressed Return to zero modulation format
CW	Continuous Wave
dB	Decibel
dBm	Decibel above/below one milliwatt
DC	Duty Cycle
DCF	Dispersion compensating fibre
DCM	Dispersion Compensation Module
DGD	Differential Group Delay
DM	Dispersion managed
DPSK	Differential Phase Shift Keying
DRB	Double Rayleigh Backscattering
DSF	Dispersion Shifted Fibre
DWDM	Dense Wavelength Division Multiplexing
EAM	Electro-absorption modulator
EDFA	Erbium Doped Fiber Amplifier
EO	Eye Opening
EOF	Eye Opening Factor
ETDM	Electrical Time Division Multiplexing
FBG	Fibre Bragg Grating
FEC	Forward Error Correction
FFT	Fast Fourier Transform
FWHM	Full width at half maximum
FWM	Four wave mixing
GVD	Group Velocity Dispersion
HNLF	Highly Non Linear Fibre
HOM	Higher Order Mode
HONLSE	Higher Order Non Linear Schrödinger equation
ISI	Intersymbol Interference
ITU	International Telecommunication Union
LEAF	Large effective area fibre
LH	Long haul
MUX / DEMUX	Multiplexing / Demultiplexing
MZDI	Mach-Zender Delay Interferometer
MZI	Mach-Zender Interferometer
MZM	Mach-Zender Modulator

NF	Noise Figure
NLSE	Non Linear Schrödinger equation
NOLM	Non Linear Optical Loop Mirror
NRZ	Non-Return to zero modulation format
NZDSF	Non Zero Dispersion-Shifted-Fibre
OADM	Optical Add Drop Multiplexer
OCCR	Optical Cross Connect Regenerator
OOK	On-Off Keying
OPC	Optical Phase Conjugation
OSNR	Optical Signal to Noise Ratio
OTDM	Optical Time Division Multiplexing
OXC	Optical Cross Connect
PBS	Polarisation Beam splitter
PCF	Photonic Crystal Fibre
PDF	Probability Density Function
PDL	Polarisation Dependent Loss
PMD	Polarisation Mode Dispersion
PMF	Polarisation maintaining fiber
PRBS	Pseudo Random Binary Sequence
QPSK	Quaternary Phase Shift Keying
RMS	Root Mean Square
Rx	Receiver
RZ	Return-to-zero modulation format
SBS	Stimulated Brillouin Scattering
SLA-IDF	Super Large Area- Inverse Dispersion Fibre
SOA	Semiconductor Optical Amplifier
SONET	Synchronous Optical Network
SPM	Self Phase Modulation
SRS	Stimulated Raman Scattering
SSMF or SMF	(Standard) single mode fibre
TOPRATE	Terabit/s optical transmission systems based on ultra-high channel bitrate
Tx	Transmitter
ULH	Ultra long haul
VIPA	Virtually Image Phased Array
VLH	Very long haul
WDM	Wavelength Division Multiplexing
XAM	Cross Absorption Modulation
XPM	Cross Phase modulation